Predicting Wave-Induced Flooding on Low-Lying Tropical Islands

Using a Bayesian Network

Stuart Grant Pearson

Technische Universiteit Delft

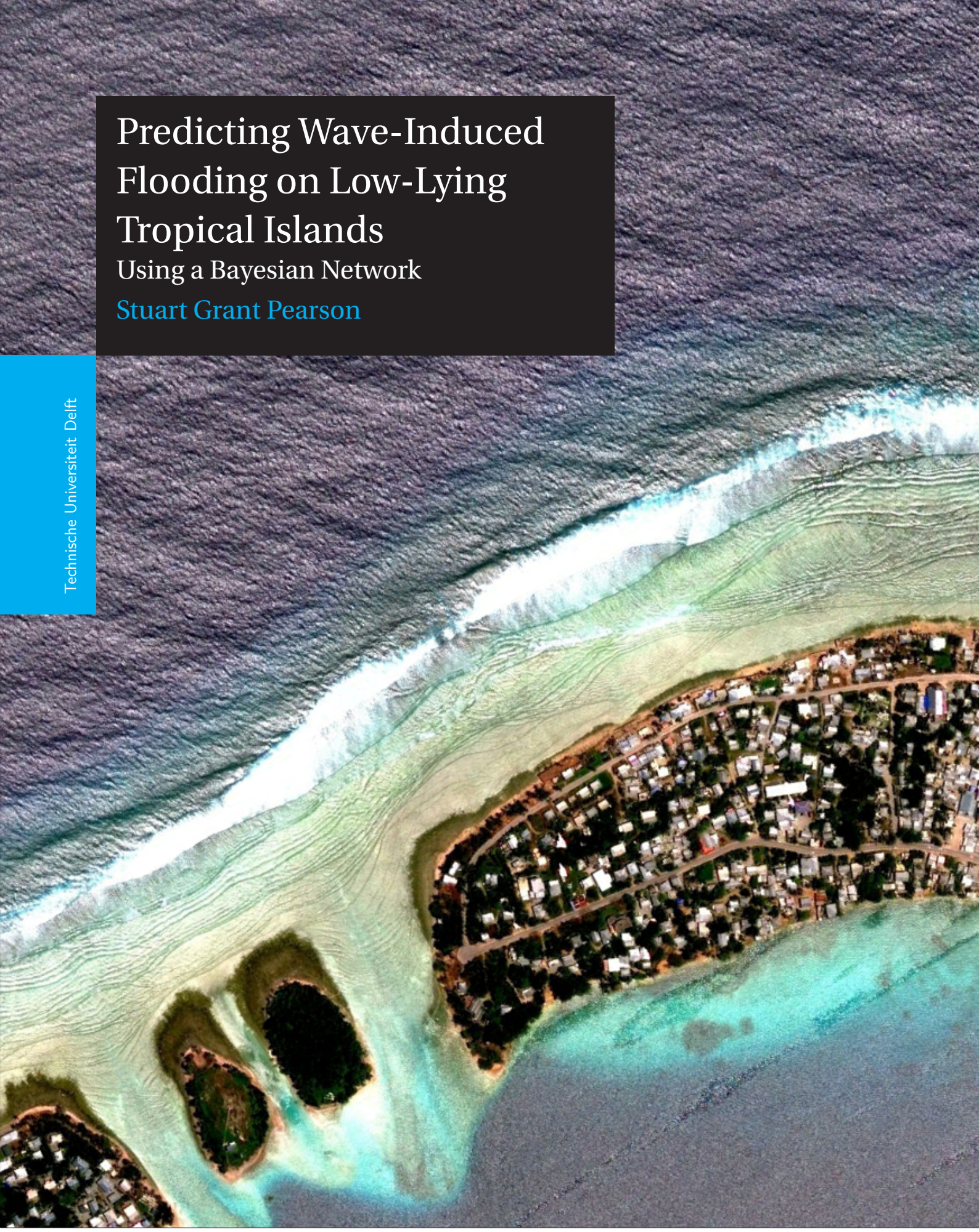

TU Delft Delft University of Technology

Challenge the future

PREDICTING WAVE-INDUCED FLOODING ON LOW-LYING TROPICAL ISLANDS

USING A BAYESIAN NETWORK

by

Stuart Grant PEARSON

in partial fulfillment of the requirements for the degree of

Master of Science
Coastal & Marine Engineering and Management

at the Delft University of Technology,
to be defended publicly on Tuesday June 28th, 2016 at 12:30 PM.

Thesis committee:
Prof. dr. ir. A.J.H.M. Reniers, TU Delft
Ir. A.R. van Dongeren, PhD, Deltares
Dr. M.F.S. Tissier, TU Delft
Dr. ir. C. den Heijer, TU Delft/Deltares

An electronic version of this thesis is available at
http://repository.tudelft.nl/

Correspondence with the author may be directed to:
stuart.pearson17@gmail.com

In collaboration with:

Keywords: Low-lying tropical islands, coral atolls, flooding, Bayesian network, disaster risk reduction, early warning system, climate change, swell, wave hydrodynamics, XBeach, non-hydrostatic, nature-based flood defenses

Front Cover: Aerial view of the reef at Majuro Atoll, Republic of the Marshall Islands. Swell from offshore breaks at the reef crest, and undular bores emerge across the shallow reef flat (identifiable by the narrow bands of short, unbroken waves). (Source: Google Earth (2014))

Back Cover: An example of wave spectral evolution across coral reefs from an XBeach model developed for this thesis. The peak incident frequency dominates at the offshore boundary (foreground), but harmonics at twice the peak frequency begin to emerge during shoaling (centre). When waves reach the reef crest, dissipation by breaking abruptly attenuates the higher frequencies. Energy is transferred to infragravity and very low frequencies on the reef flat, which reach a maximum at the shoreline (background). Some infragravity energy is also generated and directed seaward by the breakpoint mechanism (centre-left). The x-axis represents frequency, the y-axis is distance along reef profile, and the z-axis is spectral density.

The Erasmus+: Erasmus Mundus MSc in Coastal and Marine Engineering and Management is an integrated programme including mobility organized by five European partner institutions, coordinated by Norwegian University of Science and Technology (NTNU).

The joint study programme of 120 ECTS credits (two years full-time) has been obtained at two or three of the five CoMEM partner institutions:

- Norges Teknisk- Naturvitenskapelige Universitet (NTNU) Trondheim, Norway
- Technische Universiteit (TU) Delft, The Netherlands
- Universitat Politècnica de Catalunya (UPC). BarcelonaTech. Barcelona, Spain
- University of Southampton, Southampton, Great Britain
- City University London, London, Great Britain

During the first three semesters of the programme, students study at two or three different universities depending on their track of study. In the fourth and final semester an MSc project and thesis has to be completed. The two-year CoMEM programme leads to a multiple set of officially recognized MSc diploma certificates. These will be issued by the universities that have been attended by the student. The transcripts issued with the MSc Diploma Certificate of each university include grades/marks and credits for each subject.

Information regarding the CoMEM programme can be obtained from the programme coordinator:

Øivind A. Arntsen, Dr.ing.
Associate Professor in Marine Civil Engineering
Department of Civil and Transport Engineering
NTNU Norway
Telephone: +4773594625 Cell: +4792650455 Fax: + 4773597021
Email: oivind.arntsen@ntnu.no
URL: https://www.ntnu.edu/studies/mscomem

Oh the heavy water, how it enfolds
The salt, the spray, the gorgeous undertow!

British Sea Power

SUMMARY

Low-lying tropical islands are highly vulnerable to the effects of sea-level rise and climate change. Most pressing is the threat posed to their fresh water supplies by wave-induced flooding. This thesis attempts to generalize previous site-specific studies of flooding on coral atolls and apply it in a framework that can be used for early warning systems or long-term climate change impact studies. To do so, a large synthetic database of representative reef properties and hydrodynamics was developed using the numerical wave model XBeach, and then analyzed using a Bayesian probabilistic network. The resulting tool allows us to make real-time flood predictions based on offshore wave or sea level conditions, and the unique characteristics of a given island (e.g. topography).

Narrow, smooth reefs with steep fore reef slopes are the most vulnerable to runup. Extreme flooding is associated with anomalously high, resonant low frequency waves, which are more likely to occur on narrow, smooth reefs subjected to extreme swell waves (large wave heights with long periods). These extreme swells are "blue sky" events which originate from distant storms. Thus, they may thus arrive with very little warning and time for response, since they are completely independent of local weather conditions. This bolsters the need for more effective prediction tools.

Validation of the results presented in this study is limited by the small number of field observations against which the model can be compared. Thus, there is a need to develop a comprehensive database of reef morphology and hydrodynamics. Offshore wave conditions, water levels, and reef width are the most essential variables for predicting runup, so future research efforts should be directed towards collecting those data.

This model can also be used to ask questions like, "which islands will be most severely impacted by climate change?", or "can we increase flood resilience for a given island by restoring its coral reefs?". Hence, there is also potential for its use in guiding decision-makers to allocate limited funding in the places where it will have the most impact.

CONTENTS

List of Figures

List of Tables

LIST OF SYMBOLS

Symbol	Units	Description
c_f	-	Coefficient of friction
D	s^{-1}	Dissipation parameter
$f_{m-1,0}$	Hz	Spectral mean wave frequency
$f_{n,0}$	Hz	0^{th} natural resonant wave frequency
f_p	Hz	Peak wave frequency
g	m/s^2	Gravity (9.81 m/s^2)
h_{reef}	m	Mean water depth across reef flat
h_b	m	Depth at wave breaking point
H_b	m	Wave height at breaking point
$H_{s,0}/L_0$	-	Incident wave steepness
$H_{s,0}$	m	Incident offshore significant wave height
$H_{s,SS}$	m	Significant wave height at sea-swell frequencies [0.04-1 Hz]
$H_{s,IG}$	m	Significant wave height at infragravity frequencies [0.004-0.04 Hz]
$H_{s,VLF}$	m	Significant wave height at very low frequencies [0.001-0.004 Hz]
k	1/m	Wave number ($2\pi/L$)
K_R	-	Wave reflection coefficient
L	m	Local wavelength
L_0	m	Deep water wavelength ($L_0 = gT^2/2\pi$)
$q_{OT,mean}$	l/s/m	Mean overtopping discharge
$R_{2\%}$	m	Wave runup at the 2% exceedance level
S_{SS}	m	Vertical swash at sea-swell frequencies [0.04-1 Hz]
S_{IG}	m	Vertical swash at infragravity frequencies [0.004-0.04 Hz]
$T_{m-1,0}$	s	Spectral mean wave period
T_p	s	Peak wave period
W_{reef}	m	Reef flat width
x_{reef}	m	Horizontal position on the reef flat
z_{beach}	m	Beach crest elevation above reef flat
β_b	-	Beach slope
β_f	-	Fore reef slope
γ	-	Ratio of wave height to local water depth (H/h)
γ_b	-	Wave breaking parameter (H_b/h_b)
$\gamma_{JONSWAP}$	-	JONSWAP spectral shape factor (peakedness)
δ	-	Dissipative:inertial timescale parameter
η_0	m	Offshore water level
$\eta_{2\%}$	m	Inner reef flat water level at the 2% exceedance level
$\eta_{initial}$	m	Initial water level at start of simulation
$\overline{\eta}$	m	Setup on reef flat

LIST OF ABBREVIATIONS

Abbreviation	Description
BLW	Bound Long Wave
BN	Bayesian Network
DRR	Disaster Risk Reduction
ENSO	El Niño-Southern Oscillation
EWS	Early Warning System
FWL	Fresh Water Lens
HF	High Frequency (> 0.04 Hz)
GIS	Geographical Information System
RMS	Root Mean Square
IG	Infragravity (0.004 < f < 0.04 Hz)
IPCC	Intergovernmental Panel on Climate Change
JONSWAP	Joint North Sea Wave Project
LF	Low Frequency (< 0.04 Hz)
LLR	Log-Likelihood Ratio
LLTI	Low-lying Tropical Islands
MDA	Maximum Dissimilarity Algorithm
MWL	Mean Water Level
NGO	Non-governmental Organization
NH	Non-hydrostatic
OT	Overtopping
RCP	Representative Concentration Pathway
RMI	Republic of the Marshall Islands
SB	Surf Beat
SIDS	Small Island Developing States
SLR	Sea Level Rise
SS	Sea-Swell (0.04 < f < 1 Hz)
SWL	Still Water Level
TK	Traditional Knowledge
USGS	United States Geological Survey
VLF	Very Low Frequency (< 0.004 Hz)

ACKNOWLEDGEMENTS

This thesis completes the Master of Science in Coastal & Maritime Engineering and Management (CoMEM) program carried out at Delft University of Technology, the Norwegian University of Science and Technology (NTNU), and the University of Southampton. Research for this project was primarily conducted at Deltares in Delft.

The past five months spent working on this thesis and the last two years of this program have flown by. It has been a challenging but ultimately very rewarding experience. I feel extraordinarily lucky to have had this opportunity to study in Europe, to meet so many great people, and to be working in a field that I find fun and endlessly fascinating.

I would first like to thank my committee for their contributions to this project. I would like to thank Ap van Dongeren for taking me on as a student in spite of my brief timeline and for encouraging my curiosity. You helped me to stay focused and were always quick to respond with useful feedback. To Ad Reniers, for chairing the committee, keeping me on track, and always asking insightful questions. Thank you to Marion Tissier for your enthusiasm, helpful feedback, and for encouraging me to think more critically about my model and waves. Thank you also to Kees den Heijer for your guidance on interpreting Bayesian networks.

At Deltares, I would like to say a special thank you to Robert McCall. I am really grateful for your patience, useful ideas, and cheerful attitude, especially when I was getting started out with XBeach. Thank you also to Maarten van Ormondt for your MATLAB wizardry and making 300,000 model runs somehow seem like an attainable goal. Thank you to Matthijs Gawehn and Ellen Quataert for their insightful discussions and for writing the reports that made me so excited about this topic in the first place. Thank you to Laurens Poelhekke for helping me navigate the perils of Bayesian networks and log-likelihood ratios. Thank you also to Lydia Cumiskey for organizing the young scientists' workshop on Disaster Risk Reduction and introducing me to the Sendai Framework. Lastly, I would like to thank my fellow interns for the many nice lunches and walks that we shared.

At TU Delft, I want to thank Gerbrant van Vledder for his insights into modelling swell on the Pacific, constructive feedback on my report, and for sharing with me the fascinating tradition of wave piloting. Thank you, too, to Wiebke Jäger for her advice on Bayesian networks.

I would like to acknowledge the support of the US Geological Survey (USGS) who funded this study through a Cooperative Agreement with Deltares. Thank you especially to Curt Storlazzi for your continual encouragement from afar, excellent advice, and for helping me to keep everything in perspective. To Nathaniel Plant, thank you for taking the time to meet with me and for your valuable advice on Bayesian networks and MATLAB.

In Southampton, I would like to thank Andreas Payo, Robert Nicholls, and Colin Woodroffe for their time and insightful advice on my research. Thank you to Dirk Spenneman for sharing his work on the history of the Marshall Islands.

I would like to acknowledge the support of the EACEA/EU and CoMEM Board in making it possible to study in Europe for two years. *Tusen takk* to Sonja Marie Ekrann Hammer and Øivind Arntsen for organizing the CoMEM program, and to Raed Lubbad for the opportunity to try my hand at permafrost research last summer.

I am extremely grateful to my former colleagues at Baird & Associates back in Canada. Thank you first to Mike Fullarton and Pete Zuzek for giving me a chance the first time we met in 2010. Thank you especially to Rob Nairn, Alex Brunton, and Mark Kolberg for their mentorship while I was working in Oakville and for their continued support after I left to start my MSc. Thanks also to Danker Kolijn for sharing his thesis database on reefs around the world and for taking an interest in my research. Thank you to everyone else at Baird who has supported me in my career and fueled my enthusiasm for coastal engineering.

To my fellow CoMEM students here at Deltares and TU Delft—Alejandra, Ana, Gerald, John, and Yahia—from Lofoten to Louisiana and Scotland to Scheveningen, our time together went well beyond the classroom. The preposterously long coffee breaks, post-NOC pizzas, Thanksgiving dinners (Canadian and American), beers on the canal, and library camaraderie brought joy to even the most challenging days. A special gracias goes out to Alejandra for keeping me sane and for keeping me away from the stroopwafels.

You have all broadened my horizons, and have taught me about much more than just coastal engineering. I will forever be grateful for the time that we spent together, and as we go our separate ways, I will really miss each of you. I hope that the friendships we have forged here will last for a lifetime, regardless of where we all end up. Thank you also to my other CoMEM classmates, Athul, Dennis, Ilija, Kyle, Said, and Thevaher. Although we didn't get to spend as much time together, you were also an important part of this journey.

Thank you to all my friends in Canada for keeping in touch while I've been away and for the fun trips back home. Your emails and skype chats never fail to brighten my day. Thank you to my family in UK, for making me feel welcome and like I had a small piece of home on this side of the Atlantic.

Most of all, I would like to thank Mom, Dad, Cameron, and Elizabeth. Running halfway around the world to follow your curiosity is a lot less scary when you have people rooting for you at home. Thank you for your perpetual love and support.

Stuart Grant Pearson
Delft, June 2016

1

INTRODUCTION

CHAPTER SUMMARY
Coral atolls and low-lying tropical islands are subject to frequent inundation and highly vulnerable to the effects of sea-level rise and climate change. However, before they drown, these islands may succumb to thirst. The threat of sea level rise looms large for atolls and other low-lying tropical islands, but far more pressing is the threat to their fresh water supplies posed by wave-induced flooding. The severity of this hazard is likely to increase due to climate change-induced sea level rise, modifications to wave climate, and coral reef degradation. In order to better understand and predict wave-induced flooding of atolls, this study investigates the processes influencing runup and overtopping using numerical and probabilistic models.

1

1.1. MOTIVATION

This study is motivated by the looming freshwater security and safety crisis that faces low-lying tropical islands. These islands are currently vulnerable to the effects of wave-induced flooding, but may become even more exposed under climate change. The threat to low-lying tropical islands has been formally recognized by the Sendai Framework for Disaster Risk Reduction (DRR), which identifies the need for improved early-warning systems (EWS) to mitigate flood risk (UNISDR, 2015, 18(g),42).

CURRENT VULNERABILITY

Coastal flooding affects communities around the world, from New York City to remote Arctic villages. Among the most vulnerable are low-lying tropical islands. Many of these islands belong to Small Island Developing States (SIDS), a group of over 50 countries with unique socioeconomic and environmental vulnerabilities UN-OHRLLS (2015). Even though some small islands may have more elevated areas, population and critical infrastructure may be concentrated located close to sea level. In the case of Kiribati, Tuvalu, the Maldives, and the Marshall Islands, over 90% of their population and land area are located within 5 m of mean sea level (Figure 1.1). The vulnerability of SIDS to natural hazards is enhanced by their small physical size, relative isolation, and often limited resources Meheux et al. (2007).

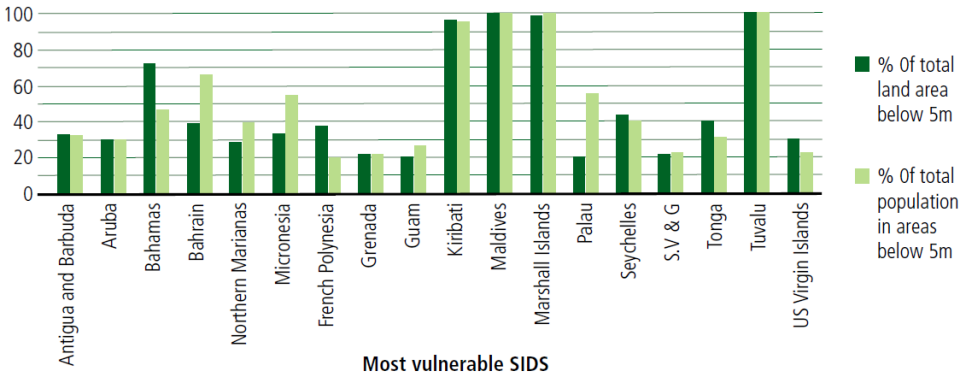

Figure 1.1: Percentage of total land area and population located within 5 m of mean sea level in Small Island Developing States (SIDS) (UN-Habitat, 2015).

Many of these islands are atolls, surrounded by and composed of coral. In addition to their intrinsic ecological value, coral reefs also provide a natural form of flood defense by dissipating waves that might otherwise inundate low-lying islands Ferrario et al. (2014). Nevertheless, reefs do not guarantee complete protection from the sea. Under extreme conditions, flooding may cause loss of life, economic damage, and contaminate drinking water supplies. Throughout recorded history and to this day, tropical cyclones (hurricanes or typhoons) have wreaked havoc on low-lying islands, causing widespread devastation to people, property, and infrastructure (Roeber and Bricker, 2015; Spennemann, 2004).

However, a direct hit by tropical cyclones is not necessary to generate devastating waves. Indeed, cyclones seldom form at the equator[1], sparing many equatorial islands the brunt of their impact. Unsheltered by continents, many atolls are directly exposed to large tracts of open ocean. Waves generated by storms in mid-high latitudes can thus travel unimpeded for thousands of kilometers to reach the islands. These swell waves tend to be smaller than those generated by cyclones, but if they coincide with higher tides or sea level anomalies, widespread inundation may occur (Hoeke et al., 2013). Furthermore, such waves may strike completely independently of the local weather, providing little warning and catching residents unprepared ("sunny day flooding").

In December 2008, two storms located in the North Pacific generated powerful swell waves which propagated south towards the western tropical Pacific and inundated numerous low-lying islands. Even though the swell was generated more than 3800 km from the island of Nukutoa in Papua New Guinea, the waves were sufficiently large to flood the island (Smithers and Hoeke, 2014). At the time of the flood, the island experienced clear skies and calm winds, highlighting the independence of swell wave-induced flooding from local weather conditions. The event ultimately submerged almost 50% of Nukutoa over a period of 4 days, a striking example of the threat posed by remotely-generated swell on atolls in otherwise low-energy environments.

Human development on atolls is most rapidly increasing on urbanized islands (e.g. Majuro in the Marshall Islands), with rapid population growth, widespread land reclamation, and the construction of “hard” coastal protection measures like seawalls and groynes (McLean and Kench, 2015). This urbanization has exacerbated flooding problems, both through human modifications to the islands and also through increased development in more vulnerable, low-lying areas McLean and Kench (2015). In contrast, Spennemann (1996) discusses how traditional indigenous settlement patterns were less vulnerable by settling in sheltered areas less prone to flooding.

Human modification of the coast may also have adverse effects on flood risk. Smithers and Hoeke (2014) observed decreased runup and damage areas protected by a seawall, although they remark that such “hard” interventions limit the ability of islands to morphodynamically adjust in a natural manner. The effect of shore protection structures on flooding of atolls is not well-documented. Payo and Muñoz Pérez (2013) caution that the excavation of pits in reef flats (to obtain aggregate for construction) (Ford et al., 2013) may increase the wave energy reaching shore and thus worsen flood risk.

The other factor that makes atolls uniquely vulnerable is the susceptibility of their fresh water supplies to salinization and drought. Potable water on coral atolls is obtained either through directly capturing rainwater, or more commonly from thin aquifers known as freshwater lenses (FWLs) (Chui and Terry, 2013). These lenses are recharged by rainwater and float within the atolls’ porous rock atop denser seawater. Freshwater lenses on atolls can be degraded by a number of natural processes including the physical erosion of an island, meteorological drought, and salinization due to overtopping by waves, or by anthropogenic influences like excessive groundwater pumping (Terry and Falkland, 2010). The recovery time of freshwater lenses depends on both the climate

[1] The Coriolis parameter (which governs the formation of coherent cyclonic vortices) is equal to zero at the equator. Hence, cyclones are generated more frequently 5° north or south of the equator (Barry and Chorley, 2004).

during the flooding event but also on the recharge of groundwater in the months that follow. For example, heavy rainfall in the wake of the incident may mitigate the salinization and increase the rate of aquifer recovery, but droughts may exacerbate the problem (Terry and Falkland, 2010).

Wave-induced flooding threatens freshwater security by increasing the salinity in FWLs to intolerable levels. As seawater overwashes an island, it seeps down through the surface to the FWL, or ponds in freshwater swamps and depressions (Figure 1.2).

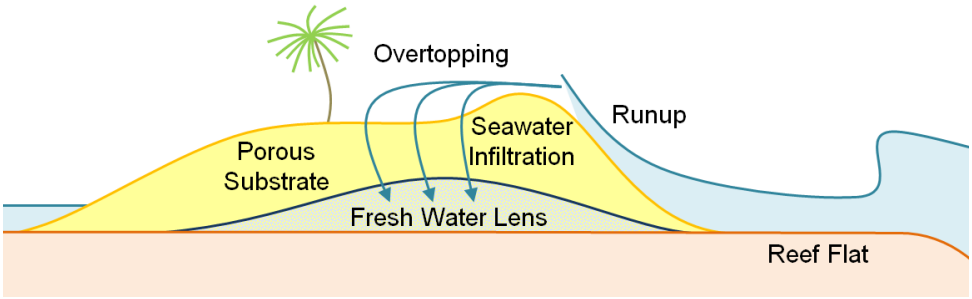

Figure 1.2: Schematic cross-section of an atoll depicting infiltration of the freshwater lens by wave-induced flooding.

Figure 1.3 demonstrates the influence of wave-induced flooding on the fresh water reserves of an atoll. When flood occurs, supplies are reduced by salinization. The magnitude of this reduction depends on both the hydrodynamic forcing (offshore wave and water level conditions) and morphology of the given island (which will determine the characteristics of the flooding). The aquifer then gradually recovers at a rate depending on recharge by rainfall. The frequency between events and subsequent rate of recovery may be influenced by climate change. Improved capabilities for estimating the magnitude of flooding can thus be used to make projections about future water scarcity and help decision-makers plan accordingly.

Desalination or importing freshwater are prohibitively expensive solutions (White et al., 2007). Hence, it is important to quantify the impact of wave-induced flooding and salinization to better understand and manage the risks to freshwater security on atolls.

CLIMATE CHANGE IMPACTS

Current threats may be compounded even further by the projected impacts of climate change. Coral atolls will be particular susceptible to changes in sea level, wave climate, and reef health. There are numerous factors which may govern an atoll's response to climate change, including location in the ocean, exposure to different wind and wave forcing, sediment characteristics, island topography and reef geometry (McLean and Kench, 2015).

Sea Level Rise

Church et al. (2006) project that rapid sea level rise in the tropical Pacific Ocean will seriously threaten island residents in the coming century. However, atolls have a certain degree of natural resilience to changes in sea level. Coral reefs naturally grow vertically,

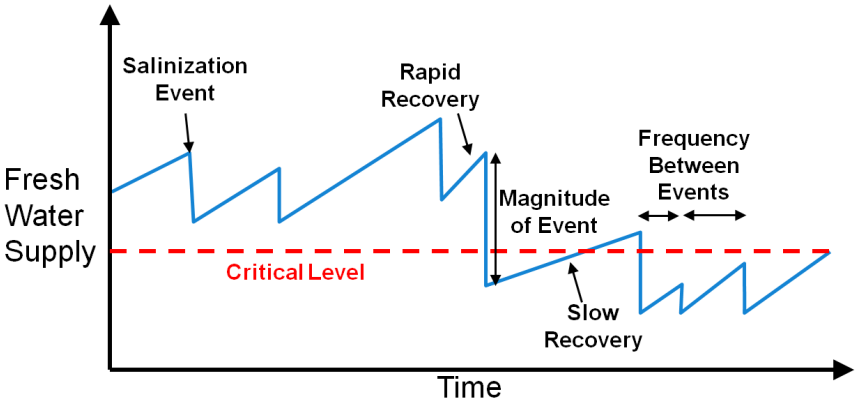

Figure 1.3: Conceptual diagram illustrating the relationship between wave-induced flood events and fresh water supplies on atolls.

and in many cases 'catch up' or 'keep up' with sea level rise (Woodroffe, 2008). However if the rate of sea level rise far outpaces the rate of vertical reef accretion, the reef 'gives up' and becomes completely submerged. Similarly, if threats to reef health reduce the rate of growth, they may also fail to keep pace with rising seas.

However, sea level rise brings not only the danger of permanent submergence, but also compounds the impact of waves. The relative increase in depth over reefs will reduce the amount of wave breaking and frictional dissipation, allowing larger waves to reach the shoreline, and thereby increasing the risk of flooding Storlazzi, Elias and Berkowitz (2015).

Wave Climate

Furthermore, the wave climate itself may be modified by climate change. Shope et al. (2015) project a decrease in extreme offshore wave heights at tropical Pacific islands, although this may be countered by the aforementioned synergy between sea level rise and nearshore wave heights. Walsh et al. (2012) project an increase in intensity but decrease in frequency of cyclones in the south Pacific, making it difficult to quantify the precise net effect of climate change on storm wave generation. Regional climate changes may shift areas of storm generation, and in doing so may alter the mean wave direction of waves at atolls (Shope et al., 2015). Previously unexposed stretches of coastline may then be subjected to increased wave forcing and shift to reach new morphological equilibria.

Reef Health

Healthy coral makes the surface of reefs hydrodynamically rough, which attenuates wave energy. Damage to coral caused by bleaching (from increased sea temperatures) and ocean acidification may effectively reduce this roughness and leave atolls more vulnerable to wave impacts (Hoegh-Guldberg et al., 2007) suggest that reduced rates of reef accretion and increased damage to coral ecosystems may increase the vulnerability of reef-lined coasts to storm and sea level rise impacts.

Morphological Response

The response of these islands to climate change varies considerably as a result of their diverse morphology, local climates, and human interventions. Atolls unconstrained by human development tend toward a dynamic equilibrium and may morphologically adjust in response to changes in forcing (McLean and Kench, 2015). Erosion on one side of an atoll due may be compensated by accretion on the opposite side. However, urbanized atolls or those with heavily modified shorelines may be have less flexibility in response to changes imposed on them. Although some atolls have been able to adjust to changes in forcing, recent monitoring has revealed the disappearance of several islands below the waves (Albert et al., 2016). Counterintuitively, Shope et al. (2015) suggest that a decrease in average wave heights may actually reduce the ability of islands to respond to sea level rise. This is because vertical accretion of atolls is driven in part by the constructive forces of large waves. Hence, a complicated suite of factors determines a given island's resilience to erosion, making it a challenge to predict potential impacts.

Implications

Flooding threatens the immediate safety of island residents, and may cause direct economic consequences in the form of damage to property and infrastructure. However, floods may also lead to indirect economic damages, long-term disruption to freshwater supplies, and ultimately the forced migration of residents (UN-OHRLLS, 2015). Hoeke et al. (2013) argue that the habitability of many Pacific islands will be more likely governed by increases in frequency and intensity of wave-driven flooding events than gradual sea level rise. As of this writing, the Marshall Islands are in the throes of a record drought, having received less than a quarter of their expected rainfall in winter 2015-2016 (Milman, 2016). Dwindling freshwater supplies leave them even more vulnerable to salinization by wave-induced flooding.

McLean and Kench (2015) assert that in spite of the common perception that Pacific atolls will disappear by the end of the next century, geomorphological trends make it likely that most islands will still remain in 100 years' time, even under IPCC AR5 sea level rise projections. However, the disruption of freshwater supplies by wave-induced flooding could make these long term predictions a moot point: the islands may physically remain but be rendered incapable of supporting human habitation. While the threat of permanent inundation may take over a century to materialize, the viability of life on these islands may cease on a much shorter timescale (Chui and Terry, 2013; Storlazzi, Elias and Berkowitz, 2015). Given the major social and economic costs that such a scenario would entail, it is vital that we improve our predictive skill for wave-driven flooding events.

SENDAI FRAMEWORK FOR DISASTER RISK REDUCTION

In light of the heavy costs to society posed by disasters of all kinds, the Sendai Framework for Disaster Risk Reduction was adopted by the United Nations (UNISDR, 2015). The framework sets out to reduce mortality and displacement of people, economic losses, damage to infrastructure, and interruption of key services. The framework specifically recognizes the threat experienced by SIDS:

> *Disasters can disproportionately affect small island developing states, owing to their unique and particular vulnerabilities. The effects of disasters, some of which have increased in intensity and have been exacerbated by climate change, impede their progress towards sustainable development (UNISDR, 2015, 42).*

Hence, it is imperative that effective tools be developed specifically to help small island developing states deal with the challenges facing them. Although there are numerous strategies proposed to mitigate disaster risk, most relevant for this study is a call to:

> *Substantially increase the availability of and access to multi-hazard early warning systems and disaster risk information and assessments to the people by 2030 (UNISDR, 2015, 18(g)).*

Although there are many components necessary for an effective early warning system: data, real-time monitoring, legal frameworks, communication networks, and response plans. This study aims to respond specifically to the need for a rapid flood forecasting system that is capable of generalizing to regional scales processes that are inherently site-specific.

Main motivation for research:

- Low-lying tropical islands are vulnerable to wave-induced flooding.
- Climate change is expected to increase their vulnerability.
- There is a recognized need for early flood warning systems in support of Small Island Developing States.

1.2. RESEARCH SIGNIFICANCE

This thesis offers a novel contribution to the existing body of research on reef hydrodynamics by generalizing the findings of previous site-specific studies and proposing new methods to predict wave-induced flooding on low-lying tropical islands.

1.2.1. CURRENT STATE OF RESEARCH

The work presented in this thesis builds on recent field and numerical modelling studies that investigated wave transformation on coral atolls in detail (Beetham et al., 2015; Cheriton et al., 2016; Gawehn, 2015; Merrifield et al., 2014; Péquignet et al., 2009; Quataert et al., 2015; van Dongeren et al., 2013). We attempt to generalize their findings and apply them on a larger scale for operational forecasting and climate change impact assessment.

Bayesian networks have become increasingly popular tools for modelling coastal environments, including as early flood warning systems (Balbi et al., 2015; Poelhekke, 2015). This study takes many of the analysis techniques used previously in storm impact (den Heijer et al., 2012; Jäger, den Heijer, Bolle and Hanea, 2015; van Verseveld et al.,

2015) and geomorphological studies (Gutierrez et al., 2015), and applies them to a coral reef setting.

Hence, to fulfill our study objectives, we require a synthesis of the latest research on reef hydrodynamics together with Bayesian network modelling techniques. We also build on recent work examining the potential of reefs as nature-based flood defenses (Ferrario et al., 2014; Narayan et al., 2016), climate change impact assessments Shope et al. (2015), and a study linking the traditional knowledge of indigenous Marshall Islanders with state-of-the-art wave modelling techniques (van Vledder, 2015).

1.2.2. IDENTIFIED KNOWLEDGE GAPS

Although studies to date have revealed much about the physical processes acting on specific sites, the tremendous diversity of atoll characteristics and huge geographical scales of atolls require a more generalized approach. Compared to sandy coastlines, coral reefs have received comparatively little attention in coastal engineering, and much is still unknown about the important processes there. As discussed in Section 1.1, there is a recognized need to improve real-time flood forecasting capabilities for low-lying islands. Furthermore, there is an interest in better understanding long-term impacts to coral atolls under different climate change scenarios, so new tools are necessary to account for both the complexity of the processes and the uncertainties inherent in climate change.

Generalized Reef Hydrodynamics

Smithers and Hoeke (2014) identify the improved understanding of coral atoll flooding due to extreme swells as a key research priority, citing limited observations, complex physical processes, and the dire implications for habitability. They recommend a probabilistic investigation of both hydrodynamic forcing (waves, water levels) and variations in reef morphology to determine how frequently the critical conditions for flooding will be exceeded. Hoeke et al. (2013) note that the challenges of predicting wave-driven flooding on atolls stem from highly site-specific interactions between offshore forcing and local reef morphology. In order to make valid predictions for individual locations, more light must first be shed on the general principles involved.

Early Flood Warning Systems (EWS)

The current forecast system for wave-induced flooding on Fiji uses only offshore wave height as a warning threshold, without considering water level or the complex interactions of waves with the reef (Bosserelle et al., 2015). Bosserelle et al. (2015) suggest that prediction of wave-induced flooding should account not just for offshore wave height, but also wave period, water level, wave groupiness, and reef characteristics. They also advocate for the use of a large number of model simulations to test a wide range of possible hydrodynamic conditions and reef morphologies. In light of the limited available field and laboratory data, numerical models provide the next best possible means to improve predictive capabilities and further elucidate the interactions between all of the relevant processes.

Bayesian networks are an attractive solution for the development of early flood warning systems, given their fast computational times, ability to incorporate diverse types of data, and inclusion of uncertainty. Although they have been applied for ecological pur-

poses in coral reef settings (Ban et al., 2015; Franco et al., 2016) and as EWS on sandy coastlines (Poelhekke, 2015), Bayesian networks are as yet untested for flood forecasting on atolls and low-lying tropical islands.

Climate Change Impact Assessments
Storlazzi, Shope, Erikson, Hegermiller and Barnard (2015) conduct a thorough study of potential changes to tropical Pacific wave climates under a range of future climate change scenarios. To estimate the potential impacts to atolls, they use Stockdon et al. (2006) to calculate runup. The methods discussed in this thesis could be used to provide a more precise estimate of how flood risk will change for low-lying tropical islands in the decades to come. For Funafuti Atoll in Tuvalu, Beetham et al. (2015) found that waves can impact the shore for significantly greater periods of time when the combined influence of high frequency waves, low frequency waves, and wave setup are accounted for, than when only mean water level is considered. Hence, a static approach to sea level rise impact assessment is insufficient (Cheriton et al., 2016), creating a need for models that predict the combined influence of waves and sea level changes.

Nature-based Flood Defenses
Recently, the value of coral reefs as nature-based flood defenses has been recognized (Ferrario et al., 2014; Narayan et al., 2016). This thesis provides a large synthetic database with reefs of varying characteristics which can be used to assess the effectiveness of different reefs at attenuating wave-induced floods. Such results can then be used to make more informed decisions about reef conservation or restoration projects.

1.2.3. FILLING KNOWLEDGE GAPS

We seek to improve the general understanding of coral processes by offering a virtual laboratory for testing alternative reef configurations and the relative influence of different parameters. This study effectively builds on the sensitivity analysis of Quataert et al. (2015). Given the relative scarcity of field measurements on fringing coral reefs and atolls, the modelling approach used here provides a valuable opportunity to experiment with a wide range of hypothetical scenarios and idealized versions of real reefs. By pre-computing a large number of different numerical model scenarios, a Bayesian network can be used to prepare real-time flood predictions. This study provides a proof-of-concept for the use of Bayesian networks as an early warning system for low-lying tropical islands.

To forecast the long-term fresh water security of atolls under projected climate change scenarios, it is important to understand how both the frequency and intensity of salinization events, as well as the system's resilience to recover. Global climate models can predict long-term rainfall, ENSO trends, and sea level rise, while regional wave models can be used to predict future wave climates. At the other side of the problem, groundwater models can be used to understand infiltration rates and aquifer recovery times. This informs our modelling approach for this study, since we need to bridge the gap between forecasting the metocean conditions and being able to predict infiltration into the freshwater lenses.

Ideally, the work presented in this thesis may contribute to more informed and ef-

fective policy and decision-making with regards to disaster risk reduction for low-lying tropical islands.

1.3. SCOPE AND RESEARCH OBJECTIVES

This section outlines the primary scope and research objectives of the thesis.

1.3.1. RESEARCH QUESTIONS

Predicting floods is a complex and uncertain science even in well-studied environments like sandy coastlines. Predicting them on low-lying tropical islands is complicated even further by wide variations in reef morphology and hydrodynamic forcing, as well as a paucity of relevant field observations. In order to refine these predictive capabilities, this thesis focuses on several key research questions:

Main Question:

How can we give estimates of flooding and runup on low-lying tropical islands, knowing only little or very approximate information about the geomorphic system or hydraulic boundary conditions?

Sub-Questions:

1. What are the most important processes that drive flooding on low-lying tropical islands?
2. Can we reproduce these processes using a detailed process-based numerical model (XBeach) together with a probabilistic (Bayesian network) model?
3. How can these tools be applied in an early warning system or to assess the impact of climate change?

In the process of answering these questions, we hope to bridge the gap between the existing body of reef hydrodynamics research and the practical implementation of an early warning system for flooding on tropical islands.

1.3.2. RESEARCH APPROACH

In order to answer those questions, five key research objectives have been set:

1. To understand the sensitivity of wave runup and overtopping to changes in reef properties and hydrodynamic forcing.
2. To develop a synthetic reef hydrodynamics database using a process-based numerical model (XBeach).
3. To develop a probabilistic Bayesian network for flood prediction using this

database.

4. To validate this prediction system using field observations from the literature.
5. To prepare a plan for the practical application of the system.

The following tasks will be carried out to meet the above research objectives:

i **Define key parameters that determine wave-induced flooding**
- Identify key processes to include in hydrodynamic and probabilistic models
- Establish range of parameter values using literature, field data, and previous model results

ii **Develop synthetic dataset using hydrodynamic model**
- Develop hydrodynamic numerical model using XBeach
- Test sensitivity and performance of idealized reef model
- Carry out multiple (O(100,000)) model simulations

iii **Cast the results in a Bayesian Network**
- Develop and test Bayesian network model in Netica
- Analyze probabilistic relationships and dependencies between key variables
- Optimize network structure for improved predictive capabilities

iv **Verification of the models**
- Validate predictive skill of Bayesian network using standard tests
- Find similar sites in literature against which to validate
- Identify and explain discrepancies between models and field observations

v **Explore future applicability**
- Propose plan for implementation in an early warning system
- Propose plan for climate change impact assessments
- Identify unresolved questions and propose next steps to solve them
- Identify opportunities for collaboration with local community partners

1.3.3. SCOPE LIMITATIONS

There are several key limitations to the scope of this study:

- **Idealized 1D Profile**
  Only a one-dimensional cross-shore reef profile is considered, for reasons of simplicity, data availability, and computational expense. The profiles are also idealized with planar fore reef and beach slopes, and a horizontal reef flat. The complex spatial variations in reef topography and roughness could not be captured in this simplified approach; nor could two-dimensional processes like alongshore currents, refraction, diffraction, or edge waves. However, it should be noted that refraction generally does not occur at large scales on atolls because of their steep sides and narrow reef flats.

Longshore variations in the shoreline, such as the narrowing of an inter-island passage on Takuu Atoll, may serve to amplify wave heights or setup (Smithers and Hoeke, 2014). In their study of Palmyra Atoll, Rogers et al. (2015) found that refraction of waves along reef flats due to varying bathymetry resulted in wave focusing at certain points. Conversely, Beetham et al. (2015) suggest that the overprediction of infragravity wave period in their 1D model may be the result of excluding longshore processes such as refraction and edge waves.

LF waves may become trapped in the nearshore depending on their frequency and angle of incidence, forming edge waves. However, for their study of Ningaloo Reef in Australia, van Dongeren et al. (2013) found that infragravity wave energy tended to be concentrated mostly in the leaky region, indicating seaward propagation rather than coastal trapping.

- **Discrete Input Parameter Distributions**
  Discrete, uniform input parameter distributions were used in the XBeach model, so there may be gaps in the range of applicability. For instance, resonant low-frequency waves can cause severe flooding (Roeber and Bricker, 2015), but require a very specific combination of reef geometry and offshore hydrodynamic forcing to occur. Although we simulated approximately 100,000 unique permutations, it is still possible that certain key combinations were missed. Furthermore, Bayesian networks cannot extrapolate beyond the parameter space in which they were constructed.

- **Limited Field Data for Validation**
  There is limited runup or wave overtopping data available to validate the model results. This is due partly to the challenges of measuring runup in the field, but also due to the relatively limited number of field studies on this topic in the literature.

- **Tropical Cyclone-Generated Waves Not Considered**
  Only remotely-generated swell waves are considered, not the large waves locally generated in tropical cyclones. This study is more concerned with flooding due to swell wave impacts for several reasons. Many islands near the equator lie outside the direct path of tropical cyclones but are still exposed to swell waves from multiple distant sources. There are also certain marginal cases in which milder forcing can lead to disproportionately high flooding (such as via resonance).

  Although smaller in magnitude, extreme swell events are expected to occur more frequently than tropical cyclones. Of most concern are events that are large enough to contaminate aquifers, but also happen regularly enough that the aquifers do not have sufficient time to recover. Hoeke et al. (2013) estimate that the major flooding event of December 2008 had a return period of less than 3 years for many islands. More than 1.5 years may be required to fully recharge a salinized freshwater lens to its pre-storm, drinkable condition (Chui and Terry, 2013).

If changes to wave climate or sea level increase the frequency of these events, they may present a more immediate threat. Cyclones that directly hit islands may cause more damage but happen less frequently than smaller-magnitude swell events. Hence, an event with smaller consequences but higher chance of occurring (e.g. swell-induced floods) may pose just as great a risk as low-probability, high-consequence events like cyclones.

Furthermore, since remotely-generated swell waves are independent of local weather conditions, there may be little advance warning of their onset ("sunny day flooding"). Hence, communities on these tropical islands may have insufficient time for evacuation or other precautionary measures. This justifies the need for an early warning system capable of detecting and analyzing the threat posed by such waves.

1.4. THESIS OUTLINE

Chapter 1 outlines the motivation and general approach for this study, and Chapter 2 provides a summary of the concepts and background information relevant to predicting flooding on coral atolls. Chapter 3 reviews the methodology used to predict flooding, and Chapter 4 presents the results of the study. Chapter 5 features a discussion of the findings and Chapter 6 summarizes the main conclusions and provides recommendations for future studies. The appendices include details about model setup and testing (A-C), as well as more detailed model results and analysis (D-G). Appendix H provides a brief overview of nautical navigation by wave piloting in the Marshall Islands and its relation to the present study.

2

BACKGROUND

CHAPTER SUMMARY

The following section provides the background information necessary to understand and predict flooding of low-lying tropical islands. Section 2.1 begins with an overview of coral reefs and atolls, identifying the unique characteristics which differentiate them from other types of coastline. We then consider the environmental forcing factors to which coral atolls are exposed, such as waves or changes in sea level (Section 2.2). Reef hydrodynamics, which concern the interaction of this external forcing with coral reefs, are treated in Section 2.3. Finally, we discuss the prediction of runup, overtopping, and inundation on atolls (Section 2.4). In doing so, we attempt to identify if there are consistent relationships between certain reef characteristics and hydrodynamic responses, and whether particular islands are more vulnerable or resilient to wave-induced flooding.

2.1. CORAL ATOLLS

Atolls are low-lying tropical islands formed from emerged coral reefs. Coral reefs are calcium carbonate structures created by small marine organisms. The skeletons of the coral accumulate over time and become cemented together into large formations. They are mainly found in tropical regions within 30° of the equator (Figure 2.1). They are of special interest to coastal engineers because of the unique properties and processes associated with them, but also because of their vulnerability to the effects of climate change.

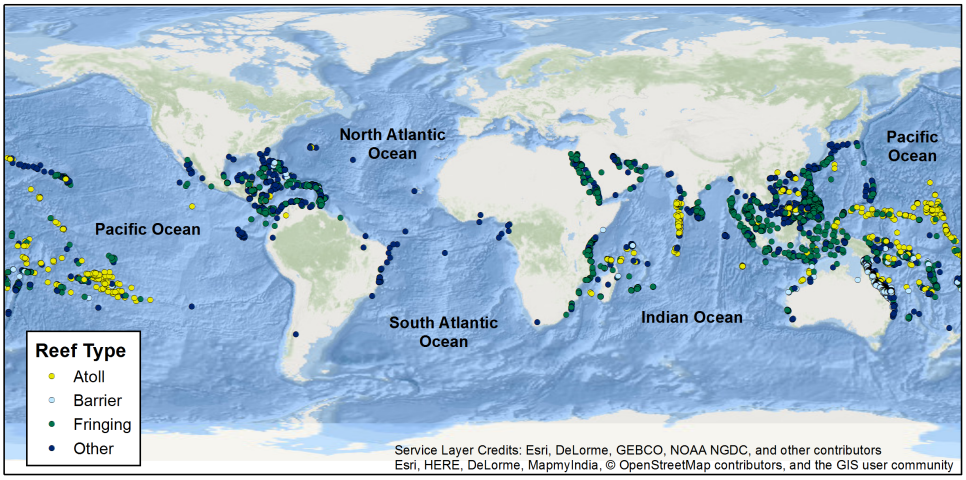

Figure 2.1: Locations of atolls, fringing, and barrier reefs around the world. Data source: (UNEP-WCMC, 2016).

Key differences between reefs and sandy coasts are the steep fore reef slope, a considerably rougher bed, and a wide platform (or lagoon) separating the breakpoint of waves from the shore (van Dongeren et al., 2013). In that regard, they have much in common with the rocky shore platforms often found on cliffed coastlines Beetham and Kench (2011). However, unlike rocky shore platforms, reefs are composed of living organisms, and hence have unique ecological dependencies. Changes to the health of the reef may have a direct feedback on its morphology (Baldock et al., 2014). The unique characteristics of coral reefs influence the hydrodynamics such that many of the usual assumptions used in coastal engineering for planar beaches do not necessarily hold true. As such, we need a better understanding of reef morphology to predict flooding.

Coral reefs can be classified by their geomorphology into three main categories: barrier, fringing, and atoll (Figure 2.2). Fringing reefs abut the coastline, whereas barrier reefs are separated from shore by a large lagoon. Atolls are ring-shaped chains of islands surrounding a lagoon, usually isolated from the mainland.

This thesis focuses primarily on atolls and fringing reefs rather than barrier reefs due to major hydrodynamic differences between them, and the shoreline protection that the former affords. Depth-limited wave breaking at the reef edge induces a high radiation stress gradient, which results in wave setup. On barrier reefs, this wave setup is partly offset by flow over the reef, although on fringing reefs the shore provides a fixed bound-

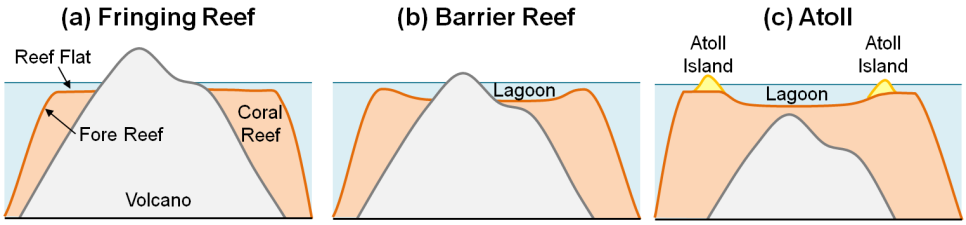

Figure 2.2: Different types of coral reefs: (a) Fringing, (b) Barrier, and (c) Atoll. Of particular interest to this project are fringing reefs and the reefs that form around the outer edge of atolls. Adapted from Woodroffe (2002).

ary and thus increases the water setup (Young, 1989). Hence the potential for flooding on land shoreward of fringing reefs or atolls is greater than on barrier reefs.

ATOLL EVOLUTION

Many low-lying tropical islands are volcanic in origin. Fringing reefs often encircle volcanic islands, and atolls tend to form as reefs built on top of eroded or subsided volcanoes Woodroffe (2002). Atolls are largely composed of unconsolidated sand and rubble originating from the adjacent coral reefs (McLean and Kench, 2015). It is within this porous material that the freshwater lenses used by inhabitants for drinking water form.

Morphological change of coral atolls is driven by extreme events (e.g. tsunamis or storms) as well as more gradual processes associated with climate change (Ford and Kench, 2015). Storms can be destructive, causing erosion of shorelines, or even constructive, transporting material from adjacent reefs to build up the island. Being subjected to different external forcing from all directions, atolls may have considerable morphological variation even on a single island (McLean and Kench, 2015).

McLean and Kench (2015) examined the vulnerability of 244 atolls in the tropical Pacific to erosion hazards. They found that erosion can be temporary or offset by accretion elsewhere. In many cases, long term trends in morphodynamic evolution may be obscured by interannual and decadal sea level variations interspersed by large storm events. Although the islands have generally persisted through recent sea level rise, they are highly dynamic systems and may still experience large spatial and temporal fluctuations in morphology. However, Albert et al. (2016) identified several atolls in the Solomon Islands which have disappeared due to erosion and permanent submergence. The differences between their findings and those of McLean and Kench (2015) underscore the challenge of predicting the geomorphological response of atolls to climate change on such large spatial and temporal scales.

The same swell generated by remote, mid-latitude storms will often reach both equatorial atolls and those located in storm belts. However, islands frequently subjected to cyclones will tend to be more robust against swell-induced floods due to island-building by onshore transport of material from adjacent reefs during the large storms (Smithers and Hoeke, 2014). Smithers and Hoeke (2014) posit that equatorial atolls not exposed to the direct impact of tropical cyclones may be less resilient to extreme swell generated by distant storms.

2.1.1. ISLAND & REEF MORPHOLOGY

Four main morphological features are of interest in predicting wave-induced flooding on reef-fronted coastlines: the fore reef, reef flat, beach, and hinterland.

FORE REEF

Waves first begin to transform from their offshore state as they travel up the fore reef towards the crest, making its slope an important variable to include in the model. Atolls are typically found at deep mid-ocean locations, so they lack the broad, gradually sloping continental shelf associated with many coastal settings. The fore reef thus typically marks an abrupt change in bathymetry, steeply rising from the deep ocean up to the reef flat. Fore reefs often feature spur and groove formations, which are shore-normal ridges and troughs that form in environments with high wave energy (Rogers et al., 2013).

Fore reef morphology depends on its sea level history, karstification and cementation, biological construction and erosion processes, and collapses or slides from major storms, tsunamis, and earthquakes (Cabioch, 2011). Duce et al. (2016) found that upper reef slopes tend to be wider and more gradual with highly developed spur and groove systems in places with higher wave exposure. They also found that windward fore reefs were wider with more gradual slopes. These trends could be used to estimate likely fore reef geometry of a given island for flood forecasting in the absence of measured data.

REEF FLAT

The reef flat is a wide platform extending from the reef crest to the shore, covered in coral, rubble, sand and algae Thornborough and Davies (2011). Typical reefs range from 40 to 2000 m in width (Kolijn, 2014; Quataert et al., 2015). The morphology of reef flats is largely dependent on the type of forcing to which they are subjected (Figure 2.3).

Reef flats are sometimes exposed at high tide, but it depends on the width of the reef flat and the relative tidal range. In some cases, the reef crest rises above the mean elevation of the reef flat, resulting in ponding at low tide (Brander et al., 2004). Locally wind-generated short waves ($T < 3$ s) thus tend to dominate ponded reef flats at during lower tidal levels, since longer period waves from offshore are effectively blocked.

Variations in reef topography exert a major influence on wave transformation across the reef flat (Brander et al., 2004). Péquignet et al. (2011) found that wave height at the shoreline is inversely proportional to reef flat width, although wave setup seems to be independent of it. Field observations of wave runup and damage during Typhoon Haiyan demonstrate a clear relationship between reef width, dominant wave period, and flooding (Gunasekara et al., 2014; Shimozono et al., 2015).

BEACH CHARACTERISTICS

After waves have propagated across the reef flat, they usually arrive at a beach and then run up the slope. Hence, the characteristics of that beach may in part govern the extent of runup and flooding.

The sensitivity of runup to beach slope on reef-fronted coasts has not been studied extensively, and there were few available measurements to serve as input for this thesis. Nevertheless, it is well-established that runup is strongly influenced by beach slope on sandy coastlines (Stockdon et al. (2006)), so it was an essential parameter to include in

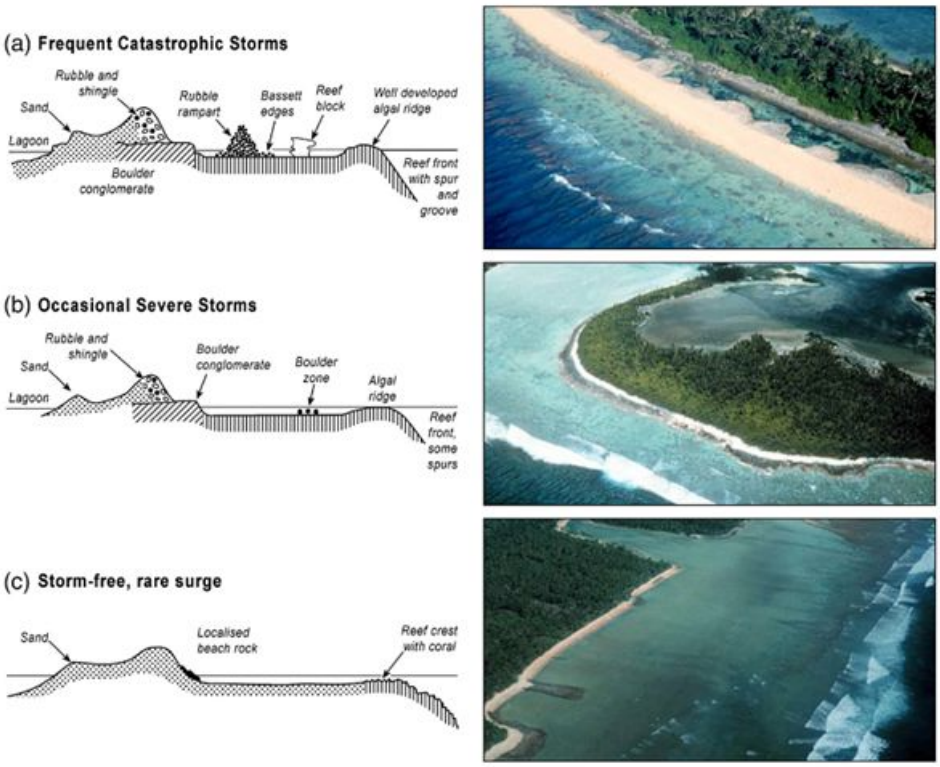

Figure 2.3: Characteristic reef flat morphology based on typical hydrodynamic forcing. Reefs frequented by large storms or cyclones are characterized by large rubble and boulder deposits with well-developed algal ridges, plus spur and groove systems on the fore reef (a). Those with only occasional exposure to major storms will tend to have a mix of sand, rubble, and shingle (b), while atolls in quiescent areas are sandier with more developed coral at the reef crest. Source: Woodroffe (2008)

this model. Wright and Short (1984) classify beaches into reflective ($\tan\beta_{beach} = 1/10 - 1/6.7$) and dissipative ($\tan\beta_{beach} = 1/100 - 1/50$) regimes. Since the majority of sea-swell wave energy is dissipated across the reef flats rather than on the beach face, most reef-fronted beaches would be classified as reflective or intermediate.

Beach sediment is typically calcium carbonate-based, originating from the coral sources on the reef and transported ashore Kench (2011). Beetham et al. (2015) suggest that beach percolation and porosity may also play a role in attenuating wave runup. These factors were not considered in the present study.

ISLAND ELEVATIONS

The extent of hinterland flooding will be governed by the minimum height of the beach crest. The highest points on atolls are typically wave-built ridges of deposited sediment, which may serve to protect the interior of islands from inundation (Smithers and Hoeke, 2014). The height of these ridges is highly dependent on sediment supply from the adjacent reef and average incident wave energy (Figure 2.3).

Table 2.1 lists the percentage of land above certain elevations on several atolls throughout the Indian and Pacific Oceans. For example, it can be inferred from this table that 99% of the Maldives are less than 3 m above sea level. The low elevations make these islands extremely susceptible to flooding.

Table 2.1: Proportion of reef islands at elevations above mean sea level (MSL) based on surveyed cross-sections (Woodroffe, 2008).

Atoll or Archipelago	% > 2 m above MSL	% > 3 m above MSL
Cocos (Keeling) Islands	33	8
Maldives	4	1
Chagos	18	7
Marakei	32	8
Gilbert Chain/Tuvalu	34	7

A key observation of Smithers and Hoeke (2014) is that older parts of the village on Nukutoa tend to be located on higher ground than newer expansions, suggesting an increased vulnerability to flooding as development increases. Hence, when choosing a representative hinterland elevation for flood prediction scenarios, it may be prudent to consider future trends in land use rather than simply accounting for existing settlements.

2.1.2. REEF ECOLOGY & ROUGHNESS

Reefs are unique among coastal environments in that friction plays a major role in the dissipation of wave energy. Reef platforms may exhibit complex topography strewn with coral and rubble (Brander et al., 2004), which increases the hydrodynamic roughness and thus frictional dissipation far beyond what is normally seen for sandy beach settings. Parameterizing hydraulic roughness of coral reefs differs from sandy beds in that bed topography can be considered fixed (Nelson, 1996).

Our understanding of coral roughness is hampered by the considerable diversity of reefs and a lack of high-resolution seabed data to characterize them. Reef bathymetry is heterogeneous and the roughness length scales may vary significantly over short distances, making it challenging to parameterize Jaramillo and Pawlak (2011). Nunes and Pawlak (2008) carried out a detailed reef survey in O'ahu, Hawaii, and found that while there was no consistent roughness length scale, roughness spectra had a characteristic slope. In general, high friction is associated with complex, healthy canopy structures Monismith et al. (2015).

The ecological health of coral reefs has a strong relationship with the hydrodynamic processes that act on them (Baldock et al., 2014). Climate change may worsen stresses experienced by coral ecosystems, driving them to the point of functional collapse (Hoegh-Guldberg et al., 2007). Reef destruction due to climate change is expected to vary spatially, temporally, and by species, depending also upon anthropogenic interventions (Pandolfi et al., 2011). At sites in the Seychelles, Sheppard et al. (2005) found that coral mortality increased the amount of wave energy reaching shore, on account of decreases in roughness and increases in reef flat depth. Hence, threats to coral health (such as bleach-

ing and ocean acidification) may worsen wave-induced flooding on reef-fronted coasts.

Coral bleaching is a phenomenon that occurs when corals are subjected to abnormally high water temperatures, and may lead to both structural weakening of the coral and dramatic losses to the surrounding reef ecosystem (Pandolfi et al., 2011). Such events often take about a decade to recover from, during which time there may be a consequent reduction in hydraulic roughness on the reef. In April 2016, reports from the Australian National Coral Bleaching taskforce found that 93% of the Great Barrier Reef had been bleached, likely due to high ocean temperatures associated with a strong El Niño event (Slezak, 2016).

Ocean acidification results when increased concentrations of carbon dioxide in the atmosphere from anthropogenic sources react with water in the oceans and produce carbonic acid (Hoegh-Guldberg et al., 2007). The production of this acid reduces the supply of carbonate available for reef-building corals to grow and repair themselves, leading to a net erosion of reefs. As a result, reefs may not only grow increasingly brittle and more susceptible to damage by waves, but also become less able to recover naturally from such events (Hoegh-Guldberg et al., 2007). This could lead to a vicious positive feedback cycle of damaged coral leading to reduced hydraulic roughness, leading to larger waves on reef platforms, and hence even further coral damage.

Beyond their intrinsic ecological value, the benefits of reefs as nature-based flood defenses are now recognized (Ferrario et al., 2014; Narayan et al., 2016). Restoration of degraded reefs may be attempted by adding artificial roughness elements and encouraging recolonization by coral through transplantation (Zimmer, 2006).

2.2. HYDRODYNAMIC FORCING

This section provides an overview of the hydrodynamic forcing that acts on coral atolls to result in flooding. The main variables are water levels and waves, which are in turn influenced by a host of different processes at multiple spatial and temporal scales (Figure 2.4). Furthermore, these variables may vary spatially depending on global distributions of tidal range or wave climate.

2.2.1. WATER LEVELS

"King Tides", the colloquially-named highest tides, frequently plague low-lying tropical islands. If these king tides coincide with swell waves, flooding can result. However, there are also episodic water level increases associated with storm surges, and regional sea level changes brought about by climatic oscillations like El Niño. These phenomena are all superimposed on top of long-term sea level rise trends associated with climate change, and together may influence the local water level at a given island in unpredictable ways.

Péquignet et al. (2011) found that wave energy on reefs has a strong dependence on depth of submergence, with more energy reaching the shoreline at higher water levels. Even though setup decreases with increasing depth, reduced dissipation on the deeper reef means that more wave energy is permitted to reach the shore. Based on the relationship between reef flat submergence and wave height at the shoreline, they predict

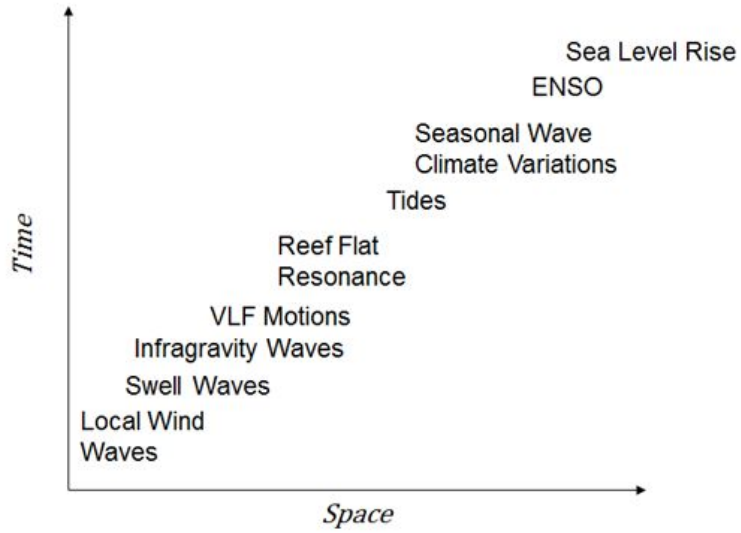

Figure 2.4: Hydrodynamic processes relevant to flooding of coral atolls, from locally-generated wind waves that act on short-term (seconds) and small scales (metres) to sea level rise which may act on much larger temporal (decades) and spatial (thousands of kilometres) scales.

increased wave energy at reefed coastlines under future sea level rise scenarios.

TIDES

Tides vary diurnally and semi-diurnally, but biweekly spring and neap or longer cycles may also be important. When islands are already so close to sea level, it does not take very large increases in water level to cause flooding.

Brander et al. (2004) found that significant wave height (Hs) across the reef platform is a function of submergence depth, with increased height at high tide and vice versa at low tide. Becker et al. (2016) find that stationary conditions are required to generate modal behaviour at low frequencies, such as at high tide for tidally-dominated reefs or when large, consistent wave setup is present on the reef flat. Therefore the tide puts temporal constraints on the windows during which significant runup can occur. Up to 30% of all reefs are tidally dominated (Lowe et al., 2015), but they are poorly studied and will not be focused on in this report.

STORM SURGE

Local sea levels may also change in response to atmospheric pressure variations, with sea surface elevation being inversely proportional to pressure (Hoeke et al., 2013). Tropical cyclones may induce wind-related or barometric storm surge along nearby coastlines, whereas many islands affected by remotely-generated swells will lie beyond the region of influence for these phenomena (Smithers and Hoeke, 2014). Furthermore, storm surge is highly dependent on offshore bathymetry. During Typhoon Haiyan, the storm surge

that devastated cities on enclosed shallow bays did not affect the reefed coast at Heinan, which abuts a deep oceanic trench Tajima et al. (2016).

REGIONAL & GLOBAL SEA LEVEL CHANGES

The threat of swell wave-induced flooding may be further compounded when sea level changes are accounted for. Changes in water level are important to flooding of coral atolls since they control both the submerged reef flat depth (which governs many key reef hydrodynamic processes) and also because they reduce the effective height of the island above the sea (freeboard). Accelerated global sea level rise and regional sea level fluctuations linked to the El Niño-Southern Oscillation (ENSO), atmospheric pressure changes, or other anomalies may greatly increase the severity of relatively minor wave events Hoeke et al. (2013).

Several interannual and decadal climate phenomenon obscure sea level rise trends, including ENSO, the Asian-Australian monsoon, and North Pacific Decadal Oscillation (Church et al., 2006). These variations introduce considerable uncertainty into predictions of sea level change in the tropical Pacific. Wunsch and Gill (1976) identify unexpected spectral peaks in Pacific island sea level records as belonging to 4-day oscillations due to equatorially-trapped internal gravity waves. The amplitude of these fluctuations was nearly 1 m, with observations generally being highest within 10 degrees of the equator. Hence, for low-latitude islands, these waves may contribute significant changes in water level beyond just daily tidal fluctuations or longer-term climatic variations. Higher-frequency variations in sea level may also be attributed to Rossby Waves (Church et al., 2006) If large swell events coincide with the peak of these oscillations, there will be an increased potential for flooding on low-lying atolls.

Sea levels at islands in the topical western Pacific Ocean are very sensitive to changes in the ENSO cycle, experiencing lower sea levels during El Niño and vice versa during La Nina. The ENSO cycle varies in duration and intensity, but Chowdhury et al. (2006) identify a strong annual signal that explains between 44-88% of the variability in sea level for northwest tropical Pacific islands. ENSO typically begins in summer, peaks in winter, then weakens by spring (Chowdhury et al., 2006). During strong and moderate La Niña years, higher sea levels (O(10cm)) are observed in the northwest tropical Pacific islands (Chowdhury et al., 2006), meaning that their vulnerability to wave-induced flooding increases due to greater reef flat submergence depths.

In the western Pacific and eastern Indian Oceans, Church et al (2006)(Church et al., 2006) report sea level rise rates approaching 30 mm/year. Even on a single atoll, relative sea level rise trends may very as a result of tectonic movement or local subsidence (Church et al., 2006). Monitoring of crustal subsidence on remote islands is limited, further adding to the challenge of predicting local sea level changes (Forbes et al., 2013). The main consequences expected from sea level rise include shoreline erosion, flooding, salinity intrusion and ensuing disruption of freshwater supplies, and decreased resilience of local ecosystems (McLean and Kench, 2015). Beetham et al. (2015) caution that even a minor sea level rise may allow increased wave energy to reach shore, increasing the potential for geomorphic change and flooding. Hence, sea level is an important consideration in predicting wave-induced floods on coral atolls.

Spatially varying interdecadal fluctuations and tectonic movements superimposed on long-term sea level rise trends will result in periods when the local rate of sea level rise

may be much higher (or lower) than global averages (Albert et al., 2016). (Barnard et al., 2015) find that fluctuations in sea level driven by ENSO could induce extreme flooding independently of global sea level rise trends. Hence, it is important to consider more than just tides and long-term sea level rise when making climate change projections for reef hydrodynamics.

2.2.2. OFFSHORE WAVES

Wave-induced flooding is the primary focus of this thesis as it presents a more imminent threat to coral atolls than flooding by mean sea level rise alone. This section highlights aspects of offshore wave forcing which are especially relevant to understanding the flooding of atolls.

Alves (2006) developed a numerical wave model in WAVEWATCH III (Tolman, 2009) to identify the influence of swell generated in specific regions of the ocean (Figure 2.5). They identify four distinct areas that contribute persistent swell to western Pacific tropical islands. Extratropical regions tend to generate swell via large storms, the same mechanism responsible for many of the wave-induced floods of concern in this thesis. Tropical regions contribute swell via tropical storms and regular trade winds.

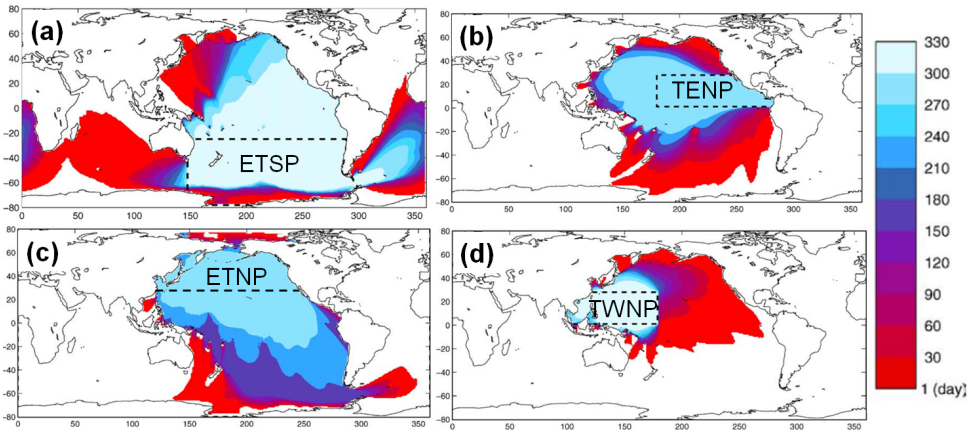

Figure 2.5: Persistence of various swell wave sources in the Pacific. The colourmap indicates the number of days per year when a given location is affected by swell originating from the area demarcated by a dashed box. The swell source areas are: (a) Extratropical south Pacific (ETSP); (b) Tropical eastern north Pacific ;(c) Extratropical north Pacific; and (d) Tropical western north Pacific (TWNP). Source: Alves (2006).

Merrifield et al. (2014) suggest that such wave models are a valuable tool to overcome the paucity of observed wave data in the Pacific, and can be used as inputs for predicting extreme water levels. In the absence of in situ wave measurements, Hoeke et al. (2013) rely on a numerical wave model to determine the wave climate driving flooding at Pacific Islands.

Waves can be classified by their frequency into several groups (Table 2.2). Sea is generated by local winds or tropical cyclones, while swell is generated far away from a given island by high-latitude storms, persistent trade winds, or far-away cyclones. Infragravity or very low frequency (VLF) waves may be generated on distant shores (Rawat et al.,

2014) but predominantly form on reefs themselves as a result of the processes discussed in Section 2.3. Although some studies classify any waves < 0.04 Hz as infragravity waves, this is our main area of interest, so it was important to make the additional distinction between infragravity and VLF waves.

Table 2.2: Classification of waves by frequency (f) and period (T).

	Wave Classification	f **[Hz]**	T **[s]**
H_{SS}	Sea/Swell	0.04 - 1.0	1 - 25
H_{IG}	Infragravity	0.004 - 0.04	25 - 250
H_{VLF}	Very Low Frequency	0.001 - 0.004	250 - 1000

LOCALLY-GENERATED SEA

Locally wind-generated sea waves are characterized by a broader spectrum and higher frequencies, with higher steepness and lower groupiness. These higher frequency waves tend to be dissipated by reefs, so they are less of a threat for flooding. However, tropical cyclones may also generate massive waves that can wreak serious devastation on low-lying tropical islands. Local wave climates may vary seasonally with monsoons or other meteorological events (Kench et al., 2009). Waves may even be generated on wider reef flats, although these will be limited by the local water depth (Nelson, 1997).

Although the inner lagoons of atolls are usually sheltered from the ocean outside, some are so large that severe waves can be generated within them[1]. This was demonstrated in a highly unseasonal July 2015 storm when Majuro Atoll, RMI, experienced flooding from the lagoon side (Australian Broadcasting Corporation, 2015). The outer coastlines may be protected to some degree from smaller locally generated waves, but since they are typically not exposed to extreme conditions, the inner side of atolls offer less protection against flooding.

REMOTELY-GENERATED SWELL

Swell is typically generated far away from the site of interest, and is the result of directional and frequency dispersion. The lower-frequency waves (typically 10-25 s) formed in storms tend to separate from the higher frequency ones as they travel further from the site, and experience less attenuation over long distances than short waves. Swell waves generated by storms may travel thousands of kilometres across entire oceans, travelling on great circle paths around the globe (Munk et al., 1963). The result is a narrow-banded, low-frequency, unidirectional, groupy wave train.

Hoeke et al. (2013) analyzed a series of floods that took place in December 2008 on islands in the Pacific Ocean. Rather than localized waves generated by tropical cyclones, the main source was identified as swell generated by distant storms in the north Pacific. They determined that swell forcing like that observed in this event has a return period of approximately 4 years, indicating that such events are relatively common. Hence,

[1] The lagoon of Kwajalein Atoll in the Marshall Islands has a maximum interior fetch of nearly 100 km.

low-probability, high-consequence storm events like tropical cyclones are not the only relevant threat to be considered when assessing flood risk on such islands. The relationship between swell waves and coastal flooding of coral atolls has poorly documented, in part due to the remoteness of the islands, limited data collection, and the insensitivity of most tidal gauges to wave-driven water level extremes (Hoeke et al., 2013). These swell waves are thus the primary focus of the present study.

There is typically a seasonal character to swell wave direction. At Palmyra Atoll (5°52'N, 162°05'W), (Rogers et al., 2015) found that during northern hemisphere winters (December-March), dominant wave energy came from the north, then shifting to the south during southern hemisphere winters. The different sources and regular patterns in wave generation mean that there are often multiple swell systems simultaneously present at a given site in the open ocean.

As illustrated in Figure 2.5, the majority of waves impacting low-lying tropical islands like the Marshall Islands are swell generated by far-away mid-latitude storms (Cheriton et al., 2016). Swell in the Marshall Islands is consistent and predictable enough that indigenous islanders were able to use it (and the resulting diffraction patterns around islands) to navigate between islands (van Vledder, 2015). The Marshallese tradition of wave piloting and its relevance to wave-induced flooding of atoll is discussed in greater detail in Appendix G.

INFRAGRAVITY & VLF WAVES

Infragravity and very low frequency (VLF) waves are much longer than the sea and swell waves examined in the previous sections. Cheriton et al. (2016) demonstrated that low-frequency waves can lead to overwash when coupled with high offshore water levels, and suggested that this will make such locations more vulnerable to flooding under future sea level rise scenarios. Infragravity waves offshore of a reef are influenced by the complex interactions between shoreward-propagating bound long waves and seaward-directed IG waves generated by the breakpoint mechanism (Pomeroy, van Dongeren, Lowe, van Thiel de Vries and Roelvink, 2012). Leaky waves from distant shores and waves generated by moving atmospheric pressure disturbances may also be relevant sources.

Bound long waves (BLW) are low frequency waves forced by nonlinear interactions between sea/swell wave components with slightly different frequencies (Herbers et al., 1994). The resulting wave groups result in radiation stress gradients which generate a phase-locked low-frequency wave. Since narrower spectra tend to result in groupier waves, remotely-generated swell is a stronger source of bound long waves than locally-generated sea waves. This explains why BLW are strongest in high energy swell conditions (Herbers et al., 1995; van Dongeren et al., 2003).

The analysis of Rawat et al. (2014) reveals that it is not only the direct impact of swell generated by large mid/high-latitude storms that may be significant for Pacific islands, but also the free infragravity waves generated by those same storms when the swell hits distant shores. Infragravity waves that reflect off the shoreline or are released seaward from the breakpoint become "leaky", as opposed to those which decay or become trapped in the nearshore. These free waves may propagate from shorelines across ocean basins to contribute (and even dominate) low-frequency wave energy on the distant opposite shore (Rawat et al., 2014). These waves are typically O(1 cm) in height on

the open sea but may transform and increase in size as they move inshore, meaning that they could contribute to coastal flooding independently of local conditions.

Most critically for the prediction of wave-induced flooding on atolls, Rawat et al. (2014) suggest that deep ocean sites in the west Pacific are dominated not by locally-generated infragravity waves, but by those that have travelled from the opposite side of the ocean. Rawat et al. (2014) find that the interaction of swell produced by large extra-tropical depressions with eastern ocean boundaries are better at generating free infra-gravity waves than hurricanes or other tropical storms. However, they do not investigate infragravity waves generated by reefed coastlines in their analysis.

VLF waves may also originate from a phenomenon known as Proudman resonance, wherein the phase speed of waves matches the speed at which the pressure disturbance associated with a storm system tracks (Benjamin, 2015; Hanafin et al., 2012; Monserrat et al., 2006; Renault et al., 2011; Vennell, 2010). These "meteo-tsunamis" can cause considerable destruction when they reach the coast (Vilibić and Šepić, 2009). This phenomenon is more likely to affect reefed coastlines in shallow seas, since atmospheric pressure waves typically travel at 20-40 m/s, which is approximately the shallow water celerity in 40-160 m depths (Monserrat et al., 2006). Hence, for atolls in the middle of the ocean or fringing reefs adjacent to deep trenches, they may not be a factor (Roeber and Bricker, 2015).

2.3. WAVE TRANSFORMATION ON REEFS

If offshore metocean conditions and reef morphology are known, we need to understand how waves transform on reefs in order to take that information and use it to predict flooding. The link between global or regional wave models and accurate prediction of extreme runup and flooding of coral atolls depends on an improved understanding of the wave transformation processes occurring on reef flats (Cheriton et al., 2016). This section describes how wave transformation processes differ on coral reefs from typical sandy coasts, and how those processes also vary between different types of reef.

As waves approach an island from offshore, they first encounter the steep fore reef. The waves rapidly shoal and then break along the upper slope of the fore reef and crest, dissipating significant energy in the process. The waves continue to propagate shoreward, losing energy as they go to breaking and frictional dissipation across the rough reef flat. By the time waves reach the shore, substantial amounts of energy have been dissipated, and the dominant frequencies become much lower. At the shoreline, these waves run up and down the beach slope, and can cause flooding if they exceed the crest elevation.

Major characteristics of wave transformation across reefs are wave height reduction and spectral evolution from high frequency dominance offshore to multimodal spectra in the middle and then low-frequency dominance at the shoreline.

Wave Height Reduction

Péquignet et al. (2011) observed a 97% reduction in wave energy across the reef flat at Ipan, Guam. Brander et al. (2004) examine wave transformation across a very wide (2.7 km) mesotidal fringing reef in Torres Strait, Australia. They observed that between 85-95pct of incident wave energy was dissipated between the reef crest and middle of reef

flat, and that there were strong, linear relationships between wave height and depth of submergence. At Funafuti Atoll, Beetham et al. (2015) observed that 78pct of incident wave energy was dissipated by the time it reached the shoreline.

Bimodal Spectra

The different spatial trends in growth and decay of high and low frequency wave components across reef flats often leads to a bimodal spectrum (Pomeroy et al., 2015). Offshore, the wave spectrum is unimodal with a HF peak, and it shifts to a unimodal spectrum with LF peak near the shoreline. In the area in between on the reef flat, a bimodal spectrum often exists as the dominance of HF and LF energy shifts.(Beetham et al., 2015) observed bimodal wave spectra during swell events at Funafuti Atoll, with distinct peaks associated corresponding to locally generated waves and the incoming swell. They also depict a clear trend in spectral evolution across the reef, with swell energy being filtered out and LF energy increasing. At Roi Namur, Cheriton et al. (2016) found that the spatial variation in wave energy was frequency dependent. Incident wave energy decreased across the reef flat, but infragravity energy peaked on mid-reef flat and VLF energy peaked at the inner reef flat.

Low Frequency Dominance

Lowe, Falter, Bandet, Pawlak, Atkinson, Monismith and Koseff (2005) liken barrier reefs to a low-pass filter, removing high frequency sea/swell energy and allowing low frequency energy to dominate at the shoreline. The fore reef and reef crest are dominated by short waves, but this shifts towards infragravity wave dominance closer to shore (van Dongeren et al., 2013). Young (1989) found that even with dissipation of short waves, there remains significant infragravity energy across the reef, which increases with water depth.

Nwogu and Demirbilek (2010) conducted a laboratory and numerical modelling study to investigate wave transformation and infragravity processes across fringing reefs. They found that infragravity energy increased across the reef flat towards shore. In their laboratory model of a fringing reef, Pomeroy et al. (2015) found that HF waves decreased rapidly at the reef crest, then more gradually across the flat. While IG waves also shoaled and then rapidly decreased in height at the crest, they instead grew higher as they propagated across the reef flat.

Pomeroy, Lowe, Symonds, van Dongeren and Moore (2012) conducted a field study of infragravity wave dynamics on Ningaloo Reef, Western Australia. They found that HF wave motions were dissipated on the reef crest, allowing infragravity motions to dominate closer to shore. In their field investigations on Rarotonga, Blacka et al. (2015) identify large fluctuations in LF energy across the reef, which lead to extreme water levels in excess of 2 m beyond the mean storm surge elevation.

2.3.1. SHOALING

As waves approach the reef, they will first begin to shoal as depth decreases across the fore reef slope. This shoaling will cause the waves to steepen and generate bound higher harmonics (corresponding to an increase in nonlinearity). For steeper fore reefs, the waves may even be reflected back offshore (Young, 1989). If the water depth increases again past the reef crest (as is typical for barrier reefs), the higher harmonics may be freed

and the wave spectrum subsequently broadened (Young, 1989). Shoaling continues until the waves steepen to the point of breaking, or if water depth increases again (as in a lagoon).

van Dongeren et al. (2007) classify the shoaling of an incoming long wave into mild-slope ($\beta_b < 0.3$) and steep-slope ($\beta_b > 1$) regimes, where:

$$\beta_b = \frac{h_x}{w}\sqrt{\frac{g}{h}} \tag{2.1}$$

and where h_x is the bed slope, w is the radial frequency of the infragravity waves, g is gravity, and h is the characteristic breaking depth. Shoaling of the incoming long waves increases for milder slopes.

Mild bed slopes tend to be more dissipative than reflective in nature. The main dissipation mechanism for long waves in this regime on sandy beaches is breaking rather than bottom friction (van Dongeren et al., 2007). Triad wave interactions also transfer energy from LF to HF waves, although the transfer process tends to be governed by self-self interactions between LF waves in very shallow water. These self-self interactions cause the long waves to steepen and break. The near-horizontal reef flat may be characterized as a very mild slope (dominated by dissipation), whereas most reef-fronted beaches are comparatively steep and thus reflect low frequency waves.

2.3.2. WAVE BREAKING

Wave breaking is an efficient means of dissipating wave energy, although unlike many coastal settings it is not the always the dominant mechanism on reefs. When waves exceed a certain steepness or relative depth, they will break. As a consequence of the abrupt change in bathymetry from deep water to shallow reef flat, wave breaking usually has zone of influence limited to the fore reef and reef crest.

Wave breaking on reefs is depth limited, although given the extreme variations in bathymetry from the steep fore reef to the near-horizontal reef flat, the ratio of wave height to depth ($\gamma = H/h$) may differ from behaviour in typical coastal settings. (γ) varies across the reef, with much lower values on the reef flat ($\gamma = 0.12 - 0.22$) than at the reef crest ($\gamma = 0.96$). This decrease across the flat is linked to dissipation due to breaking and bottom friction (Vetter et al., 2010).

The breaking threshold ($\gamma_b = H_b/h_b$) estimated by Vetter et al. (2010) at Guam varied with the magnitude of the incident waves, ranging from $\gamma_b = 0.91$ in normal conditions to $\gamma_b = 1.13$ during a cyclone. They attribute the increased threshold to the breakpoint moving further offshore under more intense wave conditions. Since gamma is sensitive to slope, it will vary depending on its position across the fore reef. Young (1989) argued that given the flat slope of the reef flat, the wave breaking depth limit is likely less than the widely-used $\gamma_b = 0.78$ threshold developed for solitary waves on sloping beaches. Blacka et al. (2015) found γ at the reef edge of 0.8, higher than the typical value of 0.55 reported for flat beds. Hence, waves may be abnormally large near the reef crest compared to typical nearshore settings of similar depth.

Salmon et al. (2015) developed a new breaking formulation based on scaling γ_b in the Battjes and Janssen (1978) model to account for bed slope (β) and kh, and applied it

to a fringing reef setting in Guam. In this particular case, their results lent support to the use of smaller γ values on reefs, although scatter was large.

Wave height depth-dependence is at its greatest when conditions are fully saturated-when every wave is breaking or broken Costa et al. (2016). Brander et al. (2004) found wave heights to lie well below the $\gamma = 0.55$ threshold on the reef flat, due to the unsaturated wave energy conditions there.

In laboratory tests, Yao et al. (2012) found that fore reef steepness constrained the width of the surf zone to a relatively narrow band. After propagating as a bore for some distance across the reef flat, sufficient energy will be lost that the wave can reform as an oscillatory wave ($\gamma < \gamma_b$), where friction will be the dominant dissipative process (Nelson, 1996; Young, 1989). In their analysis of field and laboratory data, Blacka et al. (2015) find that most waves reach a stable decayed height of ($\gamma_b \leq 0.55$) within one shallow water bore length or one quarter of the deep water wavelength ($1/4\ L_0$). These breaking conditions have been reproduced in laboratory and tests by Nwogu and Demirbilek (2010).

2.3.3. LOW FREQUENCY WAVE GENERATION

As short waves are dissipated along the outer portion of the reef, low frequency waves come to dominate at the shore. Two main low frequency wave generation mechanisms are considered here: bound long waves and breakpoint forcing.

BOUND LONG WAVES

Incident bound long waves contribute minimal infragravity energy shoreward of the reef crest on Ningaloo Reef, with the majority of them being dissipated along with short wave breaking in the surf zone Pomeroy, van Dongeren, Lowe, van Thiel de Vries and Roelvink (2012). Péquignet et al. (2014) found that strong wave breaking may decrease the bound long wave energy penetrating the surf zone, instead giving way to breakpoint generation of low frequency waves.

BREAKPOINT FORCING

Bound long waves are not the dominant source of infragravity energy on reefs; instead breakpoint forcing contributes the most. The theory was first posited by Symonds et al. (1982), who describe the generation of infragravity waves on beaches by a spatially and temporally-varying breakpoint due to wave grouping of incident waves. This breakpoint mechanism releases infragravity waves both shoreward and seaward. The amplitude of the shoreward standing wave is relatively insensitive to incident wave height, and the seaward wave depends on the mean breakpoint location, group frequency, and beach slope.

Incident waves break at different cross-shore locations depending on their height relative to the local depth. For a uniformly sloping beach, larger waves will tend to break in deeper water and thus further offshore. The breaking of waves causes a loss of momentum that must be compensated by a shoreward increase in water level (wave setup), so the width and height of this elevated region will also depend on the position of the breakpoint (Symonds et al., 1982). Hence, wave groups approaching the coast will modulate water levels at the shoreline in what is effectively a standing wave with the frequency of the wave group (Figure 2.6).

In general, larger incident waves will break further offshore in deeper water, whereas smaller waves will break closer to shore. These upper and lower incident wave heights will determine the maximum cross-shore excursion of the breakpoint, and hence the width of the surf zone, which in turn controls the setup height. The frequency of these fluctuations will depend on the length of the wave groups. Thus, the groupiness of the incident wave field plays a role in determining the efficiency of the breakpoint mechanism in generating infragravity waves. Figure 2.6 demonstrates how breakpoint generation of low frequency waves works on fringing reefs.

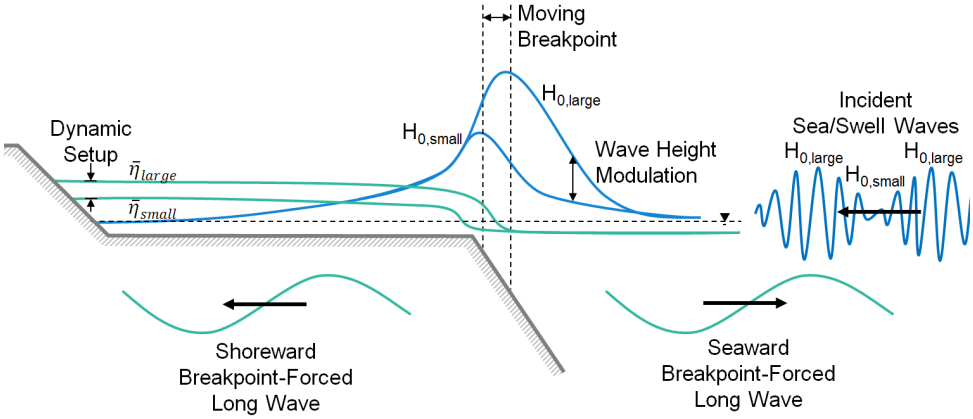

Figure 2.6: The breakpoint long wave generation mechanism on fringing reef profiles. As incident sea/swell wave height changes with wave groups, so too does the location of breaking on the fore reef and reef crest. Higher waves will break farther offshore, whereas smaller waves will break closer to shore. This horizontal movement of the breakpoint then translates to a change in the magnitude of wave setup on the reef flat. The dynamic wave setup thus fluctuates at the frequency of incident wave groups. The shifting breakpoint acts almost like a wave paddle, generating both shoreward and seaward long waves. Adapted from Symonds et al. (1982).

Péquignet et al. (2009) find that VLF motions on the reef originate from a dynamic setup generated by breaking swell waves at the reef crest. This motion is characteristic of breakpoint forcing. In a study of fringing reefs on the Marshall Islands, Merrifield et al. (2014) found shoreline water level variations at IG frequencies to be consistent with breakpoint forcing. Pomeroy, Lowe, Symonds, van Dongeren and Moore (2012) identified breakpoint forcing as the main source of infragravity waves on Ningaloo Reef, Western Australia, rather than shoaling bound waves. The dominance of this generation mechanism can be explained by the steep fore reef slope. Baldock et al. (2000) notes that the mechanism is strongest if the breakpoint excursion is small compared to the standing wavelength. Since steeper fore reefs result in a narrow breaking zone, they may prove more effective at generating low frequency waves. For this reason, Becker et al. (2014) also assume an idealized breakpoint model in their analysis.

Breakpoint forcing by the SS wave envelope is a much more efficient generator of VLF energy than bound long wave forcing (Péquignet et al., 2014). Breakpoint mechanism efficiency tends to be reduced with increasing reef flat submergence, due mainly to the decreased depth-limited breaking of short waves (Pomeroy, van Dongeren, Lowe, van

Thiel de Vries and Roelvink, 2012).

2.3.4. FRICTIONAL DISSIPATION

Although breaking is the dominant dissipation mechanism along the fore reef and reef crest, friction takes on a more important role as waves propagate across the reef flat towards shore. Frictional dissipation is closely tied to reef roughness (Section 2.1.2) and the depth of water on the reef flat.

Coral forms large, complex canopies along the seabed which may greatly distort the spatial flow structure across them Lowe and Falter (2015). The classical logarithmic flow profile which develops for turbulent flow over smooth beds is distorted by coral protruding through the boundary layer (Figure 2.7). Additional drag force from the coral slows the water passing through the canopy and provides greater resistance to flow above the canopy. The flow profile under wave-driven oscillatory currents is also distorted.

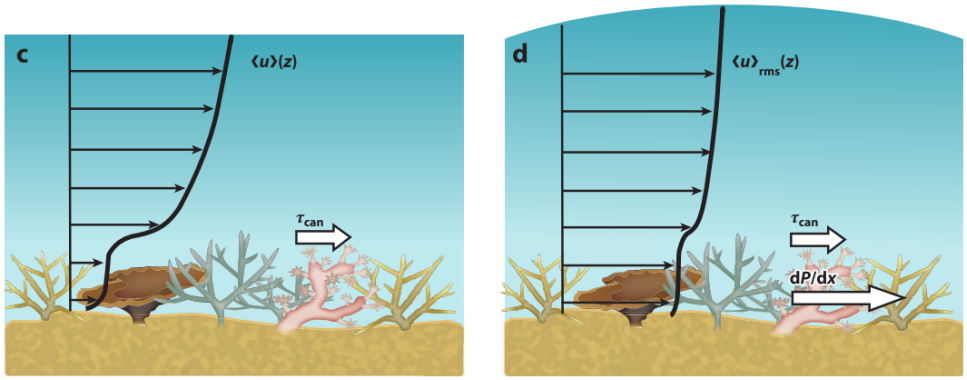

Figure 2.7: Wave and current velocity profiles illustrating flow over and through a coral canopy. Coral protruding through the boundary layer distorts the flow profiles. Source: Lowe and Falter (2015).

MORPHOLOGIC CONTROLS ON FRICTIONAL DISSIPATION

Frictional dissipation is largely dependent on the bottom roughness of a given reef. Lowe, Falter, Bandet, Pawlak, Atkinson, Monismith and Koseff (2005) found that wave energy dissipation across the reef flat is more dominated by friction than for typical sandy beach environments, due to the high bottom roughness of the reef. In an extreme case observed by Monismith et al. (2015) on Palmyra Atoll, the friction factor was more than an order of magnitude rougher than observed elsewhere. As a result, observed energy dissipation due to friction exceeded that due to breaking. Conversely, Vetter et al. (2010) examined a smoother reef and found a limited influence of frictional dissipation on cross-shore changes in momentum. Thus, variations in reef morphology make it challenging to generalize the influence of friction on reefs.

High frequency waves tend to be dissipated more through breaking than friction, although short waves that persist across the reef flat gradually attenuate (Pomeroy, Lowe, Symonds, van Dongeren and Moore, 2012). In their laboratory study, Pomeroy et al. (2015), found that bottom friction exerted more influence on LF than HF waves, and

that friction governed LF wave energy more so than submerged reef flat depth. Subject to sufficient frictional dissipation, LF energy will decay across the reef flat, tidally modulated by non-linear energy transfer and depth-varying friction (Péquignet et al., 2014). van Dongeren et al. (2013) found that frictional dissipation of IG waves play a more dominant role on reefs than on sandy beaches, where non-linear energy transfers may be more important. Furthermore, the frictional dissipation limits the IG wave steepening and breaking (bore formation) observed on sandy beaches.

However, the rate of low-frequency frictional dissipation varies with reef roughness. Cheriton et al. (2016) found that low-frequency waves on Roi-Namur underwent little frictional dissipation and increased in energy as they moved shoreward, which is consistent with other relatively smooth reef flats. Conversely, the bottom roughness of Ningaloo Reef, Western Australia, is so high that frictional dissipation dramatically attenuates outgoing infragravity waves reflecting from the shoreline (Pomeroy, Lowe, Symonds, van Dongeren and Moore, 2012), as depicted in (Figure 2.8). The result is that shoreward propagating IG waves dominate the site.

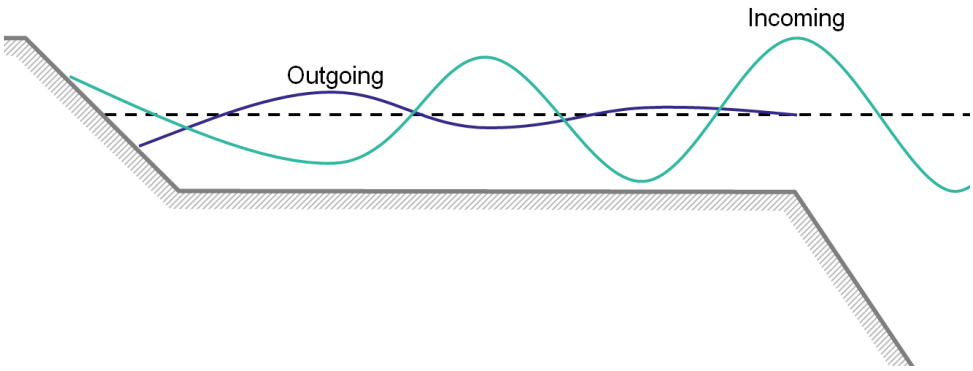

Figure 2.8: Conceptual diagram of decay of infragravity waves across the reef flat. Shoreward wave heights decrease toward the shoreline (blue line), and waves are further attenuated after they reflect off the shore and move seaward (purple line).

Monismith et al. (2015) and Young (1989) suggest scattering over rough reef topography as a possible means of decreasing energy flux, although they note that this generally occurs over length scales greater than typical wavelengths. Hence, this phenomenon might only be important for wider reef flats. Based on satellite observations of the Great Barrier Reef in Australia, Young (1989) found that wave attenuation across reef flats variations has limited sensitivity to reef porosity.

HYDRODYNAMIC CONTROLS ON FRICTIONAL DISSIPATION

Although there is considerable variation in frictional dissipation between different reefs as a result of their different morphology, it can change even for the same reef under different hydrodynamic conditions. The tidal modulation of infragravity waves was exhibited on Ningaloo Reef, where Pomeroy, Lowe, Symonds, van Dongeren and Moore (2012) found that dissipation due to friction (and thus IG wave height) varied with reef flat submergence depth. This modulation is mainly due to changes in frictional dissipation as a

function of depth over the reef, rather than variations in the rate of IG wave generation (van Dongeren et al., 2013). Water levels are not the only factor influencing frictional dissipation - Lowe, Falter, Bandet, Pawlak, Atkinson, Monismith and Koseff (2005) found that the importance of friction on the fore reef decreases with increasing wave height.

2.3.5. NON-LINEAR WAVE PROCESSES

Although much of reef hydrodynamics can be explained through linear wave theory, there are also several non-linear phenomena which redistribute energy throughout the spectrum. Nwogu and Demirbilek (2010) found that nonlinear triad wave-wave interactions on the reef flat were important for the transfer of energy to both infragravity and higher frequencies. Superharmonic wave components (at multiples of the peak frequency) are formed during the shoaling process Filipot and Cheung (2012). This energy transferred to higher frequencies by triad interactions is then more readily dissipated from the system (Sheremet et al., 2011). Péquignet et al. (2014) also found a positive non-linear energy transfer into the VLF band and growth of VLF energy flux onto the reef flat. However, Pomeroy, Lowe, Symonds, van Dongeren and Moore (2012) noted that high bottom friction on the reef flat may reduce the effect of non-linear energy transfers, especially when compared to sandy beaches.

In laboratory experiments, Nwogu and Demirbilek (2010) observed an increase in infragravity energy and decrease in short wave energy across the reef flat, with broken waves reforming as asymmetric bores. These vary from non-breaking undular bores to completely turbulent bores fronted by rollers, with larger waves propagating faster than smaller ones. Beetham et al. (2015) observed that wave period at the shoreline was tidally modulated, since HF waves tended to be filtered out at lower water levels (resulting in overall longer periods). They attribute shorter periods at high tide to waves decoupling into HF oscillations across the reef flat.

The set of processes that redistribute energy across different frequencies is complex, both spatially and temporally varying. These non-linear processes may be quantified by examining the skewness and asymmetry of waves as they propagate across the reef. Cheriton et al. (2016) observed a maximum in incident wave asymmetry at the outer reef flat, but found that IG and VLF non-linearity increased across the reef flat. In their physical model of a fringing reef, Pomeroy et al. (2015) also found strong wave asymmetry and skewness at the edge of the reef where waves first break. However, the asymmetry decreases across the reef flat as bore-like broken and breaking waves dissipate energy and reform back into oscillatory waves, as also observed by Nelson (1996).

2.3.6. REFLECTION

Although most wave energy arriving from offshore becomes dissipated on reefs, some may be reflected seawards off the face of the reef or shore. Reflection is given by comparing incoming and outgoing wave heights or energy fluxes. For cases of perfect reflection, the ratio of incoming to outgoing (reflection coefficient K_R) will equal 1. This study is focused primarily on atolls and fringing reefs rather than barrier reefs. Barrier reef hydrodynamics are different since the absence of a backing shoreline to block the flow of water means reduced setup and reflection (Young, 1989). Reflection is governed

by a combination of hydrodynamic and morphologic factors.

HYDRODYNAMIC CONTROLS ON REFLECTION

Generally, reflection is greater for longer wave periods and lower wave heights. Péquignet et al. (2009) found that wave reflection increased with decreasing wave steepness (H/L), reaching a maximum during tropical storm Man Yi and creating standing waves. Beetham et al. (2015) observe reflection of waves off the shoreline and subsequent interaction with incoming waves on the reef flat under high incident conditions.

Low frequency components are more reflective than high frequency ones (Yao et al., 2012). Roeber and Bricker (2015) note low-frequency energy in deep water offshore and identify it as free long waves reflected from shore. On the rough Ningaloo Reef, Pomeroy, Lowe, Symonds, van Dongeren and Moore (2012) observe low reflection, suggesting that shoreward-progressive rather than standing IG waves dominate there. However, on the narrower, deeper reef at Ipan, Guam, Péquignet et al. (2014) observed standing wave patterns, evidenced by near-complete reflection when measured at the outer reef.

MORPHOLOGIC CONTROLS ON REFLECTION

The slopes of both the fore reef and beach will influence the degree of reflection observed on a given reef. In laboratory experiments, Yao et al. (2012) found that reflection dramatically increases for fore reef slopes steeper than 1/4. Péquignet et al. (2014) observed partial reflection of LF waves at the reef face and near-complete reflection at the shoreline. If beach slopes are mild (< 1/20), then some dissipation at the shoreline may occur, leading to reflection coefficients less than 1 (Pomeroy, Lowe, Symonds, van Dongeren and Moore, 2012). Cheriton et al. (2016) found that a beach slope of 1/6 was fully reflective for IG and VLF waves.

2.3.7. RESONANCE

Resonance is a phenomenon where wave energy on a reef is amplified because external forcing matches a preferential frequency determined by the reef's geometry. It has been observed in the field (Cheriton et al., 2016; Péquignet et al., 2009; Pomeroy, 2011) and reproduced in laboratory settings by Nwogu and Demirbilek (2010). When the width of a reef flat is 1/4 of a given wavelength, it can act as a bounded open basin, enabling resonant oscillations (Péquignet et al., 2009). Under that scenario, a node (fixed water level) is observed at the reef crest and an antinode (varying water level) is found at the shoreline. Higher modes may also exist and become excited by shorter waves.

Resonance is depended on both morphology and hydrodynamics. The n^{th} resonant (or natural) frequency of a given reef ($f_{N,n}$) is defined by Equation 2.2:

$$f_{N,n} = \frac{(2n+1)\sqrt{g h_{reef}}}{4 W_{reef}}; \qquad T_{N,n} = \frac{1}{f_{N,n}} \tag{2.2}$$

Where n is the resonant mode $(0, 1, 2, ..., n)$, g is gravity, h_{reef} is the mean water depth on the reef flat, and W_{reef} is the width of the reef flat. $T_{N,n}$ is the resonant (or natural) period, the inverse of resonant frequency.

Resonance is important to understand, since it means that disproportionately high flooding can result for given wave conditions. Coral reefs are often thought to protect

the shore from flooding due to the dissipation of incoming wave energy (Nakaza et al., 1990). However, under resonant conditions the reefs actually spawn more harm than good, amplifying even small waves. Nakaza et al. (1990) cite bore-like surf beat from resonantly-excited wave groups as the main source of damage to coastal structures on reefed coastlines. Given typical reef flat dimensions of O(100 m), resonant waves tend to occur at infragravity and very low frequencies.

The destructive power of infragravity and VLF waves is evident in dramatic video footage of flooding in the Marshall Islands [2] and in the Philippines [3].

Reports from the December 2008 flood in Nukutoa (Smithers and Hoeke, 2014) describe surging bores with periods ranging from 6-8 minutes surging across low-lying portions of the island. These periods lie within the 0.001-0.004 Hz VLF range and are possible evidence of resonantly-amplified IG/VLF motions, similarly to those observed by Nakaza et al. (1990); Péquignet et al. (2009); Roeber and Bricker (2015); Tajima et al. (2016). Similarly, large swell events in Fiji produce tsunami-like low frequency waves (traditionally called "Loka waves" by residents) that cause considerable flooding (Bosserelle et al., 2015).

Typhoon Haiyan spawned massive low frequency waves that caused considerable destruction along the Philippine coast Roeber and Bricker (2015); Shimozono et al. (2015); Tajima et al. (2016). The waves were powerful enough to transport 2 m boulders a distance of several hundred metres (Kennedy et al., 2015)! Many reefed coastlines are strewn with boulders, originally thought to be transported by prehistoric tsunamis. However, recent investigations suggest that perhaps storm-induced waves may be responsible (Lau et al., 2016; Nott, 1997; Terry et al., 2016). Resonant amplification of low frequency waves could be a plausible explanation for these erratics and exceptional flood events.

There are three main factors which can change to initiate resonance: reef width, offshore wave forcing frequency, and water depth on the reef flat. The natural frequency of a given reef will thus vary with time depending on tidal or other water level fluctuations (Péquignet et al., 2009). Figure 2.9 shows mechanisms increasing resonant amplification.

MORPHOLOGIC CONTROLS ON RESONANCE

The main morphological properties controlling resonant amplification are reef width and roughness. Wider reefs experience greater resonant amplification, but may also experience greater damping due to frictional dissipation (Pomeroy, van Dongeren, Lowe, van Thiel de Vries and Roelvink, 2012). Furthermore, they require lower frequency forcing to become excited. Cheriton et al. (2016) posit that the narrow reef flats on Roi-Namur may contribute to resonant conditions, evidenced by increased VLF energy. Variations in cross-shore bathymetry may also disrupt resonance Ford et al. (2013).

Pomeroy, van Dongeren, Lowe, van Thiel de Vries and Roelvink (2012) note that bottom friction affects the magnitude of resonant amplification, but not the resonant frequency itself. Because of strong frictional dissipation across the reef flat, standing wave modes did not develop on Ningaloo Reef (Pomeroy, van Dongeren, Lowe, van Thiel de Vries and Roelvink, 2012).

[2] Mar. 3, 2014 on Majuro, RMI: https://youtu.be/p-FfrWubDeA

[3] Nov. 8, 2013 in Hernani, Philippines during Typhoon Haiyan https://youtu.be/rS0gv4Xbw7w?t=42s

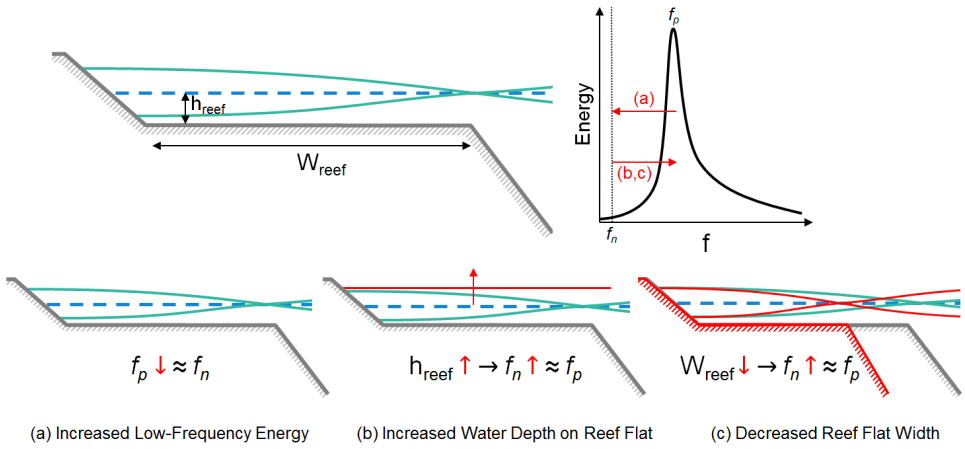

Figure 2.9: Mechanisms increasing resonant amplification, including (a) increased low-frequency energy from offshore waves (i.e. longer-period or groupier swell), (b) increased water depth on reef flat (due to tides, sea level rise, or setup), and (c) narrower reef flats. Mechanism (a) shifts the peak of the spectrum towards the resonant frequency, whereas mechanisms (b) and (c) shift the resonant frequency closer to the peak.

HYDRODYNAMIC CONTROLS ON RESONANCE

Resonance is more likely for a given reef under conditions with significant low-frequency wave energy (such as during a large storm or swell event), or where increases in water level reduce the natural frequency to match the forcing.

Péquignet et al. (2009) found that although wave motion may be highly coherent at near-resonant frequencies, they are not as energetic, since the right forcing is necessary to excite them. Péquignet et al. (2009) found that forcing at the frequencies required to induce resonant conditions was rare during typical conditions at Ipan, Guam, only occurring during storms when water depths over the reef flat were greater. Even though motion may exist on the reef flat at resonant frequencies, it will not necessarily lead to amplification, since energetic forcing at those frequencies is required (Péquignet et al., 2009). Hence, if there is strong forcing at low frequencies (such as during a large storm or swell event), there may be sufficient incident energy to excite resonant amplification.

Péquignet et al. (2009) examined the behaviour of infragravity waves on Ipan Reef, Guam during tropical storm Man Yi. They found that increased water levels on the reef flats brought the natural frequency of the reef in line with the frequency of low-frequency wave motions generated by the storm, allowing resonant amplification to occur. Péquignet et al. (2014) suggest that higher water levels will reduce dissipation due to friction and increase the likelihood of resonant conditions being reached on fringing reefs. Péquignet et al. (2009) did not observe resonant conditions outside of tropical storm Man Yi because at lower water levels, the natural frequency of the reef was too high to be excited by typical incident waves. Furthermore, as water depth increases, the natural resonant frequencies of the reef decrease, enabling low frequency wave energy to more easily amplify resonant modes (Pomeroy, van Dongeren, Lowe, van Thiel de Vries and Roelvink, 2012). Resonant excitation is more efficient when the frequency of incoming wave energy is close to the natural resonant frequency.

For a case study based in Guam, Pomeroy, van Dongeren, Lowe, van Thiel de Vries and Roelvink (2012) found that "normal" conditions (1.0 m wave height and peak period of 9.5 s in 0.5 m of water) could not produce resonant amplification because of frictional damping across the moderately rough 450 m wide reef flat. However, storm conditions corresponding to tropical storm Man-Yi (4.0 m wave height and peak period of 12.0 s in 2.0 m of water) were sufficient to cause resonant excitation. A key question is whether or not resonance happens only in big storms (e.g. (Péquignet et al., 2009; Roeber and Bricker, 2015; Shimozono et al., 2015)) or also in swell conditions. Gawehn et al. (2016) found that VLF resonance occurred 3.5% of the time during a 4 month measurement campaign at Roi Namur.

Climate change may also have dire implications for these resonant phenomena. Pomeroy, van Dongeren, Lowe, van Thiel de Vries and Roelvink (2012) suggest that sea level rise will bring increased susceptibility to infragravity resonance, on account of the increased reef flat depths. Furthermore, if ocean acidification and increased sea surface temperatures threaten the health of coral ecosystems, hydrodynamic roughness could decrease Quataert et al. (2015). This would reduce damping of resonant conditions and potentially increase the threat of flooding.

2.4. RUNUP & OVERTOPPING

2.4.1. RUNUP

Wave runup is the maximum wave-induced water level on the shoreline, measured relative to the still water level. It is important to understand and quantify runup since it is the final link in the chain of processes that transforms waves from offshore to flooding onshore.

Stockdon et al. (2006) decompose runup on sandy beaches into three main components: setup ($\overline{\eta}$), infragravity swash (S_{IG}), and incident (or sea-swell) swash (S_{inc}). Figure 2.10 illustrates the separate components.

WAVE SETUP

Setup is the difference between mean water level (MWL) and still water level (SWL), and is the result of a water level increase as hydrostatic pressure counters radiation stresses from breaking waves. On reefs, setup tends to occur on the reef flat, shoreward of the breakpoint. Bosserelle et al. (2015) found that wave setup made the most important contribution to extreme water levels.

Vetter et al. (2010) found that traditional wave setup theory developed for sandy beaches still applies well to reefs. However, reefs present additional complexity due to their geometry, highly variable roughness, and the presence of a beach or lagoon shoreward of the reef crest. Yao et al. (2012) found that spatial variation of setup depended on the surf zone width, which in turn depended on the fore reef slope. The magnitude of reef flat setup is highly correlated to incident wave height (Vetter et al., 2010).

SWASH

While setup is static at short wave timescales, swash is the oscillating component of waves that runs up and down on the beach face. Since low frequency waves dominate at the inner reef flat, infragravity swash plays an important role on the beach. Low

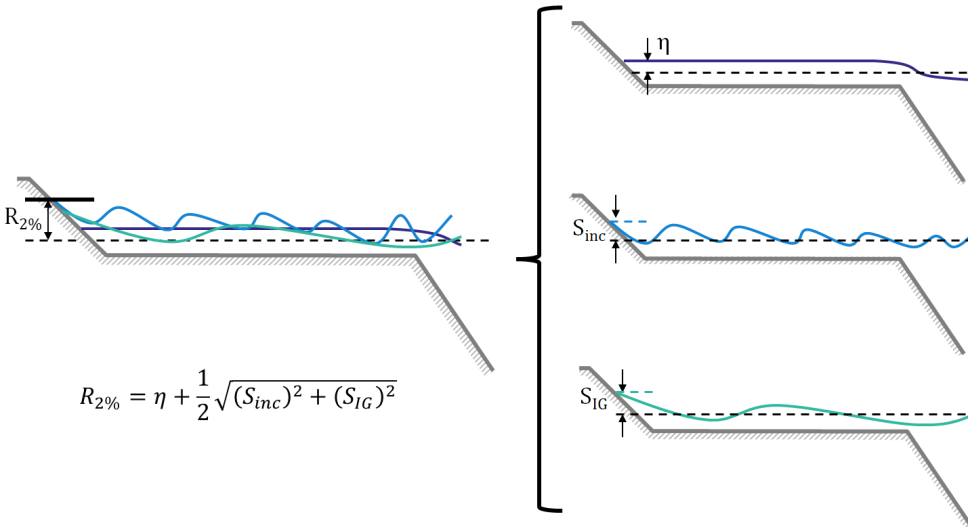

Figure 2.10: Stockdon's runup decomposition (Stockdon et al., 2006). The total runup ($R_{2\%}$) is a combination of setup ($\overline{\eta}$) and swash at incident or sea/swell (S_{inc}) and infragravity (S_{ig}) frequencies.

frequency waves and offshore water levels are the main forces driving extreme water level events at Roi Namur (Cheriton et al., 2016). In laboratory experiments, Nwogu and Demirbilek (2010) found that even though wave setup decreased with increased depth over the reef flat, increased infragravity wave contributions to runup compensated for the decrease. Although infragravity swash dominates, Gawehn (2015) determined that incident swash is still an important process to include in models of reef hydrodynamics. (Guza and Feddersen, 2012) established that infragravity swash increases with increasing frequency spread and decreases with increasing directional spread.

TIDAL MODULATION

Tidal fluctuations play an important role in determining the relative contributions of swash and setup to total runup (Becker et al., 2014; Beetham et al., 2015; Cheriton et al., 2016; Pomeroy et al., 2015; Vetter et al., 2010). Merrifield et al. (2014) found that the individual components of extreme water levels on the reef flat are tidally dependent, but tend to compensate for one another, resulting in a weak net dependency. Incident wave heights will be larger and wave setup lower at high tide, and vice versa at low tide. However, runup at the shoreline may still increase at high tide if higher energy is present on the reef flat.

Tidal fluctuations are not the only offshore water level forcing that determines runup contributions. The combination of sea-level rise and coral degradation could enable flooding of coral atolls under less extreme offshore wave heights, by increasing water depth and reducing reef flat friction, respectively (Cheriton et al., 2016). Becker et al. (2014) suggest that sea level rise will reduce the influence of wave setup on extreme water levels, since reef flat water levels and wave heights will be higher. However, Péquignet et al. (2009) suggest that this will be compensated by increased incident and infragravity

wave energy along the reef. Merrifield et al. (2014) suggest that the contribution of waves to flooding will become exponentially more important in the future than sea level rise alone, a trend that could be further compounded by changes in wave climate. Thus, it is important to understand each component of runup and how changes in forcing will influence their contributions.

2.4.2. OVERTOPPING & INUNDATION

When runup exceeds the crest elevation of the beach and begins to flow towards the hinterland, overtopping begins. Sea water overtopping an atoll due to wave action, tsunamis, or permanent submergence penetrates the porous substrate and forms a layer of denser fluid atop the freshwater lens, which then migrates downwards and mixes through the aquifer (Terry and Falkland, 2010).

Depending on the application (e.g. designing flood defense structures or evaluating pedestrian safety), different measurements of overtopping may be appropriate. Given the discontinuous nature of overtopping, a mean overtopping discharge rate may not provide enough information to characterize the situation, so maximum overtopping volumes could be more meaningful (Pullen et al., 2007).

Tolerable mean overtopping discharge rates vary depending on the safety concerns being considered. For example, (Pullen et al., 2007) define the threshold for pedestrians as 0.1 l/s/m, whereas damage to building structures begins at 1 l/s/m, and damage to grassy promenades occurs in excess of 50 l/s/m.

2.4.3. MEASUREMENT

Measurements of runup on coral atolls are scarce. Wave runup is challenging to measure in the field, since high wave forces and morphological changes in extreme events may damage in situ measurement equipment or make it difficult to relate observed runup to nearshore bathymetry Stockdon et al. (2014). Studies on Kwajalein by Quataert et al. (2015) and Cheriton et al. (2016) used a camera recording at 15 minute intervals and a series of visual markers to estimate runup height. Although this method was successful in capturing at least one major runup event, it has the disadvantage of being able to record only a small sample of actual runup conditions. Beetham et al. (2015) used a numerical model to extend their nearshore field observations to include runup, but did not have measurements at the shoreline to validate their estimates.

Runup has been measured on dikes using a series of gauges van Gent (2001), and on beaches using cameras (Ruggiero et al., 2004) and x-band radar (Hasan and Takewaka, 2009). The maximum high water mark as identified by debris can be surveyed to estimate maximum runup heights for a given event. In the absence of these sources, anecdotal evidence of flooding or crowd-sourced photographs may be used (with caution).

Since runup is so challenging to measure, Merrifield et al. (2014) instead used extreme water levels at the beach toe or inner reef flat as a proxy for runup.

2.4.4. PREDICTION

Several methods have been developed to predict runup and overtopping. Merrifield et al. (2014) suggest that it is important to break down runup into its separate components in order to better generalize formulations of the relevant processes and move away from

site-specific empirical parameterizations. Stockdon et al. (2006) developed a set of equations for beaches, van Gent (2001) for dikes, and Merrifield et al. (2014) and Blacka et al. (2015) for reefs.

Drawing on an extensive set of field observations, Stockdon et al. (2006) developed an empirical parameterization to estimate extreme runup ($R_{2\%}$) on sandy beaches. Their method decomposes total runup into time-averaged wave setup (η) and swash at both incident and infragravity frequencies (S_{SS}, S_{IG}). Stockdon et al. (2006) separate swash into separate incident and infragravity bands, since they are each forced by different processes.

A major simplification in the method of Stockdon et al. (2006) is that it relies on a single beach slope, which may not be representative of beaches that are highly concave or feature prominent bars. Abrupt changes in bathymetry at reef crests and wide, horizontal reef flats may also limit the validity of the method on coral reefs. They define beach foreshore slope ($\beta_{foreshore}$) as the average slope over the region $\pm 2\sigma$ around mean water level. They also note that for beaches, the slope of the surf zone β_{sz} (between the location of wave breaking and shoreline) may vary as a function of tide and bar evolution.

On sandy beaches, the data of Stockdon et al. (2006) suggests that infragravity waves are more efficiently generated by swell waves (characterized by low steepness (H_0/L_0)) than locally-generated sea (characterized by higher steepness). Unlike incident swash and wave setup, infragravity swash on sandy beaches shows little to no dependence on beach slope (Stockdon et al., 2006).

Stockdon et al. (2006) found that foreshore slope had a larger influence on swash than surf zone slope did. For dissipative beaches, the correlation of their formulations for swash and setup improved when slope was removed from the equation. They note that their bulk parameterization breaks down under extremely dissipative cases, which they attribute to the influence of bottom friction across wide surf zones. This may be relevant to reef settings that are dominated by dissipation due to breaking and friction, and suggest that alternative formulations may be necessary.

Further discussion about the application of Stockdon's method and other parametric runup equations to reef environments can be found in Appendix G.

3

METHODOLOGY

CHAPTER SUMMARY
This chapter explains the methods used to predict wave-induced flooding on coral atolls. First, we discuss numerical modelling with XBeach, examining the assumptions key model parameters and the general model setup. We then review the techniques used to analyze the results. We then provided background on the theory behind Bayesian networks and discuss their successful application on coastal engineering projects. The setup and use of the Bayesian network is then discussed, including the skill-testing and validation methods used.

3.1. HYDRODYNAMIC MODELLING

Bayesian networks require significant amounts of data in order to model complex phenomena like wave transformation on reefs. Datasets concerning reef morphology and hydrodynamics are few and far between. Although there is a growing number of site-specific field measurement campaigns in the literature, as yet there is no comprehensive database of the information necessary to predict wave-induced flooding of low-lying tropical islands on a large scale. To fill this need, we created a synthetic dataset by simulating many permutations of different reef characteristics and offshore forcing.

There two main approaches to hydrodynamic modelling which can be used in the creation of such a dataset: physical or numerical. Numerous studies have constructed physical scale models in laboratories to investigate reef hydrodynamics (Blacka et al., 2015; Buckley et al., 2015; Gourlay, 1994, 1996*a*,*b*; Nwogu and Demirbilek, 2010; Pomeroy et al., 2015; Yao et al., 2012). While a valuable tool for understanding physical processes in a controlled environment, physical modelling can be expensive, and it may be quite laborious to test numerous different reef configurations.

Hence, numerical modelling is an attractive solution for the development of a synthetic dataset. These models are comparatively fast, inexpensive, and offer sufficient flexibility to simulate the many permutations required. As a sort of virtual laboratory, they also allow us to test what-if scenarios that are not seen in the field, such as for climate change impact assessments There are many numerical wave models, however, and not all are equally suited to modelling reefs.

Storlazzi, Elias and Berkowitz (2015) note that passive flooding models[1], which only account for static sea level rise and not the dynamic effects of waves, are insufficient to assess flood or erosion risk on atolls.

Nwogu and Demirbilek (2010) declare that it is essential to model low-frequency waves, as well as wave breaking, setup, reflection, bottom friction, percolation, wave-induced currents, and wave-current interaction. Hence, a spectrally averaged wave model will not be sufficient to describe processes influencing reef hydrodynamics. The steep slopes and abrupt changes in bathymetry found on coral reefs may invalidate many of the assumptions inherent in numerical wave models developed for mild-sloped sandy beaches Buckley and Lowe (2013). Furthermore, wave breaking takes place in a narrower band than on sandy beaches, and frictional dissipation may be much higher, necessitating careful evaluation of a model's representation of these processes.

Long wave-resolving models like XBeach Surf Beat (XB-SB) (Roelvink et al, 2015b) are capable of reproducing low-frequency waves, and have been used successfully to model reefs (Bosserelle et al., 2015; Damlamian et al., 2015; Gawehn, 2015; Pomeroy, Lowe, Symonds, van Dongeren and Moore, 2012; Pomeroy, van Dongeren, Lowe, van Thiel de Vries and Roelvink, 2012; Quataert, 2015; van Dongeren et al., 2013). However, XB-SB cannot model incident short waves, which were identified by Gawehn (2015) as an important contribution to total runup.

Beetham et al. (2015) support the use of a short wave-resolving numerical model for representing infragravity waves and setup in simulating flooding along reefed coasts. Boussinesq models are depth-averaged and phase-resolving, solving the Boussinesq equa-

[1] "Bathtub" models, since they assume that the domain is flooded steadily and uniformly along topographic contours, much like a slowly-filling bathtub.

tions for shallow water. They have been used by Beetham et al. (2015); Kennedy et al. (2015); Nwogu and Demirbilek (2010); Roeber and Bricker (2015); Roeber and Cheung (2012); Shimozono et al. (2015); Su et al. (2015); Yao et al. (2012) to model reef hydrodynamics. Although Boussinesq wave models can be used to describe short waves, infragravity waves, and nonlinear interactions between them, Nwogu and Demirbilek (2010) caution that the use of Boussinesq wave models could be limited by steep fore reef slopes and an inability to simulate plunging breakers without a separate breaking model.

Alternatively, non-hydrostatic models can be used to resolve short waves. They do so by including a dynamic pressure term in the fluid motion equations. Wave breaking occurs when the steepness of an individual wave exceeds a pre-determined threshold. Since they represent the water surface elevation as being mono-valued, non-hydrostatic models are also unable to simulate plunging breakers. In order to simulate the vertical breaking wave face, the non-hydrostatic term is suppressed until energy is dissipated and the wave steepness drops below another prescribed threshold. Zijlema (2012) simulated wave transformation processes on a fringing reef with the non-hydrostatic model SWASH (Zijlema and Stelling, 2008; Zijlema et al., 2011), while Ma et al. (2014) used shock-capturing non-hydrostatic model NHWAVE to examine infragravity wave processes on coral reefs.

XBeach Non-Hydrostatic (XB-NH) Smit et al. (2014) has been selected for use in this thesis on the grounds of successful simulation by Quataert et al. (2015) and Gawehn (2015) of wave transformation on Kwajalein Atoll in the Marshall Islands. XB-NH is a depth-averaged model limited to relatively shallow conditions where $kh < 1$. Although it can resolve short waves, it is also computationally more expensive than its counterpart XBeach Surf Beat. This meant that certain simplifications had to be made to the model setup and parameter space in order to remain feasible.

3.1.1. PARAMETER SELECTION

The ultimate goal of the XBeach modelling phase was to develop a synthetic dataset which could be used to predict wave transformation on reefs and subsequent flooding in lieu of a dataset of field observations. Hence, it was imperative to choose parameters which were most representative of conditions to be encountered in the field.

Based on previous reef hydrodynamics studies (Chapter 2) and sensitivity analysis (Appendix B), eight primary parameters were chosen to be varied in the idealized XBeach model. Offshore water level (η_0), wave height ($H_{s,0}$), and wave steepness ($H_{s,0}/L_0$) were chosen as the hydrodynamic inputs, while fore reef slope (β_f), reef flat width (W_{reef}), beach slope (β_b), coefficient of friction (c_f), and beach crest elevation (z_{beach}) were chosen to represent the island morphology. Figure 3.1 illustrates the idealized reef profile modelled in XBeach.

Bayesian networks cannot extrapolate beyond the parameter space in which they are constructed, so the values chosen must encompass the full range of potential scenarios. However the benchmarking tests (Appendix A) established that there were strict limits to the number of parameters that could be modelled while remaining computationally feasible. Thus, the resolution of parameters within those ranges was carefully considered to provide detail for the most sensitive variables and account for the most likely scenarios. The final range of parameters selected to run in the model are summarized in Table 3.1.

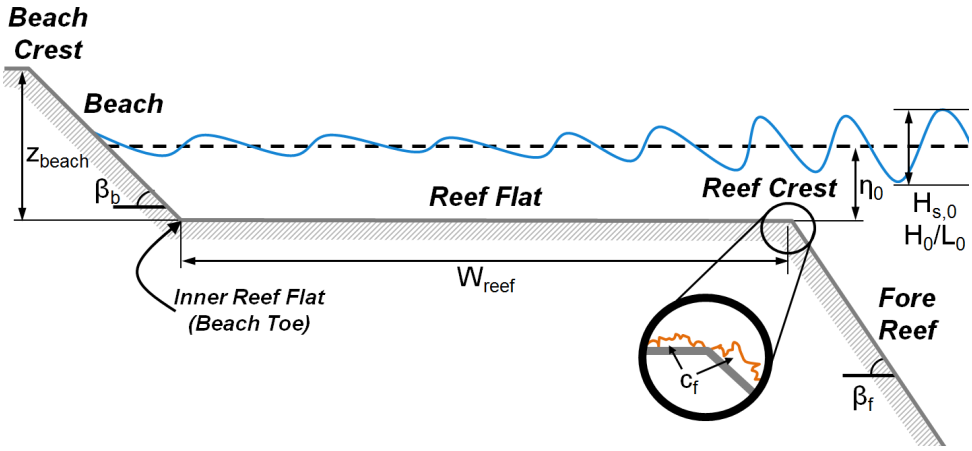

Figure 3.1: The idealized reef profile modelled in XBeach.

Table 3.1: Primary XBeach parameters and their range of values.

Symbol	Parameter	Units	Values
η_0	Offshore Water Level	m	-1, 0, 1, 2
$H_{s,0}$	Offshore Wave Height	m	1, 2, 3, 4, 5
$H_{s,0}/L_0$	Offshore Wave Steepness	-	0.005, 0.01, 0.05
β_f	Fore Reef Slope	-	1/2, 1/10, 1/20
W_{reef}	Reef Flat Width	m	0, 50, 100, 250, 500, 1000, 1500
β_b	Beach Slope	-	1/5, 1/10, 1/20
c_f	Coefficient of Friction	-	0.01, 0.05, 0.10
z_{beach}	Beach Crest Elevation	m	1, 2, 3, 4, 30

Combinations of parameters were also considered in the development of the model. For instance, scenarios with negative freeboard (where still water levels exceed the beach crest elevation) are trivial since they represent complete inundation even without considering waves. Cases like this were removed from testing to limit unnecessary computations.

Discrete uniform distributions were used for several reasons. First, there is insufficient field data to populate a dataset with real probability distributions. Secondly, at the outset of the XBeach modelling, it was unknown which parameters and combinations of parameters would be most important for the prediction of flooding, so we needed to test the whole parameter space. Future research may be able to take a more targeted approach based on the outcomes of this study. Lastly, this thesis is an attempt to generalize the findings of specific sites to a wide range of low-lying tropical islands. Thus, using the wave climate or reef characteristics of a particular island to build the model may limit its applicability. Future studies may consider a random sampling or Monte Carlo approach to provide continuous input distributions.

The following section provides brief justifications for each range of parameters used in the model based on field measurements and theory from the literature. In particular, the datasets compiled from the literature by Quataert et al. (2015) and Kolijn (2014) were valuable in deciding on suitable values.

OFFSHORE WATER LEVEL

Offshore water level is a key variable in predicting wave runup on reefs, controlling wave breaking, frictional dissipation, resonance, and reducing freeboard. Four different offshore water levels were considered to account for tidal variations and potential sea level rise. It is also important to understand how relative runup contributions of setup and wave heights at high or low frequencies changes with different tidal stages. Lowe et al. (2015) estimate that up to 30% of reefs are tidally dominated, so these variations (even at low tide) must be captured by the model in order to ensure its applicability to a wide range of locations. In his extensive review of 68 different reef sites, Kolijn (2014) found that the majority had tidal ranges between -1 to 1 m above the reef flat. Measured relative to the reef flat, we modelled offshore water levels of -1, 0, 1, and 2 m.

OFFSHORE WAVE HEIGHT

Offshore significant wave heights are also a critical parameter to include. Five different wave conditions were selected: 1, 2, 3, 4, and 5 m. As discussed in Section 1.3.3, this thesis focuses on extreme swell events expected to occur frequently enough to threaten freshwater lenses on atolls. For example, our upper bound of 5 m lies approximately within the expected 2-5 year return period range for Kwajalein in the Marshall Islands (Storlazzi, Shope, Erikson, Hegermiller and Barnard, 2015). The majority of sites compiled by Kolijn (2014) had waves less than 4.5 m, and Quataert (2015) reported a maximum observed wave height of 6 m.

OFFSHORE WAVE STEEPNESS

Wave period is a key variable in wave transformation, but for this study we instead chose to vary wave steepness. Wave steepness is the ratio between wave height and wavelength, and can be used to distinguish different sea states. Steeper waves are usually lo-

cally generated, whether by small breezes or powerful storms. On the other hand, swell waves are typically less steep. Wave period can calculated using wave height (H_0) and steepness (H_0/L_0) (Equation 3.1). This method thus produces both a broader range of wave periods with consistent sea state properties than if we varied period alone.

$$T_p = \sqrt{\frac{\left(\frac{H_0}{H_0/L_0}\right)}{g/2\pi}} \tag{3.1}$$

In order of increasing steepness, 0.005, 0.01, and 0.05 were included in the model. When combined with the five wave heights specified above, 15 unique wave periods were simulated, spanning from 3.6 (short wind waves) to 25.3 seconds (long swell waves). The full range of tested wave periods is presented in Table 3.2.

Table 3.2: Deep water peak wave periods (T_p) as a function of wave steepness and height.

	Steepness [-]		
H_0 **[m]**	**0.050**	**0.025**	**0.005**
1.0	3.6	5.1	11.3
2.0	5.1	7.2	16.0
3.0	6.2	8.8	19.6
4.0	7.2	10.1	22.6
5.0	8.0	11.3	25.3

FORE REEF SLOPE

For simplicity, a planar fore reef slope was assumed in the model. Based on measurements compiled by Quataert et al. (2015), fore reef slopes of 1/2, 1/10, 1/20 have been included in this model.

REEF FLAT WIDTH

Reef flat topography is highly variable in reality, but for simplicity a flat horizontal platform was assumed in the model. The reefs examined by Kolijn (2014) and Quataert et al. (2015) ranged from 40 to 2200 m, with an average width of 400 m. The width of a reef flat also determines its resonant frequency, so it is crucial that the parameter be modelled in enough detail to capture resonance and represent natural variability. Ultimately, we selected widths of 0, 50, 100, 250, 500, 1000, and 1500 for the model.

FRICTION COEFFICIENT

Although several studies have undertaken detailed surveys of reef roughness Jaramillo and Pawlak (2011); Nunes and Pawlak (2008); Zawada et al. (2010), the problem of translating the actual geometry of a reef into a simplified hydrodynamic roughness parameter is still largely an unresolved matter (Monismith et al., 2015). Wave friction factors change with wave and water depth conditions, whereas relative roughness remains unchanged (Nelson, 1996). Here, a dimensionless friction coefficient (c_f) with values of 0.01, 0.05,

and 0.10 were given to c_f based on numerical models for other reefs found in the literature (Table 3.3). For contrast, a typical sandy coastline has a coefficient of approximately 0.003 (Roelvink et al, 2015b), an order of magnitude less than even the smoothest reefs.

Table 3.3: Reef friction parameters from various sites in the literature. Dimensionless friction coefficients (c_f) are provided for direct comparison to the XBeach model used in this study. However, many of the sources provide only short-wave friction coefficients (f_w), which are only applicable to wave action balances and are typically an order of magnitude higher (Roelvink et al, 2015b).

	Site	c_f	f_w	Source
1	Roi-Namur, Marshall Islands	0.01-0.10	0.3	(Gawehn, 2015; Quataert et al., 2015)
2	Funafuti Atoll, Tuvalu	0.04	-	(Beetham and Kench, 2014)
3	Palmyra Atoll, Northern Line Islands	-	0.4-0.5	(Rogers et al., 2015)
4	Palmyra Atoll, Northern Line Islands	-	1.8	(Monismith et al., 2015)
5	Qita Dukais, Red Sea, Saudi Arabia	-	0.2-5.0	(Lentz et al., 2015)
6	John Brewer Reef, Australia	-	0.1	(Nelson, 1996)
7	Ningaloo Reef, Australia	0.04	0.6	(van Dongeren et al., 2013)
8	Kaneohe Bay, Hawaii, USA	-	0.3	(Lowe, Koseff, Monismith and Falter, 2005)
9	Ipan, Guam	0.06-0.20	-	(Péquignet et al., 2011)

Including spatially varying roughness in a numerical model may yield improved performance where reef topography is heterogeneous van Dongeren et al. (2013). However, Lowe, Falter, Bandet, Pawlak, Atkinson, Monismith and Koseff (2005) found that it was possible to accurately describe the effects of frictional dissipation across coral reefs by using a single hydraulic roughness value. Given that we must minimize the number of parameters in the model to maintain computational feasibility, a uniform roughness is assumed across the fore reef, reef flat, and beach.

Since roughness may also be used as a proxy for reef health (Baldock et al., 2014), incorporating it as a variable in the model lets us simulate ecological changes, whether due to climate change or reef restorations.

BEACH SLOPE

Beach slope was assumed to be planar in the model for simplicity. Based on the reflective nature of reef-fronted beaches and selected field measurements (Quataert, 2015), we selected slopes of 1/5, 1/10, 1/20 (vertical distance/horizontal distance).

BEACH CREST ELEVATION

The potential for hinterland flooding is directly related to the lowest crest elevation of an island's beach. This makes crest height a necessary parameter to investigate wave over-

topping. Greater wave reflection can be expected with a semi-infinite slope than with finite crest elevations, which could interfere with the processes on the reef flat (Nelson, 1996, 1997). However, the finite elevations complicates the calculation and comparison of runup, since runup cannot exceed the crest level. Hence for this parameter, four atoll crest heights of 1, 2, 3, and 4 m (based on Woodroffe (2008)) were simulated, along with a 30 m high semi-infinite slope for analyzing runup. This allows overtopping discharges to be computed for future use as point sources in hinterland inundation models.

3.1.2. XBEACH MODEL SETUP

This section provides an overview of the XBeach model setup and development process. Due to the dimensional limitations on the parameter space imposed by computational feasibility requirements, some parameters of interest were held fixed. Benchmarking and quality control tests were conducted to estimate simulation times and ensure a stable model. Analysis of the literature and sensitivity tests were then carried out to determine the most important parameters to include. Once the model setup had been finalized, the main simulations were run.

Four main phases of XBeach modelling were carried out:

- Model Setup
- Benchmarking & Quality Control (Appendix A)
- Sensitivity Testing (Appendix B)
- Main Simulations (Appendix D)

The procedures used to set up, preprocess, and post-process the XBeach simulations are illustrated as flow charts in Appendix C.

COMPUTATIONAL GRID AND BATHYMETRY

A one-dimensional (1D) grid was chosen with an idealized reef profile as per Figure 3.1. Modelling the wave-induced flooding of atolls using a simplified 1D model by definition may exclude several relevant processes. van Dongeren et al. (2013) found improved model performance from a 2D XBeach reef model over 1D. As islands, atolls can be affected by forcing from all directions, including from their interior if a lagoon is present (McLean and Kench, 2015). This makes atolls highly three dimensional, but in order to assess a wide range of reef morphologies and hydrodynamic forcing conditions, a simpler model was chosen to reduce computational expense.

Grid resolution varies between simulations, depending on the reef dimensions. It was determined by satisfying Courant number stability and a minimum of 64 grid points per wavelength. Maximum and minimum cell sizes were defined as 0.25 and 1 m, respectively, to ensure sufficiently high resolution in areas of interest (e.g. beach slope) but remain computationally feasible.

During initial sensitivity tests carried out to set up the model, it was discovered that estimates of runup did not converge when grid resolution was increased. This can be attributed to the steeper water surfaces at wavefronts which finer grids permit. Thus, maximum wave height has a dependency on grid resolution which is moderated by the maximum wave breaking steepness. When the steepness limit was reduced from the default 0.6 to 0.4 (as per the recommendations of Roelvink et al, 2015a), the model converged. Details of this sensitivity analysis are provided in Appendix B.

The location of the offshore boundary was dynamically adjusted depending on the hydrodynamic forcing for a given simulation. Depth at the boundary h was set such that $kh = 1$, where $k = 2\pi/L$ and L is wavelength. This limit was set to ensure that the modelled depth remained within the validity of XBeach Non-Hydrostatic's assumptions for dispersion (Smit et al., 2014). The model approximates dispersion well when $kh < 1$, but loses significant accuracy beyond that threshold since linear wave theory is no longer valid. A check was also performed to ensure that depth-limited wave breaking did not occur immediately at the boundary (Appendix B).

A short (4 grid cells) flat step extends out from the boundary before the fore reef slopes upwards at the prescribed β_f to reach the reef flat (0 m elevation). Although algal or coral ridges are frequently observed at reef crests in the field, they were excluded from the model for reasons of simplicity (see Appendix B). The reef flat extends a distance W_{reef} horizontally, and then slopes upward again at β_b. At the crest (elevation z_{beach}), there is a flat section followed by a negative slope towards the rear model boundary. This slope ensures that any water overtopping the beach crest drains promptly from the model domain so as to maintain unidirectional flow through the discharge monitoring point.

BOUNDARY CONDITIONS

The offshore boundary conditions (water level, significant wave height, and peak period) were specified as per the values chosen in Section 3.1.1, and held constant for the duration of each simulation. However, other hydrodynamic parameters were fixed for all simulations, including spectral properties. Each scenario simulated random waves according to a fixed spectrum for four 30 minute periods. Special attention was also given to setting the boundary and initial conditions such that stationary conditions were ensured during the tests.

Multimodal spectra (in both frequency and directional space) are highly prevalent in the tropical Pacific, on account of consistent swell generation by trade or monsoon winds and distant sources in mid-high latitudes (van Vledder, 2015). However, we assumed a unimodal, unidirectional JONSWAP spectrum for simplicity. Beetham et al. (2015) found that using a parametric JONSWAP wave field gives similar model results to using measured wave spectra. Incident wave direction was conservatively chosen to be shore-normal for all cases, since this should yield maximum runup for a given wave height and steepness. Furthermore, directional spreading was also fixed because of the 1D profile.

The theoretical basis for including spectral shape ($\gamma_{JONSWAP}$) is rooted in its role in determining wave groupiness. The energy in narrower spectra is clustered around a smaller frequency band, allowing for more coherent wave groups to form. Furthermore, Bosserelle et al. (2015) note that multiple swell systems converging on a site could make groupiness an important consideration. Using wavelet analysis, Li et al. (2015) found that groupiness increased as a function of $\gamma_{JONSWAP}$. The presence of wave groups will in turn affect the formation of bound long waves and the dynamic setup of the breakpoint mechanism, which should increase wave heights near the shore.

However, previous studies have found no significant correlation between offshore wave groupiness and reef flat behaviour (Cheriton et al., 2016; Gawehn, 2015; List, 1991).

A sensitivity analysis of spectral shape (specifically the peakedness of the JONSWAP spectrum, $\gamma_{JONSWAP}$) was carried out in Appendix B.2. These results suggest that there is only a very weak relationship between spectral shape and the parameters we are interested in, so $\gamma_{JONSWAP}$ was fixed in the model at the default value for wind seas of 3.3.

For computational efficiency, we reused the same hydrodynamic boundary conditions for each scenario featuring the same hydrodynamic inputs and reef width. This procedure is illustrated in Appendix C.

INITIAL CONDITIONS

A key requirement for the validity of the model simulations is stationarity. To provide meaningful assessments of how each parameter changes the output, conditions must be held fixed across the entire tested duration. Since all simulations start with still water conditions, it takes time for the model to reach a steady state with the tested parameters. This stationary state is achieved when mean water levels and wave characteristics stay consistent for the period of interest (e.g. 30 minutes). To ensure this, we allow the model to "spin up" for a brief period, before we begin recording the model outputs.

For instance, in order to calculate runup at the shoreline, waves must first propagate from the offshore boundary across the model domain to reach the shore. If the waves do not reach the shore, or if they only do so partway through the simulation, then one cannot make a fair comparison with other tested scenarios where the shore is subjected to wave action throughout the simulation period. However, it is not just waves reaching the beach that constitutes reaching stationarity- wave setup on the reef flat also needs to reach steady state. It may take quite some time for the waves to physically transport enough water onto the reef flat to fill the semi-enclosed basin and balance the radiation stresses imposed at the reef crest.

For this model, required spinup time is primarily governed by reef flat width, offshore water level, and to a lesser extent by wave height, wave period, and friction. Hence, the required spinup times may vary significantly between runs. If a fixed spinup time is used for all simulations, then we risk either not running for long enough, or unnecessarily long computational times. Early tests found that 300 seconds (5 minutes) was sufficient in 87% of simulated cases.

Even with this revised spinup, not all simulated cases reached stationary conditions. However, the increased spinup (up to 2 hours for the widest reefs) became computationally infeasible, so non-stationary runs had to be filtered out. We compared setup ($\overline{\eta}$) at the inner reef flat between the n^{th} and last of four simulated 30 min bursts. If the ratio of $\overline{\eta_n}/\overline{\eta_4}$ was < 0.95, it was assumed that the model had not yet reached stationary conditions, and the first n bursts were discarded from the analysis. Without removing them, the model results might be biased by lower water levels or wave conditions. Hence the results could be less conservative and predict reduced flooding.

In particular, simulations representing low tide (-1 or 0 m) took longer to spin up. To remedy this, a thin layer of water was initially placed on the reef flat. This was justified on the basis that under tidal conditions, the reef flats do not drain fully during the course of a single tidal cycle. Lowe et al. (2015) they found that for macrotidal reefs, ponding is usually widespread (but highly spatially variable).

To test this hypothesis for the current model setup, a series of 24 hour tests were conducted with diurnal and semi-diurnal tidal cycles. To test reef flat drainage during

rising and falling limbs of the tide, water levels were initially either +1 m or -1 m. Even for diurnal cycles (allowing 6 hours to drain), the widest reef flats (1500 m) would not fully drain ($\eta_{min,beach} = 0.08m$ for semi-diurnal cycles and $\eta_{min,beach} = 0.12m$ for diurnal cycles). On this basis, a logarithmic curve was fit to the water surface profile at low tide: $\eta(x) = 0.0105log(x - x_{crest})$, where η is initial water level, x is a given point on the reef flat, and x_{crest} is the horizontal position of the reef crest. This profile was then used to hotstart the model when water levels were less than reef flat level.

FIXED PARAMETER SETTINGS

Unless otherwise noted, all XBeach parameters were set to their default values (see Roelvink et al, 2015b). Full details of parameter specifications are provided in Appendix C. Lowe, Falter, Bandet, Pawlak, Atkinson, Monismith and Koseff (2005) cite appropriate parameterization of frictional dissipation and wave breaking processes as a key challenge to modelling wave transformation across reefs. Based on sensitivity analysis carried in Appendix B, the maximum wave breaking steepness was set to 0.4, in line with the recommendations of Roelvink et al, 2015a.

LIMITATIONS

There are several key limitations to the model developed here:

- One-dimensional model
- Simplified reef profile
- Shore-normal, long-crested waves
- Unimodal JONSWAP spectrum
- Uniform friction

These simplifications were necessary to carry out the numerous simulations needed to create the synthetic dataset.

3.1.3. ANALYSIS METHODS

This section outlines the main tools and procedures used to post-process the XBeach model results. The main post-processing procedure is illustrated as a flow chart in Appendix C. To simulate the full parameter space defined in Section 3.1.1, a total of 53,865 different permutations were required.

Each of the simulations (model runs) were broken up into 5 main segments: the spinup period (not used), and 4 × 30 minute bursts for analysis. The 30 minute bursts were chosen for reasons of stationarity (Holthuijsen, 2007) and comparability to field measurements recorded in 15-35 minute bursts Beetham et al. (2015); Bosserelle et al. (2015); Quataert et al. (2015); Stockdon et al. (2006). Furthermore, the analysis periods needed to be long enough to capture low frequency waves, which may have periods exceeding 15 minutes. To obtain the standard runup statistic $R_{2\%}$, at least 100 waves are necessary, which takes 30 minutes for 18 s swell waves. Lastly, using four 30 minute bursts increases the randomness of the dataset, since each period will experience slightly different conditions even though the average forcing is consistent.

The statistics obtained for each burst provide a unique set of data points which serve as individual "cases" in the Bayesian network analysis of Sections 3.2 & 4.2. Bursts not

satisfying the stationarity criteria specified in Section 3.1.2 were filtered from the data, leaving 186,314 bursts or cases in total. Unless otherwise specified, the analyses below were also filtered by beach crest elevation to include only scenarios with a 30 m height. This removes the cutoff effect imposed by crests of finite elevation. The final dataset used for runup comparisons thus contains 39,352 unique bursts or cases.

Six monitoring points were included in the model (Figure 3.2). They were located just inside the offshore boundary, at $kh = 0.5$ on the fore reef, at the reef crest, at the midpoint of the reef flat, at the inner reef flat (toe of beach), and at the rear of the beach crest (for measuring overtopping discharge). A runup gauge was also placed along the length of the profile to track the maximum landward extent of the water surface.

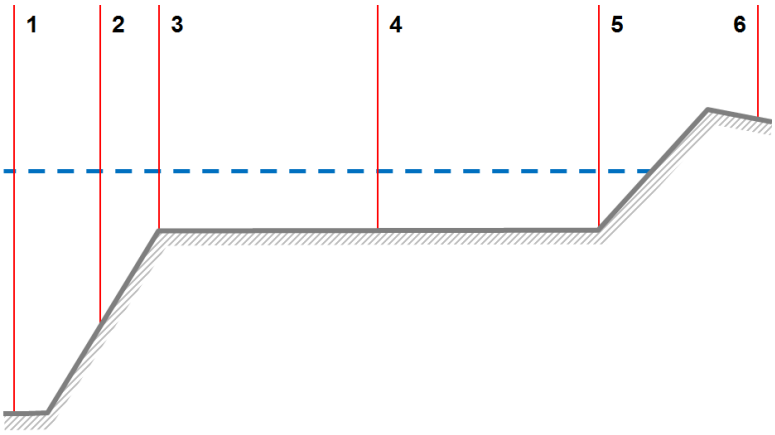

Figure 3.2: Schematic of monitoring points in the XBeach model. (1) Offshore boundary; (2) Fore reef (kh = 0.5); (3) Reef crest; (4) Midpoint of reef flat; (5) Inner reef flat/beach toe; (6) Overtopping discharge gauge at rear of beach crest; (7) Moving runup gauge (not depicted).

Runup ($R_{2\%}$) was calculated based on a time series of vertical elevation at the maximum landward excursion of the water surface. Runup values were sorted in descending order and the 2% index was selected to determine $R_{2\%}$. To calculate swash, the runup time series was split using band pass filters into high and infragravity frequencies (Table 2.2). H_{rms} for each band was then calculated based on the variance of the time series.

Overtopping discharge (q_{OT}) was determined by measuring the mean volumetric flux $[l/s/m]$ at the rear crest of the beach over the course of a 30 minute burst.

Wave height at the inner reef flat determined by detrending the water level time series and decomposing it into three frequency bands (Table 2.2). Power spectra were calculated for each separate time series, from which H_{rms} was calculated.

Wave setup ($\overline{\eta}$) was calculated by subtracting the offshore water level η_0 from mean water level at the inner reef flat. The mean water depth on the reef flat (h_{reef}) was calculated from the average depth at monitoring points 3, 4, and 5. Freeboard can be defined as the difference between the beach crest elevation and either mean or still water level. Negative freeboard thus denotes continuous inundation.

van Gent (2001) found that the mean spectral period $T_{m-1,0}$ was the most suitable characteristic wave period for estimating runup and overtopping, particularly for multi-

modal spectra. The mean spectral period at the inner reef flat was calculated by taking moments of the total spectrum ($T_{m-1,0} = m_{-1}/m_0$). The mean spectral frequency is just the inverse: $f_{m-1,0} = 1/T_{m-1,0}$.

The reflection coefficient was calculated by taking the ratio of outgoing to incoming waves near the offshore boundary, using the method of Guza et al. (1984) to separate the components using water surface elevation and pressure.

3.2. BAYESIAN NETWORK

A Bayesian network (BN) is a probabilistic graphical model. A deterministic, process-based model like XBeach provides a definite output for a given set of input parameters and initial conditions. Instead, a probabilistic model is a statistical tool that provides a probability distribution of likely outputs. As such, Bayesian networks can be used to predict the likelihood of flooding for a particular island given certain hydrodynamic forcing.

If the physical processes involved in reef hydrodynamics are too complex to fully understand, then a probabilistic model may be a useful tool for exploring the relationships between parameters. Furthermore, they can help us focus our modelling efforts or data collection to help us improve our understanding of physical processes. They also allow us to interpolate between conditions not explicitly modelled and account for the uncertainty in island properties or forcing by adjusting input distributions. Bayesian networks are also an effective data management tool for organizing large datasets and sorting or filtering them based on the causal and statistical relationships between variables.

This section provides a brief introduction to Bayesian probability, then provides examples of the use of Bayesian networks for coastal engineering applications. The setup of the Bayesian network in Netica is reviewed, and then the methods used to analyze and validate the BN are explained.

3.2.1. BAYESIAN INFERENCE

Bayesian inference is a statistical method to determine how our belief in something (or prediction) changes with evidence or new information. It is a fundamental part of reasoning both in science and in everyday life. This is done by expressing probability in terms of conditional relationships that make explicit the statistical dependencies between variables. Conditional probabilities ($P(x \mid y)$) define the likelihood of x under the assumption that y is known with absolute certainty (Pearl, 1988). At the heart of Bayesian inference is Bayes' theorem (Bayes and Price, 1763), which is given by:

$$P(x \mid y) = \frac{P(y \mid x)P(x)}{P(y)} \tag{3.2}$$

Where $P(x \mid y)$ is the conditional (posterior) probability of observing x given that y occurs, $P(y \mid x)$ is the conditional probability of observing y given that x occurs, $P(x)$ is the independent (prior) probability of x occurring, and $P(y)$ is the independent probability of y occurring.

Without any additional information, we can predict the likelihood of x using its prior probability. Consider the probability that wave heights will exceed 10 m at a given island tomorrow. The prior probability considers all possible cases, so $P(x)$ might be 1/10,000:

highly unlikely. Our "belief" is low. At this particular island, 10 m waves are typically associated with hurricanes, which occur very rarely. However, if we know that a large hurricane is tracking straight towards that island and will arrive within a few hours, the probability of 10 m waves occurring tomorrow changes drastically, and $P(x \mid y)$ becomes 1/3: very likely.

This "Bayesian updating" is a structured way to combine new information with our previous understanding of a system. Bayesian Networks allow us to determine how the degree of belief in a proposition will change depending on the available evidence (den Heijer et al., 2012).

Bayesian networks build on these concepts by graphically representing the statistical relationships between variables using a series of nodes and connections. The nodes represent different variables, and the connections (as unidirectional arrows) indicate causal relationships between them. The BN computes these conditional probabilities by learning from empirical datasets (training). With sufficient input, it can generalize probabilistic trends and be used to make predictions about new scenarios. This will be illustrated by way of an example in Section 3.2.3.

Bayesian Networks have been used in fields as diverse as medicine (Kahn et al., 1997), forestry (Zwirglmaier et al., 2013), dam safety (Hanea et al., 2015), ecology, (Gieder et al., 2014) risk and reliability assessments, and traffic prediction (Sun et al., 2006). Numerous Bayesian network software packages are available, including Netica (Norsys, 2003), Genie (Decision Systems Laboratory, 2016), and Uninet (Lighttwist Software, 2016). Based on its successful use in several coastal engineering applications, Netica has been chosen for this project.

3.2.2. BAYESIAN NETWORKS IN COASTAL ENGINEERING

Bayesian networks are an attractive tool for coastal engineering applications. Complex coastal environments are typically simulated using computationally demanding numerical models. Bayesian networks can use the results from these models to develop predictions, enabling engineers to extend their applicability probabilistically (den Heijer et al., 2012). Unlike deterministic process-based models, Bayesian Networks provide not just an expected outcome, but also indicate the uncertainty surrounding that prediction (Plant and Holland, 2011*b*). This is especially useful in situations where accurate input data is limited and prediction errors are likely, as it can prevent users from having false confidence in their model results.

They are useful where our grasp of physical processes are limited, since we can instead make sense of the system using probabilistic relationships. They are also a fast and effective tool for assimilating large datasets. Bayesian Networks can be applied for several purposes, including the calculation of posterior probabilities, most likely explanations, rational decision-making, and analyzing the effects of interventions (den Heijer et al., 2012).

The Sendai framework calls for rapid and effective disaster response (UNISDR, 2015, 34(a)). A key advantage of using Bayesian Networks instead of hydrodynamic process-based models for operational flood forecasting is their speed and portability (Jäger, den Heijer, Bolle and Smets, 2015). Process-based numerical models may require significant time to set up, run, and analyze; they also need high-performance computers. Bayesian

networks are much faster, can be run from a laptop, and can be updated in real time as conditions change or improved data becomes available. Hence, they may provide better decision-making support in emergencies.

As a result of these advantages, Bayesian networks and analysis techniques are growing in popularity for coastal applications. They have been used for studies of storm impacts (den Heijer et al., 2012; Jäger, den Heijer, Bolle and Hanea, 2015; Jäger, den Heijer, Bolle and Smets, 2015; van Verseveld et al., 2015), reliability of flood defenses (Schweckendiek et al., 2014), early flood warning systems (Balbi et al., 2015; Poelhekke, 2015), inundation pathways (Narayan et al., 2015), coastal zone management (Hoshino et al., 2015), coastal groundwater (Fienen et al., 2013), 1D surf zone wave models (Plant and Holland, 2011*a*,*b*), large-scale sea level rise vulnerability (Bulteau et al., 2015; Gutierrez et al., 2011; Lentz et al., 2016; Plant et al., 2016), wave overtopping prediction (Tolo et al., 2015), and geomorphological predictions (Audrey et al., 2013; Gutierrez et al., 2015; Hapke and Plant, 2010; Wilson et al., 2015). They have also been used in coral reef settings for ecological analyses (Ban et al., 2015; Franco et al., 2016).

In light of their successful application to other coastal environments, we have chosen to develop a Bayesian network for flood prediction on coral atolls and other low-lying tropical islands.

3.2.3. NETICA MODEL SETUP

Developing a Bayesian Network is an iterative process. den Heijer et al. (2012) identify four key steps in developing a BN: data collection, building the network, training it, and validation.

The eight primary input parameters varied in the XBeach simulations were divided into two different sets: hydrodynamic and reef morphology parameters. There are many possible output parameters to choose from, but the most useful were selected: mean overtopping discharge ($q_{OT,mean}$), runup ($R_{2\%}$), wave height at the inner reef flat for SS, IG, and VLF frequency bands ($H_{s,SS}, H_{s,IG}, H_{s,VLF}$), setup ($\overline{\eta}$), and mean spectral period ($T_{m-1,0}$) at the inner reef flat. In some tests, the overtopping was excluded because the inclusion of a finite beach crest height made it difficult to compare trends in the results. In many of the tests, wave heights, runup, and setup were normalized by offshore wave height to make it easier to identify trends independent of wave height.

Equation 3.3 shows the underlying mathematical structure of our Bayesian network, where the conditional probability of each output variable given the input variables is a function of the total probability of all the variables.

$$\begin{aligned} p(q_{OT,mean}, R_{2\%}, H_{s,SS}, H_{s,IG}, H_{s,VLF}, \overline{\eta}, T_{m-1,0} \mid \\ H_{s,0}, H_{s,0}/L_0, \eta_0, \beta_{forereef}, W_{reef}, \beta_{beach}, z_{beach}, C_f) \\ = f[p(q_{OT,mean}, R_{2\%}, H_{s,SS}, H_{s,IG}, H_{s,VLF}, \overline{\eta}, T_{m-1,0} \\ H_{s,0}, H_{s,0}/L_0, \eta_0, \beta_{forereef}, W_{reef}, \beta_{beach}, z_{beach}, C_f)] \end{aligned} \quad (3.3)$$

DATA COLLECTION

Bayesian Networks are data-intensive, requiring a large pool of information in order to calculate probabilistic relationships between the variables of interest. Ideally measured historical data should be used to construct this dataset. However, given the paucity of hydrodynamic data available for coral reefs and the diverse geography of atolls, a synthetic dataset was required.

The synthetic dataset generated using XBeach forms the basis for our Bayesian Network. However, field observations, or a synthetic dataset constructed by other means could also be used in future applications. The parameters were initially selected with the end goal of developing a BN. Ideally, the input parameters which have the greatest influence on the flooding will be used. Hence, the selection of parameter range is important.

However, it was an iterative process, and as the BN was developed, the XBeach model setup was adjusted. For instance, a maximum beach crest elevation of 5 m was originally simulated, which made direct comparisons with other runup calculations impossible when runup exceeded that value. In subsequent XBeach model runs, a semi-infinite slope was simulated to ensure comparability in later validation.

The complexity of a Bayesian Network increases with the dimensionality of the dataset being modelled (Plant and Holland, 2011*b*). As such, there is a need to strike a balance between including enough variables to represent the phenomena of interest and keeping it simple enough to be computationally feasible.

Figure C.3 in Appendix C provides a flow chart of this process.

NETWORK STRUCTURE

Bayesian Networks consist of nodes and connections, which specify variables and the relationships between them. These relationships may be causal, functional, or based on statistical correlations, and can be expressed in terms of conditional probabilities (Norsys, 2003). The input nodes are the same as the varied parameters from XBeach, and the output nodes were selected based on variables of interest for further analysis (e.g. overtopping volumes) or quantities frequently compared in the literature (e.g. transmission coefficient). Runup was selected as the main output variable, so for this analysis, simulations with finite beach crest elevations were excluded. Initially, all input nodes were connected to all output nodes, although these connections were later varied to test sensitivity.

Several different network structures were developed, although one main layout (Configuration A) was used for the majority of tests carried out. After analyzing the XBeach results (Section 4.1.2), it was clear that wave height had a direct influence on runup and overtopping. To minimize this dependency and uncover more anomalous events (as might be associated with resonance), wave heights, setup, and runup were normalized by offshore wave height in Configuration A. This exaggerated the differences between high and low values to better indicate output conditions which are surprisingly high given the input conditions. These events will be more likely to catch forecasters off guard, so it was important to understand the conditions that cause them. Figure 3.5 shows the structure of Configuration A. Full networks are shown in Appendix E.

Four other network configurations were tested in detail: Configuration B, which is identical to A but with only two bins per output parameter, and Configuration C, which

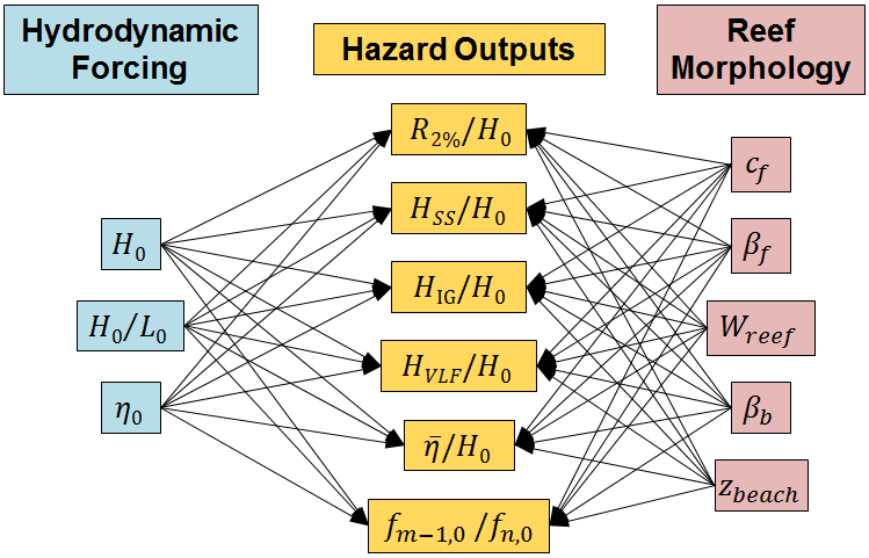

Figure 3.3: Simplified schematic of Bayesian network Configurations A & B, which features output variables normalized by offshore wave height. Hydrodynamic input variables are shaded in blue, reef morphology input variables in red, and output variables in yellow.

is also identical to A but with reef width as the only morphological input. This is meant to represent a hypothetical scenario where no information about reef characteristics is available, apart from reef widths obtained via remote sensing.

Figure 3.3 shows the structure of Configurations D and E, for which the output variables were not normalized. This version was used in the validation against field data, so as to make the inputs and outputs directly comparable with the available information.

In order to represent the model variables as probabilistic distributions, the dataset is divided into bins. Input variables were discretized using the same parameter values as were tested in XBeach, resulting in uniform, discrete distributions.

Discretization of output variables required more careful consideration, since they were continuously distributed. The chosen bins should take into account both the desired precision of the predictions and the distribution of data. For instance, resonance happens in a narrow band defined around $f_{m-1,0}/f_{n,0} = 1$, so it may be appropriate to use bins from 0.95-1.05, and much larger bins outside that range of interest. The bins may also be defined based on logical states, such as "overtopping" or "no overtopping".

Plant and Holland (2011*a*) propose three main requirements for discretizing nodes. Intervals should be:

1. As wide as possible to reduce the computational effort.
2. Sufficiently narrow to provide meaningful forecasts and resolve the uncertainty
3. Sufficiently wide to capture multiple data points (i.e. they should not be empty)

Figure 3.6 shows the discretization used for this network. A histogram with many bins was first used to get a sense of the underlying distribution of the data. Larger bins

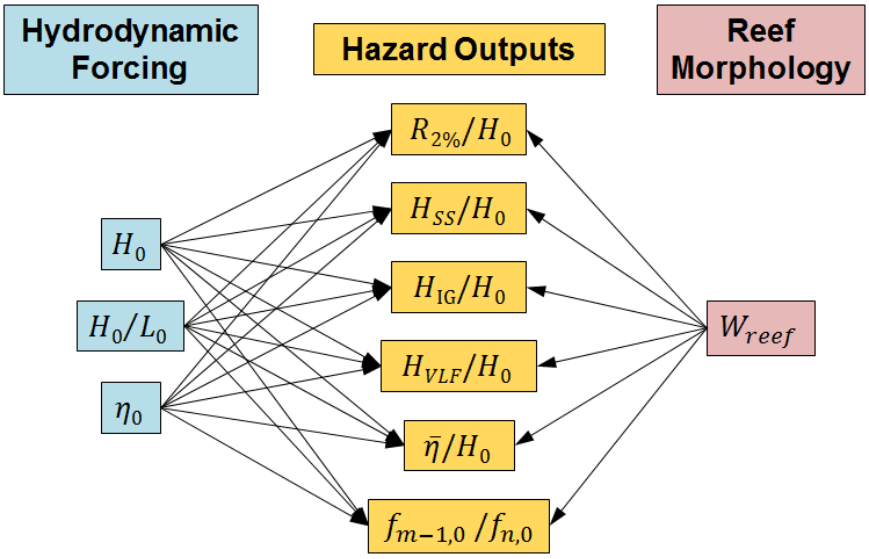

Figure 3.4: Conceptual layout of Bayesian network Configuration C, which features output variables normalized by offshore wave height, and reef width as the sole reef morphology parameter. Hydrodynamic input variables are shaded in blue, reef morphology input variables in red, and output variables in yellow.

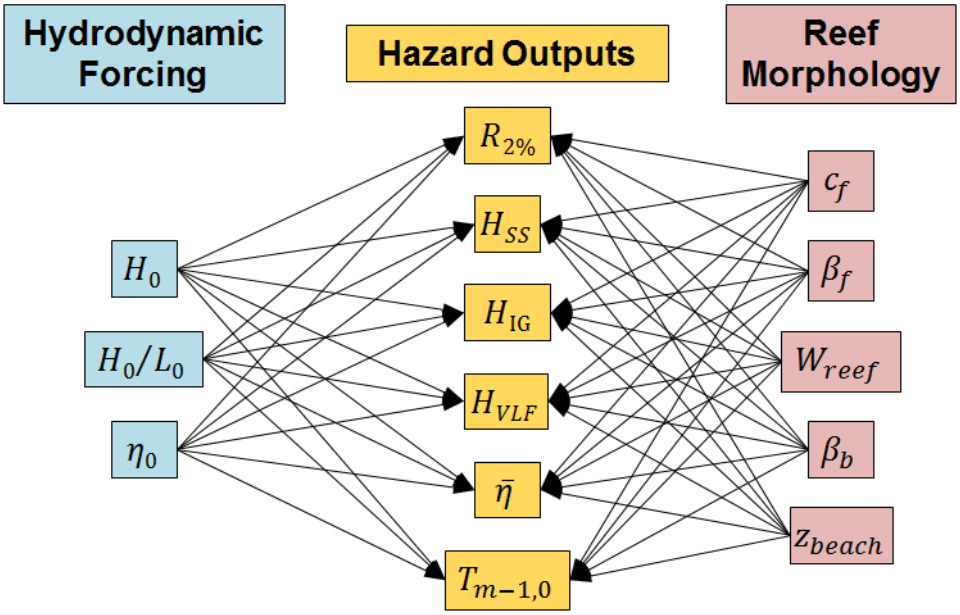

Figure 3.5: Simplified schematic of Bayesian network Configuration D. Hydrodynamic input variables are shaded in blue, reef morphology input variables in red, and output variables in yellow.

were then defined so as to break the dataset into large and groups, as per the guidelines above.

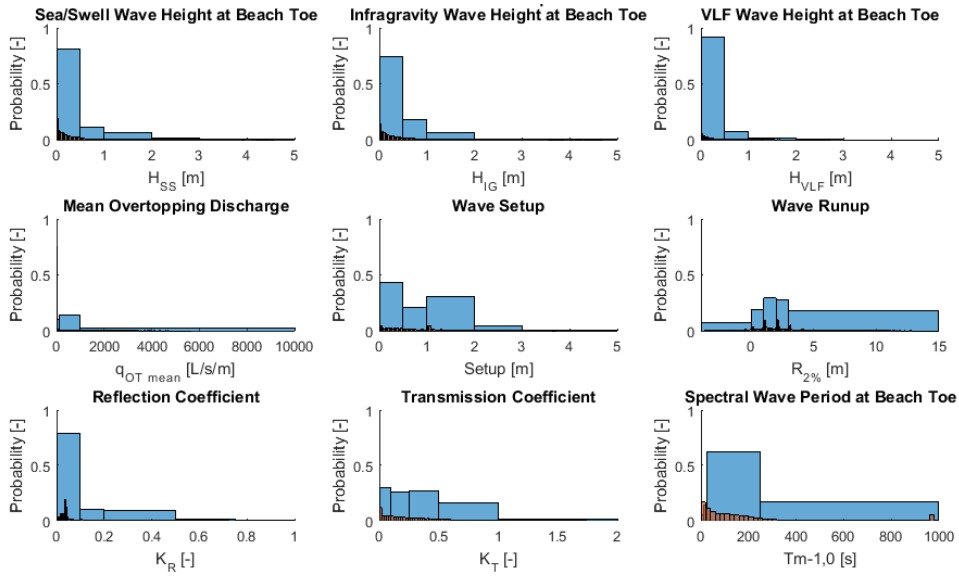

Figure 3.6: The blue bins show the groupings manually selected for use in the Bayesian network, while the very small orange bins show the underlying distribution at a much finer resolution. This distribution was used to guide the discretization process by ensuring that important breaks in the data were captured well.

In discussing discretization, it is important to consider the relative importance of precision and accuracy. A node with many bins will be more precise, for instance providing estimates of runup to within 0.1 m. However, in asking for such a precise answer, accuracy may be lower. On the other hand, a node with two bins cannot give a very precise answer (e.g. 'flooding' or 'not flooding'), but may be correct much more frequently. The choice to prioritize precision or accuracy depends very much on the intended use of the network.

TRAINING

Training a Bayesian Network entails calculating the conditional probabilities of each node in the network based on available data. A key constraint in the development of a BN is that predictions can only interpolate within the provided ranges of input data and cannot extrapolate out to parameter combinations outside those values (den Heijer et al., 2012). As such, it is important to ensure that the training dataset is large enough to encompass the natural variability expected for the site of interest.

In Netica, a "case" refers to a specific combination of modelled or observed inputs and outputs. Each of the four analysis bursts for all model runs were considered, for a total of 186,314 unique cases. Networks that compared runup and not overtopping were filtered to exclude simulations that did not meet stationarity criteria and with beach crest elevations < 30 m, resulting in a total pool of 39,352 cases. These were extracted from the

XBeach models and compiled into a single table using MATLAB. The variables of interest were then exported to Netica using the OpenEarthTools MATLAB toolkit[2].

Netica then assimilates the training cases to construct conditional probability tables (CPT). These CPTs are the reason for Bayesian networks' speed when compared to process-based models: by pre-computing all of the statistical relationships between different variables, the network can use the CPTs as a simple look-up table given user inputs. In that regard, Bayesian networks can be thought of as similar to spreadsheets or pivot tables which can filter and sort data. However, the functionality of Bayesian networks goes beyond merely filtering data and presenting it graphically, given their ability to generalize trends and predict new scenarios.

Plant and Holland (2011*b*) suggest that experimenting with Bayesian Networks can yield new insights about correlations between coastal processes and identify knowledge gaps. The combined use of all these tools enables both scientists and decision-makers to better understand coastal flooding and make decisions accordingly. This type of sensitivity testing is where some of the greatest value of Bayesian networks lies.

The spread in comparisons of predictions and observations can be reduced by increasing the number of bins used for every variable in the network, although this comes at the cost of requiring additional training data den Heijer et al. (2012).

3.2.4. ANALYSIS METHODS

A key question in the application of Bayesian networks is how well they can reproduce the observed phenomenon and model results upon which they are based (den Heijer et al., 2012). Three main analyses are carried out here for the BN: assessments of predictive skill, validation against cases from the literature, and sensitivity analyses.

The analyses of predictive skill are used to determine the ability of the network to make predictions based on our synthetic dataset. They allow us to answer questions such as:

- Which network makes the best predictions?
- Which variables are most important?
- How often do we make correct predictions?
- How well can the network learn and generalize trends?

Netica provides numerous output statistics that can be used to assess performance, but this study focuses on just three: log-likelihood, confusion matrices, and overfitting. A flow chart to demonstrate the predictive skill-testing procedures is provided in Appendix C.

However, answering those questions about predictive skill only tells us how well the network predicts the XBeach results. To ground-truth the BN, we must validate using field observations. Although the availability of useful observations is extremely limited, these tests are nevertheless an important indicator of the network's value and may provide direction for future improvements.

Having established our confidence in the network through these tests, we can then conduct sensitivity analyses to explore relationships between different variables. For

[2] Available here: https://publicwiki.deltares.nl/display/OET/OpenEarth

instance, simplified networks featuring only two or three nodes of interest can be used to isolate the influence of specific variables on complex phenomena like resonant low frequency anomalies.

LOG-LIKELIHOOD TESTS

The first test of predictive skill is the log-likelihood test. It allows us to compare the value of different network layouts and determine which variables are most important in the BN. The test is based on the log-likelihood ratio (LLR), which provides an indication of both predictive skill (how well the mean prediction approximates observed values) and the relative uncertainty (Plant and Holland, 2011*b*). The LLR for assessing a network's predictive skill relative to the prior distributions can be calculated as:

$$LLR_j = log_{10}\left\{P\left(F_i \mid \tilde{O}_j\right)_{F_i=O_j}\right\} - log_{10}\left\{P\left(F_i\right)_{F_i=O_j}\right\} \tag{3.4}$$

Where $P\left(F_i \mid \tilde{O}_j\right)_{F_i=O_j}$ is the posterior (updated) probability given some observation O_j. $P\left(F_i\right)_{F_i=O_j}$ is the prior (initial) probability for a given forecast (F_i), and j is an index denoting a particular test case. To examine the network's overall predictive skill, the sum of LLRs for all tested cases is compared.

The LLR severely penalizes "over-confident" predictions that are wrong but with a high degree of certainty more than incorrect predictions with low certainty (Plant and Holland, 2011*b*).

It is also possible to compare the predictive skill of two different networks by comparing their posterior probabilities:

$$LLR_j = log_{10}\left\{P\left(F_{1,i} \mid \tilde{O}_j\right)_{F_{1,i}=O_j}\right\} - log_{10}\left\{P\left(F_{2,i} \mid \tilde{O}_j\right)_{F_{2,i}=O_j}\right\} \tag{3.5}$$

Where $P\left(F_{1,i} \mid \tilde{O}_j\right)_{F_{1,i}=O_j}$ is the posterior probability of network 1 and $P\left(F_{2,i} \mid \tilde{O}_j\right)_{F_{1,i}=O_j}$ is the posterior probability of network 2.

Figure 3.7 demonstrates the log-likelihood calculation for an arbitrary test case with observed runup of 16 m. This value falls in the 15 to 30 m bin (highlighted in orange), so the model's predictions of this bin under various scenarios is examined. The prior prediction (a) represents the base probability distribution for all cases in the dataset, with no specific information about input conditions (i.e. wave conditions and reef characteristics). When updated input information is provided to the network for a particular case, it updates the runup probability distribution. Four examples are provided here to demonstrate what makes a particular prediction good or bad.

For a perfect prediction (b), the network predicts the correct bin with 100% certainty, resulting in the highest possible log-likelihood ratio for this case. A good prediction (d) is one that chooses the correct bin with a relatively high degree of certainty (53%). This results in a positive LLR score, since the network provides a better prediction than the prior distribution alone. A much lower LLR score is given when the network hedges and predicts a uniform probability distribution (c). A result like this indicates that uncertainty is too great for the network to make a confident prediction. Bad predictions (e) may also result from wrong but confident predictions. In this case, the network predicts that runup will fall in the 10 to 15 m range with a high degree of certainty (57.6%), and

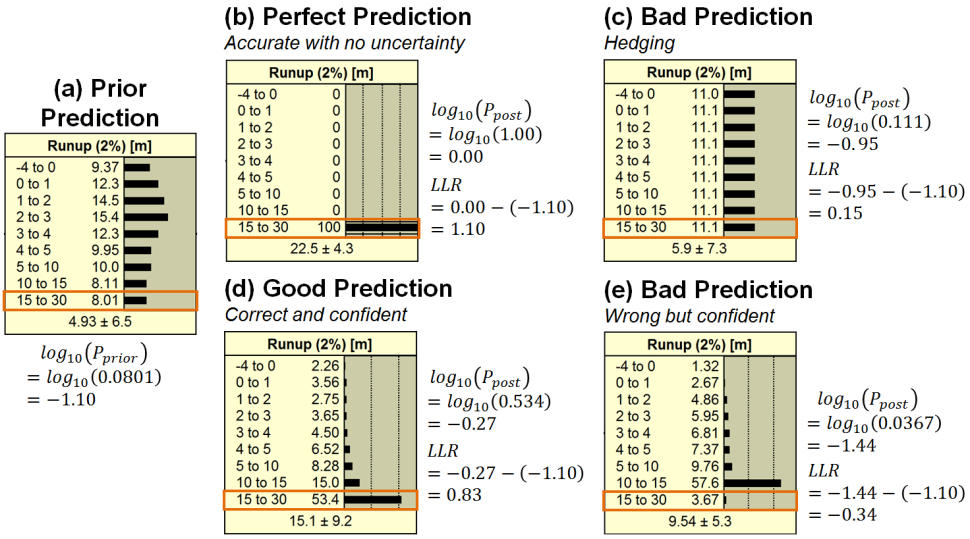

Figure 3.7: Demonstration of the log-likelihood ratio (LLR) calculation for an arbitrary test case. The bin highlighted in orange contains the observed runup value of 16 m. The prior prediction (a) indicates the base prediction of the model for all cases in the dataset, whereas the other four predictions (b-e) represent predictions made using updated input information. Predictive skill ranges from perfect to bad, depending on the log-likelihood ratio.

that runup in the correct bin is very unlikely (3.7%). The LLR is negative, which indicates that the prediction is actually worse than just assuming the prior prediction would be.

This example (e) also demonstrates the important role that discretization plays: even though the observed value of 16 lies just outside the predicted 10 to 15 m bin, the log-likelihood test considers it a bad prediction. Because we demand more precision from our network by featuring many bins, we may sacrifice accuracy. If a simpler network with fewer output bins were used instead (e.g. only <4 m and >4 m), then the observed value would fall into the most likely bin (e.g. >4 m). Hence, node discretization is a subjective but very important decision to be made in the development of a Bayesian network, and the attendant trade-offs between precision and accuracy must be carefully considered.

In addition to comparing the overall performance of different networks, log-likelihood tests can determine the relative importance of each input variable in making predictions. The first test is to develop a network featuring only a single input variable. Variables that exert more influence will have a higher LLR score, since they contribute more to the overall prediction. Variables with less influence will have a low score, which demonstrates that they alone cannot be used to make predictions: more variables are needed. If a single input variable produced the same score as the entire network, it would indicate that the other inputs are completely unnecessary to make predictions.

Another useful test is to compare networks that withhold input variables one at a time. In this way, it is possible to identify variables that the network cannot function without. More essential variables will receive lower scores, whereas unimportant ones will score similarly to the complete network. In some cases, variables which are less rele-

vant may actually score higher than the full network, which indicates that their inclusion makes predictions worse by adding uncertainty and complexity to the BN.

CONFUSION MATRICES

The second test of predictive skill is the confusion matrix, which indicates the network's accuracy. The matrix calculates the validation error rate, then breaks it down into overpredictions (false positives) and underpredictions (false negatives).

To compute the error rates and confusion matrices, a k-fold validation was performed (see Appendix D for flow chart of the full procedure). The sample set of 39,352 (160,000) cases was divided randomly into k test groups ("folds"). Each test group was withheld from the training of the $k-1$ remaining groups (training datasets), and then compared against the tested for those cases. The output statistics from each individual test were then averaged across all k tests to provide a measure of predictive skill for the entire dataset.

A confusion matrix provides a "hit rate" for the BN, identifying how often the network predicts what is observed in reality, or in this case calculated by the XBeach network. For the purposes of this study, a variable lying below a set threshold is considered negative, and positive above the threshold. For instance, the beach crest elevation of a given island could be a useful threshold for defining critical runup levels. There is no restriction on the size of confusion matrices, but since their complexity increases greatly with the number of bins for a given output node, only a binary configuration (two bins) is considered here.

Table 3.4: Confusion matrix featuring the number of correct predictions (true negatives and true positives) as well as overpredictions (false positives) and underpredictions (false negatives).

		Predicted	
		Negative	Positive
Observed	Negative	**True Negative**	**False Positive**
	Positive	**False Negative**	**True Positive**

True positives and true negatives are correct predictions. For instance, if the Bayesian network predicts that overtopping will occur and this matches the XBeach model results, we have a true positive.

False positives ("false alarms") are important for flood forecasting systems as they may undermine the apparent credibility of the predictions and reduce people's confidence in the system (i.e. "The boy who cried wolf..."). Furthermore, evacuations and other emergency preparations require significant effort and resources to mobilize.

However, false negatives are the most concerning, since they correspond to incidents where flooding occurs in the XBeach model but is not predicted by the BN. These are dangerous since they leave would leave the public unprepared for a flooding event.

To get a better sense of the predictive skill of a Bayesian network, the true/false positive/negative rates can be calculated:

$$True\ Negative\ Rate = \frac{\Sigma\ True\ Negative}{\Sigma\ All\ Observed\ Negative} \tag{3.6}$$

$$False\ Positive\ Rate = \frac{\Sigma\ False\ Positive}{\Sigma\ All\ Observed\ Negative} \tag{3.7}$$

$$False\ Negative\ Rate = \frac{\Sigma\ False\ Negative}{\Sigma\ All\ Observed\ Positive} \tag{3.8}$$

$$True\ Positive\ Rate = \frac{\Sigma\ True\ Positive}{\Sigma\ All\ Observed\ Positive} \tag{3.9}$$

For example, a false negative rate of 5% suggests that for all observed positive cases, the network makes an incorrect positive prediction 5% of the time. Conversely, the true positive rate reflects the other 95% of positive cases where the network correctly makes a positive prediction.

OVERFITTING TESTS

The third test of predictive skill examines overfitting. Is the network actually good at making predictions based on learning general trends, or is it just "memorizing" the dataset? This can be determined by comparing calibration and validation error rates.

The validation error rate is estimated by testing the network using the test dataset, and accounts for both false positive and negative predictions (Equation 3.10). Just as with the confusion matrices, the validation error rate indicates the rate at which the network makes incorrect predictions for scenarios it has not encountered before.

$$Total\ Error\ Rate = \frac{\Sigma\ (False\ Positive + False\ Negative)}{\Sigma\ All\ Observed\ Cases} \tag{3.10}$$

Conversely, the calibration error rate is estimated by testing the network using the training dataset. Although it may seem like this should give a perfect prediction, errors are introduced as a result of the discretization process.

The difference between these two error rates represents the incidence of cases that are unique to a given test dataset but not well-represented in the larger withheld dataset (Gutierrez et al., 2015). For example, extreme runup due to resonance may require very specific conditions to occur. The same reef that experiences resonant low frequency anomalies may experience relatively calm conditions under the majority of other circumstances. It can thus be challenging to predict such outliers, since they may not be captured by the training dataset. This can be quantified by calculating the overfitting ratio:

$$Overfitting\ Ratio = \frac{Calibration\ Error\ Rate}{Validation\ Error\ Rate} \tag{3.11}$$

If a system can be modelled successfully using a simpler method, then it can be said to overfit the data (Hawkins, 2004). Figure 3.8 illustrates the principle of overfitting by comparing a simple linear regression model to a complex multi-degree polynomial.

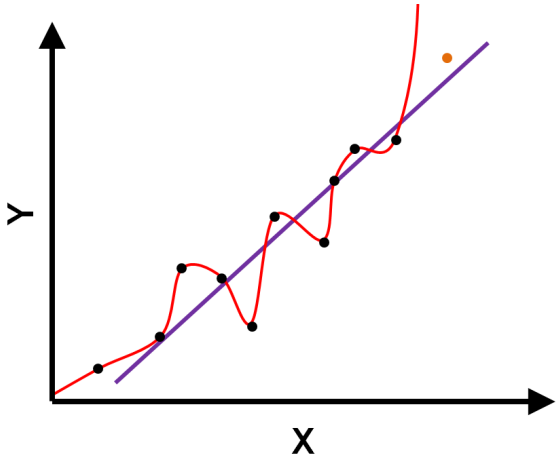

Figure 3.8: Example of overfitting, adapted from Leinweber (2007). The purple line is a simple linear regression through the black points, and the red line is a complex polynomial function that touches every point exactly. Although the red line may be able to perfectly "predict" the training data, it is not able to predict new data (orange point) well because of its complexity and how strongly it has been calibrated to the input data. We thus say that the red line is overfit. The simpler purple regression model may perform better in this case. The perils of overfitting in Bayesian networks are much the same.

The overfitting ratio as calculated with Equation 3.11 is not informative by itself; rather, we must analyze how the ratio changes with increasing network complexity. Ideally, we would like the validation error rate for our network to be as low as possible. Increasing network complexity generally decreases calibration error rates: much like the multi-degree polynomial in Figure 3.8, the network becomes able to predict the training dataset with high accuracy. However, the danger is when this improved calibration begins to increase validation errors. In the above example, the red polynomial cannot predict the orange test point because it is too tightly calibrated to the input data. The preferred network is thus one that reduces both validation and calibration error rates. This corresponds to the configuration with the minimum overfitting ratio.

Based on the outcome of the overfitting test, we can ask questions about the appropriate level of complexity in our Bayesian network. For instance, does predictive skill change when fewer input bins are used? How many folds are needed in a k-fold analysis to make meaningful comparisons? Unnecessary input variables increase the amount of data that needs to be collected to make predictions, and may add uncertainty, making predictions worse (Hawkins, 2004). As such, the outcome of this test can be used to inform decisions about future iterations of the network.

VALIDATION

A key underlying assumption for these skill prediction tests is that the XBeach model provides an accurate representation of reality. Otherwise, the BN is only good at predicting XBeach outputs and not at forecasting real floods. Hence, it is also important to test the Bayesian network using real-world cases. Table 3.5 contains field observations of runup obtained from selected case studies.

Table 3.5: Field observations from literature for validation. All water levels and crest elevations from literature have been adjusted relative to the mean reef flat level in order to be comparable to our model.

Site	H_0	T_p	η_0	c_f	β_f	W_{reef}	β_b	z_b	H_{SS}	H_{IG}	$\overline{\eta}$	$R_{2\%}$
Roi-Namur[a]	2.0	14	0.7	0.01	20	250	6	3.5	0.3	0.5	0.7	3.5
Funafuti[b]	2.1	15	0.2	0.03	2.3	100	4.6	4.4	0.3	0.6	0.9	1.1
Funafuti[c]	2.1	15	1.5	0.03	2.3	100	4.6	4.4	0.8	1.0	0.3	2.6
Funafuti[d]	1.6	13	1.9	0.03	2.3	100	4.6	4.4	0.9	0.8	0.2	2.8

[a] Nov. 17, 2013 (Gawehn, 2015)
[b] June 23, 2013 - low tide (Beetham et al., 2015)
[c] June 23, 2013 - mid tide (Beetham et al., 2015)
[d] June 23, 2013 - high tide (Beetham et al., 2015)

These values were then introduced to the network as test cases, and performance was evaluated using log-likelihoods. Not all sources had the same input or output parameters, so approximations and assumptions had to be made. Where precise values were not available for the parameters of interest, they were estimated based on descriptions in the literature. When the input data did not fit into one of the bins, the prediction used weighted probabilities to estimate equivalent conditions. This increased the uncertainty in the outputs.

SENSITIVITY TESTING

One of the benefits of Bayesian Networks is their versatility in exploring relationships and dependencies between variables. They can be used to construct different scenarios for management or future predictions. For instance, how would the likelihood of flooding change for a given reef under a certain climate change scenario?

The network is not limited to such forward predictions, but can also be used to make inverse predictions and identify the most likely input conditions contributing to a given output state. For instance, which wave conditions are most likely to induce flooding on a given island?

Plant and Holland (2011*b*) use an inverse model to predict offshore wave conditions and bathymetry based on nearshore wave characteristics. By placing certain constraints, they were able to make scenarios with only certain data available (e.g "limited remote sensing data" or "poor quality data from human observers onshore"). Certain variables can also be excluded from the network or the causal relationships changed to determine whether or not they are necessary in the model.

If withholding some of the model parameters improves predictive capability, then it suggests that those parameters are either unnecessary or inconsistent Plant and Holland (2011*b*) . For this project, removing unnecessary parameters could permit a greater range of other parameters to be varied for the same computational effort, or would reduce the amount of data that needs to be collected in the field.

4

RESULTS

CHAPTER SUMMARY

The results of the XBeach model simulations and Bayesian network are presented here. First, an example from the XBeach dataset is provided in order to illustrate some of the key hydrodynamic processes on reefs and how they are captured by the model. Then, the sensitivity of runup and other key variables to the chosen input parameters is demonstrated. A series of tests are presented to show that the XBeach model is indeed capable of representing resonant low frequency wave conditions. Lastly, the XBeach results are compared to a dataset of reef hydrodynamics for various sites around the world.

The fully-trained Bayesian network is presented, along with the results of three predictive skill tests. The log-likelihood test indicates the predictive skill of different network layouts, and identifies which parameters are most important in the model. Confusion matrices are used to categorize predictive errors into over and underpredictions, and overfitting tests assess whether the model has an appropriate level of complexity. Lastly, the network is validated using field measurements from the literature.

4.1. NUMERICAL MODELLING

This section presents the XBeach model results, beginning first with a single example of our idealized reef profile to illustrate the key aspects of the model. We then show a sensitivity analysis of key output variables to identify the most important input parameters. Next, we investigate the model's representation of low-frequency resonance. Lastly, the bulk model results are compared to field observations for validation.

4.1.1. GENERAL XBEACH MODEL RESULTS

In general, the XBeach model simulations reproduce the trends and phenomena observed for reefs in the literature. Figure 4.1 depicts spectral evolution, wave transformation, skewness, and asymmetry across the reef flat for an arbitrary example case.

The single peak of the JONSWAP spectrum applied at the boundary (a) becomes bimodal as the waves shoal up the steep fore reef slope, with a peak appearing at a higher harmonic (b). An infragravity component develops, which Pomeroy, Lowe, Symonds, van Dongeren and Moore (2012) attribute to the breakpoint generation mechanism rather than bound long waves. The higher frequency begins to dissipate by breaking at the reef crest (c), a trend which continues further as waves travel across the reef flat. At the midpoint of the reef flat (d), the bulk of the energy has shifted to lower frequencies, although the total energy of the spectrum has decreased due to continued dissipation by breaking and friction. At the inner reef flat (also the toe of the beach), infragravity and VLF energy completely dominate the spectrum (e). This qualitatively agrees with the spectral transformations observed in the literature by Becker et al. (2016); Beetham et al. (2015); Cheriton et al. (2016); Filipot and Cheung (2012); Nwogu and Demirbilek (2010); Pomeroy, Lowe, Symonds, van Dongeren and Moore (2012); Yao et al. (2012).

Wave height in the sea-swell band gradually decreases across the domain due to friction (early sensitivity tests revealed negligible numerical dissipation) (f). It then increases with shoaling on the fore reef, then abruptly drops after the crest due to breaking. After that, sea-swell wave heights experience a steady decline across the reef flat before arriving at shore. Conversely, infragravity and VLF wave height increases to shore, resulting in the dominant low frequency contribution observed in subplot (e). This increase across the surf zone and towards the shore is consistent with breakpoint forcing rather than bound long waves (Péquignet et al., 2014). Setup is relatively constant across the reef flat, although it becomes slightly larger towards shore. These patterns largely agree with the observations of Lowe, Falter, Bandet, Pawlak, Atkinson, Monismith and Koseff (2005); Nwogu and Demirbilek (2010); Pomeroy et al. (2015); Yao et al. (2012).

Wave skewness is the result of nonlinear effects due to the formation of higher harmonics in shallow water, such as during shoaling (ʌʌʌ-shaped). The pattern observed here appears qualitatively similar to observations by Cheriton et al. (2016), with the highest skewness occurring in the shoaling and breaking zones. Based on the results of Cheriton et al. (2016), slight increase in skewness at the inner reef might be attributed to increased infragravity skewness.

Wave asymmetry refers to the pitched-forward sawtooth shape often associated with breaking and broken waves (⩘⩘⩘). Pomeroy et al. (2015) and Cheriton et al. (2016) showed maximum asymmetry in the vicinity of the reef crest (point 3) and mid-reef flat (point 4), then reducing towards shore. This is due to the gradual dissipation of turbu-

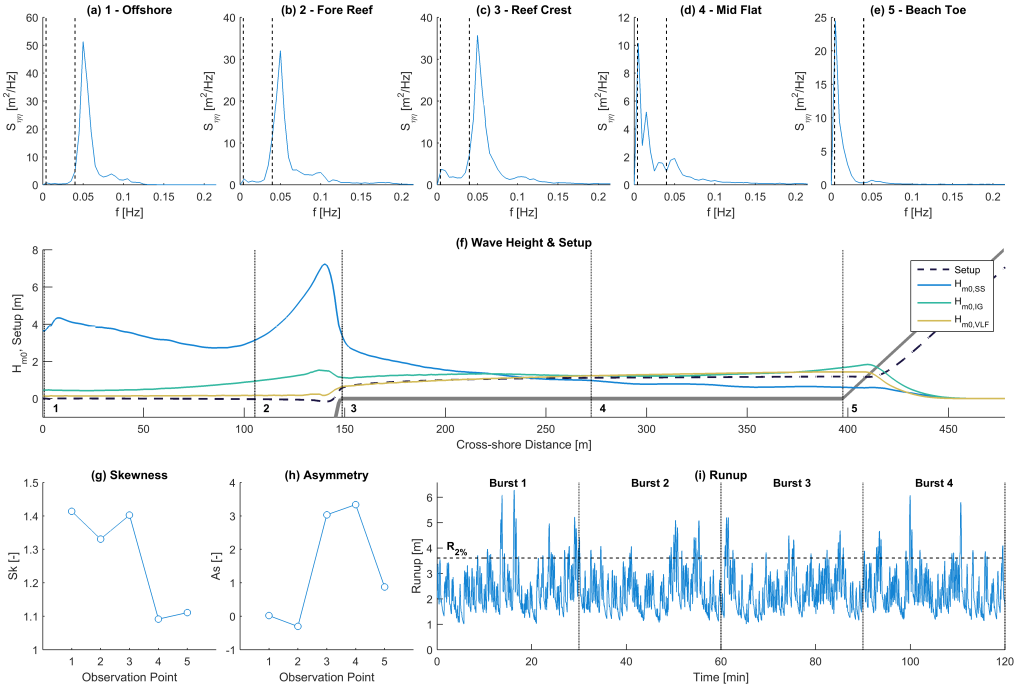

Figure 4.1: An arbitrary example from the XBeach model dataset, with $H_0 = 3m$, $H_0/L_0 = 0.005$, $\eta_0 = 1.0m$, $\beta_f = 1/2$, $W_{reef} = 250m$, $\beta_b = 1/10$, $c_f = 0.01$. Subplots (a-e) indicate the spectral evolution at five observation points across the reef. Subplot (f) shows setup and wave height at three different frequency bands (SS, IG, VLF) across the domain, and indicates the location of each observation point with a vertical dotted line. Subplots (g) and (h) illustrate wave skewness and asymmetry across the profile, respectively. Subplot (i) represents the time series of runup, indicating the $R_{2\%}$, and the four burst periods used for analysis. For illustrative purposes, all values presented in this plot are averaged across the entire simulated period (all four bursts).

lent bores and reformation of oscillatory waves on the reef flat (point 5). Undular bores are observed in many of the simulations (including this example), which may also explain the decrease in asymmetry between points 4-5, as energy is transferred from the asymmetric bores to higher frequency cnoidal waves with more symmetric forms.

The precise locations of maximum skewness and asymmetry vary between our example and the two sources above, although this can be attributed to differences in fore reef slope and wave conditions, which will govern the location of wave breaking. Since the general trends observed in our simulations resemble those in the literature, we have greater confidence in our model results.

The runup time series in subplot (i) is typical of the modelled scenarios, characterized . The highest 2% of all runup ()$R_{2\%}$) is indicated by a black dashed line on the plot, and is used as a representative value throughout this report. It should be noted that the maximum observed runup may still exceed this value by nearly double, though. This subplot could also be used to estimate the overwash potential (Matias et al., 2012) for a given island if its beach crest or maximum land elevation were known: runup exceeding the crest level would be liable to induce flooding.

Another key comparison for understanding reef hydrodynamics is an examination of how separate components of runup change with tidal elevation (Figure 4.2). Wave height (SS, IG, VLF) and setup are normalized by extreme water level ($\eta_{2\%}$) measured at the inner reef flat relative to offshore water level. Setup dominates at lower water levels, but its influence wanes with increasing depth on the reef flat. High frequency waves in the SS band become increasingly important at higher water levels. Infragravity waves make only a small contribution at low water levels, but this increases until water levels reach about 1 m above the reef flat, becoming relatively constant thereafter. VLF waves make a fairly consistent contribution across the full tidal range, albeit with a slight decrease at the highest water levels. These findings are consistent with the trends observed by (Becker et al., 2014; Beetham et al., 2015; Bosserelle et al., 2015; Merrifield et al., 2014).

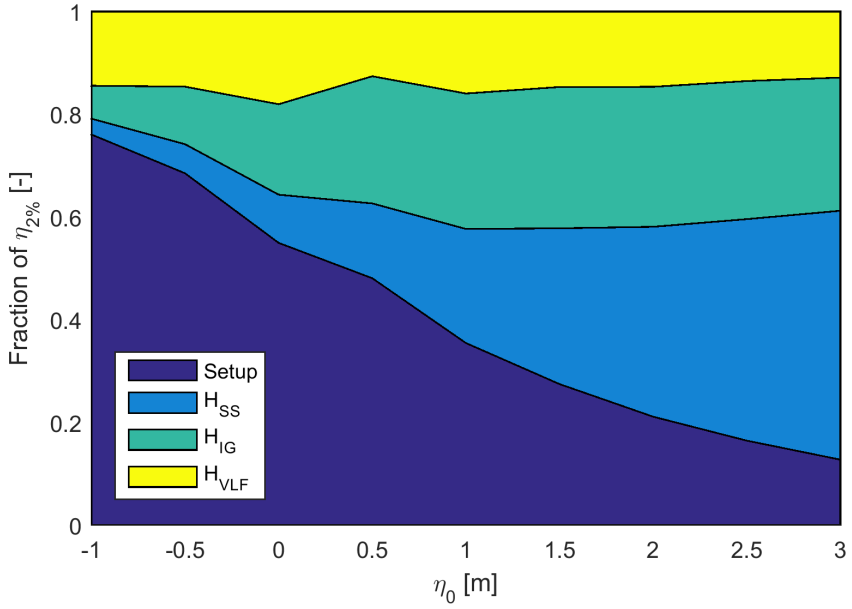

Figure 4.2: Mean relative contributions of setup and waves at different frequency bands to extreme water level ($\eta_{2\%}$), measured at the inner reef flat relative to offshore water level.

Figure 4.2 shows a clear tidal modulation in the relative importance of each hydrodynamic process. Setup dominates at low tide because depth-induced wave breaking is higher, generating larger radiation stresses and increasing the hydrostatic pressure required to balance them. The other wave components are also more easily attenuated across the reef flat in shallower water. The deeper reef flat enables SS waves to penetrate closer to shore at high tide. The low frequency components at the shore are driven by more complicated processes such as breakpoint generation and resonance, and thus exhibit less dependence on tide alone.

4.1.2. BULK MODEL RESULTS

Having examined individual cases and ensured the synthetic dataset's general agreement with measured field data, we then examined general trends in the model output. These plots illustrate the relationships between the eight primary input parameters and various output parameters. The box and whisker plots are used to illustrate the distribution of data, showing 5th, 25th, 50th, 75th, and 95th percentiles, as well as any outliers (Figure 4.3). Many of these figures have been plotted featuring only the cases with beach crest elevations of 30 m, a semi-infinite slope. This was done because overtopping and overflow conditions at discrete crest elevations tend to obscure the underlying trends in the various output parameters. Although the overtopping quantities are ultimately useful for operational flood forecasting, runup-only conditions were deemed more illustrative.

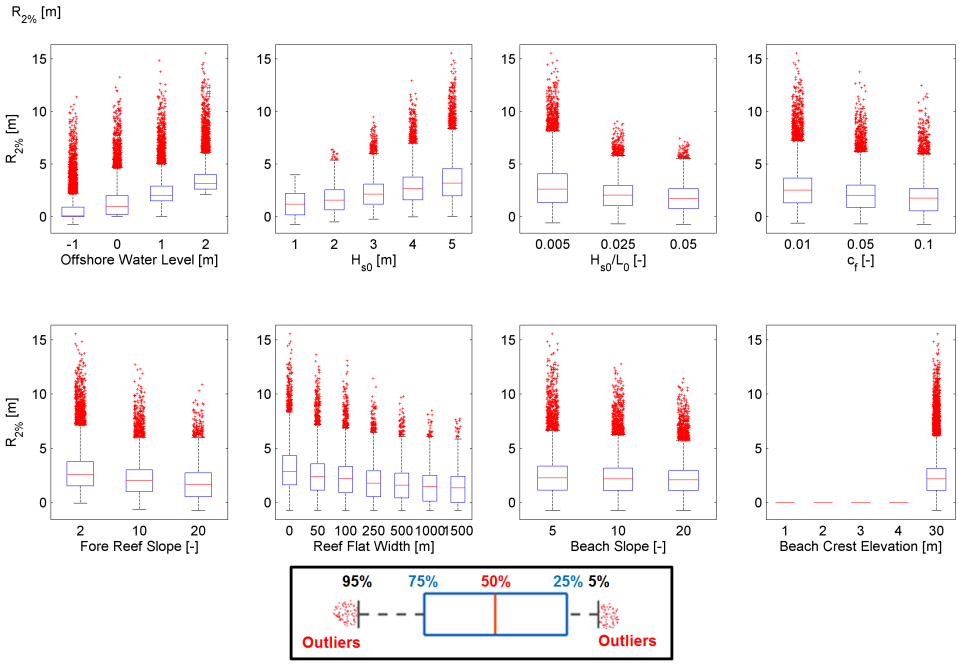

Figure 4.3: Runup as a function of the eight primary input parameters. The red centre line denotes the median value (50th percentile), while the blue box contains the 25th to 75th percentiles of dataset. The black whiskers mark the 5th and 95th percentiles, and values beyond these upper and lower bounds are considered outliers, marked with red dots.

Runup is positively correlated with offshore water level, which is in keeping with findings by Quataert et al. (2015). There is also a positive correlation with offshore significant wave height, although the spread in runup increases at higher wave heights. This is in agreement with Quataert et al. (2015) and Nwogu and Demirbilek (2010). As friction increases, runup decreases, which agrees with the findings of Quataert et al. (2015) that compares rough and smooth reefs. As the fore reef steepens, runup increases, in keeping with Quataert et al. (2015); Yao et al. (2012). Reef flat width also has a negative correla-

tion with runup, which is supported by the findings of Shimozono et al. (2015). Steeper beach slopes lead to higher runup, although it is less sensitive than to fore reef slope.

Similar plots for overtopping, setup, wave heights at the inner reef, reflection at the offshore boundary, mean spectral period, and more can be found in Appendix C.

4.1.3. RESONANCE

Since low frequency resonance may play an important role in flooding of reef-fronted coasts, we investigated whether the XBeach Non-Hydrostatic model was capable of simulating resonance, and whether there was any relationship between it and flooding.

Figure 4.4 shows the relationships between VLF wave height on the inner reef flat and each of the tested input parameters. VLF wave height reaches a maximum for reefs in the 50-100 m width range (Figure 4.4f). Since narrower reef flats are more likely to exhibit resonance Cheriton et al. (2016), it is possible that this peak represents cases where resonant conditions are achieved, amplifying VLF waves. They are not very sensitive to beach slope, which makes sense because they would be in a reflective regime.

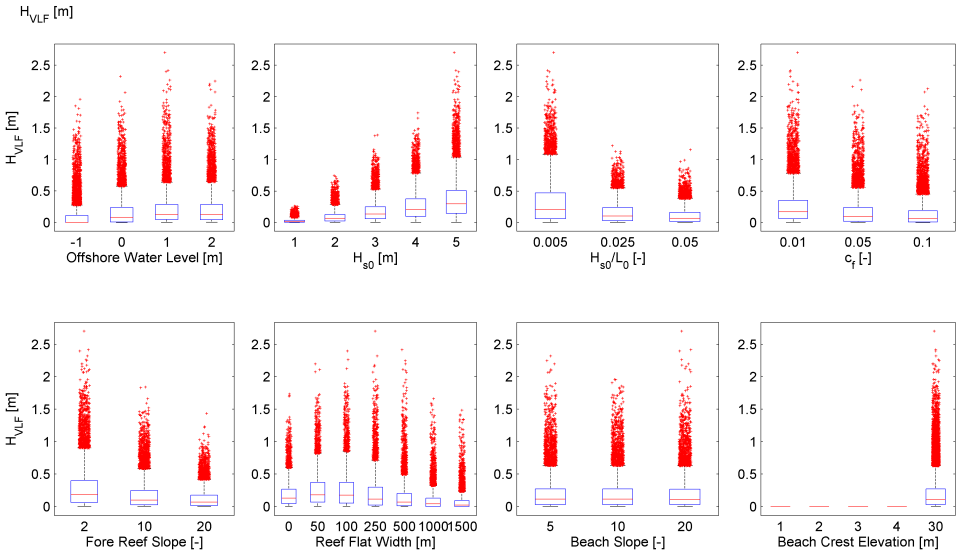

Figure 4.4: VLF wave heights as a function of the eight main input parameters.

The first question to consider was whether or not resonance was being reproduced in the XBeach model. The sensitivity analysis of VLF wave height showed a local maximum for 100 m wide reefs (Figure 4.4). Since low-frequency resonance is expected to be more likely on narrow reefs, this was a promising indication that the model was simulating resonant amplification.

As Figure 4.4 indicates, VLF wave height has a strong positive correlation with offshore wave height. To reduce this dependency and uncover more anomalous events (as might be associated with resonance), LF wave heights were normalized by offshore wave height and squared for many of the following analyses. Doing so also made differences

between high and low values more pronounced. Hence, large values of $(H_{IG}/H_0)^2$ and $(H_{VLF}/H_0)^2$ indicate low frequency waves which are surprisingly high given the input conditions. These are the events that will be more likely to catch forecasting systems off guard, so are thus important to predict.

Following the example of Gawehn et al. (2016), we next investigated anomalously high LF waves as a function of depth and observed frequency at the inner reef flat. Figure 4.5 depicts low frequency (LF) waves as a function of both offshore forcing ($f_{p,0}$, $H_{s,0}$) and mean water depth on the reef flat (h_{reef}). The pattern of anomalously high

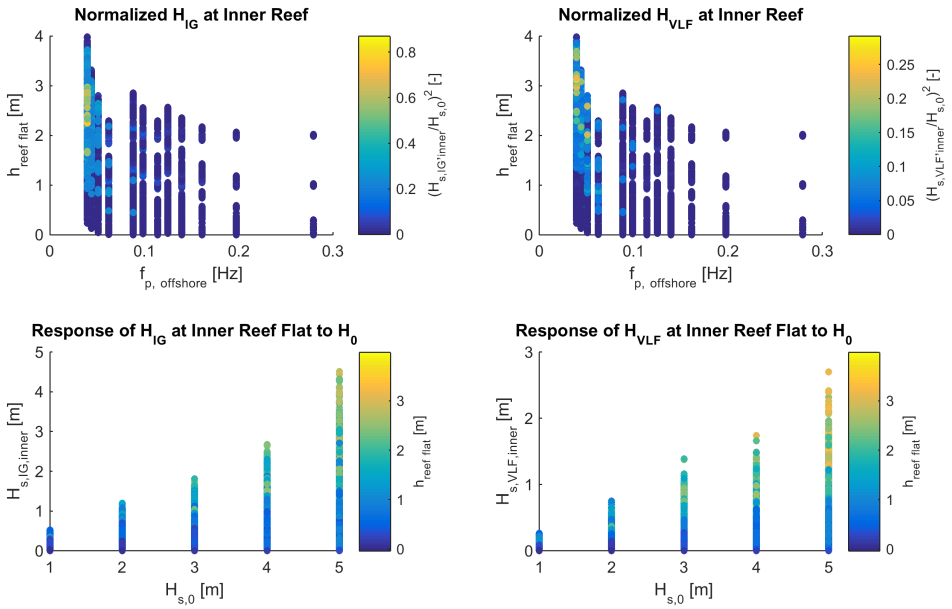

Figure 4.5: Normalized infragravity (a) and VLF (b) wave height as a function of mean reef flat depth and peak offshore frequency. Subplots (c-d) show infragravity and VLF wave height as a function of offshore significant wave height, shaded according to mean reef flat depth. The points are clustered in vertical lines because of the discrete input distributions for $H_{s,0}$ and steepness.

LF waves occurring on deeper reef flats at lower offshore wave frequencies (Figure 4.5 a,b) is also observed in the field measurements at Roi-Namur analyzed by Gawehn et al. (2016). By cross-correlating water surface time series at several points across the reef, they were able to associate this cluster of waves with resonant conditions. While such a cross-correlation analysis was beyond the scope of the present study, the similar trends suggest that resonant amplification of infragravity and VLF waves is simulated by our model.

Low frequency wave heights show a positive correlation with offshore wave heights (Figure 4.5 c,d), with also scatter increasing for higher incident waves. In the analysis by Gawehn et al. (2016), these large LF waves were also associated with resonant conditions, whereas lower ones belonged to standing, progressive, or dissipative conditions.

Observations of anomalously high LF waves alone are not enough to confirm that

resonance is occurring. Since the phenomenon occurs when the frequency of hydrodynamic forcing matches the natural resonant frequency of a given reef ($f_{n,0}$), we must examine the relationship between resonant and observed frequencies. When the natural resonant frequency is met, the ratio of $f_{m-1,0}/f_{n,0}$ approaches 1. Indeed, Figure 4.6 shows events with relatively high VLF waves clustered around the 0th resonant frequency.

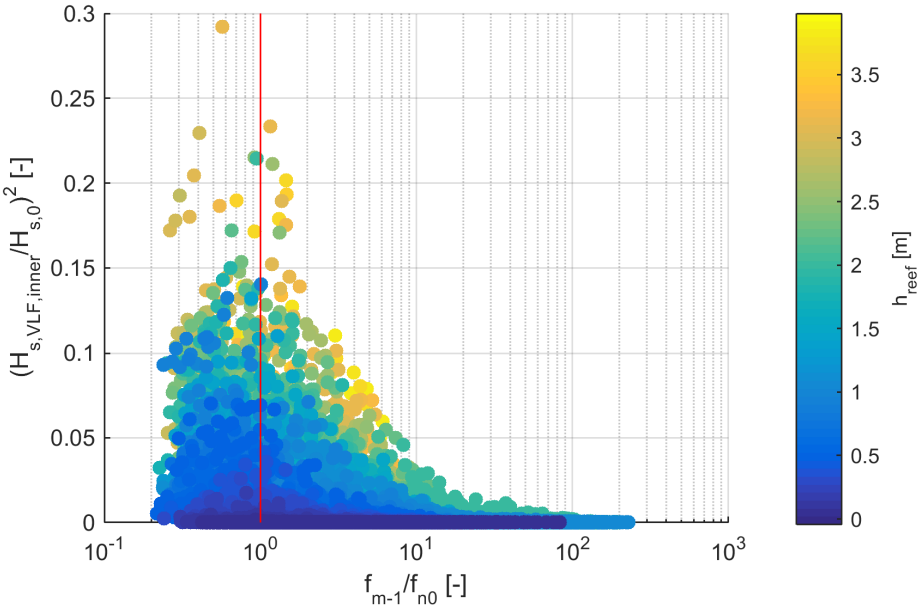

Figure 4.6: Normalized, squared VLF wave height $(H_{VLF}/H_0)^2$ as a function of the ratio between mean spectral frequency at the inner reef flat ($f_{m-1,0}$) and the reef's zeroth resonant frequency ($f_{n,0}$). Points close to $f_{m-1,0}/f_{n,0} = 1$ (10^0) are near resonance.

Consistent with the field observations of Gawehn et al. (2016), the anomalously high VLF waves observed in Figure 4.5 tend to cluster around $f_{m-1,0}/f_{n,0} = 1$. This suggests that the model is able to simulate resonant amplification even with its generalized set up. Infragravity and VLF wave response at higher modes of the natural resonant frequency is discussed further in Appendix D (Figure D.10).

Thus, multiple lines of evidence suggest that the XBeach Non-Hydrostatic model is capable of simulating low frequency resonance for generalized reef configurations.

4.1.4. VALIDATION

This section attempts to validate our numerical model by comparing it to field observations from the literature. If the results are consistent with measured values, then that gives us greater confidence in the model's predictive capability. The Bayesian analysis carried out in Section 4.2 is only as good as the underlying XBeach model which forms its underlying input dataset. Hence, it is essential to validate our model using field data

where possible.

Detailed field measurements of reef hydrodynamics are few and far between. Furthermore, we are testing an idealized reef profile with discrete input distributions designed to best represent many different reef configurations, rather than a specific site. As such, they may not be directly comparable to sites in the literature. Hence, to determine if we are reproducing general trends correctly, we can compare our results to those of Narayan et al. (2016), who aggregated wave attenuation rates from numerous sites in the literature (Figure 4.7).

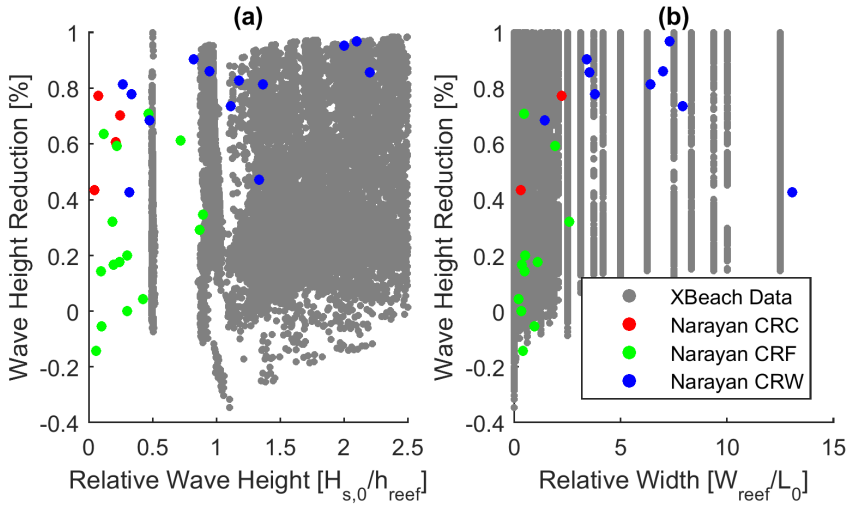

Figure 4.7: Wave height reduction rates ($R = 1 - H_{s,shore}/H_{s,0}$) as a function of (a) relative wave height and (b) reef width compared to field measurements compiled from multiple sources by Narayan et al. (2016). A reduction rate of 1 denotes complete wave attenuation, and negative values would imply amplification (possibly due to resonance or standing waves). CRC denotes measurements at the reef crest, CRF on the reef flat, and CRW across the whole reef.

In Figure 4.7 (a), most of the data points compiled by Narayan et al. (2016) tend to sit in the region where $H_{s,0}/h_{reef} < 0.5$, denoting relatively milder wave conditions or relatively deeper reef flats. The mean wave height considered in their synthesis was 0.79 m, which lies outside the 1 to 5 m parameter space that we simulated. Similarly, the mean reef flat depth in their study was 2.24 m, which also lies outside the -1 to 2 m parameter space that we simulated. Furthermore, many of their reported values were measured at the reef crest (green points), rather than at the shore (blue points) where our results are from. Hence, discrepancies in our respective results may be explained by the limited overlap in our datasets. Narayan et al. (2016) also note that their synthesis is limited by scant observations under extreme wave conditions, such as the swell-induced flood events of interest to the present study.

The comparison between our XBeach model results and the cases compiled by Narayan et al. (2016) improves when relative width is considered in Figure 4.7 (b). This is largely due to the greater overlap between our considered reef widths and incident wavelengths. Their synthesis incorporates reefs ranging from 34 to 3200 m in width ($\overline{W_{reef}}$ = 548 m),

so many of their data points lie within our modelled parameter space of 0 to 1500 m. Similarly, the observed wave periods in their analysis (used to calculate L_0) range from 4 to 14.7 s ($\overline{T_p}$ = 8.6 s), all of which are encompassed by our simulations (T_p = 3.6 to 25.3 s).

Since the data from Narayan et al. (2016) only contains mean long term wave conditions, individual data points cannot be directly validated against individual XBeach model results. This comparison thus serves as a qualitative comparison, useful mostly just in light of the limited data available for thorough 1:1 validations. The observed wave height reductions lie within the range of our XBeach results, or can else be explained, which gives us greater confidence that the model is behaving realistically.

4.2. BAYESIAN NETWORK

This section presents the main results from the Bayesian network. First, the trained network is shown to illustrate key aspects of the BN. Next, tests of the network's predictive skill are shown. Lastly, the network is validated against field observations from selected sites in the literature.

4.2.1. TRAINED NETWORK

Figure 4.8 shows the full Bayesian network trained on all data (Configuration A). The histograms in each node display the prior probabilities associated with the entire training dataset. There are uniform distributions for all inputs, with slight variations due to filtering of runs that did not meet criteria for stationary conditions. The output distributions reflect the marginal distributions for the entire range of model results. They are more variable and skewed since they are grouped by ranges of interest (e.g. resonant conditions). The negative values for $R_{2\%}/H_{s,0}$ represent runs where MWL < 0 m (below reef flat) with small waves. Waves do not reach the beach, but simply run up and down the fore reef slope.

Figure 4.9 shows the structure of Configuration D, for which the output variables were not normalized. This version was used in the validation against field data, so as to make the inputs and outputs directly comparable with the available information.

4.2.2. SKILL-TESTING

Taken at face value, a Bayesian network is an excellent tool for predicting floods. User-friendly, simple concepts, provides uncertainty, distills huge dataset and presents it in a clear way. But is the prediction actually any good? Can we predict scenarios outside the dataset with which it was trained? Did it just memorize the training data or has it actually learned to generalize the patterns? Three main predictive skill tests are prepared for this thesis: log-likelihood tests, confusion matrices, and overfitting tests.

LOG-LIKELIHOOD TESTS

The log-likelihood tests were carried out to compare the predictive skill of different network configurations and identify the relative importance of input variables. The first test examines whether using the network gives a better prediction than by estimating the outcome using only the initial distributions. Table 4.1 shows the log-likelihood test

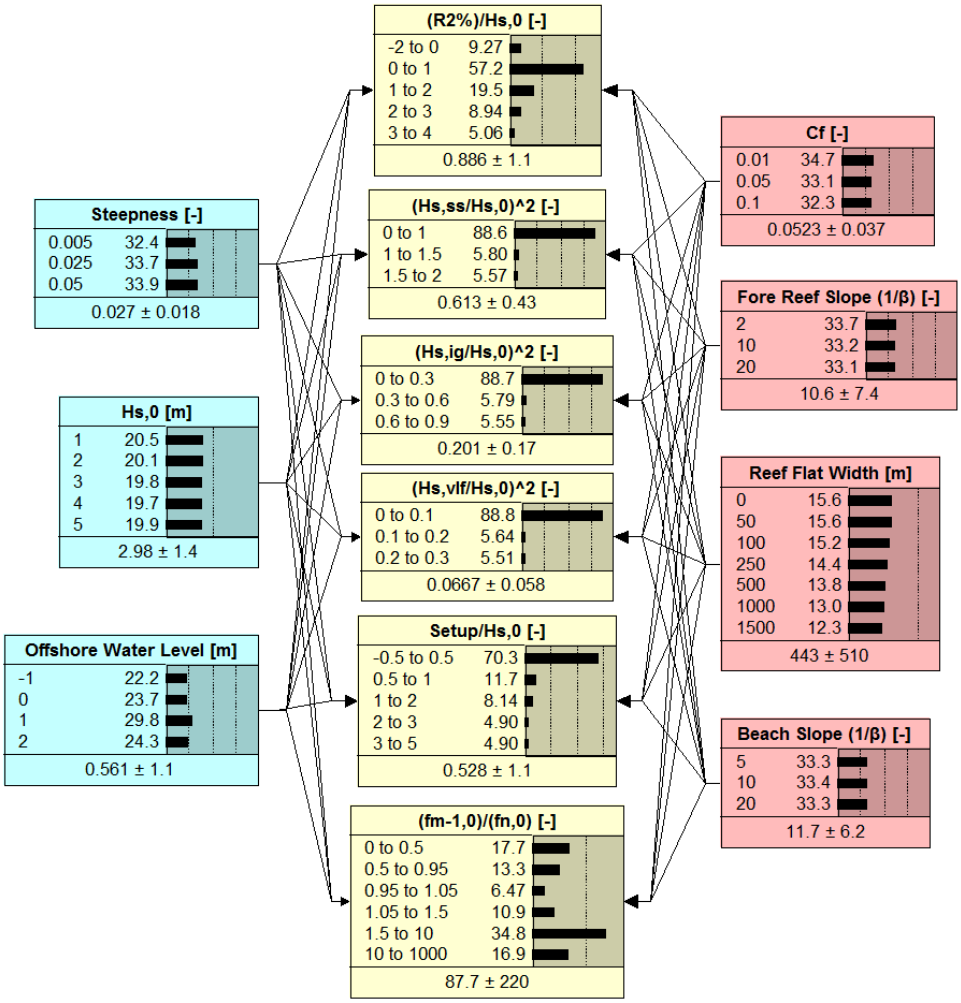

Figure 4.8: Bayesian network Configuration A, trained on all model data. Blue nodes indicate hydrodynamic input parameters, and red nodes are reef morphology inputs, while the yellow nodes are output variables. The histograms show prior distributions for all variables based on XBeach model output (filtered by 30 m beach crest). Non-uniform input distributions are the result of filtering out runs that did not meet the stationarity criteria established in Section 3.1.2. The majority of these simulations had wider reef flats, so the difference is most noticeable for the reef flat width node.

scores for the five main network layouts. The values are not directly comparable since the prior probabilities are different for each network, but the general trends are still qualitatively informative.

In order to compare the different networks directly, we calculate the log likelihood ratio of two different posterior probabilities. Table 4.2 shows the log-likelihood test scores for the three main network layouts.

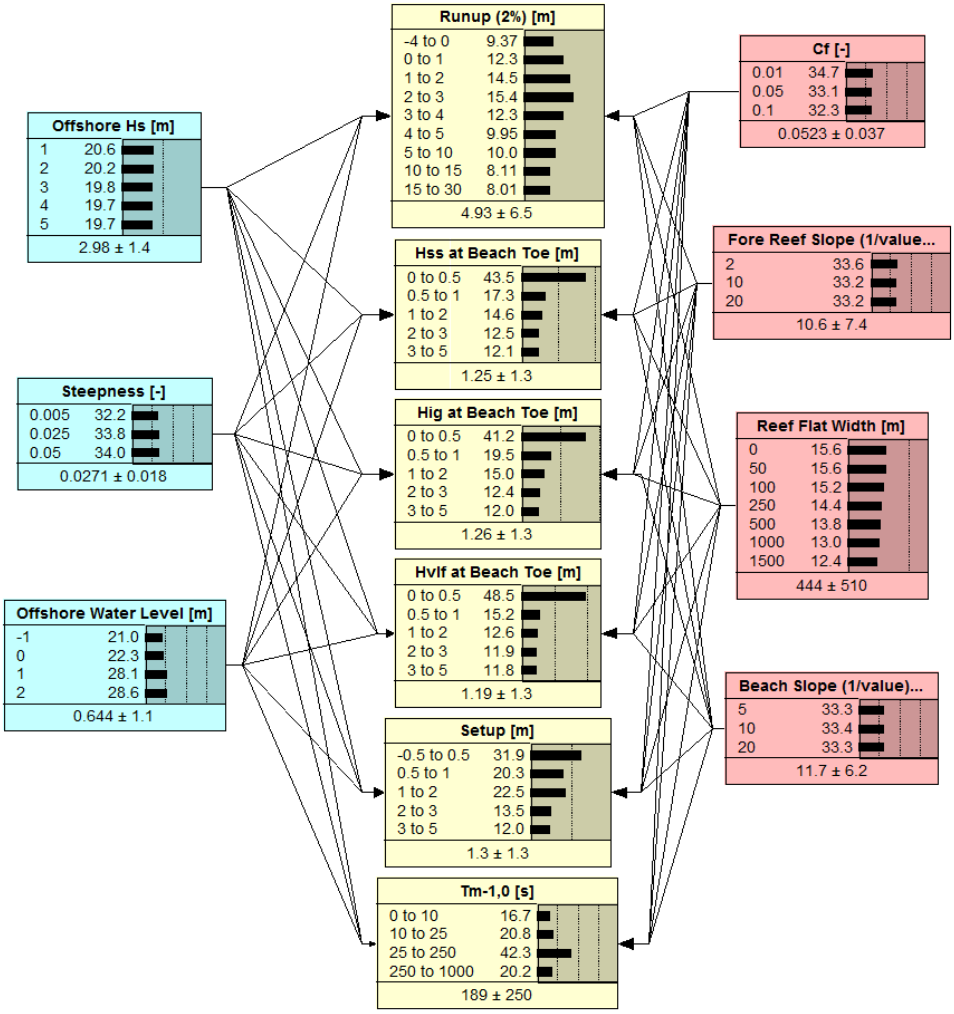

Figure 4.9: Bayesian network Configuration D, which features output variables not normalized by offshore wave height. Hydrodynamic input variables are shaded in blue, reef morphology input variables in red, and output variables in yellow. The histograms on each node indicate the prior probability distribution based on all cases in the training dataset.

Table 4.1: Log-likelihood ratios for networks, tested against themselves. A is the primary network, B is the primary network but with binary outputs, C is the primary network but with reef width as the only reef morphology input parameter. Network D features non-normalized output variables, and E is identical to D but with binary outputs. Positive values indicate that predictions using the network are better than estimates made using only the prior distributions.

Network	$R_{2\%}/H_0$	$(H_{SS}/H_0)^2$	$(H_{IG}/H_0)^2$	$(H_{VLF}/H_0)^2$	$\overline{\eta}/H_0$	$f_{m-1,0}/f_{n,0}$
A	12578	394	399	249	7084	18634
B	8002	336	334	184	6017	9575
C	11271	271	273	119	7029	17855
	$R_{2\%}$	H_{SS}	H_{IG}	H_{VLF}	$\overline{\eta}$	$T_{m-1,0}$
D	16876	6826	7611	2830	12608	9577
E	6101	5731	6464	2687	8304	5590

Table 4.2: Log-likelihood ratios comparing each network against the others. For instance the first row takes the log likelihood of A (the base network) and then subtracts the log likelihood of B (the competing network). In a comparison of (I) vs (II), negative values indicate that (I) performs better than (II) for that variable. Because their variables are different, networks D and E are not directly comparable with A, B, or C.

Comparison	$R_{2\%}/H_0$	$(H_{SS}/H_0)^2$	$(H_{IG}/H_0)^2$	$(H_{VLF}/H_0)^2$	$\overline{\eta}/H_0$	$f_{m-1,0}/f_{n,0}$
A vs B	-2914	-901	-894	-893	-2544	-6034
B vs C	3562	-709	-662	-700	576	6377
C vs A	-648	1609	1556	1593	1968	-343

In the log-likelihood ratio (LLR) tests of Tables 4.1 and 4.2, Configuration A (multiple bins for each output variable) performs better than B (only two bins for each output variable). This suggests that the output resolution of B is too coarse, or that the bin boundaries are suboptimal.

However, Configuration A is outperformed by C when predicting runup and resonance. This can be explained by revisiting the withholding/single-input tests in Figures 4.10 and 4.11.

The single-input plots in Figure 4.10 can be interpreted by looking at the performance of each input variable relative to the others for a given output. For example, in subplot (a), H_0 and η_0 score much higher than the other variables. This suggests that they are the most important parameters for predicting nondimensional runup. However, note that in both cases their LLR still falls well below that of the complete network featuring all nodes. This suggests that water level or wave height alone are not sufficient to predict runup, owing to the complex interactions between all eight inputs.

The withheld variable plots in Figure 4.11 can also be interpreted by comparing the score of individual inputs to the complete network (dashed line). These plots are perhaps even more telling than the single input plots, since they show more clearly which variables are indispensable, and which may only be contributing uncertainty to the predictions. Low scores suggest that a given input variable is important, since excluding it

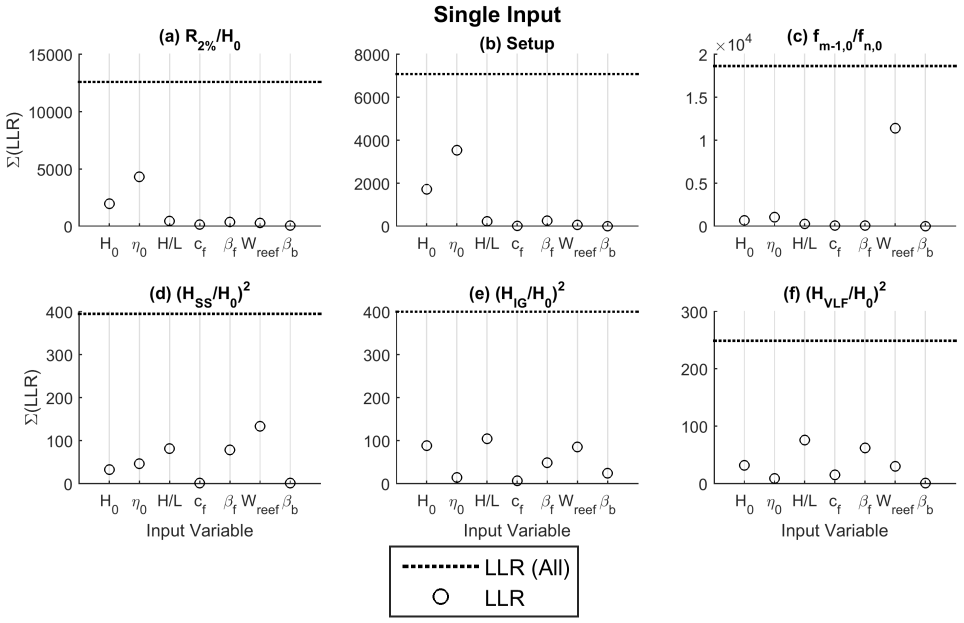

Figure 4.10: Log-likelihood ratio comparisons for single variables. The dashed line shows the LLR for all Configuration A, with all variables included. Each of the circles represents the LLR for a separate network where that variable is the only input.

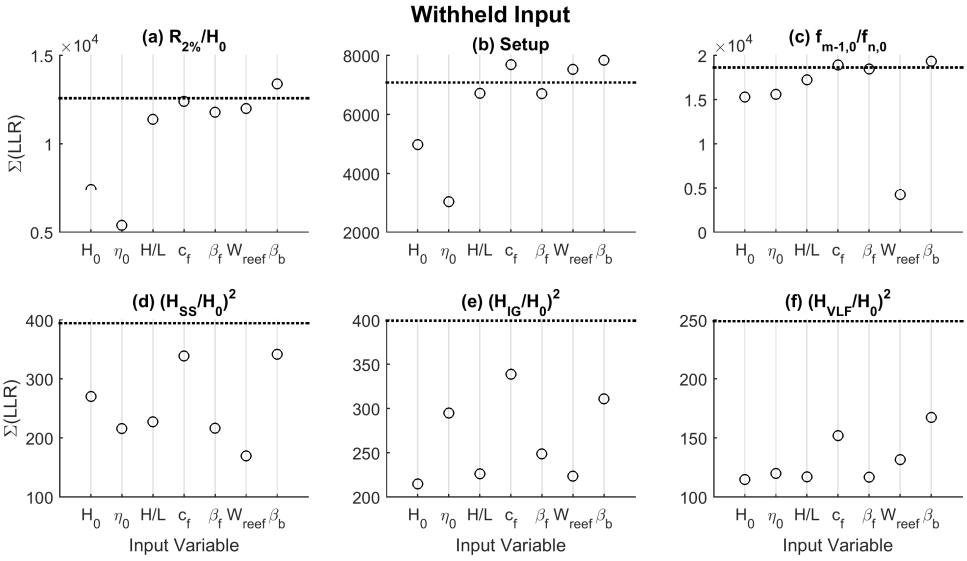

Figure 4.11: Log-likelihood ratio comparisons for withheld variables. The dashed line shows the LLR for all Configuration A, with all variables included. Each of the circles represents the LLR for a separate network where that variable has been withheld from the prediction.

from the network severely reduces predictive skill. Scores close to the dashed line indicate that removing that variable makes little difference to the prediction. At the other extreme, scores exceeding the dashed line imply that the variable actually makes predictions worse. This counterintuitive result can be explained by the additional network complexity and uncertainty that adding extra variables introduces. Hence, weakly correlated variables may only confuse the issue.

Using these results, we can explain the relative performance of networks A and C in Table 4.2. From Figures 4.10(c) and 4.11(c), it can be seen that W_{reef} is the most important variable for predicting resonance ($f_{m-1,0}/f_{n,0}$). Indeed, withholding c_f or β_b actually improves the quality of the prediction. This might be explained because low frequency waves dominate runup at the shoreline, and they are largely insensitive to β_b (Stockdon et al., 2006). Thus, by making the network simpler and removing the influence of these parameters, uncertainty reduces and predictive skill improves.

However, Configuration C shows less predictive skill for the other output variables. As indicated in Figure 4.11, these output variables generally require all inputs to make accurate predictions. In the case of $(H_{VLF}/H_0)^2$ (subplot f), the removal of any input variable significantly degrades predictive skill. This suggests that the processes driving low frequency anomalies (such as resonance) are complex with many interdependencies.

Figure 4.10 indicates that all networks have the strongest predictive skill for normalized runup, followed by setup, whereas they tend to score lower for more complex phenomena like low-frequency waves. $f_{m-1,0}/f_{n,0}$ scores high for each configuration, but this may be because non-resonant conditions dominate. The network is usually correct when it predicts non-resonant conditions and thus scores high, but because hard-to-predict resonance seldom occurs, the overall score is not much affected when the network guesses wrong.

The trends from both the single and withheld variable tests generally agree with one another: variables deemed essential in the withheld tests usually also score the highest in single variable tests. However, it is conceivable that because of the interdependencies involved, a variable which is not useful on its own could still be an indispensable part of predictions when combined with other parameters.

CONFUSION MATRICES

Confusion matrices break down predictive error rates of each variable into over and under predictions. Table 4.3 shows confusion matrices for Configuration B (two output bins). This is because confusion matrices expand rapidly in complexity with additional bins.

The confusion matrices show that the network is good at predicting setup and Hss. It is also much better at predicting low runup than high runup. Error rates are low for resonance, but because resonant conditions require at least three bins to distinguish (below resonance, at resonance, higher than resonance), this two-bin comparison is not very meaningful. This illustrates the importance of defining bins on a physically meaningful basis.

In plots d-f, excellent predictive skill is shown for low conditions, but less so for anomalously high conditions. 30% of infragravity anomalies and 100% of VLF anomalies

(a)

$R_{2\%}/H_{s,0}$ [-]	Actual	Predicted: -2 to 1	Predicted: 1 to 4
	-2 to 1	96.66	3.34
	1 to 4	**12.18**	87.82

(b)

Setup/$H_{s,0}$ [-]	Actual	Predicted: -0.5 to 0.5	Predicted: 0.5 to 5
	-0.5 to 0.5	99.40	0.60
	0.5 to 5	**1.69**	98.31

(c)

$f_{m-1,0}/f_{n,0}$ [-]	Actual	Predicted: 0 to 1.5	Predicted: 1.5 to 1000
	0 to 1.5	95.57	4.43
	1.5 to 1000	**3.73**	96.27

(d)

$(H_{s,SS}/H_{s,0})^2$ [-]	Actual	Predicted: 0 to 1	Predicted: 1 to 2
	0 to 1	99.98	0.02
	1 to 2	**4.92**	95.08

(e)

$(H_{s,IG}/H_{s,0})^2$ [-]	Actual	Predicted: 0 to 0.3	Predicted: 0.3 to 0.9
	0 to 0.3	99.96	0.04
	0.3 to 0.9	**29.85**	70.15

(f)

$(H_{s,VLF}/H_{s,0})^2$ [-]	Actual	Predicted: 0 to 0.1	Predicted: 0.1 to 0.3
	0 to 0.1	100.00	0.00
	0.1 to 0.3	**100.00**	0.00

Table 4.3: Confusion matrices depicting the accuracy of the Bayesian Network in predicting the XBeach model output for a given set of input conditions. Values in the tables indicate the percentage of observed cases falling into a given prediction bin. Green values along the main diagonal indicate correct predictions, whereas the bottom left corner indicates the false negative rate (underpredictions) and the top left indicates the false positive rate (overpredictions).

go underpredicted. It is also worth noting that although the false negative rates are high for these anomalies, the total error rates for $(H_{SS}/H_0)^2$, $(H_{IG}/H_0)^2$, and $(H_{VLF}/H_0)^2$ are less than 1%, since the anomalies represent such a small proportion of the total cases. However, the network is still not very accurate for the small minority of anomalously high waves that are of most interest to us. This can likely be attributed to the relatively few resonant cases on which the model could be trained.

OVERFITTING TESTS

The third test of predictive skill is for overfitting, to assess whether the network is actually able to learn from the input data and generalize trends, or if it is just "memorizing" the dataset. Calibration error rates are determined by testing the network using the same data it was trained with ($k-1/k$ samples), whereas validation rates are determined by testing it with data it has not seen ($1/k$ samples). The overfitting test examines how the normalized runup prediction error rate changes with the number of folds and also with the number of bins in the W_{reef} node (Figure 4.12).

Figure 4.12a indicates that the validation error rate drops significantly after 3 folds and then converges to 6.9%. This suggests that training the network with 2/3 of the dataset provides sufficient variability to conduct a meaningful k-fold analysis. Since the computational effort of carrying out k-fold tests increases with the number of folds, this is useful as it means that fewer folds may be necessary for future analyses. Variation in the error rates also decreases after 5 bins.

Based on this information, 5 folds were used to carry out the second part of the analysis (b). The number of bins for the reef width input node was varied from 2 ($\leq 250m$ and $\geq 250m$) to 7 (each of the tested values had its own bin) in order to demonstrate the effects of increasing or decreasing model complexity. W_{reef} was chosen as an example for the overfitting since 7 discrete parameter values were used, whereas the other input parameters did not have sufficient variation to conduct a meaningful analysis. Both calibration and validation error rates initially decrease as additional bins are included. This suggests that the influence of reef width on runup varies sufficiently across the tested range of parameters that 2-4 bins are inadequate for predictions. Validation error reaches a minimum at 5 bins, and then increases again for 6-7 bins, suggesting that

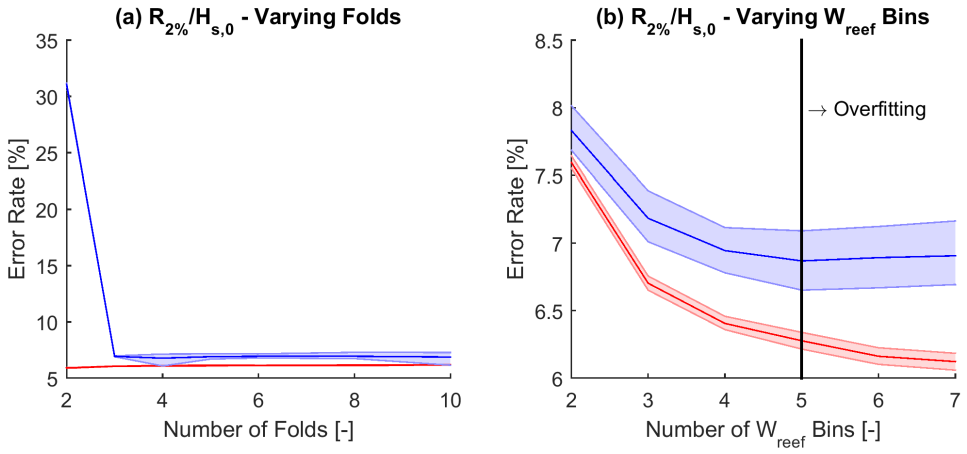

Figure 4.12: Overfitting test featuring calibration (red) and validation (blue) error rates as a function of the number of folds (a) and then as a function of the number of bins for the W_{reef} node (b). Lighter coloured bands indicate the maximum and minimum error rates across all tested folds. The solid black line at 5 bins represents the point at which validation error increases with additional network complexity (overfitting).

the complexity generated by additional bins reduces predictive skill. Meanwhile, the calibration error rate continues to drop, since the network has more resolution and is thus better able to approximate the training data. This suggests that the current model setup with 7 input bins is slightly overfit.

4.2.3. VALIDATION

Bayesian networks have not yet been applied for flood prediction on coral reefs and thus must be shown due scrutiny. Validation is used to define how well the BN can represent the desired hazard indicators (den Heijer et al., 2012). Field observations of runup on coral reefs are few and far between, limiting our ability to validate the network. The values presented in Table 3.5 were then introduced as test cases to the Bayesian network, where hazard probabilities and expected values were calculated (Table 4.4 and Figure 4.13).

Based on the log-likelihood ratios, Table 4.4 indicates poor predictive skill for runup, although generally H_{ss}, H_{ig}, and setup show improved predictions over the prior probabilities. However, the LLRs alone do not tell the whole story. When the results of the validation cases are presented graphically, other patterns emerge which improve confidence in the model's predictions (Figure 4.13).

As presented in Figure 3.7, the log-likelihood ratios may depend strongly on bin discretization. For instance, in each of the incorrect runup predictions presented above, the correct value always lies in the bin adjacent to the one with the highest predicted probability. Hence, it is quite possible that by iterating further and optimizing the bin discretization, the scores for these validation cases may improve. As the overfitting and other log-likelihood tests reveal, the network's predictive capabilities may enhanced by changing the reducing the number of bins, nodes, or connections in the model.

Table 4.4: Case study validation results. The observed values for runup, sea/swell and infragravity wave heights, and setup are indicated, along with the prior and posterior predicted values and probabilities (P_{prior},P_{post}) from the Bayesian network. Positive LLR values denote predictions that are improved over the prior distribution.

Site		$R_{2\%}$	H_{SS}	H_{IG}	$\overline{\eta}$
Roi-Namur, RMI Nov. 17, 2013	Observed Value	**3.5**	**0.3**	**0.5**	**0.7**
	Prior Value	4.9 ± 6.5	1.3 ± 1.3	1.3 ± 1.3	1.3 ± 1.3
	Post Value	4.6 ± 6.4	1.1 ± 1.3	1.2 ± 1.2	1.1 ± 1.4
	P_{prior}	0.12	0.44	0.41	0.20
	P_{post}	0.08	0.55	0.37	0.23
	LLR	**-0.20**	**0.11**	**-0.04**	**0.05**
Funafuti, Tuvalu June 23, 2013 (Low Tide)	Observed Value	**1.1**	**0.3**	**0.6**	**0.9**
	Prior Value	4.9 ± 6.5	1.3 ± 1.3	1.3 ± 1.3	1.3 ± 1.3
	Post Value	4.9 ± 6.3	1.2 ± 1.3	1.4 ± 1.2	1.6 ± 1.1
	P_{prior}	0.15	0.44	0.20	0.20
	P_{post}	0.10	0.49	0.43	0.21
	LLR	**-0.18**	**0.05**	**0.34**	**0.01**
Funafuti, Tuvalu June 23, 2013 (Mid Tide)	Observed Value	**2.6**	**0.8**	**1.0**	**0.3**
	Prior Value	4.9 ± 6.5	1.3 ± 1.3	1.3 ± 1.3	1.3 ± 1.3
	Post Value	5.4 ± 6.1	1.3 ± 1.2	1.4 ± 1.2	1.0 ± 1.4
	P_{prior}	0.15	0.17	0.20	0.32
	P_{post}	0.09	0.52	0.47	0.47
	LLR	**-0.23**	**0.47**	**0.38**	**0.17**
Funafuti, Tuvalu June 23, 2013 (High Tide)	Observed Value	**2.8**	**0.9**	**0.8**	**0.2**
	Prior Value	4.9 ± 6.5	1.3 ± 1.3	1.3 ± 1.3	1.3 ± 1.3
	Post Value	5.1 ± 6.2	1.2 ± 1.2	1.3 ± 1.2	1.0 ± 1.4
	P_{prior}	0.15	0.17	0.20	0.32
	P_{post}	0.14	0.35	0.35	0.53
	LLR	**-0.03**	**0.31**	**0.25**	**0.22**

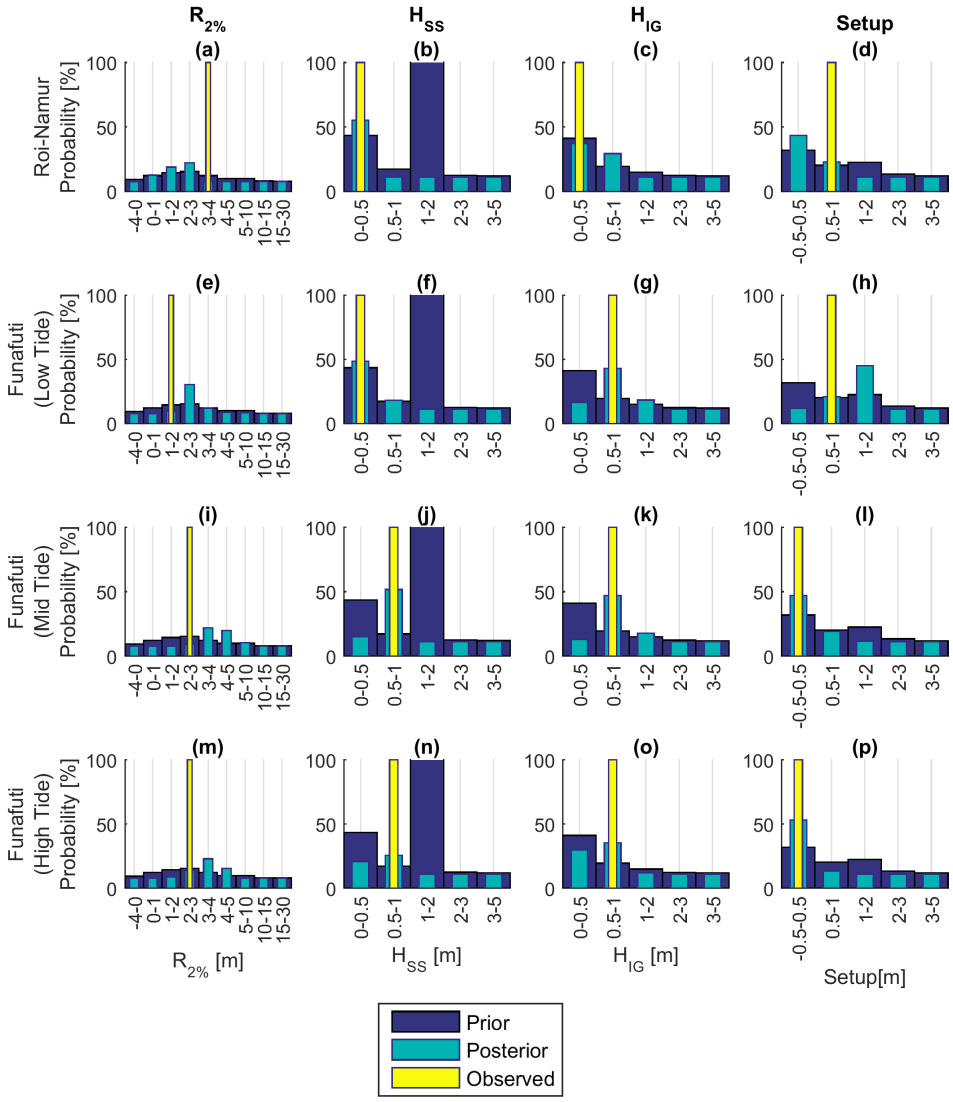

Figure 4.13: Bayesian network validation against case studies. The dark blue bars represent the prior probability distribution for all cases in the network, and the lighter blue bars represent the posterior probability distributions, based on the hydrodynamic forcing and reef characteristics of the test cases. The yellow bars indicate the observed values of each variable from the case study.

Furthermore, the incorrect runup predictions in Figure 4.13 are overestimates in 3/4 cases (false positives). Thus, the network prediction is conservative, which is preferred over false negatives for flood forecasting purposes.

5

DISCUSSION

CHAPTER SUMMARY

This chapter discusses the results from the analyses presented in Chapter 4, identifies opportunities for applications of the method, and suggests opportunities for future research. The XBeach model is generally capable of reproducing phenomena observed in the literature, such as spectral transformation to lower frequencies and resonance. Narrow, smooth reefs with steep fore reef slopes are most prone to flooding and resonant low frequency anomalies. The synthetic dataset of XBeach results should be analyzed in greater depth for future studies.

The Bayesian network provided insights into the relative importance of different parameters. The network's predictive skill was analyzed and strategies are presented for making future improvements by simplifying the BN.

The sensitivity of resonance was explored, revealing a strong dependence on reef width, fore reef slope, and wave steepness. Furthermore, a strong positive correlation between resonant low frequency anomalies and runup was established using the Bayesian network, suggesting that such phenomena may indeed be responsible for major flooding.

The application of Bayesian networks to early flood warning systems, climate change impact assessments, and the planning of reef restorations as nature-based flood defenses is also discussed here. We then outline other avenues for future research, including the investigation of undular bores, cluster and regression analysis, and the development of a reef morphology database. Lastly, the application of traditional knowledge to flood forecasting is explored.

5.1. MODEL DISCUSSION

5.1.1. XBEACH

The XBeach model is generally capable of reproducing phenomena observed in the literature, such as spectral transformation to lower frequencies and resonance. The sensitivity analysis carried out here confirms the principal findings of Quataert et al. (2015): that narrower, smoother reefs with steeper fore reef slopes are more susceptible to runup. The agreement with general trends on other sites supports the use of XBeach Non-Hydrostatic as a tool for modelling wave transformation on coral reefs and runup on low-lying tropical islands.

The modelling approach taken here was limited by several key factors, mostly related to the simplifications necessary to carry out the many simulations. The idealized one-dimensional reef profile reduces the topographic complexity present in most reefs. Most significantly, it excludes two dimensional processes which may be relevant for the prediction of flooding. Coral atolls are often relatively small and exhibit relatively large alongshore variations in morphology (e.g. spur and groove formations or highly curved coastlines). Furthermore, the influence of hydrodynamic processes like refraction, diffraction, and directional spreading is lost with the approach used here.

Furthermore, the sensitivity analyses carried out early in the model set up process revealed a dependency of wave height on grid resolution via the maximum wave breaking steepness parameter. As grid resolution was made progressively finer, modelled wave heights increased without converging on consistent values. This can be explained by higher grid resolution permitting steeper wavefronts to be resolved. The issue was satisfactorily resolved for this project by reducing the maximum allowable wave steepness to a value obtained from physical modelling tests (Roelvink et al, 2015a).

However, future studies should expand the sensitivity analysis conducted here to determine the appropriate grid resolution and breaking steepness parameters to accurately represent reef hydrodynamics in XBeach Non-hydrostatic. Physical modelling studies that specifically address breaking steepness on reefs should be carried out to determine the range of valid breaking parameters. This seems especially important for coral reefs since waves with higher breaking steepness penetrate further across the reef flat. This shifts the breakpoint shoreward and may thus influence many processes including wave attenuation, low frequency wave generation, resonance, and runup. Increasing the maximum wave steepness also seems to produce more undular bores, which may affect energy transfer between low and high frequencies.

Additional modelling carried out in the future should also consider smaller or more focused input samples. Sampling techniques such as Latin hypercubes (Helton et al., 2005) could be used to reduce the number of input parameters while maintaining a representative selection of the entire dataset. If successful, these techniques would also reduce computational requirements, since fewer XBeach simulations would need to be carried out to provide equivalent predictive skill. The tradeoffs between including more detail by running more simulations, and the value of that additional detail versus the extra runtime must be considered carefully. van Arkel (2016) found that Latin hypercube sampling yielded a more efficient sensitivity analysis for wave input reduction, speeding the process by a factor of 5 while maintaining accuracy levels.

Because this study attempted to generalize reef hydrodynamics using a simplified

model, it was challenging to directly calibrate and validate the XBeach model. Thus, additional modelling studies of XBeach Non-Hydrostatic using extensive field measurements like those of Quataert (2015) and Gawehn (2015) are recommended. Furthermore, laboratory experiments using scale models of reefs may provided useful validation of the simulations carried out here, particularly if idealized profiles are also constructed.

The tests carried out in this thesis are by no means exhaustive, considering only a fraction of the total data generated by the XBeach simulations. Given schedule limitations of the present thesis project, only selected analyses could be carried out on the synthetic dataset. On account of the sheer number of simulations, only burst-averaged statistics were examined for most cases. The high-level analysis carried out in this thesis could be used to identify simulations of interest (e.g. those with resonant low frequency anomalies). Some of the in-depth analysis procedures carried out for reef hydrodynamics in the literature (e.g. cross-correlation of waves propagating across the reef) should then be attempted on these simulations.

Lastly, the XBeach results raise questions that may lead to new lines of research. For instance, undular bores were extremely prevalent in many of the model results. Given their potential for transferring wave energy from low to high frequencies, they may play an important role in reef hydrodynamics. Thus, further investigation is required to validate their presence in the model and explain the processes involved (Section 5.3.1).

5.1.2. BAYESIAN NETWORK

Predictive skill testing, sensitivity analysis, and validation enabled us to learn much about the processes governing reef hydrodynamics. Offshore hydrodynamic forcing (water level and wave conditions) and reef width are the most essential processes to account for in predicting flooding of reef-fronted coastlines. The best-performing network configuration was one that includes all of the input variables, although certain variables like beach slope were found to contribute less to overall predictive skill. The confusion matrices revealed a tendency to underpredict low frequency resonant anomalies, illustrating the complex nature of this phenomenon.

The network tended to overpredict runup for the case studies from the literature, although in most cases showed improved predictions over the prior distribution for H_{SS}, H_{IG}, and setup. Errors may be attributed to simplifications made in transforming the observed data to the BN or discretization. Is it more important to predict a precise value for flooding or just exceedance above a threshold? If so, then perhaps a network with fewer bins would yield improved predictions. Alternative network configurations should continue to be explored.

Plant and Holland (2011*b*) found that errors in their predictions could be attributed to the relative rarity of the scenario captured by their training data (e.g. resonant anomalies). This could lead to the false conclusion that the parameter adds no value and that it is best to simply remove the parameter. A better solution is to improve the training dataset to provide a more representative range of conditions.

Through these tests, the Bayesian network demonstrated its value as a tool for data management and exploring relationships between variables within large multidimensional datasets. It also proved itself as a fast and user-friendly tool, making it a promising component in an early warning system. Furthermore, it shows potential for use as a tool

in climate change impact assessment and the planning of reef conservation or restoration projects.

LOG-LIKELIHOOD TESTS

The log-likelihood tests are valuable since they shed light on both optimal network layouts and the sensitivity of the network to different input parameters. The comparisons in Tables 4.1 and 4.2 suggest that Configuration A (multiple bins for each output variable) is the best overall network that has been tested. However, Configuration C shows better predictive skill than A when predicting runup and resonance, because these parameters may be adversely affected by unnecessary parameters.

The withheld variable plots in Figure 4.11 show which variables have the most influence, and which may worsen predictions by adding uncertainty. From these plots, it can be determined that hydrodynamic forcing (wave and water level conditions) and reef width are the most important variables to estimate flooding on reef-fronted coasts. Including other variables may improve predictive capabilities for more complex phenomena like low frequency resonance. Hence, future research should attempt to optimize the network design by using the results of this LLR test to determine the appropriate connections between nodes.

CONFUSION MATRICES

Predictive errors are highest for low frequency waves (Figure 4.3). The fact that none of the anomalously high VLF events were predicted (false negative rate of 100%) can perhaps be explained by the complex dependencies with other variables, and by their relative rarity. Such events constitute less than 1% of all tested cases, so the BN has fewer cases to learn from and characterize what leads to low frequency anomalies. If resonance only occurs for very specific combinations of reef morphology and hydrodynamic forcing, then the network may find it harder to generalize if it only has a limited number of examples to draw from.

Generally, underprediction is more common than overprediction, which is less conservative, suggesting that the current BN is better at predicting low-energy events. This is inadequate for early warning systems, since in many cases the present network would not sound the alarm and people would be caught unaware.

How can these predictive shortcomings be addressed? Additional simulations in the range of interest (e.g. narrower reefs) may help by providing the network with more examples of the conditions it is intended to predict. In Figure 4.6, the cases of interest (VLF anomalies) make up only a very small percentage of the total cases simulated. By prioritizing the inputs which are more likely to result in resonance or extreme flooding, the modelling process can be more efficient. Unlikely combinations of variables may also be filtered out, and the relationships between variables should be investigated further. There may also be output variables not considered here that could serve as better indicators for the processes of interest (e.g. Iribarren number, amplification from reef crest to shore).

OVERFITTING

For normalized runup, the model becomes overfit when more than 5 bins are used for the W_{reef} node (4.12). Given the large and diverse parameter space simulated here, it is

possible that with too many bins, the network becomes unable to generalize and learn from trends. It instead simply "memorizes" the results it was trained on (like a simple lookup table with interpolation).

The error rate and overfitting tests should also be carried out for simpler network configurations to determine whether performance gains can be made in that way. The number of input bins can be reduced for other nodes to limit network complexity. This is made challenging by the discrete input distributions currently used, which do not lend themselves well to being regrouped into bins of equal number (this is perhaps justification for a random sampling approach in future studies). Alternatively, the connections between nodes could be altered based on the outcome of the log-likelihood tests. For example, the links between reef width and setup or beach slope and infragravity wave height could be removed. If overfitting reduces for these simplified configurations, then the network's predictive skill shows an improvement.

At the heart of this optimization problem lies the balance between the size of the conditional probability tables (CPTs) calculated for the network, and amount of data available to fill each entry in the tables. The size of conditional probability tables used internally by the BN is proportional to the number of nodes and bins in the network. The BN's ability to generalize and learn from trends depends on having sufficient data to feed each entry in the table. The learning algorithm in Netica quantifies this using the concept of 'experience' (Norsys, 2003). With each additional training case, the network gains experience and is able to give predictions with greater certainty. Conversely, if the CPTs are too large and complex relative to the amount of data provided, the network will be more uncertain Poelhekke et al. (2016).

VALIDATION

When tested on case studies from the literature, the Bayesian network showed poor predictive skill for runup (Table 4.4 and Figure 4.13), although predictions for H_{SS}, H_{IG}, and setup were generally better. The LLRs and probabilities are based on the bin into which the actual observed outcome falls. If a prediction is close but on the edge of a bin (i.e. 0.99 when the threshold is 1.00), the prediction may be registered as incorrect. However, inverse predictions can be used to determine what the critical boundaries are for each parameter. By identifying sensitive spots and adding bins accordingly, we may improve our predictions.

While discretization can be held responsible for some of the errors, the main shortcoming is that only a limited number of case studies were available for calibration and validation of the models. If more data becomes available, then it should be possible to improve the models' predictive skill.

5.1.3. RESONANCE

We established from field observations that resonant low frequency waves may be significant contributors to flooding of reef-fronted coastlines. We then identified cases of anomalously high low frequency waves coinciding with the resonant frequency of a given reef. In this section we can use the Bayesian network to ask questions about the dependencies and relationships that lead to resonance.

The first question to consider was whether or not resonance was being reproduced in

the XBeach model. The sensitivity analysis of VLF wave height showed a local maximum for 100 m wide reefs (Figure 4.4). Since low-frequency resonance is expected to be more likely on narrow reefs, this was a promising indication that the model was simulating resonant amplification.

As Figure 4.4 indicates, VLF wave height is has a strong positive correlation with offshore wave height. To reduce this dependency and uncover more anomalous events (as might be associated with resonance), LF wave heights were normalized by offshore wave height and squared. Doing so also made differences between high and low values more pronounced. Hence, large values of $(H_{IG}/H_0)^2$ and $(H_{VLF}/H_0)^2$ indicate low frequency waves which are surprisingly high given the input conditions. These are the events that will be more likely to catch forecasting systems off guard, so are thus important to predict.

Following the example of Gawehn et al. (2016), we next investigated anomalously high LF waves as a function of depth and observed frequency at the inner reef flat (Figure 4.5). This reproduced similar trends, with LF anomalies clustered in the low frequency range at greater water depths. To further prove the occurrence of resonance in the model, a final test was carried out to determine if LF anomalies were also associated with the resonant frequency of each given reef (Figure 4.6). A clear peak was shown at $f_{m-1,0}/f_{n,0} = 1$, suggesting that the anomalies were indeed forced by resonant amplification. Thus, multiple lines of evidence suggest that the XBeach Non-Hydrostatic model is capable of simulating low frequency resonance for generalized reef configurations.

One of the most useful capabilities of a Bayesian network is inverse prediction. Just as we can use Bayesian networks to estimate the likelihood of effect 'A' given cause 'B' (forward prediction), we can go backwards to find the likelihood of cause 'B' as a contribution to effect 'A'. For example, we can predict runup for a given reef and forcing conditions (forward prediction) but also ask questions like "which reef widths are most associated with high runup?" (inverse prediction).

Figure 5.1 shows a three-node Bayesian network that uses normalized VLF wave height and relative resonant frequency to inversely predict reef flat width. (a) indicates the prior distributions of the unconstrained network, representing all tested cases. Reef flat width is nearly uniformly distributed, and only 2.4% of cases lie near resonant frequencies ($f_{m-1,0}/f_{n,0} = 1$). Gawehn et al. (2016) estimated that VLF resonance occurred 3.5% of the time. Similarly, in our simulations, anomalously high VLF events comprised less than 1% of all cases.

To make the inverse prediction, the VLF node is constrained by considering only anomalously high cases ($(H_{VLF}/H_0)^2 > 0.1$), and the $f_{m-1,0}/f_{n,0}$ node set equal to 1. The posterior probability distribution of reef flat width (b) then shifts to a much narrower range (a reduction in uncertainty), featuring a mean width of 114 m (down from the prior average of 443 m for all cases). This thus indicates that VLF anomalies occurring at resonant frequencies have a strong association with narrow reef flats in the 50-250 m width range. Performing a similar analysis for each input variable, Figure 5.2 was produced. It illustrates the range of input variables most likely to result in resonant VLF anomalies. Figure 5.3 shows the equivalent plots for anomalously high waves in the infragravity band.

Figures 5.2 and 5.3 reveal much about the factors contributing to resonance at low

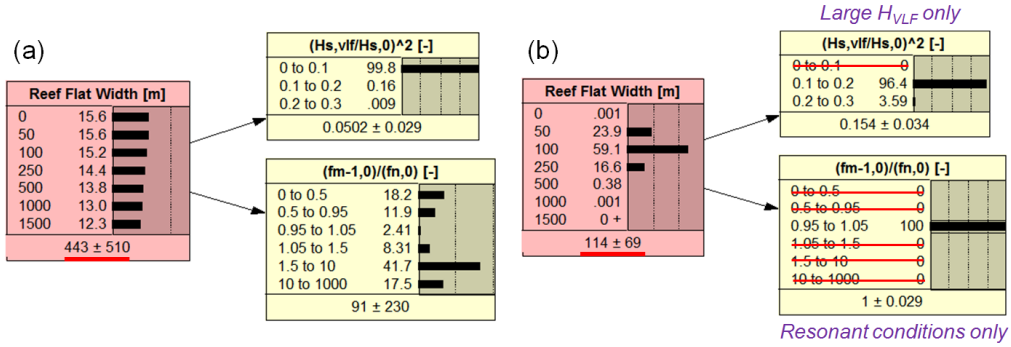

Figure 5.1: (a) A priori Bayesian network depicting the relationship between reef width, normalized VLF wave height, and relative resonant frequency. (b) Bayesian network with anomalously high VLF waves and resonant conditions selected to inversely predict reef width.

frequencies. As demonstrated in Figure 5.1, VLF resonance tends to favour narrow reefs (50-250 m) (subplot c). This is also the case for infragravity waves, although the reefs tend to be narrower (50-100 m).

Steep fore reefs are overwhelmingly associated with resonant VLF conditions (d). Breakpoint generation of low frequency waves is most effective if the breakpoint excursion is small compared to the standing wavelength (Baldock et al., 2000). This explains the strong correlation between fore reef steepness and resonance: the steeper fore reefs have a narrow breaking zone, which serves as an effective node for standing and resonant VLF waves. The dependency on fore reef slope decreases slightly for infragravity waves, but is still biased towards steep slopes.

The likelihood of resonance increases slightly with shallower beach slopes (e), a counterintuitive result, since resonance typically favours reflective conditions (i.e. steeper landward boundaries). However, this expected trend is clearly shown at infragravity frequencies, where resonance is highest for steep beaches.

Since friction (f) does not influence the geometry of the reef or offshore hydrodynamic forcing, it does not directly determine whether or not resonant conditions occur. However, it can have a damping effect on resonant amplification (Pomeroy et al, 2012a), which explains why lower friction is more likely to contribute to resonant anomalies. This trend also holds true for infragravity waves, although the sensitivity is less. This relationship does not bode well for reefs with failing health: if reefs become smoother due to dying coral, then resonant amplification would become more likely.

Although the infragravity and VLF wave heights were normalized by offshore wave height, it still exerts an influence on the variables considered here. VLF anomalies have a bimodal offshore wave height distribution, with the main peak at 5 m and a smaller peak at 3 m. This may be explained in part by the dependencies between wave height and period created by our choice of wave steepness as a varying parameter. Resonance is highly dependent on incident wave period, and each wave period is tied to a particular wave height (Table 3.2). It is possible that 3 m waves (with 19.6 s periods at steepness of 0.005) are particularly prone to exciting one of the reef configurations modelled here,

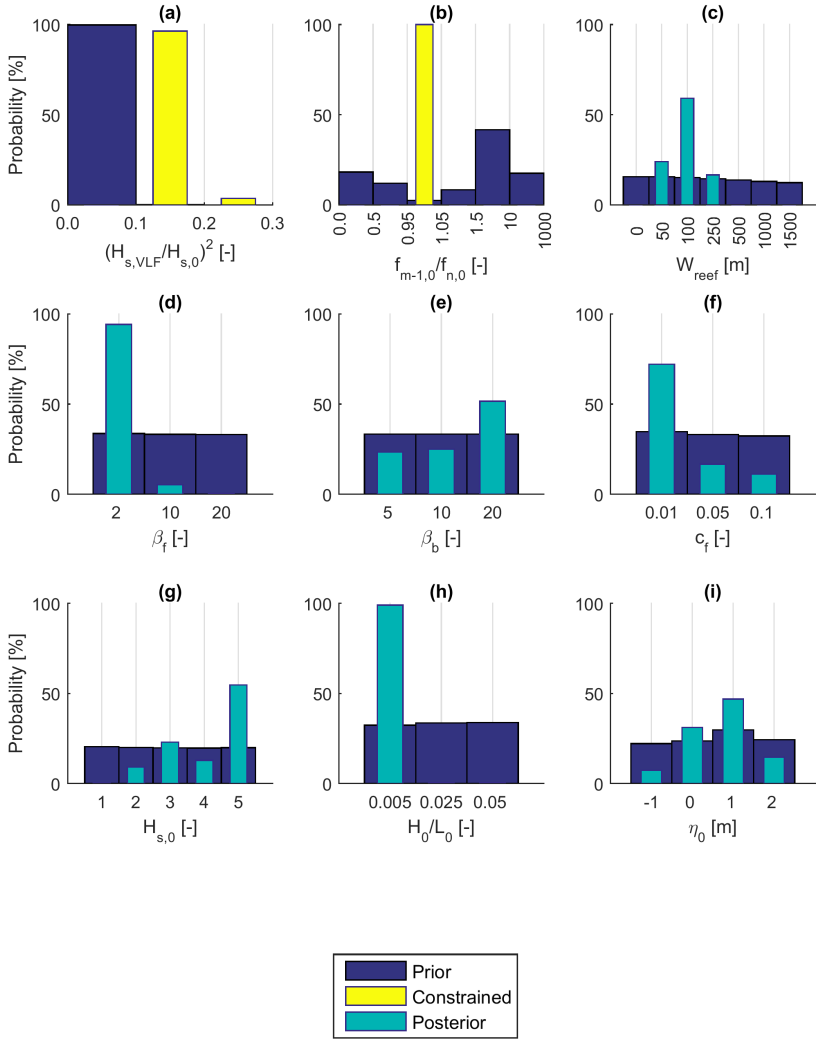

Figure 5.2: Sensitivity analysis of resonant VLF waves using the Bayesian network. The dark blue prior distributions represent the initial probability of occurrence for each variable based on all cases in the synthetic dataset. The $(H_{VLF}/H_0)^2$ and $f_{m-1,0}/f_{n,0}$ variables were then constrained to include only anomalously high VLF waves ($(H_{VLF}/H_0)^2 > 0.1$) and cases at the resonant frequency ($f_{m-1,0}/f_{n,0} = 1$), depicted in yellow (subplots a-b). The teal posterior distributions represent inverse predictions for the input variables based on the constrained nodes (subplots c-i). Hence, they show which input conditions the resonant events are most likely to be associated with.

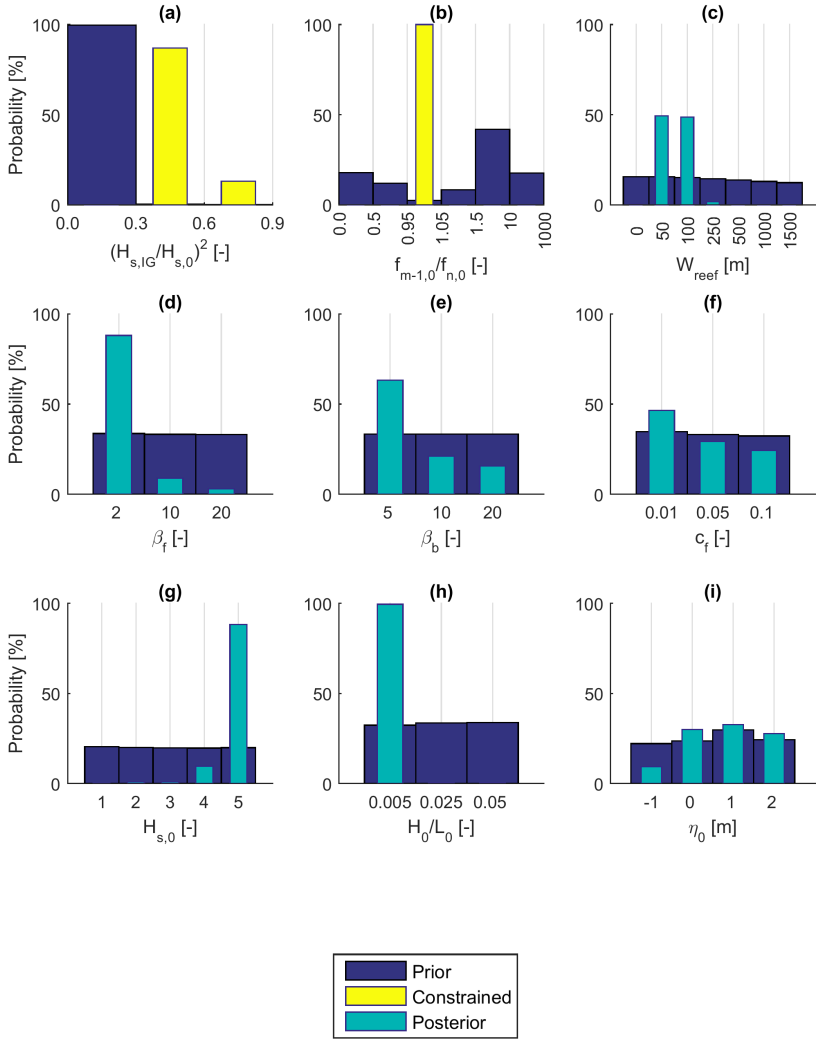

Figure 5.3: Sensitivity analysis of resonant IG waves using the Bayesian network. The dark blue prior distributions represent the initial probability of occurrence for each variable based on all cases in the synthetic dataset. The $(H_{VLF}/H_0)^2$ and $f_{m-1,0}/f_{n,0}$ variables were then constrained to include only anomalously high IG waves ($(H_{VLF}/H_0)^2 > 0.1$) and cases at the resonant frequency ($f_{m-1,0}/f_{n,0} = 1$), depicted in yellow (subplots a-b). The teal posterior distributions represent inverse predictions for the input variables based on the constrained nodes (subplots c-i). Hence, they show which input conditions the resonant events are most likely to be associated with.

explaining the peak. However, for infragravity frequencies, resonant anomalies are overwhelmingly correlated to the highest offshore waves.

As alluded to above, wave steepness plays an important role in determining resonance since it controls wave period in our analysis. The distribution in subplot (h) for both infragravity and VLF cases shows a near-100% likelihood that resonant anomalies have low wave steepness. Whether this is because of wave steepness or just its role in controlling period remains to be seen. Regardless, it underscores the threat that remotely generated swell waves (characterized by long periods and low steepness) pose for creating resonant conditions.

Lastly, offshore water levels are considered in (i). In both cases, the distributions peak at 1 m before dropping again at 2 m. This may seem to contradict the notion that increasing water depths on the reef flat create more favourable conditions for resonant, but this is not necessarily the case. Offshore water levels have a strong moderating effect on wave setup (illustrated in Figure 4.2), which also changes the depth of water on the reef flat. Since wave setup decreases with increasing offshore water level, there may be a compensating effect where the high setup generated at 0 and 1 m water levels actually increases total depth more than at 2 m where setup is lower. Thus, the relationship between future sea level rise and resonance is not straightforward, and may vary from reef to reef.

Following a similar line of reasoning, we produced Table 5.1, using W_{reef}, η_0, and $T_{n,0}$ to inversely predict T_p. This table presents the offshore peak wave period most likely to result in resonant conditions for a given reef and water level.

Table 5.1: Table of resonance risk derived from inverse Bayesian network predictions. Shorter reefs with greater water depths have the lowest resonant periods, making it more likely that they will be excited by offshore waves. For a 1000 m wide reef, the resonance period is 1806 seconds (30 mins), which is generally beyond what you would observe in nature. Prior prediction for all cases is 12.2 ± 7.5. (*) denotes cases where uniform distributions are returned, indicating total uncertainty.

W_{reef}	η_0	$T_{n,0}$	T_p
50	1.0	64	11.5 ± 5.8
	2.0	45	13.1 ± 5.5
100	1.0	128	14.0 ± 6.1
	2.0	90	17.3 ± 6.8
250	1.0	319	20.2 ± 6.4
	2.0	226	23.6 ± 4.6
500	1.0	639	20.3 ± 7.8
	2.0	452	14.5 ± 7.4*
1000	1.0	1277	14.5 ± 7.4*
	2.0	903	14.5 ± 7.4*

Curiously, peak offshore periods increase for deeper reef flats, which is counterintuitive. This might be explained because the water level on the reef flat that determines resonance is not necessarily the offshore water level. As Péquignet et al. (2009) found on Guam, increased reef flat depth due to setup under large storm waves may enable

resonance even at lower still water levels. $T_{m-1,0}/T_{n,0}$ thus has a dependency on wave setup that is not accounted for here. The transformation complex that converts offshore T_p to $T_{m-1,0}$ at the shoreline is complex, and merits further investigation. In Table 5.1, uncertainty (σ) grows with reef width. Further complicating the matter, T_p in these simulations is directly dependent on H_0 through wave steepness (H_0/L_0), such that longer periods are associated with higher waves. To negate this dependency in future simulations, T_p should be varied independently of H_0. Nonetheless, this table provides a useful insight into the offshore conditions that may most affect a certain island.

Figure 4.11 shows that friction is not necessary to predict resonance but that it is required to predict VLF anomalies. This concurs with the findings of Pomeroy, van Dongeren, Lowe, van Thiel de Vries and Roelvink (2012), who note that bottom friction only controls damping of the amplification, not the resonant frequency itself.

More detailed site-specific analysis could be used to construct similar hazard tables for individual islands. When forecast offshore peak periods fall into the danger zone, warnings should be activated. This is much cruder than using the full Bayesian network to predict flooding but may still have value as a first-order estimate of resonant conditions.

We have shown so far that XBeach can simulate low frequency resonance, and that there are clear relationships with forcing and morphology. However, what are the consequences of low frequency resonance in terms of flooding? To make this connection, a simple three-node Bayesian network (Figure 5.4) was constructed with only $(H_{IG}/H_0)^2$, $(H_{VLF}/H_0)^2$, and $R_{2\%}$ (as a proxy for flooding).

Anomalously high infragravity and VLF wave events (defined here by $(H_{IG}/H_0)^2 > 0.3$ and $(H_{VLF}/H_0)^2 > 0.1$, respectively) make up less than 1% of all simulated cases. When the remaining 99.5% are removed from consideration, the mean runup increases dramatically from 2.3 m to 9.3 m. Even when the large uncertainties in the estimate are accounted for ($\pm$3.7 m), there is a clear increase. This strong positive correlation suggests that these anomalously high LF waves are associated with high runup and hence inundation. Given the strong correlation between anomalously high LF waves and resonant conditions established in Figure 4.6, our model results suggest that resonant conditions can be associated with large inundation events.

This is supported by Figure 5.5, which shows a positive correlation between low frequency anomalies and runup. The scatter at infragravity frequencies (a) is less than that observed for the VLF band (b). This suggests that while nearly all high runup events have a relatively strong infragravity component, there is less of a dependency on anomalously high VLF waves. The highest values of $(H_{VLF}/H_0)^2$ do not lead to the highest runup.

It should be noted that uncertainty (represented in Figure 5.4 by the standard deviation) increases from 2.2 to 3.7 m. This indicates that even if the occurrence of resonance can be predicted, the degree of resonant amplification remains uncertain. Future research should seek to quantify this amplification so as to provide more precise runup estimates.

The main conclusion of this resonance analysis is that XBeach Non-Hydrostatic is capable of modelling resonant low frequency anomalies, but that it is challenging to predict when they will occur. Generally, narrow, smooth reefs with steep fore reefs exposed to large, less steep waves are most prone to resonant VLF conditions. Hence, extreme

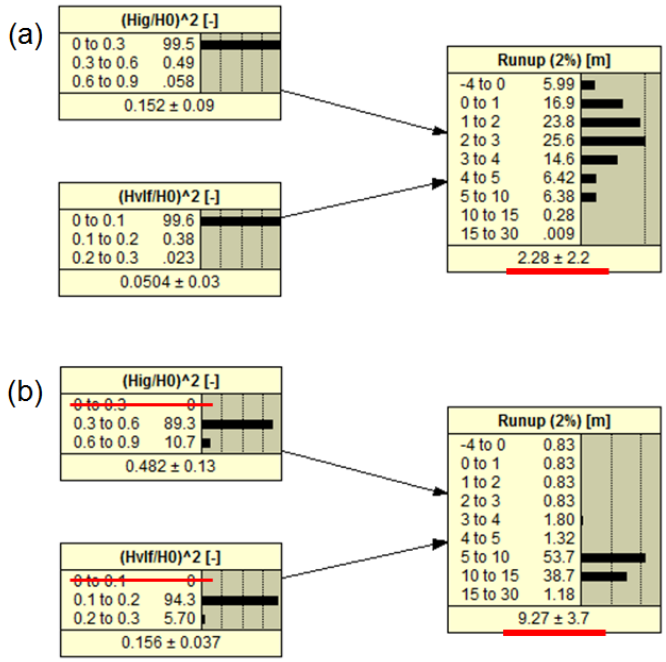

Figure 5.4: (a) Unconstrained Bayesian network. (b) Bayesian network with only anomalously high IG and VLF waves selected.

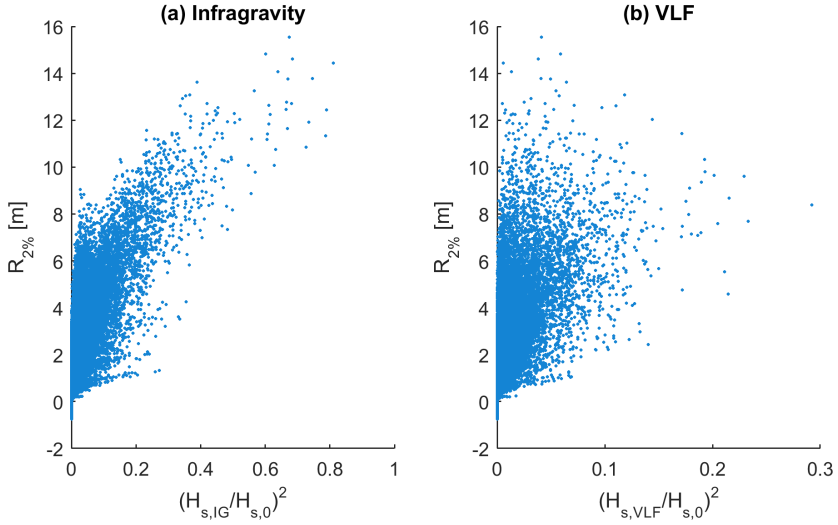

Figure 5.5: Runup as a function of low frequency anomaly height in (a) the infragravity band, and (b) the VLF band.

swell poses a significant threat. Early warning systems should always be wary of large waves, but understanding resonance will help to better predict "surprise" flooding cases.

5.2. APPLICATIONS

There are three main applications for the tools presented in this thesis: early warning systems, climate change impact assessments, and the analysis of nature-based flood defenses. Although most of the cases analyzed in this study were based on atolls in the tropical Pacific, the methods used here could be widely applied to low-lying tropical islands and fringing reef coastlines elsewhere. The highest priority should be given to populated areas and critical infrastructure. Marginally-inhabited outer islands that are threatened may drive the first wave of migration to major population centres, so they also require due consideration. Even uninhabited tropical islands hold tremendous ecological value, so it is worth understanding the consequences of wave-induced flooding for them, too (Andréfouët et al., 2015). Understanding the fate of these islands will help inform conservation efforts.

5.2.1. EARLY WARNING SYSTEMS

The main deliverable outcome of this thesis is a flood prediction model that can form the basis for an early warning system. The synthetic dataset and Bayesian network serve as a proof-of-concept for how these tools might be applied in reality.

High tides are deterministic and simple to predict, but they alone are insufficient to make real-time flood predictions. The task of predicting wave climates for islands in the western tropical Pacific ocean is made challenging by the limited observational data available (e.g. wave buoys), and the important role of long-period swell generated by distant storms rather than local conditions (Storlazzi, Shope, Erikson, Hegermiller and Barnard, 2015). Hence, global or regional wave models such as WAVEWATCH III (Tolman, 2009) may be useful tools for generating hindcasts or forecasts that can serve as inputs for site-specific models like ours.

The prediction methods developed for this thesis add value to existing tidal predictions by considering the unique interactions between waves, water levels, and a given island. If supported by hydrodynamic inputs from a regional wave model and a database of reef characteristics for each island, it should be possible to create custom flood forecasts for individual islands. A conceptual example of this is provided in Figure 5.6.

Although XBeach alone could be used to develop a flood forecast system (Bosserelle et al., 2015), the chief advantages of Bayesian networks are their speed and capability to account for uncertainty.

Given that the area of interest spans several thousand kilometers and includes many different countries, a multi-scale, cross-disciplinary approach will be needed to implement the model. Other key considerations include how to effectively communicate across islands where the hazard levels might be very different, and how to encourage international cooperation between different island groups facing similar threats.

Pilot studies should be considered first, starting with high-priority sites with highly populated areas or critical infrastructure. Key infrastructure to protect may include villages, roads, airports, ports (van Dongeren et al., 2016), military installations, places of

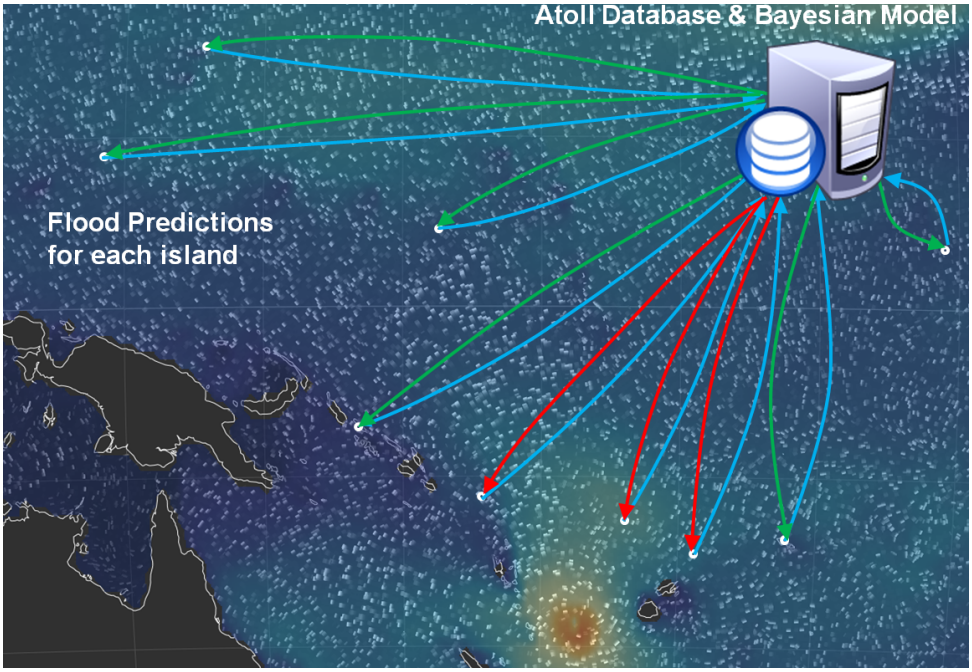

Figure 5.6: A conceptual diagram illustrating how a database of reef morphology and offshore wave heights from a global or regional wave model could be used in a Bayesian network to predict flooding for different islands across the tropical Pacific. Blue lines represent wave and water level data fed retrieved from regional wave and climate models, while the red and green lines represent positive or negative predictions of flooding derived from the Bayesian network. Source for background rendering of MMAB/EMC/NCEP/NWS/NOAA WAVEWATCH III outputs: Beccario (2016).

cultural significance, cemeteries, or aging radioactive waste disposal sites (Hamilton, 2013).

Anthropogenic modifications to the shoreline and could also be implemented in the network. For instance, shore protection structures or flood defenses could be represented by varying beach steepness and crest height.

Although the emphasis in this report is on the potential for Bayesian networks on real-time early warning systems, they could also be used in the development of flood risk maps for land use planning and evacuation purposes. If coupled with 2D inundation models like LISFLOOD, detailed hazard maps could be produced to identify vulnerable areas and estimate life safety risk. Furthermore, if building characteristics are known, damage to structures could also be estimated using simple stage-damage relationships or more sophisticated approaches (where sufficient data is available). van Verseveld et al. (2015) and Jäger, den Heijer, Bolle and Hanea (2015) use Bayesian networks to predict direct economic damage to houses and infrastructure as a result of flooding.

A simple alternative prior to the implementation of a fully-fledged EWS could be a simple lookup table customized for a specific island or town. The key reef characteristics could be obtained from remote sensing data, and then entered into the Bayesian

network to determine combinations of wave conditions and water levels (generated by wave and tidal models) which may cause flooding in locations below a certain elevation. This could improve on existing warning systems which focus only on "King Tides" by including the effects of wave-induced flooding.

5.2.2. CLIMATE CHANGE IMPACT PROJECTIONS

Real-time flood forecasting is not the only use of the Bayesian network developed here. What-if analyses can be conducted to investigate hypothetical climate change scenarios, such as changes to sea level, wave climate, reef roughness, or mitigation measures (Section 5.2.3). For instance, Shope et al. (2015) use the formulation of Stockdon et al. (2006) to estimate runup under future climate change scenarios. The Bayesian network developed for this study might be able to provide a more detailed estimate by considering the full suite of processes involved in reef hydrodynamics.

This thesis may also be useful for improving our understanding of the morphological evolution of atolls under future scenarios. Since many of the forces driving morphological changes are the same as those responsible for flooding, it is possible that these changes could be predicted by including variables related to sediment transport.

From the predictions of wave overtopping, time series of discharge could also be produced and coupled with inundation models like LISFLOOD (van der Knijff et al., 2010) for individual islands (e.g. Figure 5.7). Alternatively, the results from this study can be used to iteratively develop new parametric equations for runup on reefed coastlines (see Appendix G), which may be incorporated directly into large-scale models.

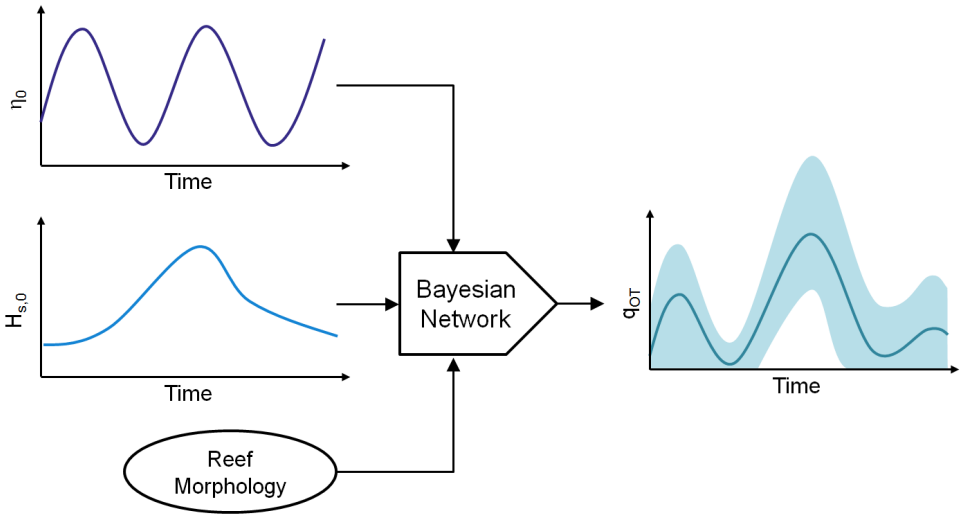

Figure 5.7: Hypothetical overtopping time series based on forecast hydrodynamic input and reef characteristics. The probabilistic nature of the Bayesian network would also allow uncertainty to be computed for the prediction (light blue shaded bands).

These could be coupled with groundwater models to investigate the threat to freshwater supplies under future conditions and examine, for instance, how long a given is-

land has before its supplies reach critical levels.

5.2.3. NATURE-BASED FLOOD DEFENSES

The reaction to climate change does not have to be passive—mitigating measures can be taken by affected islands to improve resilience to flooding. The value of coral reefs as nature-based flood defenses can also be analyzed with this model and used to prioritize conservation or restoration efforts. Given scarce resources available for such projects, this tool can be used to understand which areas are most vulnerable and where the best value for money lies. A potential strategy could be to identify resonance-prone reefs near populated areas, as these will be a higher priority for restoration.

As coastal engineers, the only variable on reefs over which we have control is roughness. Since reef roughness is correlated to its health, restoration efforts that improve coral ecosystem quality may increase roughness and thus provide more effective wave attenuation. Runup as a function of reef width and roughness is examined in Figure 5.8.

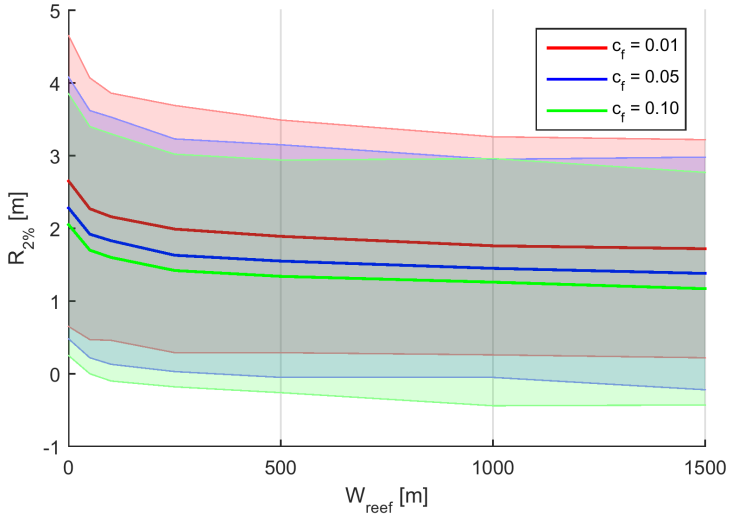

Figure 5.8: Runup as a function of reef width and roughness as determined by three-node Bayesian Network. Bands indicate uncertainty.

Worth examining is the difference in runup attenuation for a reef of a given width. That is, do we see bigger gains by increasing roughness of shorter or wider reefs? In Figure 5.8, relative attenuation is almost constant for a given c_f. The spread across all scenarios decreases with width, which suggests that variability in offshore conditions gets damped out by breaking and friction. Narayan et al. (2016) found that reef restoration costs vary considerably from site to site. If these costs are considered fixed per unit area restored, then a shorter reef would be less expensive to restore. Hence, more short reefs could be restored for the same cost as fewer wide reefs, allowing limited resources to go further.

A potential strategy is to carry out a sort of "triage", identifying suitable pilot sites en

masse with GIS analysis. Narrow reefs in high risk urban areas with a history of disruptive floods should be the first priority. This is a gross oversimplification given the aforementioned challenges of associating c_f to reef health, but it at least provides a high-level conceptual estimate of potential restoration sites.

5.3. NEXT STEPS

There are many additional analyses and ideas that lay beyond the scope of this thesis. This section describes some promising avenues for future research and proposes plans for further investigation. The existing dataset is massive and could benefit from further data mining and filtering to explore trends and derive new parametric relationships. Furthermore, the development of a database with field observations of reefs could be used to further refine the methods used here, and also provide valuable data for further validation of predictive capabilities. Lastly, the traditional knowledge of people indigenous to low-lying tropical islands may be a valuable source of information.

5.3.1. UNDULAR BORES

Bores develop where there is a local difference in the water surface elevation, as is the case when a wave surges onto the relatively shallow reef flat (Figure 5.9a). The amplitude of the wave increases the local water depth, so the crest propagates faster than the trough ahead of it: $h_{crest} > h_{trough} \therefore c_{crest} = \sqrt{gh_{crest}} > c_{trough} = \sqrt{gh_{trough}}$ (Benjamin and Lighthill, 1954). This results in a gradual steepening of the wavefront, which continues until there is a balance with horizontal pressure gradients due to local vertical accelerations, or the wave breaks (Peregrine, 1966).

The nature of the bore depends on the ratio between the height of the wave front (H_{bore}) and the local depth (h). If the wave front is relatively high, ($H_{bore} > 0.75h$) (Peregrine, 1966), turbulent bores will form, as typically seen in surf zones on sandy beaches (Figure 5.9b). For relatively low wave fronts ($H_{bore} < 0.28h$) (Peregrine, 1966), undular bores form, which feature high frequency oscillations at their crest (Figure 5.9d). The wavelength and amplitude of these undulations decreases with distance from the bore front (Gallagher, 1972). The maximum amplitude of these undulations is restricted by breaking, and so a transitional state between $0.28h < H_{bore} < 0.75h$ exists where both turbulent breaking and undulations occur (Peregrine, 1966).

Undular bores are most frequently observed as tidal bores that propagate up rivers or in canals as gates open and close (Chanson, 2010). However, tsunamis have also been found to transform into undular bores (Grue et al., 2008; Madsen et al., 2008; Tissier et al., 2011). Most significantly for this project, undular bores have been observed on fringing reefs in the field (Gallagher, 1972) and on reef-shaped profiles in laboratory conditions (Nwogu and Demirbilek, 2010; Roeber and Cheung, 2012), but not examined in detail.

Two key features of reefs favour the generation of undular bores (Gallagher, 1972):

1. Steep fore reef slope abruptly changing to extensive reef flat
2. Rough bottom

Waves break and form a bore at the reef crest, but unlike sandy beaches with constantly-sloping bathymetry, the seabed then remains flat, so shoaling and breaking eventually

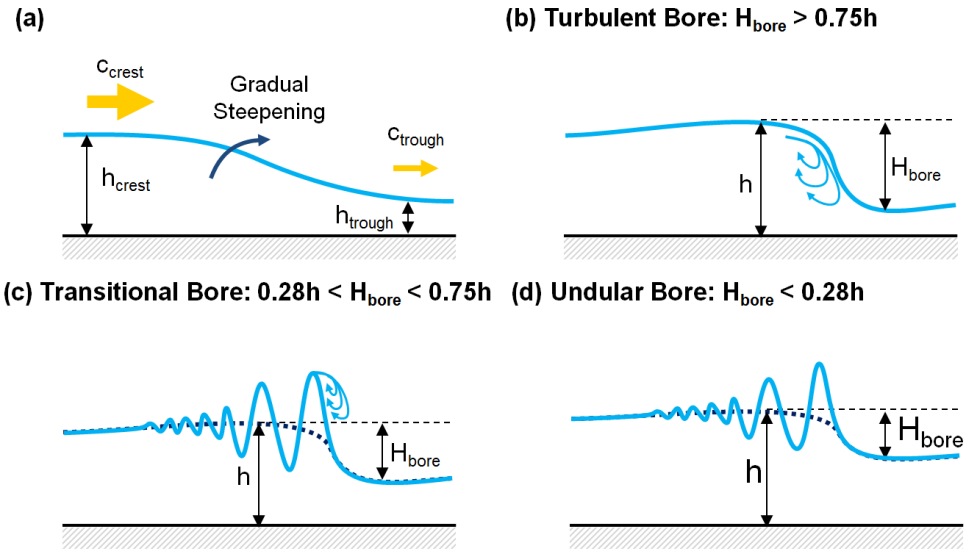

Figure 5.9: (a) Bores form as the crest of a wave moves faster than the preceding trough, steepening the wave front. The wavefront steepens until balanced by horizontal pressure gradients or the wave breaks. (b) Turbulent bores; (c) Transitional bores; (d) Undular bores.

cease. The energy available to be converted into undulations is greatest at this point, so here the seaward radiation of short waves is strongest (Gallagher, 1972). Radiation reduces as the waves travel shoreward and the bore decays. In idealized frictionless cases, energy is removed from the bore by turbulence at the breaking wavefront and by radiation of these small waves. However, given the high roughness of reefs, there will be additional dissipation by friction which may affect the short wave radiation. This influence is poorly quantified in the literature and should be studied further.

Unlike turbulent bores where energy is directly dissipated, undular bores transfer wave energy from lower frequencies to higher frequencies. These high frequency waves are then more easily dissipated by breaking or friction. Hence, undular bores may play an important role in reducing infragravity or VLF wave energy on reef flats.

The evolution of the bores is clearly illustrated in Figure 5.10, with undulations beginning to form just shoreward of the reef crest. By the time the bore reaches the 200 m mark, a full train of undulations has developed behind the bore front. As the bore continues to propagate, the undulations disperse and the height of the underlying long wave reduces. At the shoreline, the bore has completely decayed, leaving only the high frequency oscillations[1].

If allowed to propagate indefinitely, an undular bore eventually disperses into a se-

[1] In summary:
The curious undular bore
Propagates onward to shore
The energy flies
From low freqs to high
Until the wavefront is no more

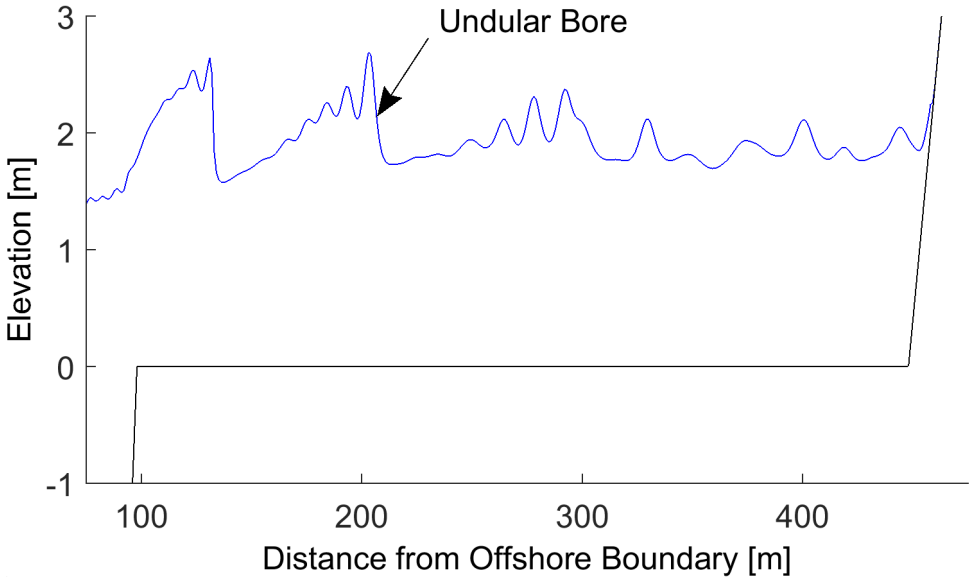

Figure 5.10: Example of undular bores forming on the reef flat in the XBeach model. It corresponds to a 350 m wide reef with high friction ($c_f = 0.1$) and a 1/2 fore reef slope, approximating the conditions at Diamond Head, Oahu, Hawaii when undular bores were observed there by Gallagher (1972). The water level was estimated as $\eta_0 = 1.5$, and $H_0 \approx 2m$, with waves of low steepness ($H_0/L_0 = 0.005$).

ries of cnoidal or solitary waves (Peregrine, 1966). However, there may be insufficient space for this to occur on shorter reefs, as the bore will first encounter the shore. Tissier et al. (2011) found that the undulations were not a primary control of runup, but that locally increasing the height of the main front could increase the impact on coastal structures. Zhao et al. (2016) further investigated the role of undular bores on runup using a Boussinesq model and analytical solutions to the nonlinear shallow water equations. They found that indeed, maximum runup coincides with the leading undulations of a bore. They also observe that the relative runup of each undulation (R_{und}/A_{und}) decreases more slowly for waves with more undulations. In the context of flooding, Madsen et al. (2008) cautions that it may be misleading to focus on these shorter oscillations, since the volume of water carried by the underlying low frequency bore is much greater.

Undular bores have been observed in many of the XBeach simulations carried out for this project (e.g. Figure 5.10), but have not been quantified. Future investigations should mine the synthetic model dataset to identify the presence of undular bores and determine any correlations with the input conditions. Physical modelling studies focusing specifically on the generation of undular bores across reefs would also be valuable for validating the behaviour shown in the model.

Field observations from remote sensing or in-situ wave measurements may also shed light on the circumstances surrounding undular bore generation. A cursory examination of aerial photos obtained through Google Earth for several fringing reefs and atolls around the Pacific suggests that undular bores are relatively common (e.g. Figure 5.11).

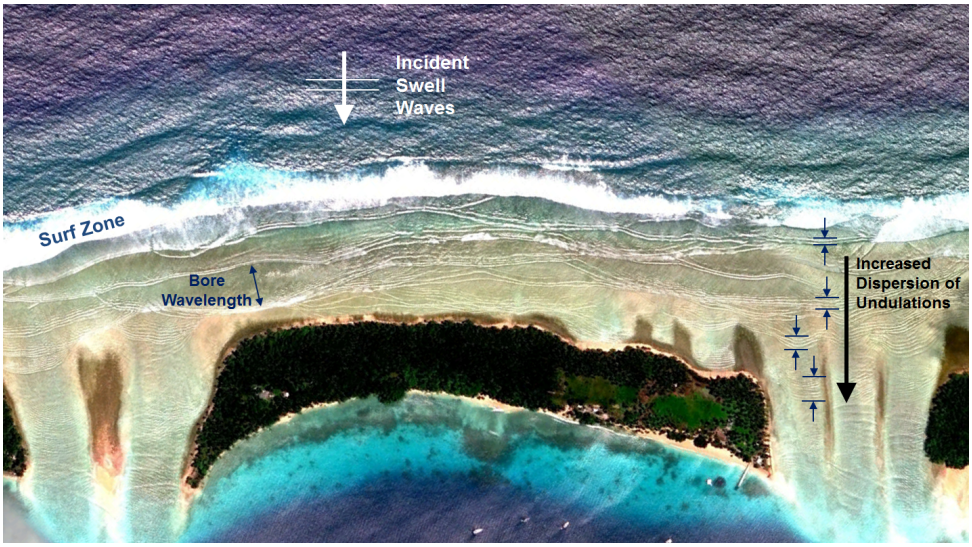

Figure 5.11: Aerial image of suspected undular bores on a reef flat in Majuro, RMI (Google Earth, 2014). Shoreward of the surf zone, narrow bands of high frequency waves appear at regular intervals similar to the swell wavelengths observed offshore. The bands further from the surf zone are more dispersed, in agreement with the processes described by Peregrine (1966) and Gallagher (1972). At the edge of the lagoon, the bands are indistinguishable, suggesting that the undular bores may have disintegrated as they travelled across the reef flat.

Future studies should determine if: (a) the formation of undular bores and turbulent bores can be correlated to specific hydrodynamic forcing or reef geometries and (b) if undular bores lead to greater runup and flooding than purely turbulent conditions.

5.3.2. CLUSTER & REGRESSION ANALYSIS OF MODEL RESULTS

Cluster analysis refers to a series of data analysis techniques which can be used to classify large datasets into meaningful groups. The techniques have been used successfully for wave climate reduction (Camus et al., 2011; Mortlock and Goodwin, 2015; Olij, 2015; **?**), morphological classification (Costa et al., 2016; Duce et al., 2016; Tomás et al., 2015), and identifying tropical cyclone trajectories (Camargo et al., 2007*a*,*b*).

It could thus be useful here as both a pre- and post-processing tool. For preprocessing, it could be used to group input conditions for XBeach model runs or planning Bayesian network bin boundaries. For post-processing, it could be used to identify patterns or to develop multiple regressions for different wave regimes.

Tomás et al. (2015) developed a flood risk assessment framework for the Spanish coast. They use the Stockdon et al. (2006) equations to estimate runup for each profile along the entire coastline. This sort of Bayesian method may thus also be useful in similar large scale flood risk assessments.

Rather than running a numerical model simulation for each profile along the entire coastline, they use k-means cluster analysis to identify similar non-dimensional profiles. This reduces the number of profiles from 5,000,000 to 121. The dimensionless

profiles are then converted back into real profiles which the numerical model can use. In reducing their required number of simulations by a factor of O(1000), Tomás et al. (2015) demonstrate the usefulness of cluster analysis for aggregating large morphological datasets. A similar approach could be taken for coral reefs if sufficient data becomes available.

Duce et al. (2016) use k-means clustering (Section F.2) to differentiate classes of spur and groove formations on coral reefs. By iteratively combining different morphological parameters and numbers of classes, they were able to maximize variability between classes but minimize variability within those classes.

Regression analysis entails curve-fitting and development of empirical equations like Stockdon's runup formulation (Stockdon et al., 2006). These equations may be faster and simpler than a Bayesian network, so it could be useful to establish the ranges of validity for existing expressions on coral reefs, but also to use the synthetic dataset to develop a new, reef-specific formulation.

These are discussed in greater depth in Appendices F and G.

5.3.3. REEF MORPHOLOGY DATABASE

This thesis revealed an urgent need for real-world data against which to calibrate and validate the models. Hence, one of the key priorities for future research is data collection. McLean and Kench (2015) advocate the targeting of more vulnerable islands in climate change adaptation efforts, as well improved collection of data to catalogue the existing state of atoll coastlines.

The three hydrodynamic input parameters (η_0, $H_{s,0}$, and $H_{s,0}/L_0$) and five reef morphology parameters (β_f, W_{reef}, β_b, c_f, and z_{beach}) used in this study should be collected. Data can be acquired through a combination of field surveys (expensive but detailed), remote sensing (less expensive but less detailed), and real time hydrodynamic monitoring. For instance, offshore buoys or wave gauges on reefs could be deployed to produce similar datasets to those developed for Roi Namur (Cheriton et al., 2016; Quataert et al., 2015) or Funafuti (Beetham et al., 2015).

As in all field campaigns, the trade-offs between feasibility and expense should be weighed carefully against the value of the information that would be obtained from an investigation. The log-likelihood analysis in Section 5.1.2 revealed that the importance of each input parameter varied depending on the output parameter. For instance, beach slope has relatively little influence on runup (Figure 4.11), so it may not be worth the extra effort to measure it in the field. Data collection in the surf zone is made challenging by breaking waves (Becker et al., 2014). However, fore reef slope is an important parameter for many of the tested outputs (especially low-frequency anomalies), so it may still be necessary to measure it. Today, there is relatively little observed information about infragravity or VLF waves on reefed coastlines, due in part to a paucity of data in remote locations and a historical bias towards studying sea and swell (van Dongeren et al., 2016).

These sources can be used to provide model inputs and better characterization of specific sites. By prioritizing and triaging more vulnerable areas, better use of limited resources can be made. If done in partnership with ecological researchers working on reefs, field investigations may be planned for mutual benefit. Innovative survey techniques such as the drifter-mounted sensors developed by Xanthidis et al. (2016) may also

be useful. They were able to provide dense randomized coverage of reefs in Barbados, along with data on currents.

After the database has been assembled, a Bayesian network can be constructed to classify morphology (and possibly predict morphological change). Such a network may be able to draw inferences from studied sites to characterize the many thousands of tropical islands which might be at risk but which cannot be surveyed due to practical limitations.

BAYESIAN NETWORKS FOR ESTIMATING REEF MORPHOLOGY

This Bayesian network has been developed with the end goal of developing an operational flood forecast system for atolls and low-lying tropical islands. The global/regional wave forecast and climate models required to generate hydrodynamic input conditions already exist (e.g. WAVEWATCH III (Tolman, 2009)). However, the other critical component for analysis is a database containing the basic morphological characteristics for each island of interest (e.g. reef flat width, roughness). Without this information, the network's use is restricted to the handful of sites which have already been studied in detail (e.g. Kwajalein (Cheriton et al., 2016; Quataert et al., 2015)).

Something else to consider is the availability of data in the literature and feasibility of collecting that data for future studies. Some are available from remote sensing, others need to be measured in situ (wave heights) or calculated based on detailed field surveys (e.g. bed roughness or fore reef slope).

Unfortunately, the tremendous geographic range and diversity of tropical islands makes detailed bathymetric surveys of every atoll unfeasible. Hence, the most cost-effective solution would be to compile data based on existing sources. Certain reef properties can be obtained through remote sensing, such as aerial photographs (Yamano, 2007) or multispectral satellite imagery (Hochberg et al., 2003).

Can we digitize coastlines and wave breaking locations to get a rough estimate of reef flat widths from aerial photos (e.g. Figure 5.12)? There would be uncertainties related to timing (with respect to tide) as this will shift the shoreline and breakpoint, although these may be small relative to the total width of the reefs. Steepness of fore reef will determine in part the width and location of the breakpoint. The fore reef slope could be determined by assuming that deepest visible part of the reef is approximately 25 m below the surface (Curt Storlazzi, personal communication, June 16, 2016). High-resolution LiDAR bathymetry may extend to 40 m depths (Pittman et al., 2013).

The data-mining and machine-learning techniques explored earlier in this thesis may also conveniently be applied in the assembly of this database. Duce et al. (2016) used Geographical Information System (GIS) software (ArcMap) in conjunction with cluster analysis to classify morphological features on coral reefs from remote sensing data. Their study focused on spur and groove formations along the fore-reef, but the same approach could be applied to other aspects of reef morphology.

Although the type of data most useful to coastal engineers may not be available for coral atolls, there is considerable information available on the ecological characteristics of reefs (UNEP-WCMC, 2016). By combining datasets for reefs where both hydrodynamic properties and ecological characteristics are known, it may be possible to construct a Bayesian network describing the probabilistic relationships between the two.

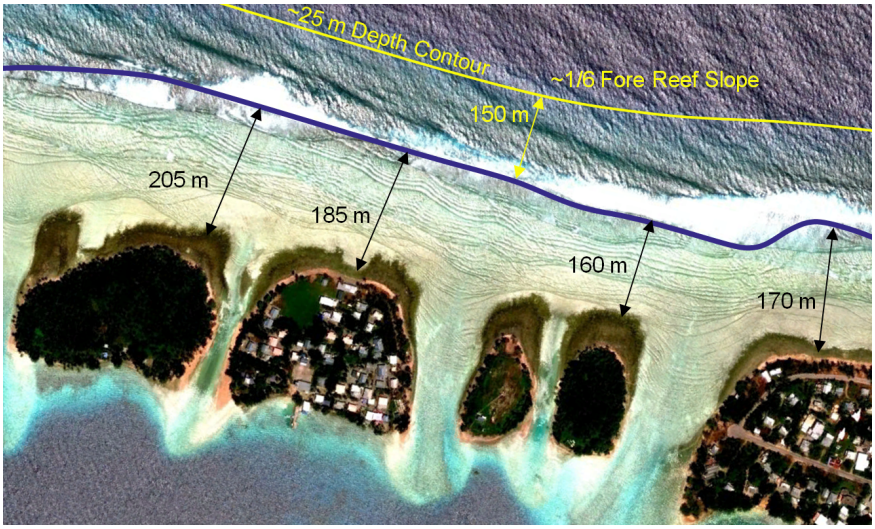

Figure 5.12: Example of measuring reef flat width from remote sensing data at Majuro Atoll, RMI. The wave breaking point visible in photos is used as a proxy for the reef crest. Also note the longer wavelengths of incoming swell versus the shorter wavelengths of high frequency oscillatory waves on the reef flat. Image source: Google Earth (2014).

A conceptual network linking the different concepts discussed in this thesis with other morphological and ecological indicators is proposed in Figure 5.13.

These sorts of approaches may also be useful for estimating future changes in island morphology (similar to work of McLean and Kench (2015)). These Bayesian networks could also be used to predict contamination of freshwater lenses by salinization, similarly to how Fienen et al. (2013) used a BN to study groundwater on islands. Existing BNs developed for coral reef management (Ban et al., 2015) may also be useful.

However, as a caveat, McLean and Kench (2015) note that as a consequence of the wide variety in reef characteristics and forcing, a “one-size-fits-all” approach to understanding climate change impacts to atolls will not be sufficient.

5.3.4. TRADITIONAL KNOWLEDGE

The Sendai Framework also includes a call to incorporate "traditional knowledge" of indigenous peoples into scientific approaches to disaster risk reduction (UNISDR, 2015, 24(i)). Marshall Islanders have a unique tradition of navigation at sea by using patterns in swell waves. For 3000 years their way of life has been intrinsically linked with being able to "read" and interpret waves. Perhaps now that these same swell waves are threatening their way of existence, flood prediction methods can benefit from their knowledge.

In the absence of measured wave or water level records, oral tradition from indigenous Pacific islanders can be a source of anecdotal evidence of past flood events, as used by Smithers and Hoeke (2014) to estimate return periods of extreme swells on Nukutoa, Papua New Guinea. Furthermore, even where measured wave and water level data exist, information about runup and inundation characteristics may be limited, so local/tradi-

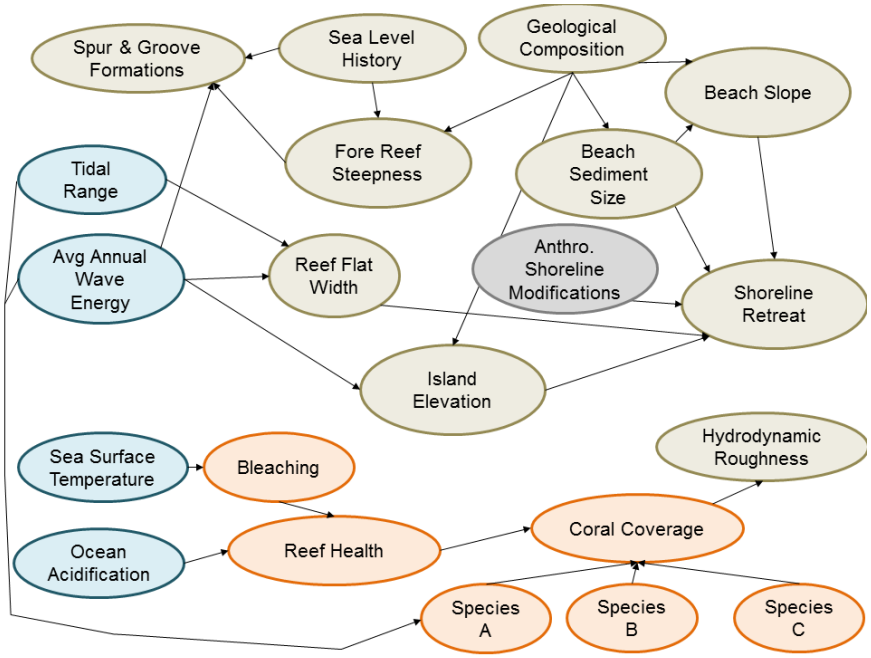

Figure 5.13: Conceptual diagram of Bayesian network relating hydrodynamic and morphological parameters to ecological characteristics

tional knowledge may serve as a valuable supplement to scientific studies like this one. Traditional knowledge could be used to qualitatively validate some of the phenomena discussed here.

More information about the fascinating tradition of wave piloting and application of traditional knowledge to flood prediction can be found in Appendix G.

6

CONCLUSIONS AND RECOMMENDATIONS

CONCLUSIONS:

- Islands with narrow, smooth reef flats and steep fore reefs are most vulnerable to wave-induced floods and resonant low frequency anomalies
- Resonant low frequency anomalies are linked with increased runup and hence greater flooding
- Wave conditions, water level, and reef width are the most important variables to estimate flooding on reef-fronted coasts
- General trends from XBeach model results are supported by field observations in the literature at specific sites
- An early warning system could be developed by using a Bayesian network to couple regional wave models with a reef database and XBeach
- Bayesian networks can be used to estimate climate change impacts by examining causal relationships and what-if scenarios
- The network may be improved by reducing its complexity

RECOMMENDATIONS:

- Collect more reef hydrodynamics field data
- Conduct out laboratory experiments to validate model
- Carry out more model simulations in the range of interest
- Build database of atoll properties relevant to hydrodynamic modellers
- Analyze database with cluster analysis, Bayesian networks, and regression analysis
- Develop Early Warning System pilot study

THIS study attempts to generalize the findings of previous research concerning reef hydrodynamics at specific sites in order to develop a flood prediction system. A synthetic dataset of runup and overtopping under varying reef characteristics and hydrodynamic conditions was generated using the XBeach non-hydrostatic wave model. These model results were then aggregated into a Bayesian network to understand the probabilistic relationships between the input conditions and flooding. The model's predictive capabilities were then tested using several case studies from the literature.

6.1. CONCLUSIONS

KEY FINDINGS

At the beginning of this study, we posed several main research questions. Based on the outcome of our study, here are the key findings:

1. **How can we give estimates of flooding and runup on coral atolls, knowing only little or very approximate information about the geomorphic system or hydraulic boundary conditions?**
   Hydrodynamic conditions can be obtained from regional/global wave models, tidal predictions, sea level rise projections, and field measurements. Similarly, reef characteristics (especially reef width and fore reef slope) can be measured from field surveys, remote sensing, and ecological studies. Using this information, a synthetic dataset of wave transformation and runup can be created using a process-based model. This may provide insights into the relevant processes in the absence of measured data. The resulting dataset can then be analyzed using a Bayesian network to identify relationships between different reef characteristics, hydrodynamic forcing, and flooding.

2. **What are the most important processes that drive flooding on low-lying tropical islands?**
   Islands with narrow, smooth reef flats and steep fore reefs are most vulnerable to wave-induced flooding and resonant low frequency anomalies. These resonant low frequency anomalies are linked with increased runup, and hence greater flooding. Hydrodynamic forcing (wave and water level conditions) and reef width are the most important variables to estimate flooding on reef-fronted coasts. Including other variables may improve predictive capabilities for more complex phenomena like low frequency resonance.

3. **Can we reproduce these processes using a detailed process-based model (XBeach) together with a probabilistic (Bayesian network) model?**
   General trends from XBeach model results are supported by field observations in the literature at specific sites. Multiple lines of evidence suggest that the XBeach Non-Hydrostatic model is capable of simulating resonant low frequency waves: (1) peak in low-frequency wave heights for narrow reefs; (2) presence of anomalously high infragravity and VLF waves at deeper reef flats; (3) low frequency anomalies tend to cluster around the resonant frequency. The Bayesian network shows variable accuracy when validated against specific runup events from the literature,

with mainly correct predictions for wave heights and setup, but a tendency to over-predict runup. Predictive skill testing indicated that it was challenging to predict low frequency anomalies using the Bayesian Network. However, the model may be improved by reducing network complexity and filtering input data.

4. **How can these tools be applied in an early warning system or to assess the impact of climate change?**
   Bayesian networks are an effective tool for organizing large datasets and exploring relationships between variables. They are a rapid, user-friendly tool for early warning systems in keeping with goals of Sendai Framework for Disaster Risk Reduction. An early warning system could be developed by using a Bayesian network to couple regional wave models like WAVEWATCH III with a database of reef characteristics and XBeach model. Furthermore, Bayesian networks can be used to estimate climate change impacts by examining causal relationships and what-if scenarios. They can also be used to prioritize sites for reef conservation and restoration. Narrow reefs adjacent to high population/value sites should be the first targets for reef restoration measures.

6.1.1. ADVANCES

Detailed hydrodynamic studies have only been carried out at a limited number of sites. By constructing a synthetic dataset, this study samples the influence of a wider range of reef morphologies, effectively simulating a large number of islands. The general conclusions drawn from this dataset are consistent with findings in the literature. It also derives general relationships between resonant low frequency waves and flooding.

To the author's knowledge, this is the first study to apply Bayesian networks for flood risk assessments on coral atolls. This marks a step forward in the development of an operational flood forecasting system for low-lying tropical islands. This thesis serves as a proof-of-concept, and demonstrates the potential for Bayesian networks in early warning systems. It may also be useful in developing projections of future climate change impacts or planning reef conservation and restoration efforts.

6.1.2. LIMITATIONS

Ultimately, this study was limited by two main factors: the simplifications necessary to feasibly simulate a large number of permutations, and the paucity of field observations against which to calibrate and validate the models.

Key limiting model assumptions included:

- Idealized 1D profile consisting of planar fore reef and beach slopes with a horizontal reef flat
- Discrete input parameter distributions
- Limited field data for validation
- Tropical cyclone-generated waves not considered
- Single-peaked JONSWAP spectra
- No directional spreading

- Spatially uniform roughness
- No 2D effects (e.g. edge waves or longshore currents)

Nonetheless, this study serves as a proof of concept, and the techniques used herein could be improved with more data and iterations.

6.2. RECOMMENDATIONS

Based on the findings of this report, we make several recommendations for future research and practical applications.

1. **Collect more field data**
   A scarcity of field data on which to validate the network is one of the key limitations of this thesis. Hence, additional data collection is essential for future work. Specifically, wave conditions offshore and on the reef flat should be measured, along with reef dimensions. Reefs near centres of high population density or critical infrastructure should be prioritized. Furthermore, joint probability distributions for input variables should be considered to see if the modelled parameter space can be reduced. Further analysis with the Bayesian network may also reveal dependencies that mean fewer variables (and hence less data) are needed to make accurate predictions.

2. **Carry out laboratory experiments to validate model and explore processes**
   Physical models should be used to validate the numerical model as well as provide more insight into the processes of interest. Resonant conditions should be simulated to determine whether the general principles gleaned from this numerical modelling study hold true in reality. The behaviour of undular bores in the numerical model could also be validated by a physical model to determine how well they are represented and their relevance to flooding. In addition, wave breaking steepness on reefs should be studied to determine the range of valid breaking parameters for XBeach Non-Hydrostatic.

3. **Carry out more model runs in range of interest and/or sample randomly**
   If this Bayesian model can be validated on additional sites and found useful in predicting floods, then the number of parameters evaluated should be expanded so as to capture a wider range of reef diversity. The parameter space should also be randomly sampled to obtain smoother input distributions. Techniques such as Latin Hypercube sampling may reduce the number of simulations required to obtain a representative sample.

4. **Build database of atoll properties relevant to hydrodynamic modellers**
   Existing remote sensing and ecological data should be collected and analyzed in a desktop study prior to carrying out new fieldwork. For instance, first-order estimates of reef widths and fore reef slopes could easily obtained using tools like Google Earth. Habitat maps from ecological studies may be useful for estimating reef roughness.

5. **Cluster analysis and BNs for classifying morphology**
   Cluster analysis is a promising tool for the classification of key reef properties such as representative bathymetric profiles. It may be useful for categorizing input data into physically meaningful groups for use in a Bayesian network. Furthermore, Bayesian networks could be used to identify relationships between hydrodynamics and morphology.

6. **Cluster analysis to explore dataset**
   The synthetic dataset developed in this thesis is extremely large and has only been explored in limited detail. Cluster analysis and additional filtering should be used to further elucidate relationships or regimes in the data. Other techniques like the Maximum Dissimilarity Algorithm are promising since they may better capture outliers than the k-means method used in this study.

7. **Regression analysis to fit new parametric equations** The XBeach Non-Hydrostatic model resolves the physical processes of reef hydrodynamics in detail, but at high computational expense. If a simpler parametric model could be derived using the dataset derived here, it would enable more rapid assessment of the potential for flooding on atolls. These equations should account for decay and amplification of waves across reef flats.

8. **Investigate role of undular bores on reefs**
   Undular bores have been observed on reefs in the field, in model simulations, and in laboratory studies. Their role in transforming wave energy on reefs and in subsequent flooding is poorly understood. The synthetic model database developed for this thesis should be mined to identify the presence of undular bores. The formation of undular bores in the Xbeach model should be validated using field data or laboratory simulations. To obtain field observations, locals should be trained to recognize, measure, and report on the occurrence of undular bores. Then, general relationships between reef morphology, hydrodynamic forcing, the generation of undular bores, and flooding should be determined.

9. **Early Warning System Pilot Study**
   This thesis was a proof-of-concept for flood prediction on low-lying tropical islands using a Bayesian network. The next step is to identify specific sites for an early warning system pilot study. The network could be validated using measured data from these locations, and practical questions of implementation could be addressed. EWS developers should work in collaboration with local communities, stakeholders, and indigenous people, in keeping with Sendai Framework goals.

10. **Climate change impact assessments**
    The capability to make forward or inverse predictions and test "what-if" scenarios is one of the most valuable uses of Bayesian networks. Hence, they may be able to predict climate change impacts in large scale studies like that of Shope et al. (2015). It may also be useful for predicting the fate of freshwater resources on low-

lying tropical islands by coupling with 2D inundation and groundwater models.

11. **Focus conservation and restoration efforts on narrower reefs**
    Coral reefs are effective nature-based flood defenses, so reef restoration and rehabilitation are promising approaches to combating flooding of low-lying tropical islands. As identified in this thesis, narrower reefs are more vulnerable to resonance and extreme water levels, so they may make more effective targets for remedial measures. Given their smaller surface area, narrower reefs may be less expensive to restore. By reducing the costs of restoration, scarce financial resources would go further and enable protection of more sites.

Although the future prospects are daunting for low-lying tropical islands, the fight is not over yet. Given the right tools and support, they can build their resilience against flooding and face the future with a sense of hope.

BIBLIOGRAPHY

Akcay, H. G. and Aksoy, S. (2008), 'Automatic detection of geospatial objects using multiple hierarchical segmentations', *IEEE Transactions on Geoscience and Remote Sensing* **46**(7), 2097–2111.

Albert, S., Leon, J. X., Grinham, A. R., Church, J. A., Gibbes, B. R. and Woodroffe, C. D. (2016), 'Interactions between sea-level rise and wave exposure on reef island dynamics in the Solomon Islands', *Environmental Research Letters* **11**(5), 054011.
URL: *http://stacks.iop.org/1748-9326/11/i=5/a=054011?key=crossref.06d94f96482fe76552e2dc5047ae69b8*

Alves, J. H. G. M. (2006), 'Numerical modeling of ocean swell contributions to the global wind-wave climate', *Ocean Modelling* **11**(1-2), 98–122.

Anderson, A., Chappell, J., Gagan, M. and Grove, R. (2006), 'Prehistoric maritime migration in the Pacific Islands: an hypothesis of ENSO forcing', *The Holocene* **1**(2006), 1–6.
URL: *http://dx.doi.org/10.1191/0959683606hl901ft*

Andréfouët, S., Aucan, J., Jourdan, H., Kench, P. S., Menkes, C., Vidal, E. and Yamano, H. (2015), 'Conservation of low-islands: High priority despite sea-level rise. A comment on Courchamp et al.', *Trends in Ecology and Evolution* **30**(1), 1–2.

Audrey, B., Thomas, B., Lise, P., Manuel, G., Ywenn, D. L. T. and Gonéri, L. C. (2013), Testing the Bayesian network method for exploring the shoreline mobility causes on volcanic islands: The case study of La Réunion (Indian Ocean), *in* 'Coastal Engineering 2013', pp. 139–150.

Australian Broadcasting Corporation (2015), 'Chaotic unseasonal storms strike Marshall Islands and Guam as eight systems threaten western Pacific'.
URL: *http://www.abc.net.au/news/2015-07-04/chaotic-unseasonal-storms-strike-marshall-islands-and-guam/6595124*

Balbi, S., Villa, F., Mojtahed, V., Hegetschweiler, K. T. and Giupponi, C. (2015), 'A spatial Bayesian network model to assess the benefits of early warning for urban flood risk to people', *Natural Hazards and Earth System Sciences Discussions* **3**(10), 6615–6649.
URL: *http://www.nat-hazards-earth-syst-sci-discuss.net/3/6615/2015/nhessd-3-6615-2015.html*

Baldock, T. E., Golshani, A., Callaghan, D. P., Saunders, M. I. and Mumby, P. J. (2014), 'Impact of sea-level rise and coral mortality on the wave dynamics and wave forces on barrier reefs', *Marine Pollution Bulletin* **83**(1), 155–164.
URL: *http://dx.doi.org/10.1016/j.marpolbul.2014.03.058*

Baldock, T. E., Huntley, D. A., Bird, P. A. D., O'Hare, T. and Bullock, G. N. (2000), 'Breakpoint generated surf beat induced by bichromatic wave groups', *Coastal Engineering* **39**(2-4), 213–242.

Ban, S. S., Pressey, R. L. and Graham, N. a. J. (2015), 'Assessing the effectiveness of local management of coral reefs using expert opinion and spatial Bayesian modeling', *PLoS ONE* **10**(8), 1–16.

Barnard, P. L., Short, A., Harley, M. D., Splinter, K. D., Vitousek, S., Turner, I. L., Allan, J., Banno, M., Bryan, K. R., Doria, A., Hansen, J. E., Kato, S., Kuriyama, Y., Randall-goodwin, E., Ruggiero, P., Walker, I. J. and Heathfield, D. K. (2015), 'Coastal vulnerability across the Pacific dominated by El Niño/Southern Oscillation', *Nature Geoscience* **8**(September), 801–808.

Barry, R. G. and Chorley, R. J. (2004), *Atmosphere, Weather and Climate*, 8th edn, Routledge, London.

Battjes, J. and Janssen, J. (1978), 'Energy Loss and Set-Up Due To Breaking of Random Waves', *Proceedings of 16th Conference on Coastal Engineering, ASCE* (1), 569–587.

Bayes, T. and Price, M. (1763), 'An Essay towards solving a Problem in the Doctrine of Chances', *Philosophical Transactions of the Royal Society of London* **53**(0), 370–418.
URL: *http://rstl.royalsocietypublishing.org/content/53/370.full.pdf*

Beccario, C. (2016), 'Earth'.
URL: *https://earth.nullschool.net/*

Becker, J., Johnston, D., Lazrus, H., Crawford, G. and Nelson, D. (2008), 'Use of traditional knowledge in emergency management for tsunami hazard: A case study from Washington State, USA', *Disaster Prevention and Management* **17**(4), 488–502.

Becker, J. M., Merrifield, M. A. and Ford, M. (2014), 'Water level effects on breaking wave setup for Pacific Island fringing reefs', *Journal of Geophysical Research: Oceans* **119**(2), 914–932.
URL: *http://doi.wiley.com/10.1002/2013JC009373*

Becker, J. M., Merrifield, M. A. and Yoon, H. (2016), 'Infragravity waves on fringing reefs in the tropical Pacific: dynamic setup', *Journal of Geophysical Research: Oceans* pp. 1–47.

Beetham, E. P. and Kench, P. S. (2011), 'Field observations of infragravity waves and their behaviour on rock shore platforms', *Earth Surface Processes and Landforms* **36**(14), 1872–1888.

Beetham, E. P. and Kench, P. S. (2014), 'Wave energy gradients and shoreline change on Vabbinfaru platform, Maldives', *Geomorphology* **209**, 98–110.
URL: *http://dx.doi.org/10.1016/j.geomorph.2013.11.029*

Beetham, E. P., Kench, P. S., O'Callaghan, J. and Popinet, S. (2015), 'Wave transformation and shoreline water level on Funafuti Atoll, Tuvalu', *Journal of Geophysical Research: Oceans* **120**, 1–16.

Benjamin, M. (2015), 'A mathematical study of meteo and landslide tsunamis: the Proudman resonance', *Nonlinearity* **28**(11), 4037–4080.
URL: *http://stacks.iop.org/0951-7715/28/i=11/a=4037?key=crossref.5222ab682386c3b4fedd1f8aa832a011*

Benjamin, T. B. and Lighthill, M. J. (1954), 'On cnoidal waves and bores', *Proceedings of the Royal Society A* **244**(1159), 448–460.

Blacka, M. J., Flocard, F., Splinter, K. D. and Cox, R. J. (2015), 'Estimating Wave Heights and Water Levels inside Fringing Reefs during Extreme Conditions', *Coast and Ports 2015* (September), 1–7.

Bonney, R., Cooper, C. B., Dickinson, J., Kelling, S., Phillips, T., Rosenberg, K. V. and Shirk, J. (2009), 'Citizen Science: A Developing Tool for Expanding Science Knowledge and Scientific Literacy', *BioScience* **59**(11), 977–984.

Booij, N., Ris, R. C. and Holthuijsen, L. H. (1999), 'A third-generation wave model for coastal regions: 1. Model description and validation', *Journal of Geophysical Research* **104**(C4), 7649.

Bosserelle, C., Kruger, J., Movono, M. and Reddy, S. (2015), Wave inundation on the Coral Coast of Fiji, *in* 'Australasian Coasts & Ports Conference 2015', Engineers Australia and IPENZ, Auckland, New Zealand, pp. 96–101.

Brander, R. W., Kench, P. S. and Hart, D. (2004), 'Spatial and temporal variations in wave characteristics across a reef platform, Warraber Island, Torres Strait, Australia', *Marine Geology* **207**(1-4), 169–184.

Buckley, M. L. and Lowe, R. J. (2013), Evaluation of Nearshore Wave Models in Steep Reef Environments, *in* 'Coastal Dynamics 2013', number October 2013, pp. 249–260.
URL: *http://www.coastaldynamics2013.fr/pdf_files/023_Buckley_Mark.pdf*

Buckley, M. L., Lowe, R. J., Hansen, J. E. and van Dongeren, A. (2015), 'Dynamics of wave setup over a steeply-sloping fringing reef', *Journal of Physical Oceanography* (September 2015).
URL: *http://journals.ametsoc.org/doi/abs/10.1175/JPO-D-15-0067.1*

Bulteau, T., Baills, a., Petitjean, L., Garcin, M., Palanisamy, H. and Le Cozannet, G. (2015), 'Gaining insight into regional coastal changes on La Réunion island through a Bayesian data mining approach', *Geomorphology* **228**, 134–146.
URL: *http://dx.doi.org/10.1016/j.geomorph.2014.09.002*

Cabioch, G. (2011), 'Forereef/Reef Front'.
URL: *http://link.springer.com/10.1007/978-90-481-2639-2*

Camargo, S. J., Robertson, A. W., Gaffney, S. J., Smyth, P. and Ghil, M. (2007*a*), 'Cluster analysis of typhoon tracks. Part I. General properties', *Journal of Climate* **20**(14), 3635–3653.

Camargo, S. J., Robertson, A. W., Gaffney, S. J., Smyth, P. and Ghil, M. (2007*b*), 'Cluster Analysis of Typhoon Tracks. Part II: Large-Scale Circulation and ENSO', *Journal of Climate* **20**(14), 3654–3676.
URL: *http://journals.ametsoc.org/doi/abs/10.1175/JCLI4203.1*

Camus, P., Mendez, F. J., Medina, R. and Cofino, A. S. (2011), 'Analysis of clustering and selection algorithms for the study of multivariate wave climate', *Coastal Engineering* **58**(6), 453–462.

Chanson, H. (2010), 'Undular Tidal Bores: Basic Theory and Free-Surface Characteristics', *Journal of Hydraulic Engineering* **136**(November), 940–944.

Cheriton, O. M., Storlazzi, C. D. and Rosenberger, K. J. (2016), 'Observations of wave transformation over a fringing coral reef and the importance of low-frequency waves and offshore water levels to runup, overwash, and coastal flooding', *Journal of Geophysical Research: Oceans* **121**, 1–20.

Chowdhury, M. R., Chu, P.-S. and Schroeder, T. (2006), 'ENSO and seasonal sea-level variability – A diagnostic discussion for the U.S.-Affiliated Pacific Islands', *Theoretical and Applied Climatology* **88**(3-4), 213–224.
URL: *http://link.springer.com/10.1007/s00704-006-0245-5*

Chui, T. F. M. and Terry, J. P. (2013), 'Influence of sea-level rise on freshwater lenses of different atoll island sizes and lens resilience to storm-induced salinization', *Journal of Hydrology* **502**, 18–26.
URL: *http://www.sciencedirect.com/science/article/pii/S002216941300591X*

Church, J. A., White, N. J. and Hunter, J. R. (2006), 'Sea-level rise at tropical Pacific and Indian Ocean islands', *Global and Planetary Change* **53**(3), 155–168.

Costa, M. B. S. F., Araujo, M., Araujo, T. C. M. and Siegle, E. (2016), 'Influence of reef geometry on wave attenuation on a Brazilian coral reef', *Geomorphology* **253**, 318–327.
URL: *http://dx.doi.org/10.1016/j.geomorph.2015.11.001*

Damlamian, H., Bosserelle, C., Kruger, J., Raj, A., Begg, Z., Kumar, S., Lowe, R. J., Buckley, M. L. and Baleilevuka, A. (2015), Bonriki Inundation Vulnerability Assessment: Inundation Modelling of Bonriki Islet, Tarawa, Kiribati, Technical report, Secretariat of the Pacific Community, Suva, Fiji.

de Bakker, A. T. M., Tissier, M. F. S. and Ruessink, B. G. (2014), 'Shoreline dissipation of infragravity waves', *Continental Shelf Research* **72**, 73–82.
URL: *http://dx.doi.org/10.1016/j.csr.2013.11.013*

Decision Systems Laboratory (2016), 'GeNIe Documentation'.
URL: *https://dslpitt.org/genie/wiki/GeNIe_Documentation*

den Heijer, C., Knipping, D. T., Plant, N. G., van Thiel de Vries, J. S. M., Baart, F. and van Geer, P. (2012), 'Impact Assessment of Extreme Storm Events Using a Bayesian Network', *Coastal Engineering Proceedings* p. 15.
URL: *https://journals.tdl.org/icce/index.php/icce/article/view/6677*

Duce, S., Vila-Concejo, a., Hamylton, S., Webster, J., Bruce, E. and Beaman, R. (2016), 'A morphometric assessment and classification of coral reef spur and groove morphology', *Geomorphology* .
URL: *http://linkinghub.elsevier.com/retrieve/pii/S0169555X16302288*

Ferrario, F., Beck, M. W., Storlazzi, C. D., Micheli, F., Shepard, C. C. and Airoldi, L. (2014), 'The effectiveness of coral reefs for coastal hazard risk reduction and adaptation', *Nature Communications* **5**(May), 1–9.
URL: *http://www.nature.com/doifinder/10.1038/ncomms4794*

Fienen, M. N., Masterson, J. P., Plant, N. G., Gutierrez, B. T. and Thieler, E. R. (2013), 'Bridging groundwater models and decision support with a Bayesian network', *Water Resources Research* **49**(10), 6459–6473.

Filipot, J. F. and Cheung, K. F. (2012), 'Spectral wave modeling in fringing reef environments', *Coastal Engineering* **67**, 67–79.
URL: *http://dx.doi.org/10.1016/j.coastaleng.2012.04.005*

Finney, B. (1998), Nautical Cartography and Traditional Navigation in Oceania, *in* 'The History of Cartography: Cartography in the Traditional African, American, Arctic, Australian, and Pacific Societies', Vol. 2, University of Chicago Press, Chicago, chapter 13, pp. 443–492.

Forbes, D. L., James, T. S., Sutherland, M. and Nichols, S. E. (2013), 'Physical basis of coastal adaptation on tropical small islands', *Sustainability Science* **8**(3), 327–344.
URL: *http://link.springer.com/10.1007/s11625-013-0218-4*

Ford, M. (2012), 'Shoreline Changes on an Urban Atoll in the Central Pacific Ocean: Majuro Atoll, Marshall Islands', *Journal of Coastal Research* **279**(2001), 11–22.
URL: *http://www.bioone.org/doi/abs/10.2112/JCOASTRES-D-11-00008.1*

Ford, M., Becker, J. M. and Merrifield, M. A. (2013), 'Reef Flat Wave Processes and Excavation Pits: Observations and Implications for Majuro Atoll, Marshall Islands', *Journal of Coastal Research* **288**, 545–554.
URL: *http://www.jcronline.org/doi/abs/10.2112/JCOASTRES-D-12-00097.1*

Ford, M. and Kench, P. S. (2015), 'Multi-decadal shoreline changes in response to sea level rise in the Marshall Islands', *Anthropocene* (2015).
URL: *http://dx.doi.org/10.1016/j.ancene.2015.11.002*

Franco, C., Hepburn, L. A., Smith, D. J., Nimrod, S. and Tucker, A. (2016), 'A Bayesian Belief Network to assess rate of changes in coral reef ecosystems', *Environmental Modelling & Software* **80**, 132–142.
URL: *http://www.sciencedirect.com/science/article/pii/S1364815216300494*

Gallagher, B. (1972), 'Some qualitative aspects of nonlinear wave radiation in a surf zone', *Geophysical Fluid Dynamics* **3**(1), 347–354.
URL: *http://www.tandfonline.com/doi/abs/10.1080/03091927208236086*

Gallien, T. W. (2016), 'Validated coastal flood modeling at Imperial Beach , California: Comparing total water level, empirical and numerical overtopping methodologies', *Coastal Engineering* **111**, 95–104.
URL: *http://dx.doi.org/10.1016/j.coastaleng.2016.01.014*

Gawehn, M. (2015), Incident, infragravity and very low frequency wave motions on an atoll reef platform, Master's thesis, Delft University of Technology.
URL: *http://resolver.tudelft.nl/uuid:5d45bce9-ef29-459c-a659-417342a875e9*

Gawehn, M., van Dongeren, A., van Rooijen, A., Storlazzi, C. D., Cheriton, O. M. and Reniers, A. (2016), 'Identification and classification of very-low frequency waves on a coral reef flat', *Submitted to Journal of Geophysical Research: Oceans, Under Review* .

Genz, J. H., Aucan, J., Merrifield, M. A., Finney, B. and Joel, K. (2009), 'Wave navigation in the Marshall Islands: Comparing indigenous and Western scientific knowledge of the ocean', *Oceanography* **22**(2), 234–245.

Gieder, K. D., Karpanty, S. M., Fraser, J. D., Catlin, D. H., Gutierrez, B. T., Plant, N. G., Turecek, A. M. and Thieler, E. R. (2014), 'A Bayesian network approach to predicting nest presence of the federally-threatened piping plover (Charadrius melodus) using barrier island features', *Ecological Modelling* **276**(April), 38–50.

Google Earth (2014), 'Majuro Atoll, Republic of the Marshall Islands, 7.125885°N, 171.353389°E, March 6, 2014'.
URL: *http://www.google.com/earth/*

Gourlay, M. R. (1994), 'Wave transformation on a coral reef', *Coastal Engineering* **23**(1-2), 17–42.

Gourlay, M. R. (1996*a*), 'Wave set-up on coral reefs. 1. Set-up and wave-generated flow on an idealised two dimensional horizontal reef', *Coastal Engineering* **27**(3-4), 161–193.

Gourlay, M. R. (1996*b*), 'Wave set-up on coral reefs. 2. Set-up on reefs with various profiles', *Coastal Engineering* **28**(1-4), 17–55.

Grue, J., Pelinovsky, E. N., Fructus, D., Talipova, T. and Kharif, C. (2008), 'Formation of undular bores and solitary waves in the Strait of Malacca caused by the 26 December 2004 Indian Ocean tsunami', *Journal of Geophysical Research: Oceans* **113**(5), 1–14.

Gunasekara, K. H., Tajima, Y. and Shimozono, T. (2014), 'Variation of Impact along the East Coast of Eastern Samar Due to Typhoon Haiyan in the Philippines', *Journal of Japan Society of Civil Engineers* **70**(2), I_241–I_245.
URL: *http://jlc.jst.go.jp/DN/JALC/10041329183?from=Google*

Gutierrez, B. T., Plant, N. G. and Thieler, E. R. (2011), 'A Bayesian network to predict coastal vulnerability to sea level rise', *Journal of Geophysical Research* **116**(F2), F02009.
URL: *http://doi.wiley.com/10.1029/2010JF001891*

Gutierrez, B. T., Plant, N. G., Thieler, E. R. and Turecek, A. (2015), 'Using a Bayesian network to predict barrier island geomorphologic characteristics', *Journal of Geophysical Research: Earth Surface* **120**, 2452–2475.

Guza, R. and Feddersen, F. (2012), 'Effect of wave frequency and directional spread on shoreline runup', *Geophysical Research Letters* **39**(11), n/a–n/a.
URL: *http://doi.wiley.com/10.1029/2012GL051959*

Guza, R., Thornton, E. and Holman, R. (1984), 'Swash on steep and shallow beaches', *Coastal Engineering Proceedings* **1**(19), 708–723.
URL: *https://icce-ojs-tamu.tdl.org/icce/index.php/icce/article/view/3829*

Hamilton, T. (2013), A Visual Description of the Concrete Exterior of the Cactus Crater Containment Structure, Technical Report LLNL-TR-648143, Lawrence Livermore National Laboratory, US Department of Energy, Livermore, CA.
URL: *https://marshallislands.llnl.gov/ccc/Hamilton_LLNL-TR-648143_final.pdf*

Hanafin, J. A., Quilfen, Y., Ardhuin, F., Sienkiewicz, J., Queffeulou, P., Obrebski, M., Chapron, B., Reula, N., Collard, F., Cormand, D., Vandemark, D., de Azevedo, E. B. and Stutzmann, E. (2012), 'Phenomenal sea states and swell from a North Atlantic Storm in February 2011: a comprehensive analysis', *Bulletin of the American Meteorological Society* **93**(December), 1825–1832.

Hanea, A., Morales Napoles, O. and Ababei, D. (2015), 'Non-parametric Bayesian networks: Improving theory and reviewing applications', *Reliability Engineering and System Safety* **144**, 265–284.
URL: *http://dx.doi.org/10.1016/j.ress.2015.07.027*

Hapke, C. and Plant, N. G. (2010), 'Predicting coastal cliff erosion using a Bayesian probabilistic model', *Marine Geology* **278**(1-4), 140–149.
URL: *http://dx.doi.org/10.1016/j.margeo.2010.10.001*

Hasan, G. M. J. and Takewaka, S. (2009), 'Wave Run-Up Analyses Under Dissipative Condition Using X-Band Radar', *Coastal Engineering Journal* **51**(2), 177–204.

Hawkins, D. M. (2004), 'The Problem of Overfitting', *Journal of Chemical Information and Computer Sciences* **44**(1), 1–12.

Helton, J. C., Davis, F. J. and Johnson, J. D. (2005), 'A comparison of uncertainty and sensitivity analysis results obtained with random and Latin hypercube sampling', *Reliability Engineering and System Safety* **89**(3), 305–330.

Hennings, I. (2015), 'New perspectives on indigenous navigation tradition', *Hydrographische nachrichten* (02), 54–58.

Herbers, T. H. C., Elgar, S., Guza, R. and O'Reilly, W. C. (1994), 'Infragravity-Frequency (0.005–0.05 Hz) Motions on the Shelf. Part I: Forced Waves'.

Herbers, T. H. C., Elgar, S., Guza, R. and O'Reilly, W. C. (1995), 'Infragravity-Frequency (0.005-0.05 Hz) Motions on the Shelf. Part II: Free Waves', *Journal of Physical Oceanography* **25**, 1063–1079.

Hiwasaki, L., Luna, E., Syamsidik and Shaw, R. (2014), 'Process for integrating local and indigenous knowledge with science for hydro-meteorological disaster risk reduction and climate change adaptation in coastal and small island communities', *International Journal of Disaster Risk Reduction* **10**, 15–27.
URL: *http://dx.doi.org/10.1016/j.ijdrr.2014.07.007*

Hochberg, E. J., Atkinson, M. J. and Andréfouët, S. (2003), 'Spectral reflectance of coral reef bottom-types worldwide and implications for coral reef remote sensing', *Remote Sensing of Environment* **85**(2), 159–173.

Hoegh-Guldberg, O., Mumby, P. J., Hooten, A. J., Steneck, R. S., Greenfield, P., Gomez, E., Harvell, C. D., Sale, P. F., Edwards, A. J., Caldeira, K., Knowlton, N., Eakin, C. M., Iglesias-Prieto, R., Muthiga, N., Bradbury, R. H., Dubi, A. and Hatziolos, M. E. (2007), 'Change and Ocean Acidification', *Science* **318**(December 2007), 1737–1742.
URL: *http://www.sciencemag.org/content/318/5857/1737.short*

Hoeke, R. K., McInnes, K., Kruger, J., McNaught, R. J., Hunter, J. R. and Smithers, S. G. (2013), 'Widespread inundation of Pacific islands triggered by distant-source wind-waves', *Global and Planetary Change* **108**, 128–138.
URL: *http://linkinghub.elsevier.com/retrieve/pii/S0921818113001483*

Holden, H. and LeDrew, E. F. (1998), 'Spectral Discrimination of Healthy and Non-Healthy Corals Based on Cluster Analysis, Principal Components Analysis, and Derivative Spectroscopy', *Remote Sensing of Environment* **65**(February), 217–224.

Holthuijsen, L. H. (2007), *Waves in Oceanic and Coastal Waters*, Cambridge University Press, Cambridge, UK.

Hoshino, E., van Putten, I., Girsang, W., Resosudarmo, B. P. and Yamazaki, S. (2015), 'A Bayesian belief network model for community-based coastal resource management in the Kei Islands, Indonesia', *Ecology and Society* **21**(2), 16.

Huang, N. E., Shen, Z. and Long, S. R. (1999), 'A New View of Nonlinear Water Waves: The Hilbert Spectrum', *Annual Review of Fluid Mechanics* **31**(1), 417–457.
URL: *http://www.annualreviews.org/doi/abs/10.1146/annurev.fluid.31.1.417\npapers2://publicatio*

Hughes, M. G., Moseley, A. S. and Baldock, T. E. (2010), 'Probability distributions for wave runup on beaches', *Coastal Engineering* **57**(6), 575–584.
URL: *http://dx.doi.org/10.1016/j.coastaleng.2010.01.001*

Jäger, W. S., den Heijer, C., Bolle, A. and Hanea, A. (2015), A Bayesian Network Approach to Coastal Storm Impact Modeling, *in* '12th International Conference on Applications of Statistics and Probability in Civil Engineering', Vol. 12.

Jäger, W. S., den Heijer, C., Bolle, A. and Smets, S. (2015), Resilience-Increasing Strategies for Coasts – Toolkit D3.3 Bayesian Decision Support System, Technical report.

Jaramillo, S. and Pawlak, G. (2011), 'AUV-based bed roughness mapping over a tropical reef', *Coral Reefs* **30**(SUPPL. 1), 11–23.

Jiminez, J. A., Armaroli, C., Berenguer, M., Bosom, E., Ciavola, P., Ferreira, O., Plomaritis, T. A., Roelvink, J. A., Sanuy, M., Sempere, D. and Spencer, T. (2015), Resilience-Increasing Strategies for Coasts – Coastal Hazard Assessment Module, Technical report.

Kahn, C. E., Roberts, L. M., Shaffer, K. A. and Haddawy, P. (1997), 'Construction of a Bayesian network for mammographic diagnosis of breast cancer', *Computers in Biology and Medicine* **27**(1), 19–29.

Kench, P. S. (2011), 'Sediment Dynamics'.
URL: *http://link.springer.com/10.1007/978-90-481-2639-2*

Kench, P. S., Brander, R. W., Parnell, K. E. and O'Callaghan, J. M. (2009), 'Seasonal variations in wave characteristics around a coral reef island, South Maalhosmadulu atoll, Maldives', *Marine Geology* **262**(1-4), 116–129.
URL: *http://dx.doi.org/10.1016/j.margeo.2009.03.018*

Kennedy, A. B., Mori, N., Zhang, Y., Yasuda, T., Chen, S.-E., Tajima, Y., Pecor, W. and Toride, K. (2015), 'Observations and Modeling of Coastal Boulder Transport and Loading During Super Typhoon Haiyan', *Coastal Engineering Journal* **58**(1), 1640004.
URL: *http://www.worldscientific.com/doi/10.1142/S0578563416400040*

Kolijn, D. J. (2014), Effectiveness of a multipurpose artificial underwater structure as a coral reef canopy, Master's thesis, Delft University of Technology.
URL: *http://resolver.tudelft.nl/uuid:7794dcfc-0971-4646-9ea2-25f8894176c3*

Lau, A. Y. A., Terry, J. P., Ziegler, A. D., Switzer, A. D., Lee, Y. and Etienne, S. (2016), 'Understanding the history of extreme wave events in the Tuamotu Archipelago of French Polynesia from large carbonate boulders on Makemo Atoll, with implications for future threats in the central South Pacific', *Marine Geology* .
URL: *http://dx.doi.org/10.1016/j.margeo.2016.04.018*

Leinweber, D. J. (2007), 'Stupid Data Miner Tricks: Overfitting the S&P 500', *The Journal of Investing* **16**(1), 15–22.

Lentz, E. E., Thieler, E. R., Plant, N. G., Stippa, S. R., Horton, R. M. and Gesch, D. B. (2016), 'Evaluation of dynamic coastal response to sea-level rise modifies inundation likelihood', *Nature Climate Change* (March), 1–6.
URL: *http://www.nature.com/doifinder/10.1038/nclimate2957*

Lentz, S. J., Churchill, J. H., Davis, K. A. and Farrar, J. T. (2015), 'Surface gravity wave transformation across a platformcoral reef in the Red Sea', *Journal of Geophysical Research: Oceans* **121**, 1–13.

Li, J., Yang, J., Liu, S. and Ji, X. (2015), 'Wave groupiness analysis of the process of 2D freak wave generation in random wave trains', *Ocean Engineering* **104**, 480–488.
URL: *http://linkinghub.elsevier.com/retrieve/pii/S0029801815002188*

Lighttwist Software (2016), 'Uninet Help'.
URL: *http://www.lighttwist.net/wp/wp-content/doc/UninetHelp.pdf*

List, J. H. (1991), 'Wave groupiness variations in the nearshore', *Coastal Engineering* **15**(5-6), 475–496.
URL: *http://www.sciencedirect.com/science/article/B6VCX-47XNJCM-2J/2/ca7c810e6f5a5fcbf2803b01b35dbbf2*

Lowe, R. J. and Falter, J. L. (2015), 'Oceanic Forcing of Coral Reefs', *Annual Review of Marine Science* **7**(1), 43–66.
URL: *http://www.annualreviews.org/doi/abs/10.1146/annurev-marine-010814-015834*

Lowe, R. J., Falter, J. L., Bandet, M. D., Pawlak, G., Atkinson, M. J., Monismith, S. G. and Koseff, J. R. (2005), 'Spectral wave dissipation over a barrier reef', *Journal of Geophysical Research* **110**(C4), C04001.
URL: *http://doi.wiley.com/10.1029/2004JC002711*

Lowe, R. J., Koseff, J. R., Monismith, S. G. and Falter, J. L. (2005), 'Oscillatory flow through submerged canopies: 2. Canopy mass transfer', *Journal of Geophysical Research: Oceans* **110**(10), 1–14.

Lowe, R. J., Leon, A. S., Symonds, G., Falter, J. L. and Gruber, R. (2015), 'The intertidal hydraulics of tide-dominated reef platforms', *Journal of Geophysical Research: Oceans* **120**, 4845–4868.

Ma, G., Su, S.-F., Liu, S. and Chu, J. C. (2014), 'Numerical simulation of infragravity waves in fringing reefs using a shock-capturing non-hydrostatic model', *Ocean Engineering* **85**, 54–64.
URL: *http://dx.doi.org/10.1016/j.oceaneng.2014.04.030*

Madsen, P. a., Fuhrman, D. R. and Schaffer, H. a. (2008), 'On the solitary wave paradigm for tsunamis', *Journal of Geophysical Research: Oceans* **113**(12).

Matias, A., Williams, J. J., Masselink, G. and Ferreira, O. (2012), 'Overwash threshold for gravel barriers', *Coastal Engineering* **63**, 48–61.
URL: *http://dx.doi.org/10.1016/j.coastaleng.2011.12.006*

McAdoo, B. G., Moore, A. and Baumwoll, J. (2009), 'Indigenous knowledge and the near field population response during the 2007 Solomon Islands tsunami', *Natural Hazards* **48**(1), 73–82.
URL: *http://www.scopus.com/inward/record.url?eid=2-s2.0-57749187853&partnerID=40&md5=bc7f636484426edb2fc7a8cfb599b16a*

McCormick, T. H., Ferrell, R., Karr, A. F. and Ryan, P. B. (2010), 'Complex Networks as a Unified Framework for Descriptive Analysis and Predictive Modeling in Climate Science', *Science And Technology* **4**(5), 497–511.

McLean, R. F. and Kench, P. S. (2015), 'Destruction or persistence of coral atoll islands in the face of 20th and 21st century sea-level rise?', *Wiley Interdisciplinary Reviews: Climate Change* **6**(October), n/a–n/a.
URL: *http://doi.wiley.com/10.1002/wcc.350*

Meheux, K., Dominey-Howes, D. and Lloyd, K. (2007), 'Natural hazard impacts in small island developing states: A review of current knowledge and future research needs', *Natural Hazards* **40**(2), 429–446.

Mercer, J., Dominey-Howes, D., Kelman, I. and Lloyd, K. (2007), 'The potential for combining indigenous and western knowledge in reducing vulnerability to environmental hazards in small island developing states', *Environmental Hazards* **7**(4), 245–256.

Merrifield, M. A., Becker, J. M., Ford, M. and Yao, Y. (2014), 'Observations and estimates of wave-driven water level extremes at the Marshall Islands', *Geophysical Research Letters* pp. 7245–7253.
URL: *http://dx.doi.org/10.1002/2014GL061005*

Milman, O. (2016), 'Obama declares disaster as Marshall Islands suffers worst-ever drought'.
URL: *http://www.theguardian.com/world/2016/apr/28/obama-marshall-islands-drought*

Monismith, S. G., Rogers, J. S., Koweek, D. A. and Dunbar, R. B. (2015), 'Frictional wave dissipation on a remarkably rough reef', *Geophysical Research Letters* pp. 4063–4071.

Monserrat, S., Vilibić, I. and Rabinovich, a. B. (2006), 'Meteotsunamis: atmospherically induced destructive ocean waves in the tsunami frequency band', *Nat. Hazards Earth Syst. Sci.* **6**, 1035–1051.

Mortlock, T. R. and Goodwin, I. D. (2015), 'Directional wave climate and power variability along the Southeast Australian shelf', *Continental Shelf Research* **98**, 36–53.
URL: *http://dx.doi.org/10.1016/j.csr.2015.02.007*

Munk, W. H., Miller, G. R., Snodgrass, F. E. and Barber, N. F. (1963), 'Directional recording of swell from distant storms', *Philosophical Transactions of the Royal Society. Series A, Mathematical and Physical Sciences* **255**(1062), 505–584.
URL: *http://www.ncbi.nlm.nih.gov/entrez/query.fcgi?cmd=Retrieve&db=PubMed&dopt=Citation&list_ui*

Nakaza, E., Tsukayama, S. and Hino, M. (1990), 'Bore-like surf beat on reef coasts', *Proc. 22nd Int. Conf. Coastal. Eng.* pp. 743–756.
URL: *http://journals.tdl.org/icce/index.php/icce/article/viewArticle/4486*

Narayan, S., Beck, M. W., Reguero, B. G., Losada, I. n. J., van Wesenbeeck, B., Pontee, N., Sanchirico, J. N., Ingram, J. C., Lange, G.-M. and Burks-Copes, K. A. (2016), 'The Effectiveness, Costs and Coastal Protection Benefits of Natural and Nature-Based Defences', *Plos One* **11**(5), e0154735.
URL: *http://dx.plos.org/10.1371/journal.pone.0154735*

Narayan, S., Simmonds, D., Nicholls, R. J. and Clarke, D. (2015), 'A Quasi-2D Bayesian network model for assessments of coastal inundation pathways and probabilities', *Journal of Flood Risk Management* pp. 1–28.

Nelson, R. C. (1996), 'Hydraulic roughness of coral reef platforms', *Applied Ocean Research* **18**(5), 265–274.

Nelson, R. C. (1997), 'Height limits in top down and bottom up wave environments', *Coastal Engineering* **32**, 247–254.

Ng, H., Ong, S., Foong, K., Goh, P. and Nowinski, W. (2006), 'Medical Image Segmentation Using K-Means Clustering and Improved Watershed Algorithm', *2006 IEEE Southwest Symposium on Image Analysis and Interpretation* pp. 61–65.
URL: *http://ieeexplore.ieee.org/lpdocs/epic03/wrapper.htm?arnumber=1633722*

Norsys (2003), Netica - Application for Belief Networks and Influence Diagrams: User's Guide, Technical report, Norsys Software Corp., Vancouver, BC.

Nott, J. (1997), 'Extremely high-energy wave deposits inside the Great Barrier Reef, Australia: Determining the cause-tsunami or tropical cyclone', *Marine Geology* **141**(1-4), 193–207.

Nunes, V. and Pawlak, G. (2008), 'Observations of Bed Roughness of a Coral Reef', *Journal of Coastal Research* **24**(Figure 1), 39–50.

Nwogu, O. and Demirbilek, Z. (2010), 'Infragravity Wave Motions and Runup over Shallow Fringing Reefs', *Journal of Waterway, Port, Coastal, and Ocean Engineering* **136**(December), 295–305.

Olij, D. J. C. (2015), Wave climate reduction for medium term process based morphodynamic simulations with application to the Durban Coast, Master's thesis, Delft University of Technology.

Pandolfi, J., Connolly, S. R., Marshall, D. J. and Cohen, A. L. (2011), 'Ocean Acidification', *Science* **333**, 418–422.

Payo, A. and Muñoz Pérez, J. J. (2013), 'Discussion of Ford, M.R.; Becker, J.M., and Merrifield, M.A. 2013. Reef Flat Wave Processes and Excavation Pits: Observations and Implications for Majuro Atoll, Marshall Islands. Journal of Coastal Research, 29(3), 545–554.', *Journal of Coastal Research* **290**, 1236–1242.
URL: *http://www.bioone.org/doi/abs/10.2112/JCOASTRES-D-13-00051.1*

Pearl, J. (1988), 'Probabilistic Reasoning in Intelligent Systems'.

Péquignet, A.-C., Becker, J. M. and Merrifield, M. A. (2014), 'Energy transfer between wind waves and low-frequency oscillations on a fringing reef, Ipan Guam', *Journal of Geophysical Research: Oceans* pp. 6709–6724.
URL: *http://doi.wiley.com/10.1002/2014JC010179*

Péquignet, A.-C., Becker, J. M., Merrifield, M. A. and Aucan, J. (2009), 'Forcing of resonant modes on a fringing reef during tropical storm Man-Yi', *Geophysical Research Letters* **36**, 1–6.

Péquignet, A.-C., Becker, J. M., Merrifield, M. A. and Boc, S. J. (2011), 'The dissipation of wind wave energy across a fringing reef at Ipan, Guam', *Coral Reefs* **30**(SUPPL. 1), 71–82.

Peregrine, D. H. (1966), 'Calculations of the development of an undular bore', *Journal of Fluid Mechanics* **25**, 321.

Pittman, S. J., Costa, B. and Wedding, L. M. (2013), *Coral Reef Remote Sensing*.
URL: *http://link.springer.com/10.1007/978-90-481-9292-2*

Plant, N. G. and Holland, K. T. (2011*a*), 'Prediction and assimilation of surf-zone processes using a Bayesian network. Part I: Forward models', *Coastal Engineering* **58**(1), 119–130.
URL: *http://linkinghub.elsevier.com/retrieve/pii/S0378383910001353*

Plant, N. G. and Holland, K. T. (2011*b*), 'Prediction and assimilation of surf-zone processes using a Bayesian network. Part II: Inverse models', *Coastal Engineering* **58**(3), 256–266.
URL: *http://dx.doi.org/10.1016/j.coastaleng.2010.11.002 http://linkinghub.elsevier.com/retrieve/pii/S03783*

Plant, N. G., Thieler, E. R. and Passeri, D. L. (2016), 'Coupling centennial-scale shoreline change to sea-level rise and coastal morphology in the Gulf of Mexico using a Bayesian network', *Earth's Future* .

Poelhekke, L. (2015), Predicting Coastal Hazards with a Bayesian Network, Master's thesis, Delft University of Technology.
URL: *http://resolver.tudelft.nl/uuid:8875d3be-5686-4272-b8e5-394f760157cf*

Poelhekke, L., Jäger, W. S., van Dongeren, A., Plomaritis, T. A., McCall, R. T. and Ferreira, O. (2016), 'Predicting Coastal Hazards for Sandy Coasts with a Bayesian Network', *Submitted to Coastal Engineering, Under Review* .

Pomeroy, A. (2011), Low Frequency Wave Resonance on Fringing Reefs, PhD thesis, TU Delft.

Pomeroy, A., Lowe, R. J., Symonds, G., van Dongeren, A. and Moore, C. (2012), 'The dynamics of infragravity wave transformation over a fringing reef', *Journal of Geophysical Research: Oceans* **117**(11), 1–17.
URL: *http://doi.wiley.com/10.1029/2012JC008310*

Pomeroy, A., Lowe, R. J., van Dongeren, A., Ghisalberti, M. and Bodde, W. (2015), 'Spectral wave-driven sediment transport across a fringing reef', *Coastal Engineering* **98**, 78–94.
URL: *http://dx.doi.org/10.1016/j.coastaleng.2015.01.005*

Pomeroy, A., van Dongeren, A., Lowe, R. J., van Thiel de Vries, J. S. M. and Roelvink, J. A. (2012), Low-frequency wave resonance in fringing reef environments, *in* 'Coastal Engineering 2012', pp. 1–10.

Pullen, T., Allsop, N., Bruce, T., Kortenhaus, A., Schüttrumpf, H. and van der Meer, J. W. (2007), *EUROTOP Manual*, HR Wallingford Ltd, Wallingford, UK.
URL: *www.overtopping-manual.com*

Punj, G. and Stewart, D. W. (1983), 'Cluster analysis in marketing research: Review and suggestions for application', *Journal of marketing research* **20**(2), 134–148.

Quataert, E. (2015), Wave runup on atoll reefs, Master's thesis, Delft University of Technology.
URL: *http://resolver.tudelft.nl/uuid:f9ba5835-66bf-4907-9823-4ff56edf5909*

Quataert, E., Storlazzi, C. D., Rooijen, A., Cheriton, O. M. and van Dongeren, A. (2015), 'The influence of coral reefs and climate change on wave-driven flooding of tropical coastlines', *Geophysical Research Letters* pp. 1–9.

Rawat, A., Ardhuin, F., Ballu, V., Crawford, W., Corela, C. and Aucan, J. (2014), 'Infragravity waves across the oceans', *Geophysical Research Letters* **41**(22), 7957–7963.

Renault, L., Vizoso, G., Jansá, A., Wilkin, J. and Tintoré, J. (2011), 'Toward the predictability of meteotsunamis in the Balearic Sea using regional nested atmosphere and ocean models', *Geophysical Research Letters* **38**(May), 1–7.

Roeber, V. and Bricker, J. D. (2015), 'Destructive tsunami-like wave generated by surf beat over a coral reef during Typhoon Haiyan.', *Nature communications* **6**, 7854.
URL: *http://www.nature.com/ncomms/2015/150806/ncomms8854/full/ncomms8854.html*

Roeber, V. and Cheung, K. F. (2012), 'Boussinesq-type model for energetic breaking waves in fringing reef environments', *Coastal Engineering* **70**, 1–20.
URL: *http://linkinghub.elsevier.com/retrieve/pii/S0378383912001081*

Roelvink, J. A., Dastgheib, A., Spencer, T., Moller, I., Christie, E., Berenguer, M., Sempere, D., van der Meer, J. W., Seyyedabdolhossein, M., Nederhoff, K. and Vermin, W. (2015), Resilience-Increasing Strategies for Coasts - Toolkit - Improvement of physical processes XBeach improvement & validation; wave dissipation over vegetated marshes and flash flood module, Technical report.

Roelvink, J. A., van Dongeren, A., McCall, R. T., Hoonhout, B., van Rooijen, A., van Geer, P., de Vet, L., Nederhoff, K. and Quataert, E. (2015), XBeach Technical Reference : Kingsday Release, Technical report.

Rogers, J. S., Monismith, S. G., Feddersen, F. and Storlazzi, C. D. (2013), 'Hydrodynamics of spur and groove formations on a coral reef', *Journal of Geophysical Research: Oceans* **118**(April), 3059–3073.

Rogers, J. S., Monismith, S. G., Koweek, D. A. and Dunbar, R. B. (2015), 'Wave dynamics of a Pacific Atoll with high frictional effects', *Journal of Geophysical Research: Oceans* **120**, 1–18.

Różyński, G. and Reeve, D. (2005), 'Multi-resolution analysis of nearshore hydrodynamics using discrete wavelet transforms', *Coastal Engineering* **52**(9), 771–792.
URL: *http://www.sciencedirect.com/science/article/pii/S0378383905000736*

Ruggiero, P., Holman, R. A. and Beach, R. A. (2004), 'Wave run-up on a high-energy dissipative beach', *Journal of Geophysical Research C: Oceans* **109**(6), 1–12.

Salmon, J. E., Holthuijsen, L. H., Zijlema, M., van Vledder, G. P. and Pietrzak, J. D. (2015), 'Scaling depth-induced wave-breaking in two-dimensional spectral wave models', *Ocean Modelling* **87**, 30–47.
URL: *http://dx.doi.org/10.1016/j.ocemod.2014.12.011*

Schweckendiek, T., Vrouwenvelder, a. C. W. M. and Calle, E. O. F. (2014), 'Updating piping reliability with field performance observations', *Structural Safety* **47**, 13–23.
URL: *http://dx.doi.org/10.1016/j.strusafe.2013.10.002*

Sheppard, C., Dixon, D. J., Gourlay, M. R., Sheppard, A., Payet, R. and Sheppard, C. (2005), 'Coral mortality increases wave energy reaching shores protected by reef flats: Examples from the Seychelles', *Estuarine, Coastal and Shelf Science* **64**(2-3), 223–234.

Sheremet, A., Kaihatu, J. M., Su, S.-F., Smith, E. R. and Smith, J. M. (2011), 'Modeling of nonlinear wave propagation over fringing reefs', *Coastal Engineering* **58**(12), 1125–1137.

Shi, F., Kirby, J. T., Harris, J. C., Geiman, J. D. and Grilli, S. T. (2012), 'A high-order adaptive time-stepping TVD solver for Boussinesq modeling of breaking waves and coastal inundation', *Ocean Modelling* **43-44**, 36–51.
URL: *http://dx.doi.org/10.1016/j.ocemod.2011.12.004*

Shimozono, T., Tajima, Y., Kennedy, A. B., Nobuoka, H., Sasaki, J. and Sato, S. (2015), 'Combined infragravity wave and sea-swell runup over fringing reefs by super typhoon Haiyan', *Journal of Geophysical Research: Oceans* **120**, 1–24.

Shope, J. B., Storlazzi, C. D. and Hegermiller, C. A. (2015), Modeled Changes in Extreme Wave Climates of the Tropical Pacific Over the 21st Century: Implications for US and US-Affiliated Atoll Islands, *in* 'Coastal Sediments 2015', World Scientific, San Diego, pp. 1–13.

Slezak, M. (2016), 'Great Barrier Reef: 93% of reefs hit by coral bleaching'.
URL: *http://www.theguardian.com/environment/2016/apr/19/great-barrier-reef-93-of-reefs-hit-by-coral-bleaching*

Smit, P. B., Roelvink, J. A., van Thiel de Vries, J. S. M., McCall, R. T., van Dongeren, A. and Zwinkels, J. R. (2014), XBeach: Non-hydrostatic model, Technical report, Deltares, Delft, The Netherlands.

Smithers, S. G. and Hoeke, R. K. (2014), 'Geomorphological impacts of high-latitude storm waves on low-latitude reef islands - Observations of the December 2008 event on Nukutoa, Takuu, Papua New Guinea', *Geomorphology* **222**, 106–121.
URL: *http://dx.doi.org/10.1016/j.geomorph.2014.03.042*

Smithsonian National Museum of Natural History (2016), 'Marshall Islands Stick Navigation Chart'.
URL: *http://www.smithsonianmag.com/arts-culture/science-and-tradition-are-resurrecting-lost-art-wave-piloting-180958005/?no-ist*

Spennemann, D. H. R. (1996), 'Nontraditional settlement patterns and typhoon hazard on contemporary Majuro atoll, Republic of the Marshall Islands', *Environmental Management* **20**(3), 337–348.

Spennemann, D. H. R. (2004), *Typhoons in Micronesia: A History of Tropical Cyclones and their Effects until 1914*, CNMI, Saipan.

Stockdon, H. F., Holman, R. A., Howd, P. A. and Sallenger, A. H. (2006), 'Empirical parameterization of setup, swash, and runup', *Coastal Engineering* **53**(7), 573–588.
URL: *http://linkinghub.elsevier.com/retrieve/pii/S0378383906000044*

Stockdon, H. F., Thompson, D. M., Plant, N. G. and Long, J. (2014), 'Evaluation of wave runup predictions from numerical and parametric models', *Coastal Engineering* **92**, 1–11.
URL: *http://linkinghub.elsevier.com/retrieve/pii/S0378383914001239*

Storlazzi, C. D., Elias, E. P. L. and Berkowitz, P. (2015), 'Many atolls may be uninhabitable within decades due to climate change', *Nature Scientific Reports* pp. 1–9.
URL: *http://dx.doi.org/10.1038/srep14546*

Storlazzi, C. D., Shope, J. B., Erikson, L., Hegermiller, C. A. and Barnard, P. L. (2015), Future wave and wind projections for United States and United States-affiliated Pacific Islands, Technical report, U.S. Geological Survey, Santa Cruz, CA.

Su, S.-F., Ma, G. and Hsu, T. W. (2015), 'Boussinesq modeling of spatial variability of infragravity waves on fringing reefs', *Ocean Engineering* **101**, 78–92.
URL: *http://dx.doi.org/10.1016/j.oceaneng.2015.04.022*

Sun, S., Zhang, C. and Yu, G. (2006), 'A Bayesian Network Approach to Traffic Flow Forecasting', *IEEE Transactions on Intelligent Tra* **7**(1), 124–132.

Symonds, G., Huntley, D. A. and Bowen, A. J. (1982), 'Two-dimensional surf beat: Long wave generation by a time-varying breakpoint', *Journal of Geophysical Research* **87**(C1), 492.

Tajima, Y., Shimozono, T., Gunasekara, K. H. and Cruz, E. C. (2016), 'Study on Locally Varying Inundation Characteristics Induced by Super Typhoon Haiyan Part 2: Deformation of Storm Waves on the Beach with Fringing Reef along the East Coast of Eastern Samar', *Coastal Engineering Journal* **58**(1).

Tan, P.-N., Steinbach, M. and Kumar, V. (2005), 'Chap 8 : Cluster Analysis: Basic Concepts and Algorithms', *Introduction to Data Mining* p. Chapter 8.
URL: *http://www-users.cs.umn.edu/ kumar/*

Terry, J. P. and Falkland, A. C. (2010), 'Responses of atoll freshwater lenses to storm-surge overwash in the Northern Cook Islands', *Hydrogeology Journal* **18**(3), 749–759.
URL: *http://link.springer.com/10.1007/s10040-009-0544-x*

Terry, J. P., Oliver, G. J. and Friess, D. A. (2016), 'Ancient high-energy storm boulder deposits on Ko Samui, Thailand, and their significance for identifying coastal hazard risk', *Palaeogeography, Palaeoclimatology, Palaeoecology* .
URL: *http://linkinghub.elsevier.com/retrieve/pii/S0031018216301298*

Thornborough, K. J. and Davies, P. J. (2011), 'Reef Flats'.
URL: *http://link.springer.com/10.1007/978-90-481-2639-2*

Tingley, K. (2016), 'The Secrets of the Wave Pilots'.
URL: *http://www.nytimes.com/2016/03/20/magazine/the-secrets-of-the-wave-pilots.html?mabReward=A3&_r=1*

Tissier, M. F. S., Bonneton, P., Marche, F., Chazel, F. and Lannes, D. (2012), 'A new approach to handle wave breaking in fully non-linear Boussinesq models', *Coastal Engineering* **67**, 54–66.
URL: *http://dx.doi.org/10.1016/j.coastaleng.2012.04.004*

Tissier, M. F. S., Bonneton, P., Marche, F., Chazel, F., Lannes, D., Montpellier, D. and Eugène, P. (2011), 'Nearshore Dynamics of Tsunami-like Undular Bores using a Fully Nonlinear Boussinesq Model', *Journal of Coastal Research* **Special Is**(64), 603–607.

Tolman, H. L. (2003), 'Treatment of unresolved islands and ice in wind wave models', *Ocean Modelling* **5**(3), 219–231.

Tolman, H. L. (2009), User manual and system documentation of WAVEWATCH-IIITM version 3.14, Technical Report 3.14.
URL: *http://polart.ncep.noaa.gov/mmab/papers/tn276/MMAB_276.pdf\ npapers2://publication/uuid/298*
957F-4D13-A6AB-ABE61B08BA6B

Tolo, S., Patelli, E. and Beer, M. (2015), 'Enhanced Bayesian Network approach to sea wave overtopping hazard quantification', (April), 1983–1990.

Tomás, A., Méndez, F. J., Medina, R., Jaime, F. F., Higuera, P., Lara, J. L. and Álvarez de Eulate, M. F. (2015), 'A methodology to estimate wave-induced coastal flooding hazard maps in Spain', *Journal of Flood Risk Management* pp. 1–17.

UN-Habitat (2015), Urbanization and Climate Change in Small Island Developing States, Technical report, United Nations Human Settlements Programme (UN-Habitat), Nairobi.
URL: *https://sustainabledevelopment.un.org/content/documents/2169(UN-Habitat, 2015) SIDS_Urbanization.pdf*

UN-OHRLLS (2015), Small Island Developing States in Numbers (Climate Change Edition 2015), Technical report, Office of the High Representative for the Least Developed Countries, Landlocked Developing Countries and Small Island Developing States (UN-OHRLLS).

UNEP-WCMC (2016), 'ReefBase - ReefGIS'.
URL: *http://www.reefbase.org/gis_maps/*

UNISDR (2015), Sendai Framework for Disaster Risk Reduction 2015-2030, Technical report, United Nations Office for Disaster Risk Reduction (UNISDR), Sendai, Japan.

van Arkel, M. (2016), Towards an efficient sensitivity analysis of wave forcing in coastal erosion studies, Master's thesis, Delft University of Technology.
URL: *http://repository.tudelft.nl/islandora/object/uuid:3bfe1ad0-426d-4671-810f-2110724c3385*

van der Knijff, J. M., Younis, J. and De Roo, a. P. J. (2010), 'LISFLOOD: A GIS-based distributed model for river basin scale water balance and flood simulation', *International Journal of Geographical Information Science* **24**(2), 189–212.

van Dongeren, A., Battjes, J. A., Janssen, T. T., van Noorloos, J., Steenhauer, K., Steenbergen, G. and Reniers, A. (2007), 'Shoaling and shoreline dissipation of low-frequency waves', *Journal of Geophysical Research* **112**(C2), 1–15.
URL: *http://doi.wiley.com/10.1029/2006JC003701*

van Dongeren, A., de Jong, M., van der Lem, C., van Deyzen, A. and den Bieman, J. (2016), 'Review of Long Wave Dynamics over Reefs and into Ports with Implication for Port Operations', *Journal of Marine Science and Engineering* **4**(1), 12.
URL: *http://www.mdpi.com/2077-1312/4/1/12*

van Dongeren, A., Lowe, R. J., Pomeroy, A., Trang, D. M., Roelvink, J. A., Symonds, G. and Ranasinghe, R. (2013), 'Numerical modeling of low-frequency wave dynamics over a fringing coral reef', *Coastal Engineering* **73**, 178–190.
URL: *http://linkinghub.elsevier.com/retrieve/pii/S0378383912001779*

van Dongeren, A., Reniers, A., Battjes, J. A. and Svendsen, I. A. (2003), 'Numerical modeling of infragravity wave response during DELILAH', *Journal of Geophysical Research* **108**(C9), 1–19.

van Gent, M. (2001), 'Wave Runup on Dikes with Shallow Foreshores', *Journal of Waterway, Port, Coastal, and Ocean Engineering* **127**(October), 254–262.

van Verseveld, H., van Dongeren, A., Plant, N. G., Jäger, W. S. and den Heijer, C. (2015), 'Modelling multi-hazard hurricane damages on an urbanized coast with a Bayesian Network approach', *Coastal Engineering* **103**, 1–14.
URL: *http://linkinghub.elsevier.com/retrieve/pii/S0378383915000927*

van Vledder, G. (2015), Swell-Wave Island Interaction and Piloting in the Southern Pacific Ocean, *in* '36th IAHR World Congress', number 1963, pp. 1–5.

Veltcheva, A. D. (2002), 'Wave and Group Transformation By a Hilbert Spectrum', *Coastal Engineering Journal* **44**(04), 283–300.

Vennell, R. (2010), 'Resonance and trapping of topographic transient ocean waves generated by a moving atmospheric disturbance', *Journal of Fluid Mechanics* **650**, 427.

Vetter, O., Becker, J. M., Merrifield, M. A., Péquignet, A.-C., Aucan, J., Boc, S. J. and Pollock, C. E. (2010), 'Wave setup over a Pacific Island fringing reef', *Journal of Geophysical Research: Oceans* **115**(September), 1–13.

Vilibić, I. and Šepić, J. (2009), 'Destructive meteotsunamis along the eastern Adriatic coast: Overview', *Physics and Chemistry of the Earth* **34**(17-18), 904–917.

Walsh, K. J. E., McInnes, K. and McBride, J. L. (2012), 'Climate change impacts on tropical cyclones and extreme sea levels in the South Pacific - A regional assessment', *Global and Planetary Change* **80-81**, 149–164.
URL: *http://dx.doi.org/10.1016/j.gloplacha.2011.10.006*

Weisler, M. I. and Woodhead, J. D. (1995), 'Basalt Pb isotope analysis and the prehistoric settlement of Polynesia.', *Proceedings of the National Academy of Sciences of the United States of America* **92**(6), 1881–5.
URL: *http://www.pubmedcentral.nih.gov/articlerender.fcgi?artid=42386&tool=pmcentrez&rendertype=al*

White, I., Falkland, A. C., Perez, P., Dray, A., Metutera, T., Metai, E. and Overmars, M. (2007), 'Challenges in freshwater management in low coral atolls', *Journal of Cleaner Production* **15**(16), 1522–1528.

Wilson, K. E., Adams, P. N., Hapke, C., Lentz, E. E. and Brenner, O. (2015), 'Application of Bayesian Networks to hindcast barrier island morphodynamics', *Coastal Engineering* **102**, 30–43.
URL: *http://linkinghub.elsevier.com/retrieve/pii/S0378383915000794*

Woodroffe, C. D. (2002), Reef Coasts, *in* 'Coasts: Form, Process, and Evolution', Cambridge University Press, Cambridge, chapter 5, pp. 189–241.

Woodroffe, C. D. (2008), 'Reef-island topography and the vulnerability of atolls to sea-level rise', *Global and Planetary Change* **62**(1-2), 77–96.

Wright, L. D. and Short, A. (1984), 'Morphodynamic variability of surf zones and beaches: A synthesis', *Marine Geology* **56**(1-4), 93–118.
URL: *http://citeseerx.ist.psu.edu/viewdoc/download?doi=10.1.1.175.7797&rep=rep1&type=pdf*
http://linkinghub.elsevier.com/retrieve/pii/0025322784900082

Wunsch, C. and Gill, A. (1976), 'Observations of equatorially trapped waves in Pacific sea level variations', *Deep Sea Research and Oceanographic Abstracts* **23**(5), 371–390.
URL: *http://www.sciencedirect.com/science/article/pii/0011747176908354\nhttp://linkinghub.elsevier.com*

Xanthidis, M., Li, A. Q. and Rekleitis, I. (2016), Shallow Coral Reef Surveying by Inexpensive Drifters, *in* 'IEEE OCEANS 2016 - Shanghai', IEEE, Shanghai, pp. 1–9.

Yamano, H. (2007), 'The use of multi-temporal satellite images to estimate intertidal reef-flat topography', *Journal of Spatial Science* **52**(May), 73–79 ST – The use of multi–temporal satellite im.

Yao, Y., Huang, Z., Monismith, S. G. and Lo, E. Y. M. (2012), '1DH Boussinesq modeling of wave transformation over fringing reefs', *Ocean Engineering* **47**, 30–42.
URL: *http://dx.doi.org/10.1016/j.oceaneng.2012.03.010*

Young, I. R. (1989), 'Wave Transformation Over Coral Reefs', *Journal of Geophysical Research* **94**(C7), 9779–9789.

Zawada, D. G., Piniak, G. A. and Hearn, C. J. (2010), 'Topographic complexity and roughness of a tropical benthic seascape', *Geophysical Research Letters* **37**(14), 1–6.

Zhao, X., Liu, H. and Wang, B. (2016), 'Tsunami Waveforms and Runup of Undular Bores in Coastal Waters', *Journal of Engineering Mechanics* **0**(0), 6016003.
URL: *http://ascelibrary.org/doi/abs/10.1061/(ASCE)EM.1943-7889.0001086*

Zijlema, M. (2012), 'Modelling wave transformation across a fringing reef using SWASH', *Coastal Engineering 2012* pp. 1–12.
URL: *http://journals.tdl.org/icce/index.php/icce/article/view/6479*

Zijlema, M. and Stelling, G. (2008), 'Efficient computation of surf zone waves using the nonlinear shallow water equations with non-hydrostatic pressure', *Coastal Engineering* **55**(10), 780–790.

Zijlema, M., Stelling, G. and Smit, P. B. (2011), 'SWASH: An operational public domain code for simulating wave fields and rapidly varied flows in coastal waters', *Coastal Engineering* **58**(10), 992–1012.
URL: *http://dx.doi.org/10.1016/j.coastaleng.2011.05.015*

Zimmer, B. (2006), Coral reef restoration: an overwiew, *in* 'Coral Reef Restoration Handbook', chapter 3, p. 384.

Zwirglmaier, K., Papakosta, P. and Straub, D. (2013), 'Learning a Bayesian network model for predicting wildfire behavior', pp. 3115–3121.

A

XBEACH BENCHMARK TESTS

A

To generate the large synthetic dataset at the heart of this study, the desire for a wide and varied range of model scenarios had to be balanced with computational feasibility. This section reviews first the methodology used to define the feasible scope of the project, and then the sensitivity tests conducted to set up the model.

The more model simulations that can be run, the larger the resulting synthetic database. However, an unlimited number of simulations cannot realistically be completed, owing to several key constraints:

- Computational expense of the chosen model
- Schedule of the thesis project
- Availability of computer resources
- Time required for model pre-/post-processing
- Time required for carrying out additional simulations
- File storage space

Together, these limitations determined the feasible scope of the project. The project schedule and availability of shared modelling computers meant that there was approximately 1 month in which to carry out all of the required simulations. We also felt it necessary to include contingency time for re-running the model to make any necessary corrections that come to light after the initial attempt. Hence, a full batch of model runs should take between 5-10 days.

For the first benchmark tests, I tested extreme values of each parameter (max/min values) to get a sense of the potential range of results and any problems that might arise. After completion of these runs, they were analyzed to identify ways in which the model could be sped up without sacrificing quality. Also, by extensively testing the model beforehand, the pre- and post-processing tools could be developed and debugged, reducing the likelihood of costly errors during the production run phase.

The computer specifications used for both the initial model tests and final production runs are given in Table A.1.

Table A.1: Specifications of modelling computers.

Type	Number of Computers	Processor Speed [GHz]	Number of Cores	RAM [GB]	Capacity [GB]
WCF	1	2.60	4	16	100
WCP	9	2.60	8	32	100

For the initial benchmark tests, a total of 384 simulations were carried out, representing 2 variations of 9 parameters with unrealistically steep wave combinations excluded. In non-hydrostatic mode of XBeach, the 30 minute simulations took between 2-26 mins to complete, with an average of 9 mins.

A.1. PREDICTED SIMULATION TIMES

To get a sense of how many simulations we could feasibly run, we took the average run times from the benchmark tests and multiplied them by different hypothetical numbers

of simulations. The number of simulations depends on the number of parameters tested and how many different variations there are for each parameter. The required number of simulations can be calculated with equation A.1:

$$\textit{Total required number of simulations} = \prod_{i=1}^{n} v_i \tag{A.1}$$

Where n is the number of parameters, i is a given parameter, and v is the number of variations for a given parameter. For instance, testing 3 parameters with 4 variations each would require $4 \times 4 \times 4 = 64$ runs in total.

Table A.2 shows the estimated total simulation times (in number of days) for different numbers of parameters and variations. The total duration also depends on the number of processing cores available. It is assumed that the total number of simulations is divided evenly between all of the cores. The chosen maximum permissible run time of 10 days was used to eliminate combinations of parameters and variations that would be infeasible (red text). For simplicity, linear scaling of run times with the number of simulations was assumed.

Table A.2: Number of days required to complete full batch of runs for 8 parameters and the given number of variations. Red text denotes total projected runtimes exceeding 10 days (infeasible) and green text denotes runtimes 10 days or less (feasible).

8 Parameters		**Number of Cores**					
Variations	**# of Runs**	**1**	**4**	**8**	**16**	**32**	**80**
2	256	**2**	**0**	**0**	**0**	**0**	**0**
3	6,561	**41**	**10**	**5**	**3**	**1**	**1**
4	65,536	**410**	**102**	**51**	**26**	**13**	**5**
5	390,625	**2,441**	**610**	**305**	**153**	**76**	**31**
6	1,679,616	**10,498**	**2,624**	**1,312**	**656**	**328**	**131**
7	5,764,801	**36,030**	**9,008**	**4,504**	**2,252**	**1,126**	**450**
8	16,777,216	**104,858**	**26,214**	**13,107**	**6,554**	**3,277**	**1,311**
9	43,046,721	**269,042**	**67,261**	**33,630**	**16,815**	**8,408**	**3,363**

As Table A.2 demonstrates, the number of required simulations becomes infeasible quite quickly. Hence, careful consideration is necessary to determine precisely which parameters are most important. The feasible number of simulations was determined to be O(50,000). Based on these estimates, we decided that 8 parameters with between 3-7 variations was the optimal combination. The number of variations for each parameter was chosen based on the sensitivity of runup and overtopping to them. Ultimately, eight parameters were selected to run:

- Significant Offshore Wave Height (H_{s0}) [m]
- Wave Steepness (H_{s0}/L_0) [-]
- Offshore Water Level (η_0) [m]
- Hydrodynamic Roughness (C_f) [-]

A

- Fore Reef Slope (β_f) [-]
- Beach Slope (β_b) [-]
- Reef Flat Width (W_{reef}) [m]
- Beach Crest Elevation (z_{beach}) [m]

A.2. ACTUAL RUN TIMES

Throughout the duration of the project, it became important to monitor run times so as to ensure efficient use of computing resources. Given the limited time constraints of the project, we could not afford to leave computers sitting idle. Furthermore, monitoring simulation times informed decisions about how many other runs can be completed, and whether or not there is sufficient time to rerun problematic runs. Figure A.1 shows the distribution of model run time depending on different parameters. Reef width has the greatest influence, since it extends the size of the model domain and thus the number of grid points at which calculations must be performed.

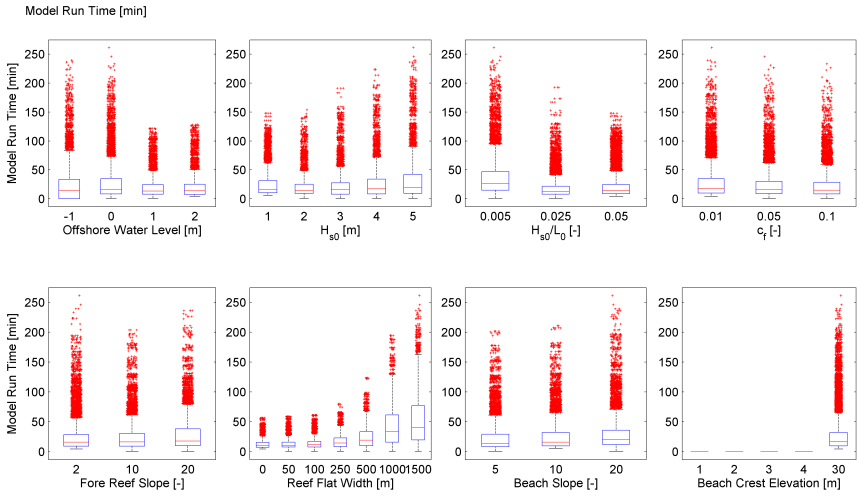

Figure A.1: Diagram illustrating the influence of different model parameters on run time.

A.3. STORAGE

A 30 min simulation output globally every second resulted in an average file size of 133 MB, which in total quickly reaches terabytes of data for even small numbers of simulations. The main consideration for file size rests less with the parameters chosen, than with the output file specifications. Hence, it was necessary to determine which parameters to output and at what frequencies. The following output settings were chosen:

- Global output every second (`zb, zs`)
- Mean statistics across entire profile at end of simulation (`zb, zs, qx`)
- Point output (x7) for fore reef, reef flat, runup gauge and overtopping measurement (1 s output)

B

XBeach Sensitivity Tests

The overall aim of this project was to determine the sensitivity of flooding to variations in hydrodynamic forcing and reef morphology. In order to do this, sensitivity testing first had to be carried out to determine appropriate values for other model parameters that would remain fixed through the main tests. Grid resolution, representation of idealized bathymetry, numerical dispersion, spectral shape, offshore boundary settings, and model spinup were all examined to ensure reliable results.

B.1. Grid Resolution & Wave Breaking Steepness

The resolution of the numerical grid in XBeach is one of the main factors controlling runtimes. Doubling the grid resolution effectively doubles the number of calculations that need to be made at each timestep, which increases the total run time. However, numerous factors such as the numerical stability of the model, accuracy, and precision of outputs are improved with higher grid resolution. Hence, trade-offs must be made between providing sufficient detail to resolve the processes in the model and remaining computationally feasible.

An initial minimum grid resolution of 1 m was tested. Then, we decreased grid resolution to see if this could reduce run times. How coarse can the model become without sacrificing performance? However, when we did this, overtopping discharges and runup decreased. To determine if the results converged with greater resolution, the grid was made finer. However, it was found that runup and overtopping increased further, and did not converge at higher resolutions (Figure B.1).

Grid resolution is determined through a number of criteria: Courant number for numerical stability, number of points per wavelength, and manual upper and lower limits for grid cell sizes. We varied the `maxbrsteep` parameter (default value = 0.6), which controls the steepness of a wave front before breaking. Larger steepnesses enabled waves to grow higher before breaking, which led to higher runup and overtopping predictions. However, the model was also much more sensitive to grid resolution at high steepnesses, since only finer models could simulate the steeper water surfaces. Similar relationships

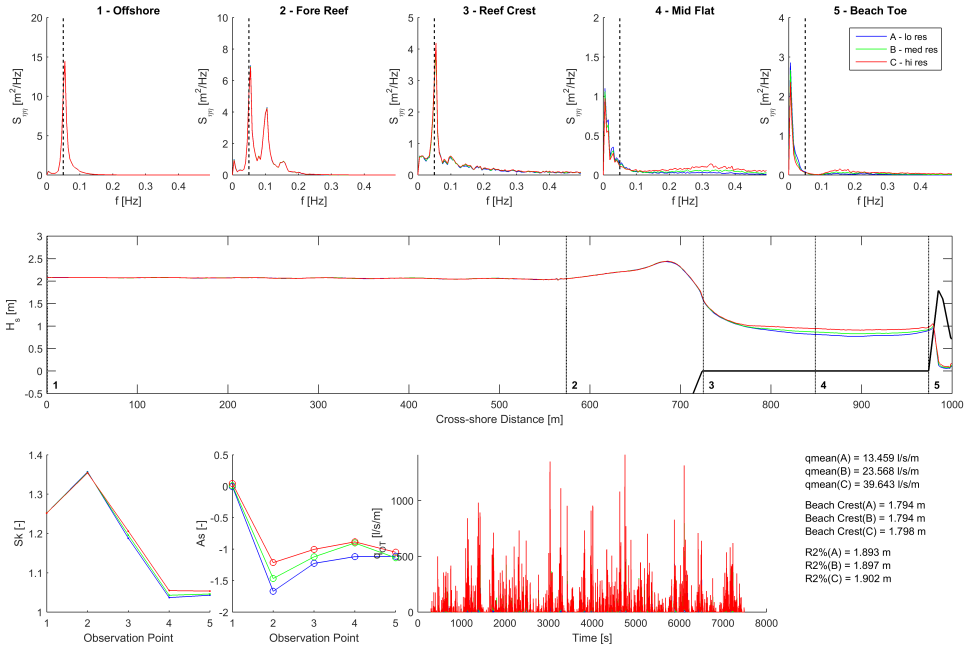

Figure B.1: A diagnostic plot showing the difference between grid resolutions of 0.25 (lo res), 0.50 (med res), and 1.00 m (hi res), for the default `maxbrsteep = 0.6`

between wave height, wave front steepness, and grid spacing have been noted by Tissier et al. (2012) and Shi et al. (2012).

Ultimately, `maxbrsteep = 0.4` was justified based on laboratory overtopping tests by Roelvink et al, 2015a. Lower steepnesses also had the effect of reducing dependency on grid resolution, since finer spacing was not required to resolve the steep wave fronts. As a consequence, the non-convergence observed with the default breaking steepness disappeared. Nonetheless, future studies should investigate the model's sensitivity to grid resolution and breaking steepness in greater detail.

B.2. SPECTRAL SHAPE

In the early stages of the project, spectral shape was investigated as a potentially important parameter for reef hydrodynamics, since it controls wave groupiness. However, previous studies of reef hydrodynamics have found negligible influence between runup or reef flat behaviour and spectral shape or groupiness (Cheriton et al., 2016; Gawehn, 2015).

To determine if there was any correlation in the present model, we carried out a sensitivity analysis, changing spectral shape from 1 to 15, representing fully developed sea state (1) through to an extremely peaked swell spectrum (15) (Figure B.2).

We investigated the sensitivity of key outputs to spectral shape (Figure B.3).

We then examined the relationship between peakedness and VLF anomalies at the

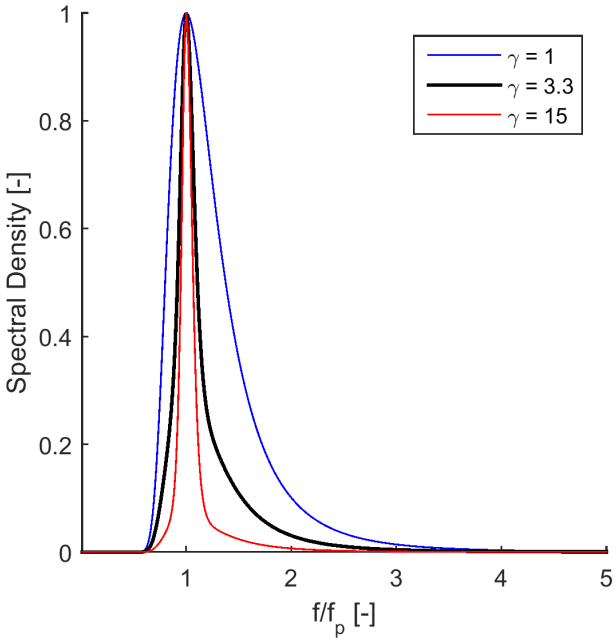

Figure B.2: Spectral shape with varying $\gamma_{JONSWAP}$ values. $\gamma_{JONSWAP} = 1$ represents a fully-developed sea (Pierson-Moskowitz Spectrum), $\gamma_{JONSWAP} = 3.3$ is the default shape for developing seas, and $\gamma_{JONSWAP} = 15$ represents an extremely peaked case (for illustrative purposes only).

resonant frequency (Figure B.4) but found little influence.

A simplified Bayesian network was set up to examine the dependencies between spectral shape and various outputs. Figure B.5 shows the network constrained by (a) higher runup values and (b) VLF anomalies, the mean spectral shape shifts towards higher values

The mean prior prediction of spectral shape across all tested cases here is $\overline{\gamma} = 6.27$. Figure B.5 suggests that large runup events cannot be exclusively attributed to higher spectral shapes ($\overline{\gamma} \rightarrow 6.53$). However, anomalously high VLF events are dominated by wave conditions with more peaked spectra ($\overline{\gamma} \rightarrow 8.16$). This suggests that although spectral shape may not have a strong relationship with runup, there may yet be some connection to anomalously large low frequency motions on the reef.

Spectral shape was ultimately not included in the main analysis for reasons of computational feasibility, but future studies should investigate its role further.

B.3. OFFSHORE BOUNDARY

Model boundaries should be far enough from area of interest to limit spurious effects but close enough to remain computationally feasible. In this study, that means that the model needs sufficient space for waves to develop, and to avoid unrealistic frictional or numerical dispersion effects. The boundary was initially set at a distance of $3 \times L_0$

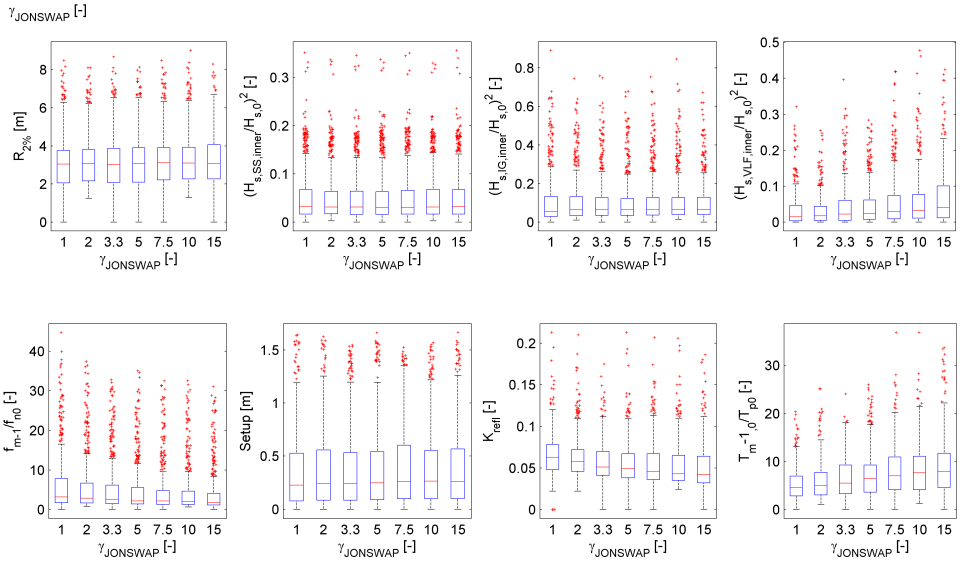

Figure B.3: This plot demonstrates the relationship between key output parameters and spectral shape.

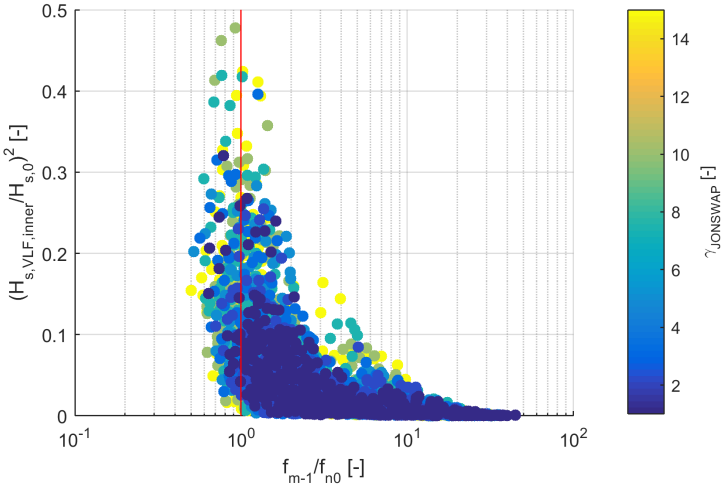

Figure B.4: Normalized, squared VLF wave height $(H_{VLF}/H_0)^2$ as a function of the ratio between mean spectral frequency at the inner reef flat ($f_{m-1,0}$) and the reef's zeroth resonant frequency ($f_{n,0}$). Points close to $f_{m-1,0}/f_{n,0} = 1$ (10^0) are near resonance. The colour of the points indicates peakedness, with yellow representing more peaked spectra.

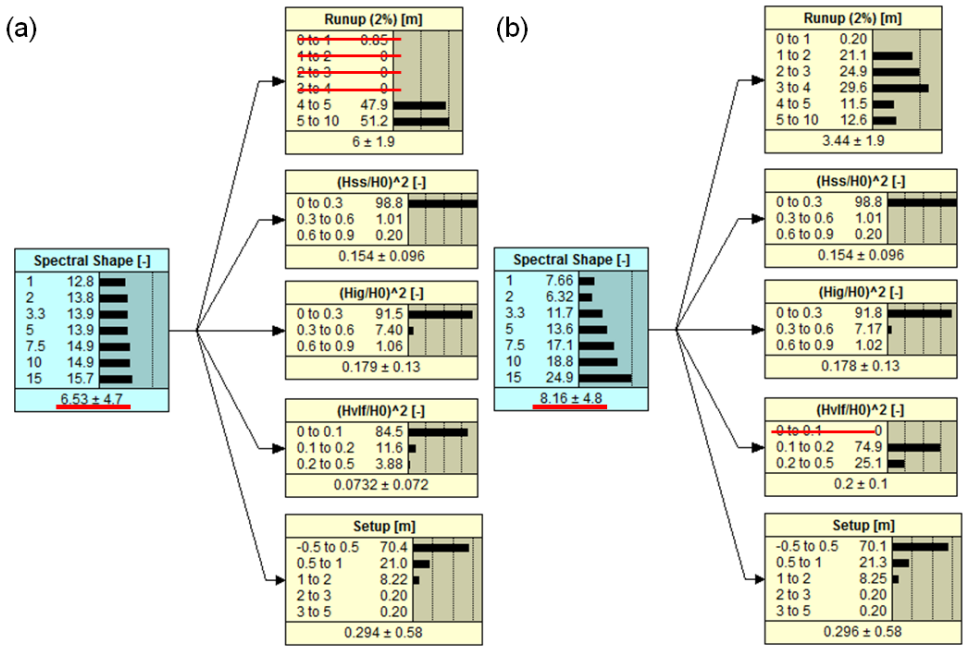

Figure B.5: (a) Shows the Bayesian network constrained on runup and (b) shows the Bayesian network constrained on VLF overtopping. The prior prediction of spectral shape based upon the uniform input distribution is 6.27.

from the toe of the fore reef slope, but this led to physically unrealistic and significant frictional losses across the horizontal step. Hence, we implemented a dynamic offshore boundary depth and model domain width governed by the incident wave characteristics ($kh = 1$). This ensures that the XBeach Non-Hydrostatic dispersion requirements are satisfied Smit et al. (2014).

It was also important to ensure that waves did not break at the offshore boundary. Hence, the ratio of $H_{s,0}/d_{offshore} = \gamma_b$ was calculated for each unique permutation of hydrodynamic boundary conditions at $k = 1.5, 1.0, 0.5$. It was thus necessary to establish an acceptable limit for γ_b. $\gamma_b = 0.78$ is commonly used for solitary waves, and $\gamma_b = 0.55$ for flat bathymetry. The literature (Section 2.3.2) suggests that wave breaking thresholds are typically higher on reefs due to the steep fore reef slope. Figure B.6 shows γ_b as function of kh with various breaking thresholds on it. Since the plotted points at $kh = 1$ all lie well below even the most conservative breaking threshold, this diagram proves that we are in an acceptable range and do not have wave breaking at the model boundary.

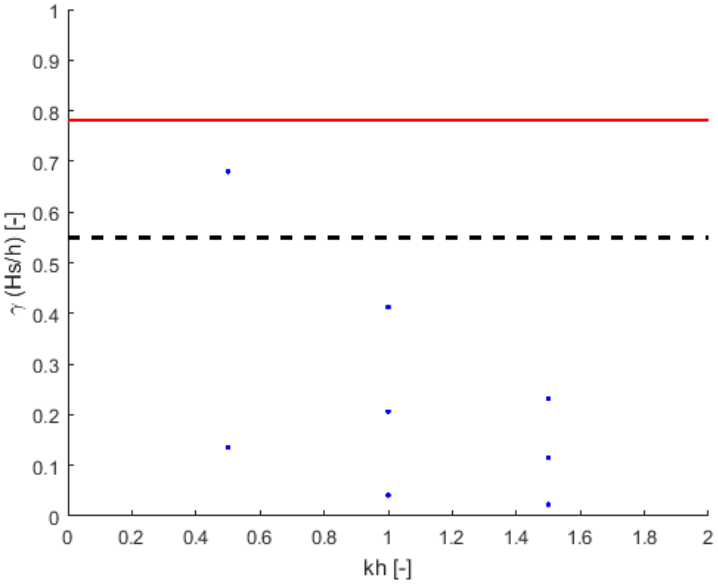

Figure B.6: γ_b as function of kh with common breaking thresholds on it.

B.4. MODEL SPINUP TIMES

Stationary conditions are necessary to make meaningful model assessments. Hence, sufficient "spinup" time is required to allow the model to reach this state. For instance, in order to calculate runup at the shoreline, waves must first propagate from the offshore boundary across the model domain to reach the shore. If the waves do not reach the shore, or if they only do so partway through the simulation, then one cannot make a fair comparison with other tested scenarios where the shore is subjected to wave action

throughout the simulation period. However, it is not just waves reaching the beach that constitutes reaching stationarity- wave setup on the reef flat also needs to reach steady state. It may take quite some time for the waves to physically transport enough water onto the reef flat to balance the radiation stresses imposed at the reef crest.

For this model, required spinup time is primarily governed by reef flat width, offshore water level, and to a lesser extent by wave height, wave period, and friction. Hence, the required spinup times may vary significantly between runs. If a fixed spinup time is used for all simulations, then we risk either not running for long enough, or unnecessarily long computational times. Early tests found that 300 seconds (5 minutes) was sufficient in 87% of simulated cases.

Even with this revised spinup, not all simulated cases in the second batch of runs reached stationary conditions, so these had to be filtered out (Figure B.7). We compared mean water levels at the inner reef flat between the nth and last of four simulated 30 min bursts. If the ratio of last/n^{th} was < 0.95, it was assumed that the model had not yet reached stationary conditions, and the first n bursts were discarded from the analysis. shows non-stationary conditions that had to be filtered from results.

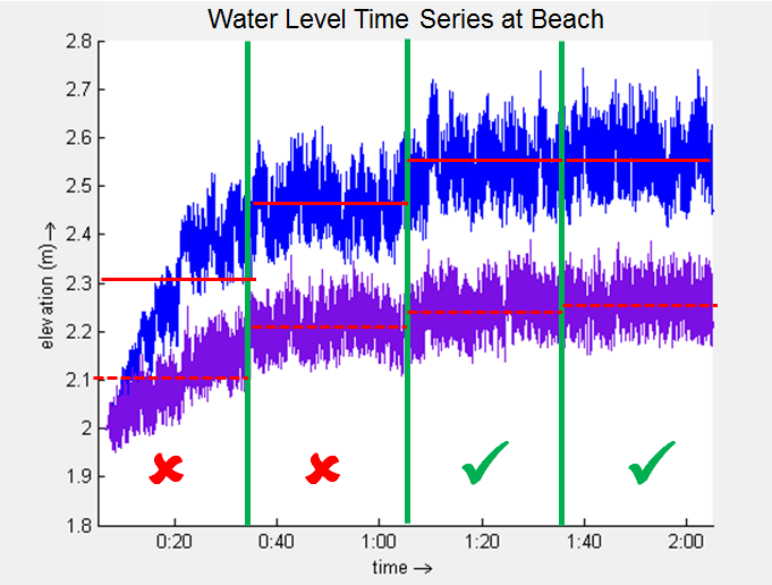

Figure B.7: Example of water level time series for runs that did not achieve stationarity in all simulated bursts. The cases on the left are less than 95% of the final water level, which

Based on initial final setup, we used the spinup times in Table B.1. This dramatically increased the total duration of simulations, and meant that more than half of the total time spent running models was devoted to 1000 and 1500 m profiles.

B

Table B.1: XBeach model spinup times based on reef width (W_{reef}).

W_{reef} **[m]**	**Spinup Time [min]**
< 250	15
250	30
500	60
1000	90
1500	120

C

Model Pre- and Post-Processing

THIS section describes the methods developed to execute multiple XBeach simulations and construct a Bayesian network from the model results.

C.1. XBEACH PRE- AND POST-PROCESSING

Figure C.1 shows the preprocessing procedure for XBeach, and Figure C.2 illustrates the post-processing procedure.

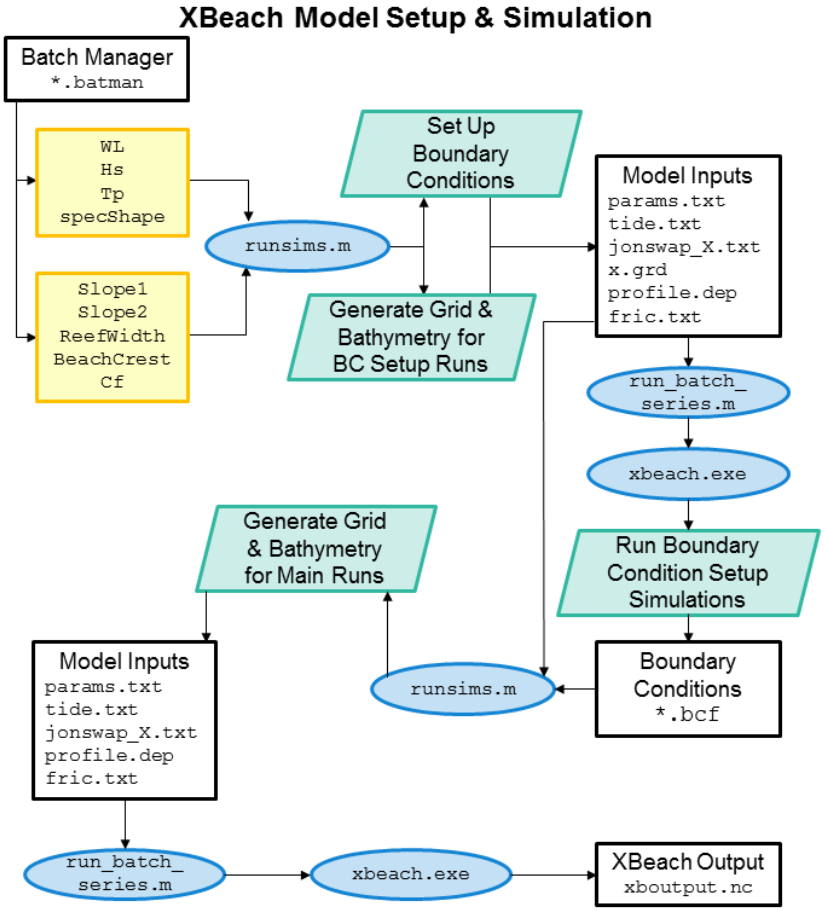

Figure C.1: XBeach pre-processing procedure. The code that forms the basis for `runsims.m` and `run_batch_series.m` was developed by Maarten van Ormondt at Deltares.

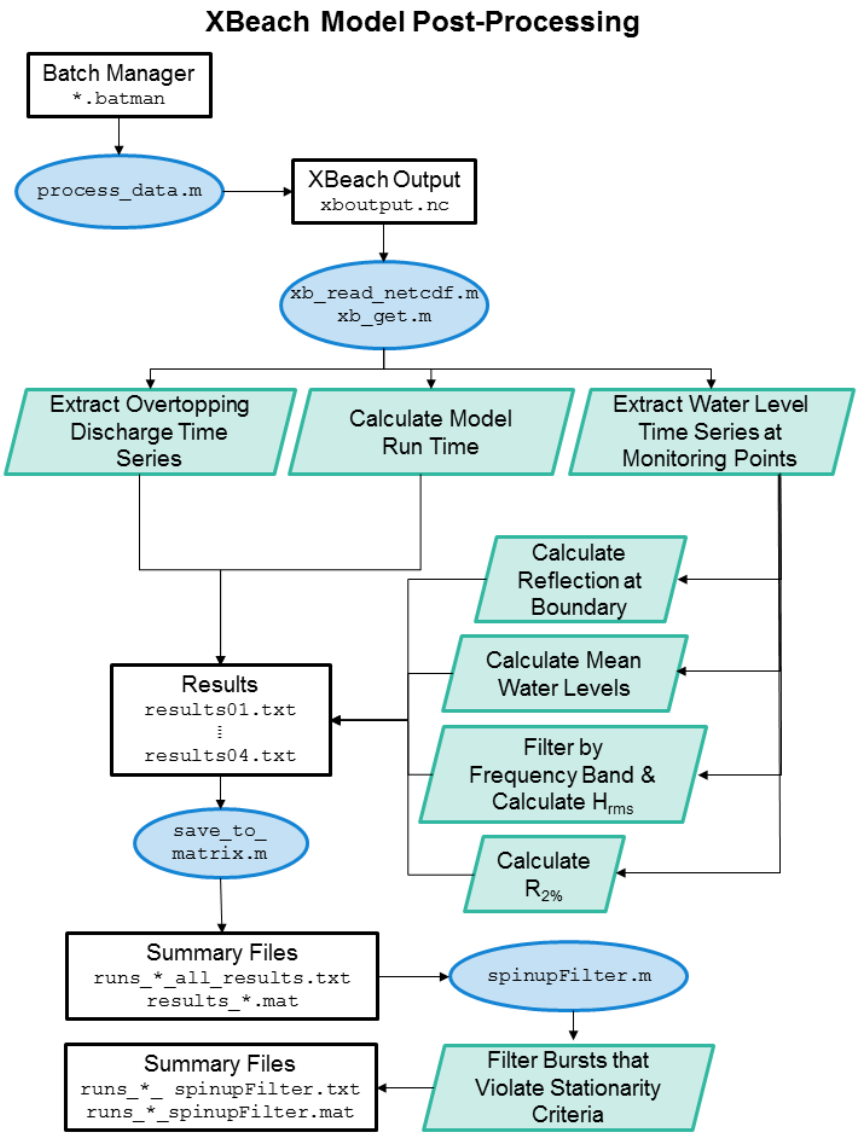

Figure C.2: XBeach post-processing flow chart procedure. The code that forms the basis for `process_data.m` and `save_to_matrix.m` was developed by Maarten van Ormondt at Deltares. The `xb_read_netcdf.m` and `xb_get.m` functions can be found in the OpenEarthTools library available here: https://publicwiki.deltares.nl/display/OET/OpenEarth.

C.2. NETICA PRE- AND POST-PROCESSING

Figure C.3 shows the main pre- and post-processing procedures for Netica. Figure C.4 describes the procedure for calculating log-likelihood ratios, Figure C.5 outlines how the confusion matrices were prepared, and Figure C.6 demonstrates the overfitting tests.

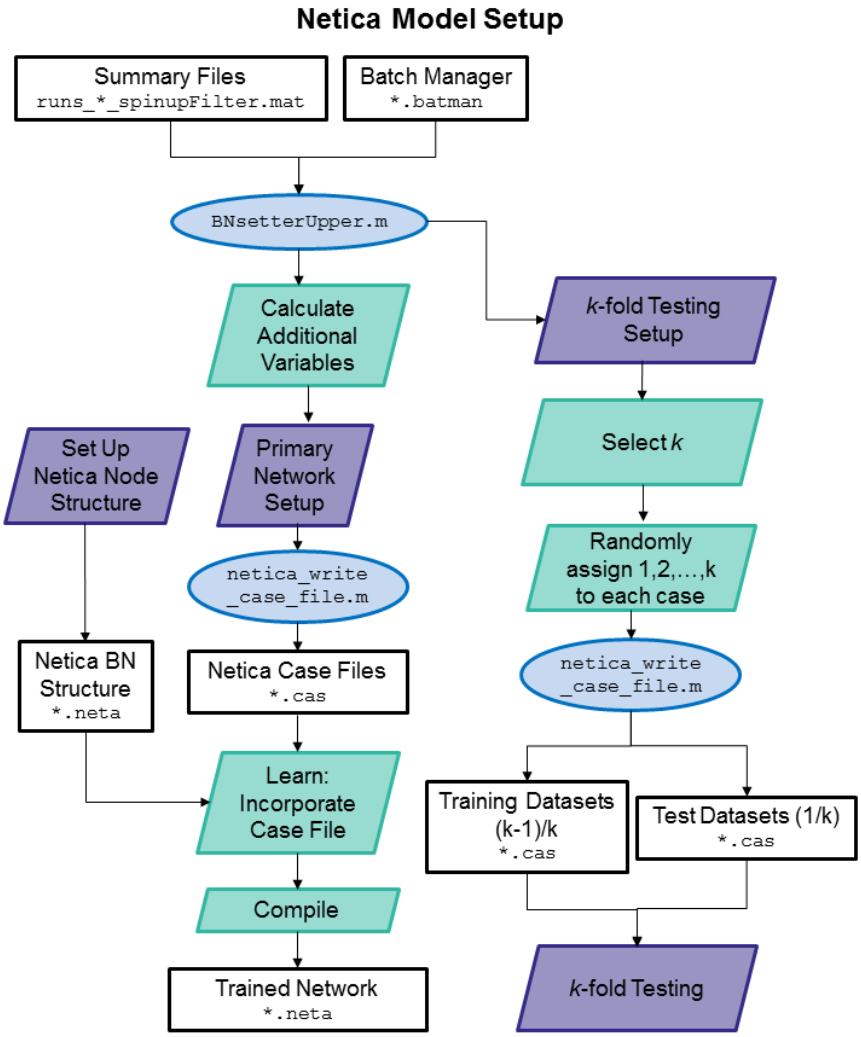

Figure C.3: Netica pre- and post-processing procedure. The `netica_write_case_file.m` function can be found in the OpenEarthTools library available here: https://publicwiki.deltares.nl/display/OET/OpenEarth..

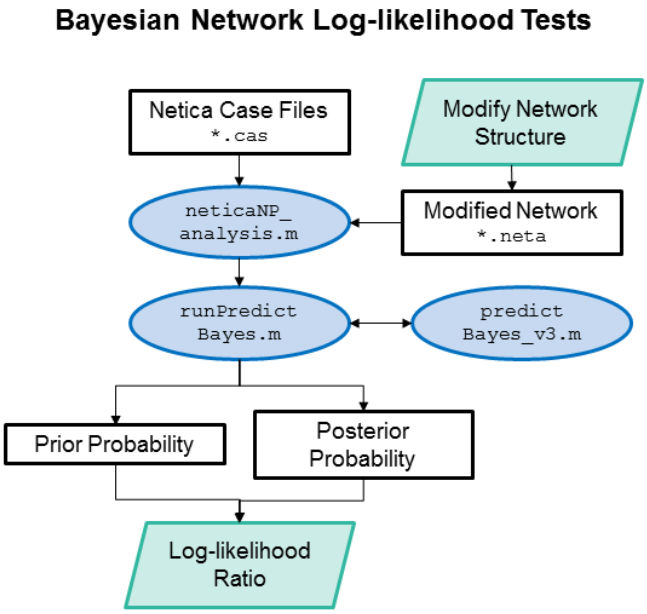

Figure C.4: Netica log-likelihood testing procedure. The `neticaNP_analysis.m`, `runPredictBayes.m`, and `predictBayes_v3.m` functions were originally developed by Nathaniel Plant at USGS.

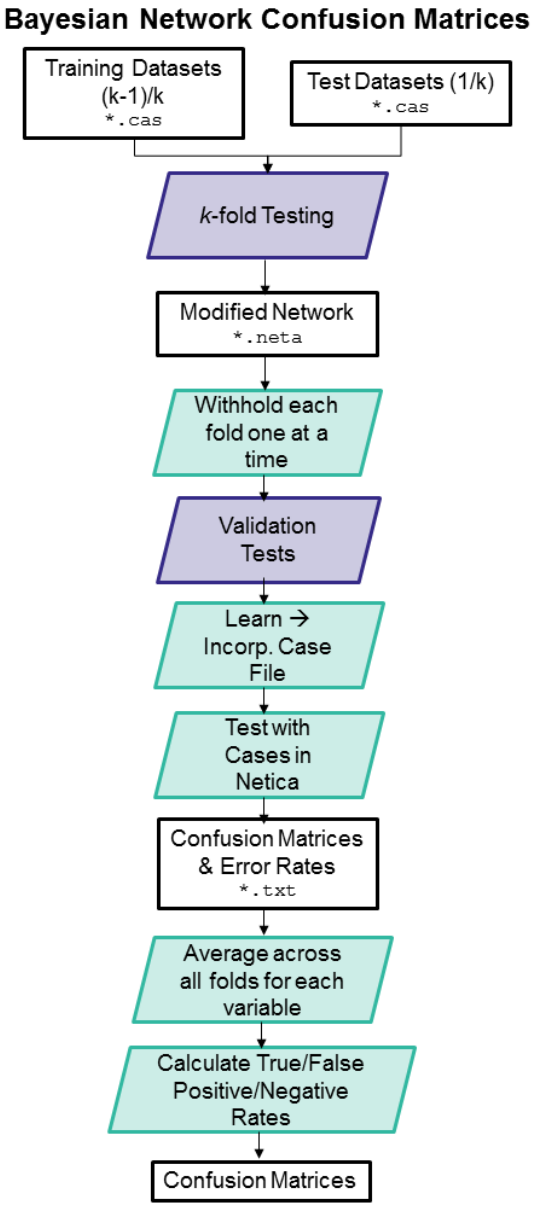

Figure C.5: Netica confusion matrix testing procedure.

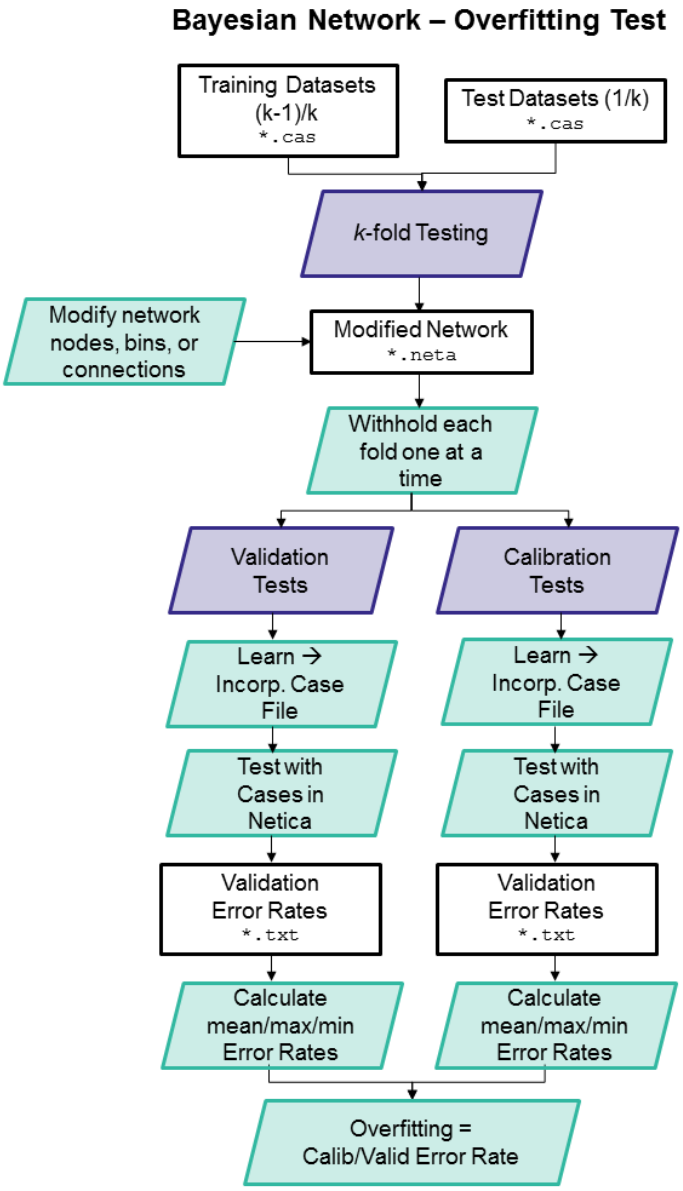

Figure C.6: Netica overfitting test procedure.

C

C.3. XBEACH INPUT FILES

This section contains examples of the XBeach input files used to set up the model. The batch manager file (`*.batman`) is used to specify the main parameters to be varied for a particular batch of runs, as well as other parameters manipulated during initial tests. This is a sample batch manager (`*.batman`) file:


```
%% BATCH MANAGER

% Run directory names
bc_AllRuns,     % bcdir - folder with boundary condition runs
runs_AllRuns,   % runsdir - folder with full set of runs
1,              % mkbct - flag for making boundary conditions (1=yes; 0=no)
1,              % mkinp - flag for making input parameter files (1=yes; 0=no)

% Initialize parameter ranges
2,1,0,-1,          % wl - water level above reef flat (when reefheight=0) [m]
1,2,3,4,5,         % hs - significant wave height [m]
0.05,0.025,0.005, % steep - H0/L0 steepness [-]
3.3,               % specShape - JONSWAP peak enhancement factor [-]
2,10,20,           % slope1=[1V/(slope1)H] - slope 1 (fore-reef) [-]
5,10,20,           % slope2=[1V/(slope2)H] - slope 2 (beach) [-]
0,50,100,250,500,1000,1500, % reefwidth - reef flat width [m]
0,                 % reefheight - reef flat elevation above 0 datum [m]
1,2,3,4,30,        % beachCrest - max elevation of beach crest [m]
0.01,0.05,0.1,     % cf - coefficient of friction [-]

% Model duration and output intervals
7200,    % runDur - total run duration without spinup [s] (1 hr = 3600s)
300,     % model spinup time when dynamic spinup disabled [s] (5 min)
1800.0, % tintm - mean output interval [s]
0.4,     % maxbrsteep - max wave breaking steepness [-]

% Grid resolution settings
0.25,    % dxmin - minimum dx for main model runs
1.0,     % dxmax - maximum dx for main model runs
64,      % np - number of gridpoints per wavelength
270,     % mainang - primary wave direction
10,      % s - directional spreading
0.005,   % dfj - step size frequency used to create input JONSWAP spectrum
```

The `params.txt` file is the standard XBeach input specification file. See Roelvink et al, 2015b for detailed information on the meaning of each parameter. The variables designated by —KEY are substituted dynamically for each run based on the values specified in the `*.batman` file or calculated based on other input parameters. This is a sample `params.txt` file:

```
%%%%%%%%%%%%%%%%%%%%%%%%%%%%%%%%%%%%%%%%%%%%%%%%%%%%%%%%%%%%%%%%%%%%%%%%%%%%%%%
%%% XBeach parameter settings input file                                      %%%
%%%                                                                           %%%
%%% date:     07-Apr-2016 12:53:50                                            %%%
%%% function: xb_write_params                                                 %%%
%%%%%%%%%%%%%%%%%%%%%%%%%%%%%%%%%%%%%%%%%%%%%%%%%%%%%%%%%%%%%%%%%%%%%%%%%%%%%%%

cmax         = 0.3
bedfriction = cf
bedfricfile = fric.txt
facua        = 0.1
sedtrans     = 0
morphology   = 0
gammax       = 2.0
taper        = TAPERKEY
nonh         = 1
swave        = 0
front        = nonh_1d
back         = abs_1d
maxbrsteep   = MAXBRSTEEPKEY

%%% Flow boundary condition parameters %%%%%%%%%%%%%%%%%%%%%%%%%%%%%%%%%%%%%%%

epsi         = -1

%%% Grid parameters %%%%%%%%%%%%%%%%%%%%%%%%%%%%%%%%%%%%%%%%%%%%%%%%%%%%%%%%%

nx        = NXKEY
ny        =  0
vardx     =  1
dy        =  5.0
xori      = 0.00
yori      = 0.00
alfa      = 0.0
depfile   = profile.dep
xfile     = x.grd
posdwn    = -1
thetamin = 45.000000
thetamax = 225.00000
dtheta    = 15
thetanaut= 1

%% Model time %%%%%%%%%%%%%%%%%%%%%%%%%%%%%%%%%%%%%%%%%%%%%%%%%%%%%%%%%%%%%%%

tstop        = TSTOPKEY

%% Morphology parameters %%%%%%%%%%%%%%%%%%%%%%%%%%%%%%%%%%%%%%%%%%%%%%%%%%%%

morfac       = 1

%% Sediment transport parameters %%%%%%%%%%%%%%%%%%%%%%%%%%%%%%%%%%%%%%%%%%%%

bulk         = 0
```

```
%% Tide boundary conditions %%%%%%%%%%%%%%%%%%%%%%%%%%%%%%%%%%%%%%%%%%%%%%%%%%%%

zs0file      = tide.txt
paulrevere   = land
tideloc      = 2
zs0          = ZS0KEY

%% Wave boundary condition parameters %%%%%%%%%%%%%%%%%%%%%%%%%%%%%%%%%%%%%%%%%%

instat       = INSTATKEY
bcfile       = BCFILEKEY

%% Output variables %%%%%%%%%%%%%%%%%%%%%%%%%%%%%%%%%%%%%%%%%%%%%%%%%%%%%%%%%%%

outputformat = netcdf
tint         = TINTMKEY
tintm        = TINTMKEY
tstart       = TSTARTKEY
tintp        = 1.0

npoints = 6
OBSPT1KEY 1. offshore
OBSPT2KEY 1. forereef1
OBSPT3KEY 1. reefcrest
OBSPT4KEY 1. midflat
OBSPT5KEY 1. beachtoe
QGAUGEKEY 1. overtop

npointvar = 3
zs
uu
qx

nrugauge     =1
RUGAUGEKEY 1
rugdepth     = 0.1

nglobalvar   = 2
zs
zb

nmeanvar = 3
zs
uu
qx

%%%%%%%%%%%%%%%%%%%%%%%%%%%%%%%%%%%%%%%%%%%%%%%%%%%%%%%%%%%%%%%%%%%%%%%%%%%%%%
```

The `jonswap.txt` is used to specify the wave boundary conditions for a given run, and is generated automatically by the batch model preprocessor using values determined from the `*.batman` file. This is a sample `jonswap.txt` file:

```
Hm0         =     1.0000
Tp          =    11.3180
mainang     =   270.0000
gammajsp    =     3.3000
s           =    10.0000
dfj         =     0.0050
```

D

XBeach Model Results

D.1. BOX AND WHISKER PLOTS

These plots illustrate the relationships between the eight primary input parameters and various output parameters. The box and whisker plots are used to illustrate the distribution of data, showing 5th, 25th, 50th, 75th, and 95th percentiles, as well as any outliers (Figure D.1). Many of these figures have been plotted featuring only the cases with beach crest elevations of 30 m, a semi-infinite slope. This was done because overtopping and overflow conditions at discrete crest elevations tend to obscure the underlying trends in the various output parameters. Although the overtopping quantities are ultimately useful for operational flood forecasting, runup-only conditions were deemed more illustrative.

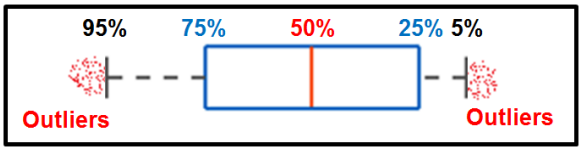

Figure D.1: Legend for box and whisker plots. The red centre line denotes the median value (50th percentile), while the blue box contains the 25th to 75th percentiles of dataset. The black whiskers mark the 5th and 95th percentiles, and values beyond these upper and lower bounds are considered outliers, marked with red dots.

Figures D.2 and D.3 show how runup and overtopping discharge vary with the eight primary input parameters. The general trends are similar for both variables, with runup/overtopping increasing due to offshore water level and wave height ($H_{s,0}$). Runup and overtopping tend to decrease with increasing steepness, friction, fore reef and beach slopes, and reef flat width. The majority of overtopping discharges are plotted as outliers, which is due to the fact that the majority of the modelled scenarios do not result in overtopping.

Figure D.4 shows the relationships between sea/swell wave height on the inner reef flat and each of the tested input parameters. Waves in this frequency band [0.04-1 Hz] may include short waves that propagate from offshore without breaking, waves that reform after breaking, or waves generated through non-linear energy transfers (such as in undular bores). The general trends are similar to those observed with runup, albeit with several key exceptions. Sea-swell waves are relatively insensitive to the friction coefficient, suggesting that their dissipation is governed mainly by breaking rather than friction. Most notable is their sensitivity to reef flat width. Wave heights decrease significantly with distance, suggesting that much of the energy in this frequency band is dissipated by breaking in the vicinity of the reef crest. H_{ss} shows little sensitivity to beach slope. This might be because runup is governed by low frequency waves at the shoreline, which are in a reflective regime and thus change little with beach slope.

Figure D.5 shows the relationships between infragravity wave height on the inner reef flat and each of the tested input parameters. Infragravity waves show less spread in their dependency on offshore wave height. They are also more susceptible to frictional dissipation than sea-swell waves. Lower wave steepness results in higher infragravity wave heights, since the wave period is proportionally longer for a given wave height.

Figure D.6 shows the relationships between VLF wave height on the inner reef flat

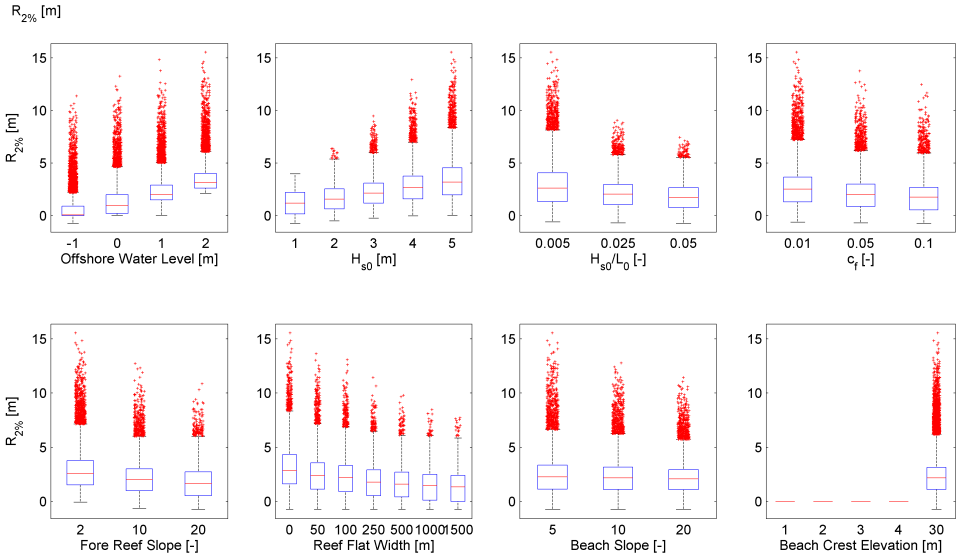

Figure D.2: Runup as a function of the eight primary input parameters.

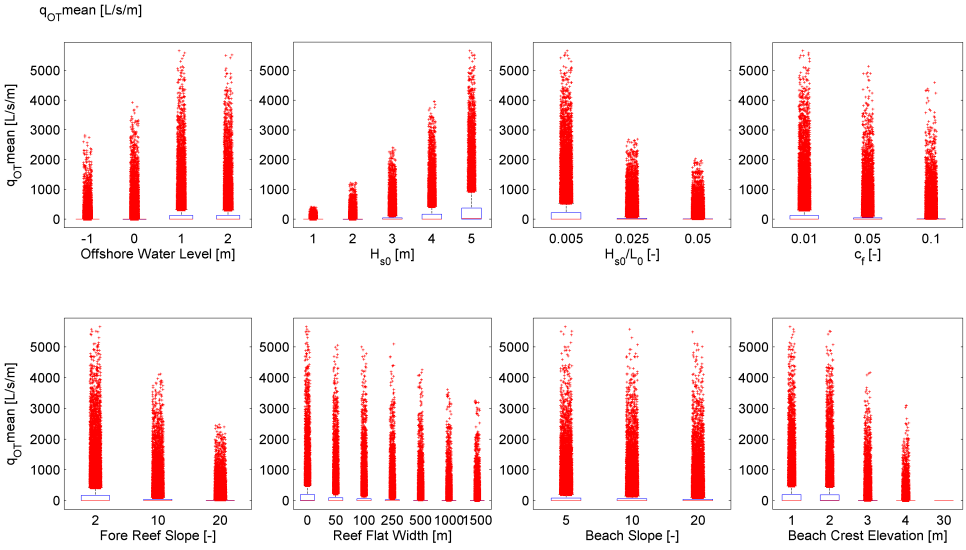

Figure D.3: Mean overtopping discharge as a function of the eight primary input parameters.

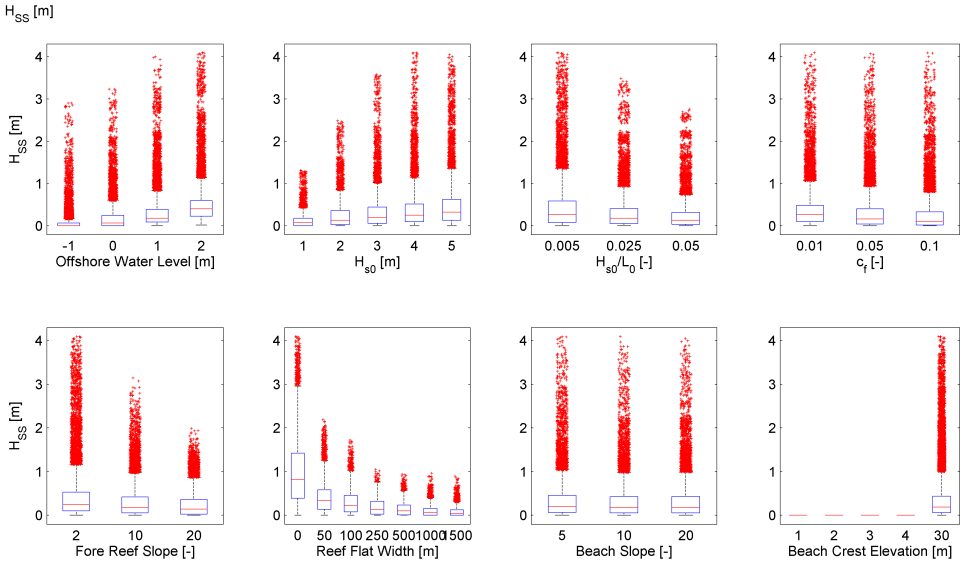

Figure D.4: Wave height in the sea/swell (SS) frequency band (0.04-1 Hz) at the inner reef flat as a function of the eight primary input parameters.

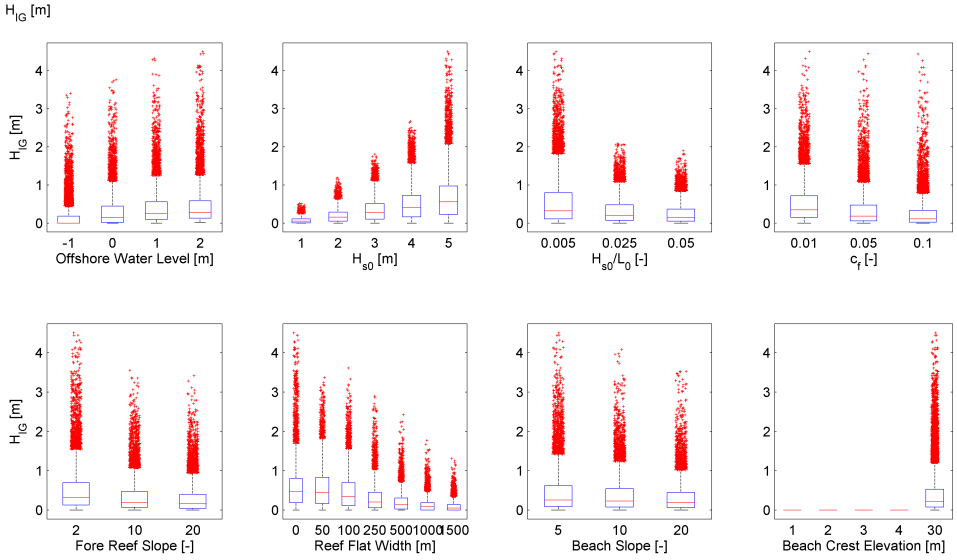

Figure D.5: Wave height in the infragravity (IG) band (0.004 - 0.04 Hz) at the inner reef flat as a function of the eight primary input parameters.

and each of the tested input parameters. VLF waves are smaller than sea-swell and infragravity waves under most circumstances. Most interestingly, VLF wave height shows a maximum for reefs in the 50-100 m width range. Since narrower reef flats are more likely to exhibit resonance, it is possible that this peak represents cases where resonant conditions are achieved, amplifying VLF waves. They are not very sensitive to beach slope, which makes sense because they would be in a reflective regime.

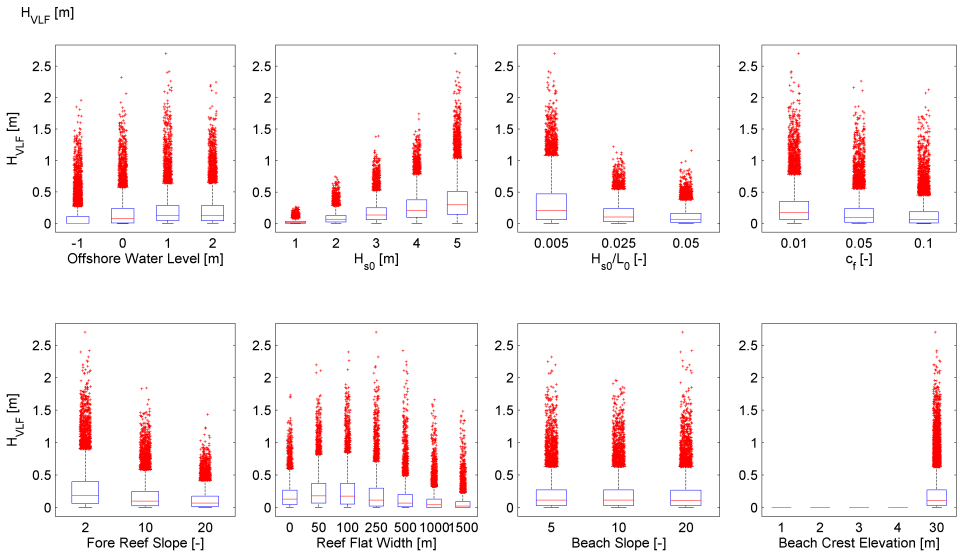

Figure D.6: Wave height in the very low frequency (VLF) band (< 0.004 Hz) at the inner reef flat as a function of the eight primary input parameters.

Figure D.7 shows the relationships between wave setup on the inner reef flat and each of the tested input parameters. Setup increases with offshore wave height but decreases at higher offshore water levels. This supports the tidal modulation discussed in Section 2.4. Setup is also greater for waves with mild steepness and steeper fore reefs. Becker et al. (2014) note that the tidal dependency of setup depends on whether or not the breakpoint is fixed, since that will increase tidal modulation of depth-induced breaking. This accounts for the dependency on fore reef slope, since the width of the breakpoint is driven in part by fore reef steepness.

Pomeroy et al. (2015) found that bottom roughness had limited influence on wave setup in their physical model, which agrees with the results here. However, Yao et al. (2012) noted that roughness could reduce setup in cases with mild fore reef slopes. Setup is largest for narrow reefs and then declines with increasing width. This might be attributed to the greater distance between the surf zone and the inner reef flat where setup is measured.

Figure D.8 shows the relationships between the reflection coefficient at the offshore boundary and each of the tested input parameters. Reflection is greatest when the offshore water level is at the same level as the reef flat. There is a slight increase in the median reflection coefficient with offshore wave height, although there is a consistently

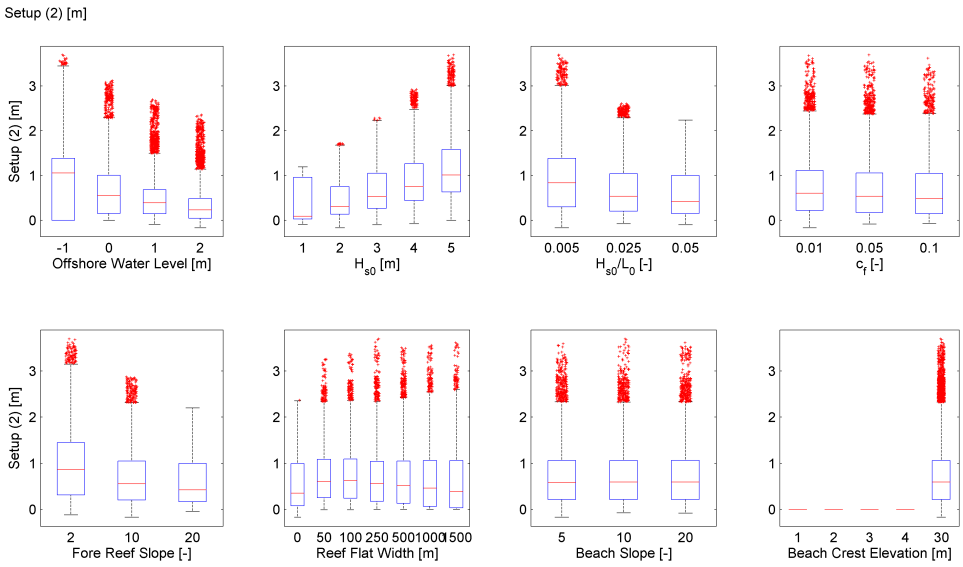

Figure D.7: Setup at the inner reef flat as a function of the eight primary input parameters.

broad spread across all wave heights. Steeper waves show much less reflection. Rougher reefs slightly reduce reflection, which makes sense because waves would experience frictional dissipation on both their shoreward and seaward journeys across the reef flat. The most significant factor in determining reflection seems to be fore reef slope. Steeper reefs reflect more energy than those with shallower slopes. There is a small negative correlation with reflection and reef flat width, but there is considerable spread in the outliers. Reflection at the offshore boundary is almost completely insensitive to beach slope.

The latter three observations suggest that reflected waves offshore are largely generated on the fore reef and reef crest. Any waves that cross the reef flat tend to be dissipated via friction and breaking, since they must effectively cross it twice. This may also be explained by the breakpoint forcing of infragravity waves, which tends to be the dominant IG wave generation mechanism on coral reefs. This phenomenon generates a strong shoreward-directed wave which may then be reflected back, as well as a seaward component. However the reflected shoreward component may dominate.

Figure D.9 shows the relationships between mean spectral wave period on the inner reef flat and each of the tested input parameters.

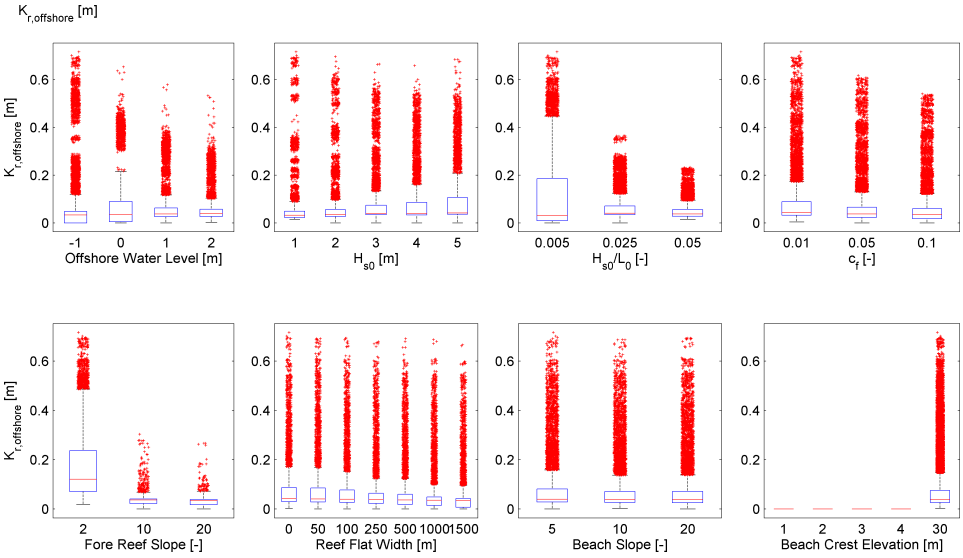

Figure D.8: Reflection coefficient at the offshore boundary (outgoing wave height/incoming wave height) as a function of the eight primary input parameters.

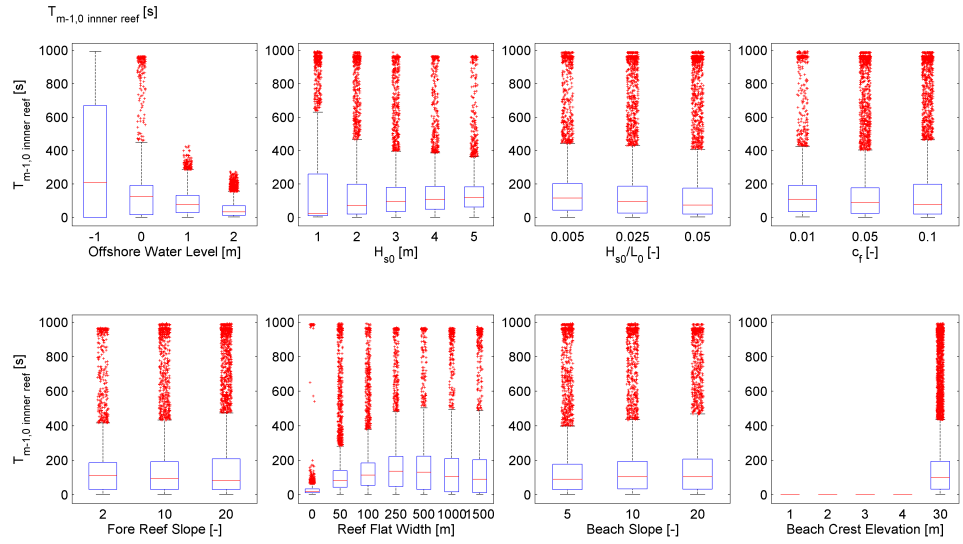

Figure D.9: Mean spectral period ($T_{m-1,0}$) at the inner reef flat as a function of the eight primary input parameters.

D.2. RESONANCE

Figure D.10 plots normalized squared infragravity (a-c) and VLF wave heights (d-f) against the observed frequency divided by natural resonant frequencies. Subplots (a,d) use the zeroth resonant frequency, while the lower plots show higher harmonics. Subplots (b,e) use the first resonant frequency, and subplots (c,f) show the second resonant frequency. The peaks of both the infragravity and VLF wave heights coincide with $f_{m-1}/f_{n0} = 1$, which suggests resonant conditions. Even though the majority of points fall close to the x-axis, most of the anomalously high values are clustered in the same zone. In their analysis of infragravity waves during Typhoon Haiyan, Roeber and Bricker (2015) observe energy at the first superharmonic of the resonant frequency. However, no additional peaks are observed at the first and second resonant frequencies, which agrees with the findings of Gawehn et al. (2016) who noted that the higher harmonics tend to get damped out.

Upon closer inspection, the secondary peak observed in plots (a-c) of infragravity wave heights is not associated with higher harmonics of the resonant frequency. The cases falling in this region all have offshore water levels and wave heights of 2 m and 1 m, respectively. Furthermore, the coefficient of friction is 0.01, representing a relatively smooth reef. When time series of several simulations were visually examined, undular bores were observed but not especially prevalent when compared to other scenarios outside the secondary peak.

Hence, we hypothesize that the anomalously high infragravity waves are explained by bound long waves that reach the shore. There is minimal attenuation of short waves across the deep, smooth reef flat ($\gamma_b \approx 0.5$, so little breaking occurs). Hence, the mean spectral periods of this cluster (7-23 s) lie within the sea-swell rather than infragravity band as is the case for most of the other tested configurations. The breakpoint mechanism might be less active in this case, so infragravity energy reaching the shore could be due to bound long waves that reach the shore relatively unimpeded. However, the cross-correlation analysis needed to prove the phase relationships between incoming short waves and infragravity waves at the shoreline was considered beyond the scope of the present study. Future research should investigate this phenomenon in greater detail and determine if there are any precedents in existing field datasets.

D.3. DISSIPATION VS INERTIA

Figure D.11 is based on a figure from Becker et al. (2016) in which they compare their non-dimensional dissipation/inertial timescale parameter (δ) with infragravity motion (Equation D.1).

$$\delta = \frac{DW_{reef}}{\sqrt{gh_{reef}}} \tag{D.1}$$

Where D is an empirical dissipation parameter, W_{reef} is reef width, g is gravity, and h_{reef} is water depth on the reef flat. Higher values of δ denote greater dissipation, whereas lower values are inertially dominant. Standing and resonant waves would fall into this category. Figure D.11 reproduces similar trends to Becker et al. (2016), although we see a broader range given that our model has a wider parameter space than their limited range of test sites. Given that most of the low frequency anomalies correspond to the

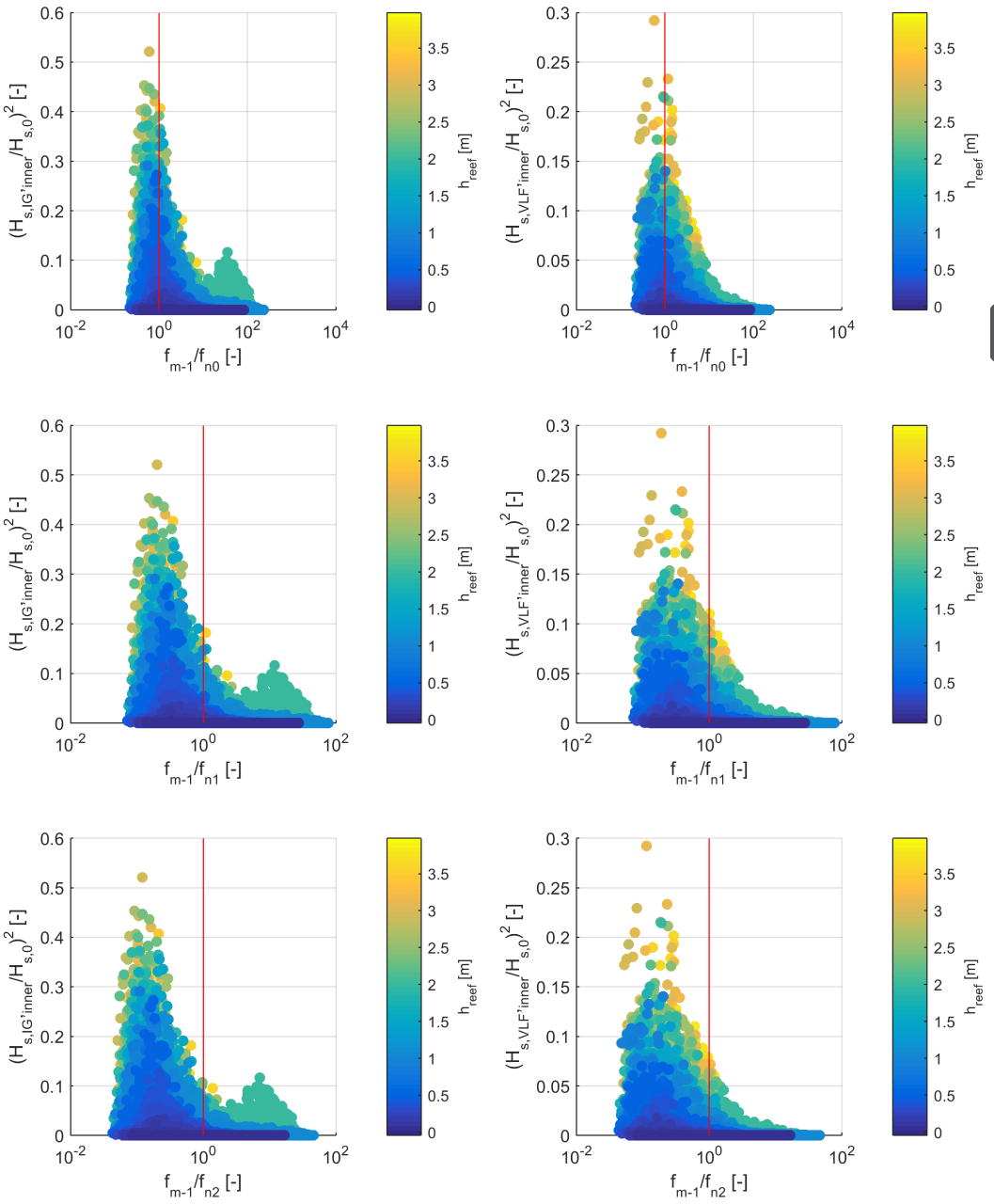

Figure D.10: Similar to Figure 4.6 but also with higher harmonics of resonant frequencies on lower plots...

inertial range, this lends support to the notion that resonant amplification is damped out by friction on rougher or wider reefs. It also illustrates clearly the relationship between reef width and dissipation: narrower reefs tend to fall more within the inertial range, whereas wider reefs are almost completely dissipative.

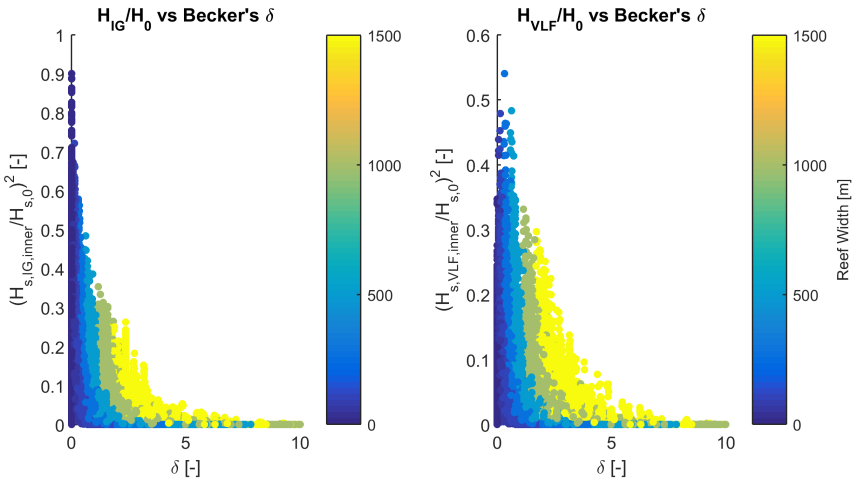

Figure D.11: Becker's δ shows the ratio between inertial and dissipative forces. High values are dissipative, low are inertial.

E

BAYESIAN NETWORK OUTPUT

Correlation doesn't imply causation, but it does waggle its eyebrows suggestively and gesture furtively while mouthing 'look over there'.

Randall Munroe

E.1. ALTERNATIVE NETWORK LAYOUTS

This section shows alternative network layouts that were tested. Configuration A (Figure E.1) is the primary Bayesian network layout, which features output parameters normalized by offshore wave height ($H_{s,0}$).

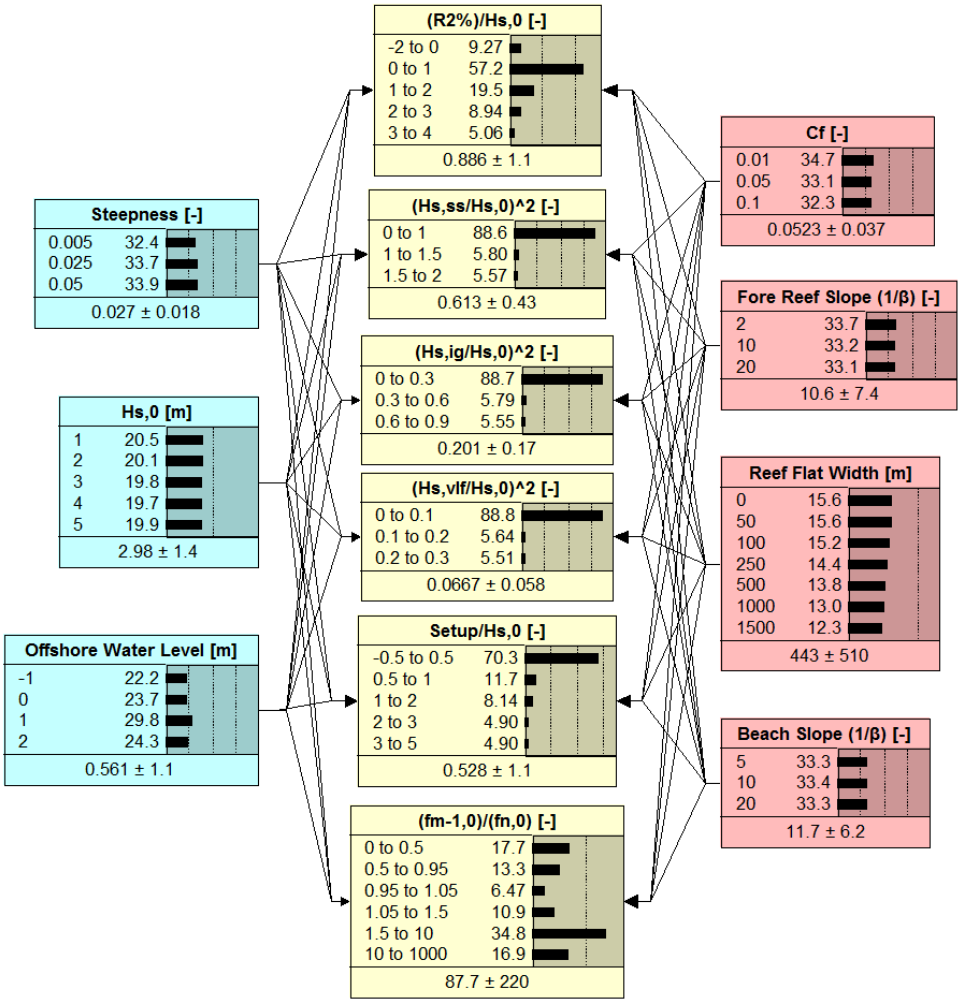

Figure E.1: Bayesian Network Configuration A

Configuration B (Figure E.2) has an identical layout to Configuration A, except that the output variables have only two bins.

Configuration C (Figure E.3) is identical to Configuration A except that the coefficient of friction (c_f), fore reef slope (β_f), and beach slope (β_b) have been removed. This leaves reef flat width (W_{reef}) as the only reef morphology input parameter. Since friction, fore reef slope, and beach slope require topographic and bathymetric surveys, they

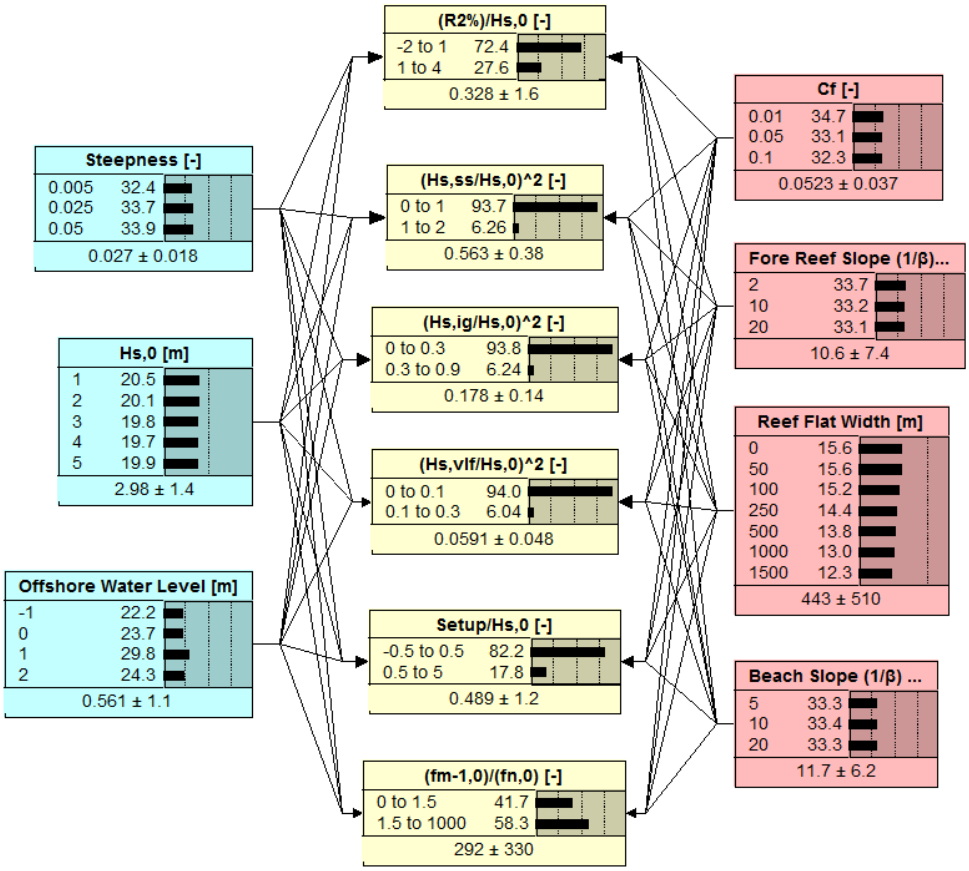

Figure E.2: Bayesian Network Configuration B

may not be easily available for all locations of interest. By contrast, reef flat width can be estimated from aerial photography or other remote sensing images. Sensitivity testing in Section 5.1.2 revealed that reef flat width was also the most important reef morphology parameter in determining runup. Thus by happy coincidence, reef width is both the most useful parameter and the easiest to estimate.

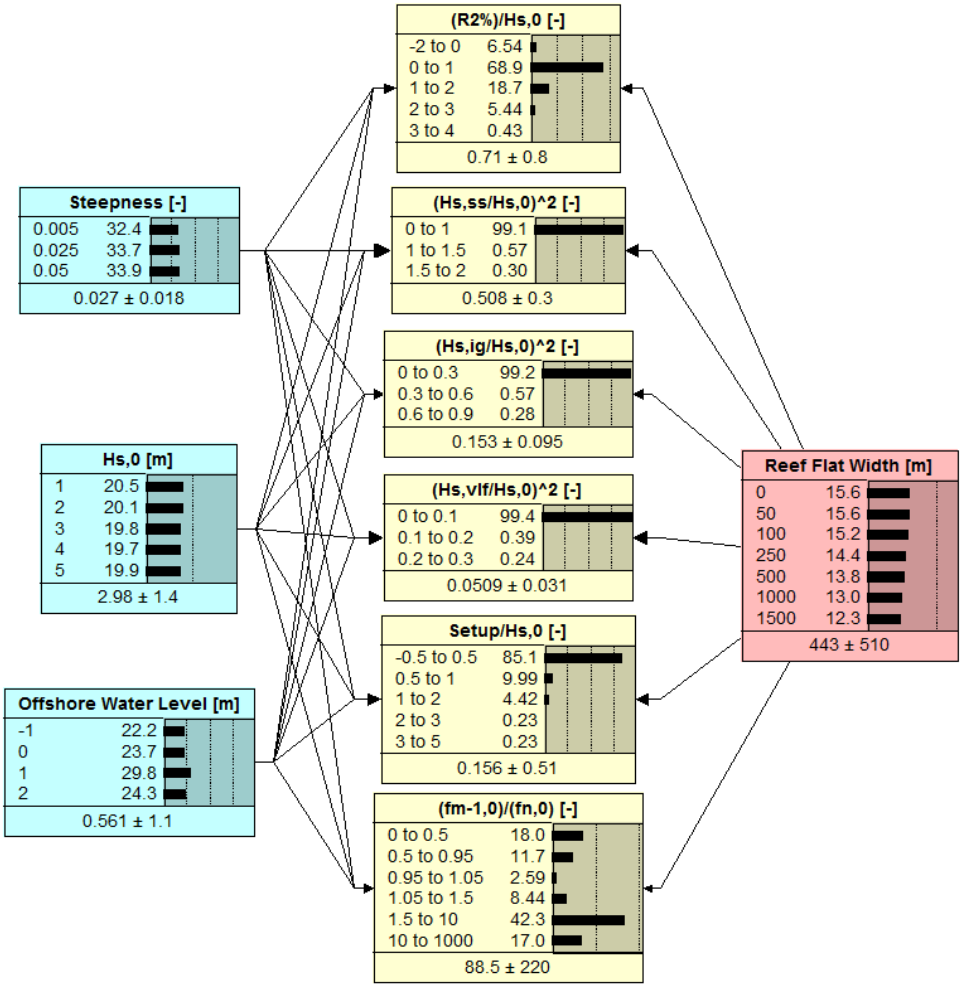

Figure E.3: Bayesian Network Configuration C

Figure E.4 shows the structure of Configuration D, for which the output variables were not normalized. This version was used in the validation against field data, so as to make the inputs and outputs directly comparable with the available information.

Figure E.5 shows the structure of Configuration E, which is identical to Configuration D but with only two bins per output node.

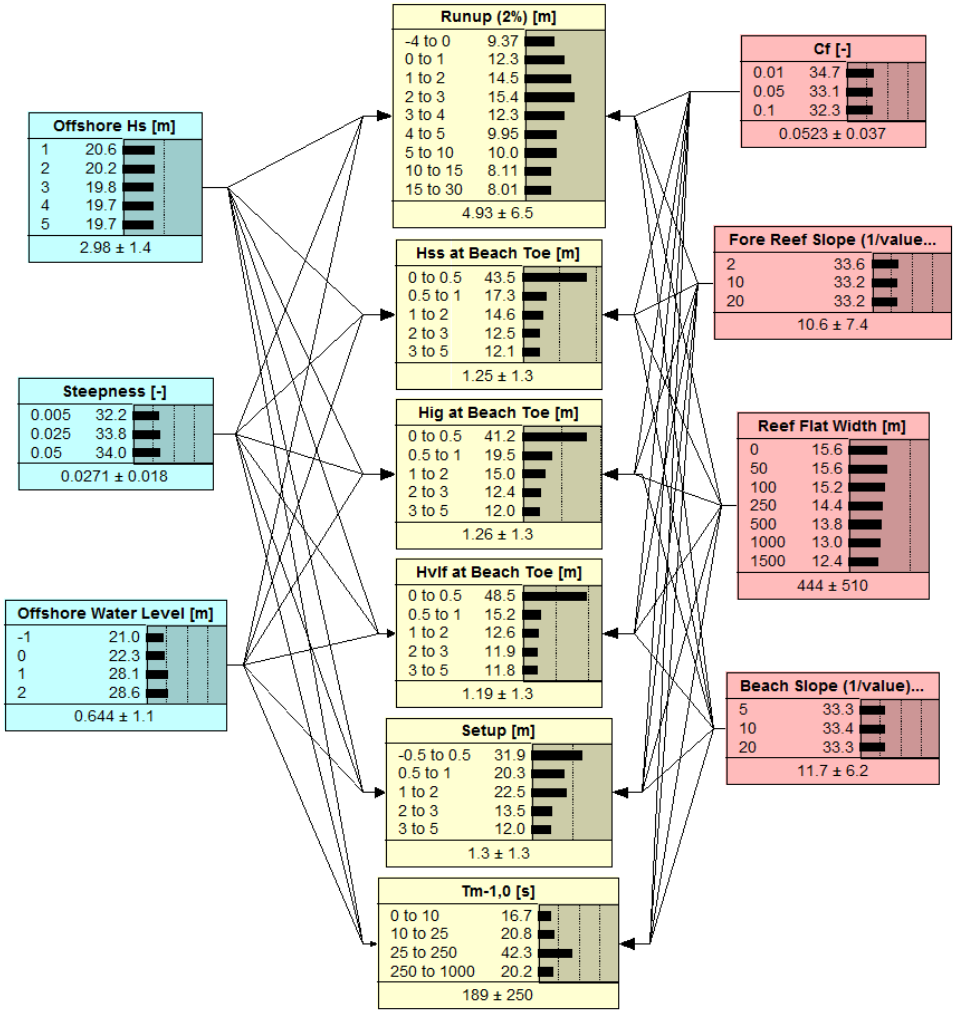

Figure E.4: Bayesian network Configuration D.

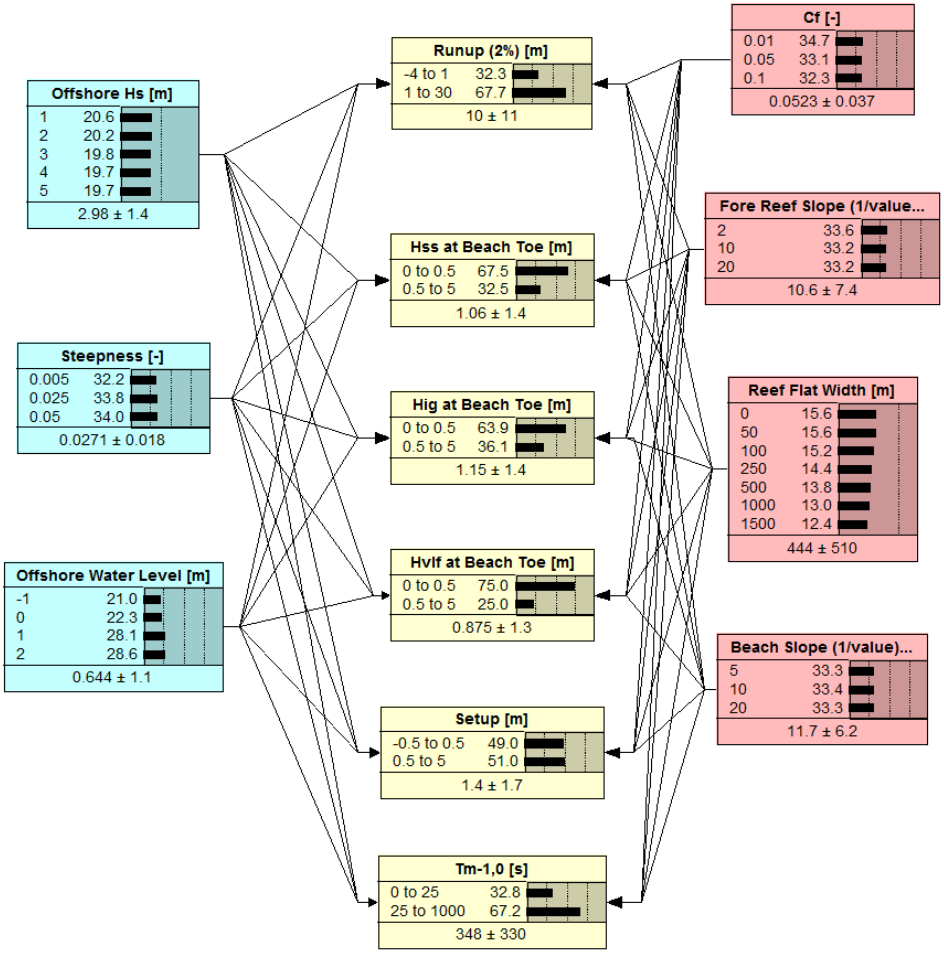

Figure E.5: Bayesian network Configuration E.

E.2. LOG-LIKELIHOOD TESTS

This section contains the data tables which form the basis of the log-likelihood plots in Section 4.2.

Table E.1 shows the log-likelihood test scores of Configuration A with input variables included in the network one at a time. This allows us to see which inputs are essential to predictions of a certain output variable.

Table E.1: Log-likelihood ratios for networks with a single input. Higher scores relative to the base network indicate more important parameters.

Included	$R_{2\%}/H_0$	$(H_{SS}/H_0)^2$	$(H_{IG}/H_0)^2$	$(H_{VLF}/H_0)^2$	$\overline{\eta}/H_0$	$f_{m-1,0}/f_{n,0}$
Config A	*12578*	*394*	*399*	*249*	*7084*	*18634*
H_0	1981	32	88	32	1716	695
H_0/L_0	469	81	104	76	222	247
η_0	4305	46	14	9	3539	1054
c_f	142	1	7	15	9	67
β_f	373	78	48	62	252	87
W_{reef}	278	133	85	30	55	11406
β_b	50	1	24	1	0	12

Table E.2 shows the log-likelihood test scores of Configuration A with input variables withheld from the network one at a time. This allows us to see which variables can be removed from the network without degrading predictive skill.

Table E.2: Log-likelihood ratios for networks withholding variables one at a time. Lower scores relative to the base case indicate that the network's performance drops considerably when that variable is not included.

Withheld	$R_{2\%}/H_0$	$(H_{SS}/H_0)^2$	$(H_{IG}/H_0)^2$	$(H_{VLF}/H_0)^2$	$\overline{\eta}/H_0$	$f_{m-1,0}/f_{n,0}$
Config A	*12578*	*394*	*399*	*249*	*7084*	*18634*
H_0	7413	270	215	115	4976	15280
H_0/L_0	11383	227	226	117	6715	17252
η_0	5391	216	295	120	3043	15583
c_f	12390	339	339	152	7685	18906
β_f	11785	216	249	117	6700	18459
W_{reef}	11991	169	223	132	7531	4282
β_b	13387	342	311	167	7832	19347

NOTE: When we prepare a 'single output' table, the LLRs are the same as for the whole network, since there are no connections defined between the outputs.

F

Cluster Analysis

THE XBeach modelling in Section 3.1 generated over 186,000 unique 30 minute bursts. 47 variables were extracted from each of the bursts, creating nearly 9 million data points to analyze. Extracting meaningful relationships or patterns from such a large dataset is a challenging task, since there may be significant noise obscuring the relevant signals.

To explore the model results, we used cluster analysis, a series of mathematical techniques for examining large datasets. Cluster analysis seeks to classify data into different groups based on common characteristics. Ideally, the points in each cluster should be similar to each other, while also being different from the points that belong to other clusters (Tan et al., 2005). The stronger the similarity within clusters and differences between them, the more distinct the clustering.

This appendix investigates the application of cluster analysis for two main purposes: finding patterns and separating the synthetic XBeach dataset into different regimes, and the classification of reef morphology for future studies.

F.1. BACKGROUND

Cluster analysis has been successfully used in many different fields, from remote sensing (Akcay and Aksoy, 2008) to climate science McCormick et al. (2010), to marketing Punj and Stewart (1983) and medicine (Ng et al., 2006). Of particular interest to this study is the technique's application in coastal engineering and coral reef settings. It has been used successfully for wave climate reduction (Camus et al., 2011; Mortlock and Goodwin, 2015; Olij, 2015), morphological classification (Costa et al., 2016; Duce et al., 2016; Tomás et al., 2015), and identifying tropical cyclone trajectories (Camargo et al., 2007*a*,*b*).

Given that certain phenomena like resonance happen under very specific circumstances, it would be useful to isolate those conditions from the point cloud. If reef hydrodynamics are too complex for simple empirical runup formulas like Stockdon et al. (2006), then perhaps multiple equations can be created to suit different clusters of input conditions. Furthermore, these techniques could also be used to define meaningful groups for discretizing nodes in a Bayesian network.

Cluster analysis also has potential for use in classifying reef morphology, should more data become available for future studies. Costa et al. (2016) used cluster analysis to classify reef geometry along a stretch of the Brazilian coast into 4 "typical" reef profiles. They were then able to determine the differences in wave dissipation across those sections. Tomás et al. (2015) followed a similar process, using cluster analysis to classify >100,000 cross-sections of the entire Spanish coastline into 100 representative profiles for subsequent flood modelling. Duce et al. (2016) sorted spur and groove formations on fore reefs into 4 main classes, and Holden and LeDrew (1998) used similar techniques to analyze coral health. Together, these studies show that cluster analysis may be an effective tool for mining large datasets of reef morphology to serve as numerical model inputs.

F.2. METHODOLOGY

There are numerous techniques when fall under the umbrella of cluster analysis, including k-means, maximum dissimilarity algorithm, and self-organizing maps Camus et al. (2011). The k-means algorithm has been selected for use in this study on the basis of its

prior applications on coastal engineering projects (Camus et al., 2011; Duce et al., 2016; Olij, 2015; Tomás et al., 2015) and relative simplicity to implement. The specific algorithm used in this study has been adapted from that used by Olij (2015). This k-means cluster analysis should not be confused with the k-fold verification discussed in Section 3.2.4.

The k-means algorithm begins by choosing k points to serve as initial centroids for the data. The remaining points in the dataset are assigned to their nearest centroid to form k clusters. A new centroid is then calculated for the points in each of these clusters. At this point, new centroids are chosen based on an objective function which seeks to minimize the distance between points within each cluster and/or maximize the distance between cluster centroids. The optimal clustering is reached when the centroids no longer move between iterations (Tan et al., 2005).

The k-means objective function is minimized by well-separated, globular clusters of equal size and density, so it may not effectively capture oddly-shaped patterns, outliers, or natural point clusters with heterogeneous sizes and densities (Tan et al., 2005). Camus et al. (2011) note that k-means is not a good technique for capturing the edges of the dataset/outliers, so it may not be a good choice for capturing anomalous resonance events. While this sort of procedure may be good for developing a representative average long-term wave climate, it may not be as well-suited to identifying extreme events. Conversely, Camus et al. (2011) suggest that the maximum dissimilarity algorithm (MDA) is better suited to examining the boundaries of a dataset, and hence may be more appropriate for analyzing uncommon sea states. van Arkel (2016) combined the k-harmonic algorithm with MDA for wave climate reduction, and found it an effective technique for capturing the diversity of their dataset.

F.3. RESULTS

Figure F.1 shows clustering for runup as a function of reef width and water depth on the reef flat. The discrete input bins have biased the clustering. Note that wide reefs are further apart in the parameter space than the narrow reefs simulated (i.e. $1500-1000=500m$, $1000-500=500m$ vs $100-50=50m$), so they tend to get their own clusters, while all the details in the shorter reefs are grouped together.

Figure F.2 shows clustering for normalized VLF wave height as a function of water depth on the reef flat and spectral mean frequency normalized by natural resonant frequency. Although the continuous data distribution allows distinct clusters to be formed, most of the points are located in the low VLF range, so outliers of interest (such as anomalous or resonance events) are not well-represented.

Based on these preliminary cluster analysis results, it seems that the k-means algorithm is inappropriate for both the available data distributions and the intent of the analysis. The two key problems with using the k-means algorithm to analyze this dataset are:

- Discrete input distributions bias the clusters
- Outliers are not well-represented

Hence, future studies should consider approaches that give more priority to outliers, such as the maximum dissimilarity algorithm. Furthermore, future modelling efforts

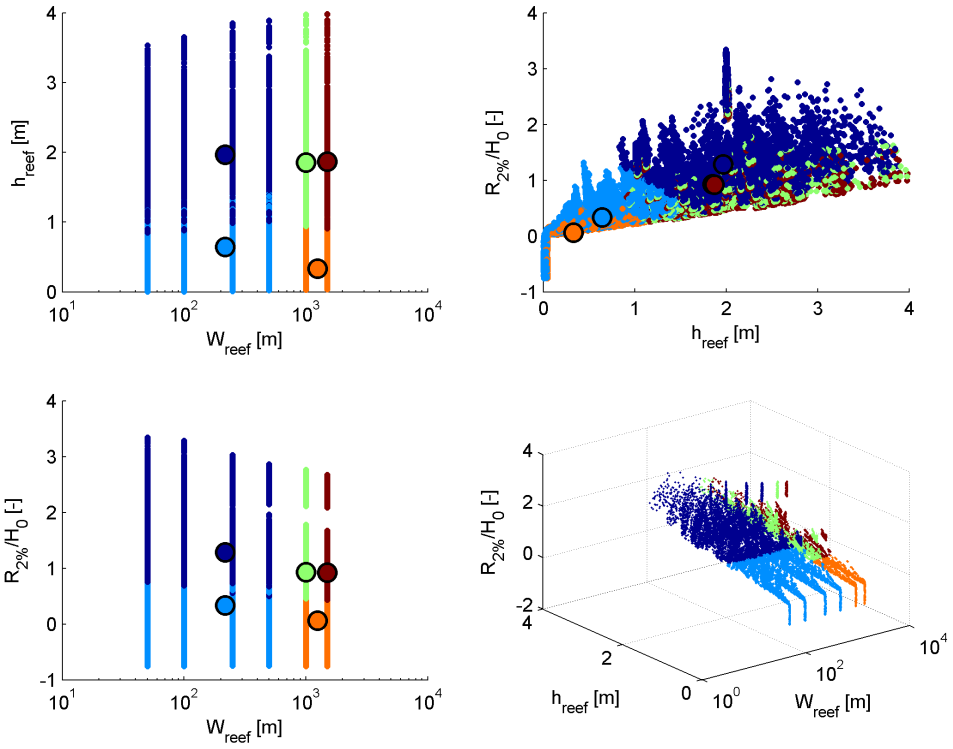

Figure F.1: Cluster analysis of runup, reef width, and depth. Points are coloured differently according to their membership in a cluster, and the large circles represent the centroid of each cluster.

should consider a random sampling approach to choosing input parameters to allow for more continuous distributions.

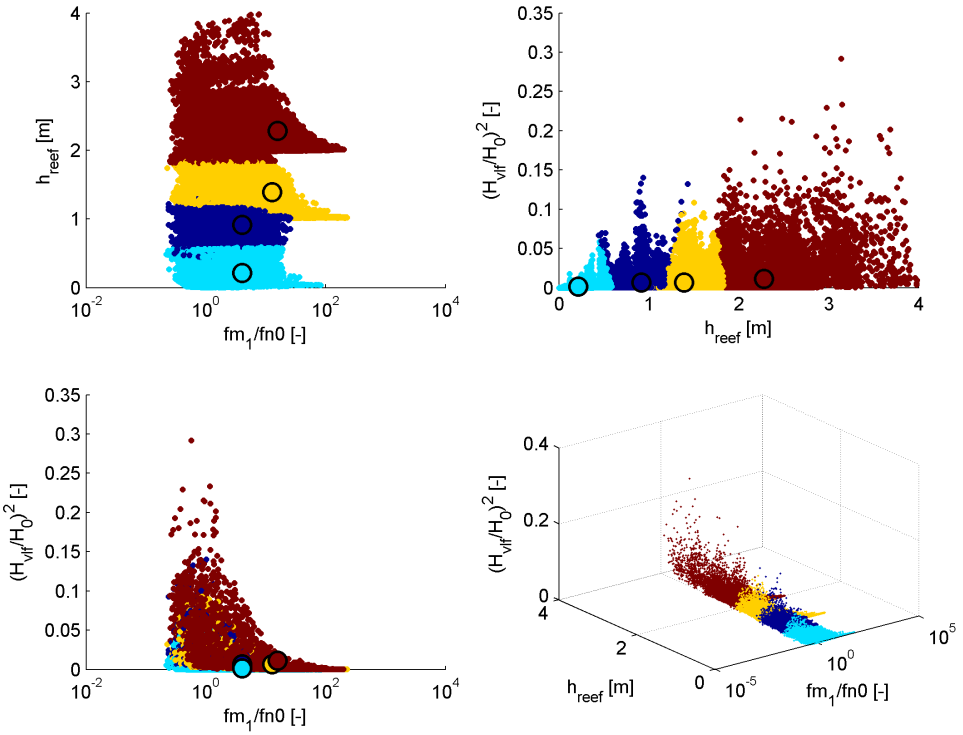

Figure F.2: Cluster analysis of VLF wave height and resonance. Points are coloured differently according to their membership in a cluster, and the large circles represent the centroid of each cluster.

F

G

Empirical Parameterization

SPEED is of the essence in early flood warning systems. Decision-makers and emergency response teams need to make fast, informed decisions under potential flood situations so that they can minimize casualties or damage and bring swift relief. Even though numerical modelling of floods has become much easier and faster with the advent of more powerful computers, such models may still cost precious time to run. For the purposes of this project, it would be challenging to coordinate and run full XBeach simulations for all islands across the Pacific in real time. Hence, faster alternative solutions like Bayesian networks are attractive.

Even simpler than Bayesian networks are empirical parameterizations like the method of Stockdon et al. (2006) for calculating runup on sandy beaches. An algebraic solution like those may also be easier to implement within a larger model.

The considerable variation in reef properties and hydrodynamic conditions and their interaction to produce LF waves generates considerable uncertainty in the estimation of wave-induced flooding on reefed coastlines. This complexity means that a simple empirical prediction has thus far eluded researchers Bosserelle et al. (2015). Many of the empirical relations developed to predict nearshore wave transformation were not intended to be used for complex reef morphologies or extreme events Blacka et al. (2015).

This section applies existing empirical runup equations to our synthetic dataset. Comparing commonly-used runup formulations on our dataset may also give us insight to how reefs differ from sandy beaches, as well as indications of the applicability limits of these formulations. While the formulation of a new empirical expression is beyond the scope of the present study, the lessons learned here may provide some insight into sensitivities and what needs to be included in future parameterizations.

G.1. COMPARISON WITH EXISTING METHODS

This section reviews some of the existing prediction methods for runup and their application to this dataset.

G.1.1. STOCKDON ET AL. (2006)

The empirical runup formulations of Stockdon et al. (2006) are widely used in coastal engineering de Bakker et al. (2014); Gallien (2016); Hapke and Plant (2010); Hughes et al. (2010); Jiminez et al. (2015); Matias et al. (2012); Shope et al. (2015) for estimating runup on beaches. See Section 2.4 for more information about Stockdon's method.

Stockdon et al. (2006) use dimensional parameterization and regressions through the origin to avoid non-physical effects, They suggest that variations in nearshore bathymetry between different experiments may introduce considerable noise into the development of empirical relationships. Hence, the complex topography of reef flats and steep fore reef slopes complicate such matters. The selection of an appropriate input wave height for empirical runup equations should be carefully considered. Stockdon et al. (2006) compare locally-measured significant wave height (H_s), deep water equivalent wave height (H_0), and breaking wave height (H_b), and ultimately use H_0. However, they caution that because of wave transformations, using an offshore wave height may overestimate runup.

Based on their analysis of field datasets, Stockdon et al. (2006) proposed the following

empirical expressions to quantify wave runup:

$$R_{2\%} = 1.1\left(\langle\eta\rangle + \frac{S}{2}\right) \tag{G.1}$$

$$\langle\eta\rangle = 0.35\beta_{foreshore}\left(H_0 L_0\right)^{1/2} \tag{G.2}$$

$$S = \sqrt{S_{inc}^2 + S_{IG}^2} \tag{G.3}$$

$$S_{inc} = 0.75\beta\left(H_0 L_0\right)^{1/2} \tag{G.4}$$

$$S_{IG} = 0.06\left(H_0 L_0\right)^{1/2} \tag{G.5}$$

Where $R_{2\%}$ is the highest 2% of runup, $\langle\eta\rangle$ is setup, S is total swash, S_{inc} is incident (sea-swell) swash, S_{IG} is infragravity swash, $\beta_{foreshore}$ is foreshore slope, H_0 is offshore wave height, and L_0 is offshore wavelength,

90% of dissipative beaches analyzed by Stockdon et al. (2006) are dominated by infragravity energy at the shoreline, which is similar to the conditions on many reefs. Hence, they propose a separate bulk swash term for dissipative beaches to characterize both the (dominant) infragravity and (negligible) incident components:

$$R_{2\%} = 0.043\left(H_0 L_0\right)^{1/2} \quad \text{for } \xi < 0.3 \tag{G.6}$$

Where ξ is the Iribarren number or surf similarity parameter:

$$\xi = \frac{\tan\beta}{\sqrt{H_0/L_0}} \tag{G.7}$$

In these dissipative cases, it should be noted that the runup formulation is not a function of beach slope. This concurs with the log-likelihood analysis conducted in Section 4.2, which found that including beach slope in runup predictions degraded predictive skill by adding uncertainty.

G.1.2. VAN GENT (2001)

The use of offshore wave characteristics to estimate runup in shallow foreshore settings may lead to errors since wave spectra may transform. For instance, energy will likely dissipate across the foreshore, and unimodal spectra may split into double or multi-peaked spectra. Using empirical methods that do not account for this transformation in shallow water may significantly underestimate runup van Gent (2001). It has been used successfully by Quataert et al. (2015) to estimate runup on reef-fronted beaches based on numerical model outputs.

van Gent (2001) proposed an empirical runup formulation for dikes with shallow foreshores to account for arbitrary spectra (including those with multiple peaks):

$$\frac{z_{2\%}}{\gamma H_s} = c_0\xi_{s,-1} \quad \text{for } \xi_{s,-1} \leq p \tag{G.8}$$

$$\frac{z_{2\%}}{\gamma H_s} = c_1 - \frac{c_2}{\xi_{s,-1}} \quad \text{for } \xi_{s,-1} \geq p \tag{G.9}$$

Where $z_{2\%}$ is runup, γ is an empirical reduction factor to account for roughness and oblique wave incidence, $H_s = H_{m0}$, and $\xi_{s,-1} = \tan\varphi / \sqrt{2\pi/g \cdot H_s / T^2_{m-1,0}}$. For the total energy spectrum including both long and short waves, c_0 is 1.45, c_1 is 3.8, $c_2 = 0.25c_1^2/c_0$, and $p = 0.5c_1/c_0$. Equations G.8 and G.9 are valid for $1 \leq \xi_{s,-1} \leq 10$ and $2.5 \leq \tan\varphi \leq 6$. Hence, they may not be applicable for shallower beach slopes.

G.1.3. MERRIFIELD ET AL. (2014)

Merrifield et al. (2014) developed empirical formulations for extreme water level near the shoreline of fringing reefs due to waves. The first parameterization is specified by Equation G.10 and the second by Equation G.11.

$$\hat{\eta}_2 = \bar{\eta} + b\sigma; \quad \sigma = 0.25\sqrt{(H_{ss}^2 + H_{IG}^2)} \tag{G.10}$$

$$\hat{\eta}_2 = b_1 \hat{H}_{br} + b_0; \tag{G.11}$$

Breaking wave height is defined by:

$$\hat{H}_{br} = [(H_0^2 T_0)/4\pi\sqrt{\gamma_s 9.81}]^{2/5} \tag{G.12}$$

And setup is estimated using:

$$\hat{\bar{\eta}} = \frac{5}{32}\gamma_s(\hat{H}_{br} - 1.2H_{ss}) \tag{G.13}$$

Where empirical coefficients $b = 2.22$; $b_1 = 0.32$; $b_0 = -0.12$; and $\gamma_s = 1.2$ are estimated based on average values from two different sites in the Marshall Islands.

G.1.4. BLACKA ET AL. (2015)

Blacka et al. (2015) developed a set of empirical relations to predict wave setup across reefs on Rarotonga in the Cook Islands under extreme events, based on a series of laboratory experiments. To account for the complex bathymetry, roughness, and permeability typical of reefs, they used a reef profile factor (K_p), ranging from 0 to 0.8. They also define reflection and transformation coefficients (K_R, K_r) to describe the transformation of waves across the reef crest.

Blacka et al. (2015) observe significant scatter in their data when comparing non dimensional surf beat (IG wave height) to reef width and submerged reef flat depth, and their best-fit curve tends to underpredict wave height. In their field observations on Rarotonga, Blacka et al. (2015) found that extreme water levels tended to increase with increasing reef flat width, albeit with considerable scatter in the data. The equations below were developed for conditions with reef widths of 150 m and a still water depth of 0 m on the reef flat.

The 1% exceedance water level on reef flat (Blacka et al., 2015):

$$\eta_{1\%} = 0.216(H_{s0}^2 T_p)^{0.325} \tag{G.14}$$

Setup on the reef flat can be estimated with the following equation (Blacka et al., 2015):

$$\overline{\eta_r} = -0.92 + 0.77 \log_{10}(H_{s0}^2 T_p) \tag{G.15}$$

To test the range of applicability for each of the empirical formulations above, they were plotted against our dataset.

G.2. RESULTS

For these runup comparisons, only the 30 m beach crest runs were included, because the shorter crests that permit overtopping tend to truncate the distribution of runup. In some cases, the runs without a reef flat ($W_{reef} = 0m$) are highlighted in red. Since the Stockdon equation was developed for coasts without a reef flat, this enables a more fair comparison between our model results and their method.

Figure G.1 shows the method of Stockdon et al. (2006) applied to our datset. When all reefs are considered (blue dots), Stockdon overpredicts runup. This is likely because wave energy is dissipated across the wider reef flats, leading to reduced runup when compared to a typical beach under the same forcing. However, even when the input dataset is filtered to include only scenarios without a reef flat, there is still considerable spread around the data, although it follows the mean trend. Stockdon tends to overpredict setup and incident swash. When the formulation for dissipative beaches (Equation G.6) is used, it tends to underpredict total runup.

Figure G.2 shows the method of van Gent (2001) applied to our dataset This formulation is slightly conservative in its prediction of both total runup and setup, although there is considerably less spread than for Stockdon. The reduced spread may be attributed to the fact that the equations use wave height at the toe of the beach for their inputs (rather than offshore, as with the other formulations). Thus, the reef morphology has less influence on the prediction when compared to Stockdon, which uses offshore wave conditions as input. This prediction could be improved by calibrating the empirical coefficients of the formulation.

Figure G.3 shows a comparison between XBeach results and Merrifield's extreme WL estimate (Merrifield et al., 2014). Equation G.10 tends to underestimate extreme water levels when compared to the XBeach model, although the spread of points is fairly narrow. Equation G.11 has a much wider spread than Equation G.10. Merrifield's setup estimate also shows considerable scatter, and appears to be truncated at a limit of 1.5 m. Their equation was calibrated using data from two specific sites in the Marshall Islands, so it is possible that the wider parameter space modelled in this project can explain the differences seen here. A cursory attempt at calibration reveals that when the empirical coefficient b is changed to 5, the visual fit with the main point cloud improves, and with $b = 8$, points in the 250-350 m reef width range fit better. Further calibration of the parameters should be carried out in a more statistically rigorous manner.

Figure G.5 shows a comparison between XBeach results and Blacka's extreme WL estimate (Blacka et al., 2015). Equation G.15 and Equation G.14 both show considerable scatter, although this can likely be attributed to the wider range of conditions modelled. To better reflect the conditions on Ratrotonga for which the equations were developed,

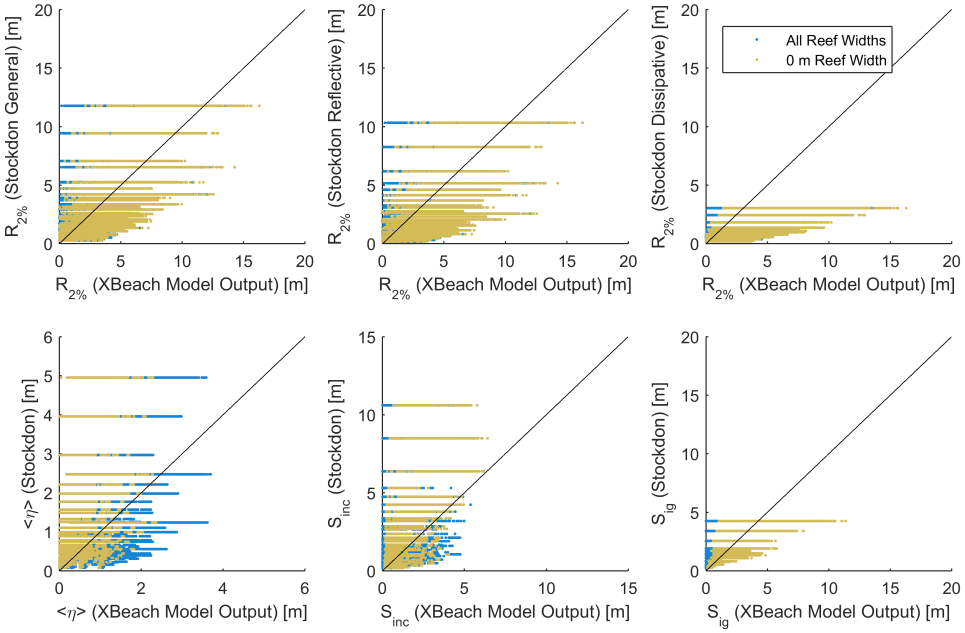

Figure G.1: Comparison between XBeach results and predictions using Stockdon et al.'s method (2006) based on offshore wave conditions and beach characteristics.

G

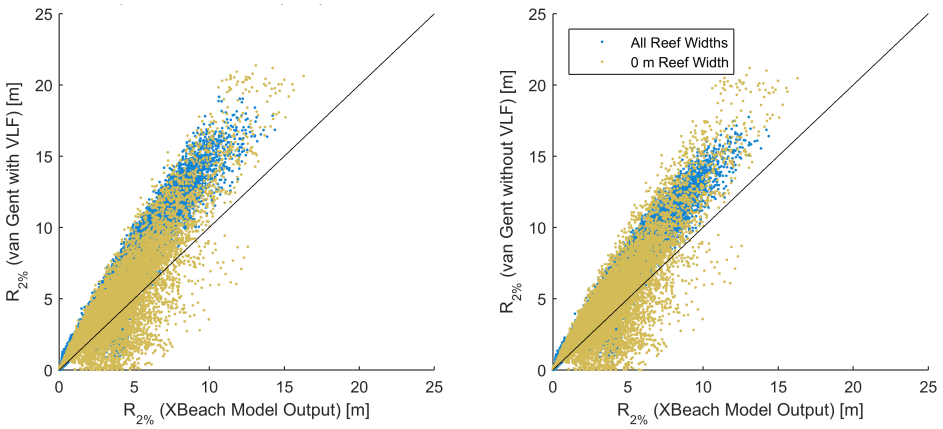

Figure G.2: Comparison between modelled runup and runup estimated by van Gent's method (2001) using wave conditions at the inner reef flat.

cases with with reef widths of 150 m and a still water depth of 0 m on the reef flat have been highlighted. These results show a better visual fit.

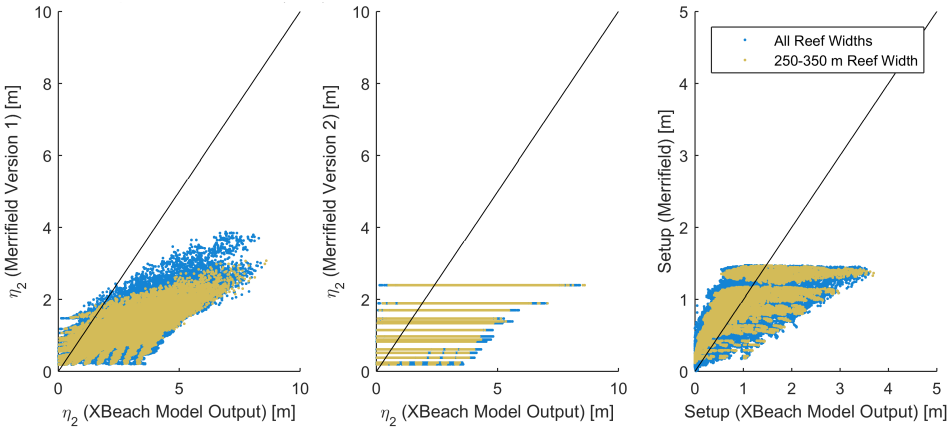

Figure G.3: Comparison between modelled extreme water levels/setup and extreme water levels/setup estimated by Merrifield's method (2014). This simulation uses the default b coefficient of 2.2.

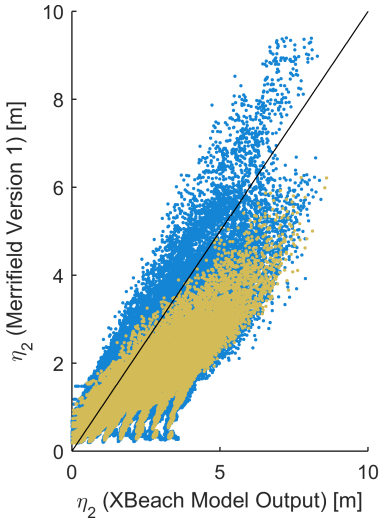

Figure G.4: Calibrated comparison between modelled extreme water levels and extreme water levels estimated by Merrifield's method (2014). The calibration parameter b has been adjusted to from 2.2 to 6.

G.3. RECOMMENDATIONS

Based on the outcome of these tests, it appears that existing formulations for runup show varying levels of applicability to reefs. The wide range of conditions simulated in our dataset and the differences between reef hydrodynamics and those on sandy beaches may account for the spread in many of the results. Furthermore, these expressions have all been developed based on specific sites or laboratory experiments, which may contribute to the differences. Additional calibration of empirical coefficients may yield improved fitting of the equations. It is challenging to isolate patterns and trends from the

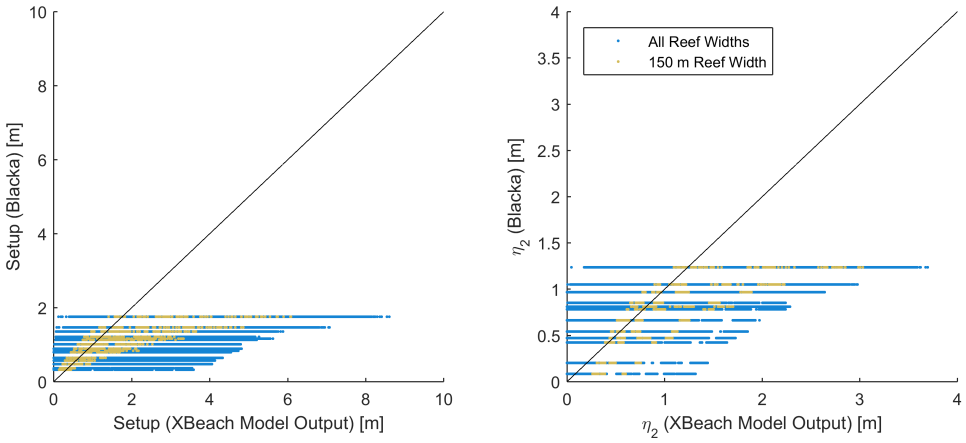

Figure G.5: Comparison between modelled setup/extreme water levels and setup/extreme water levels estimated by Blacka's formulations (2015).

present dataset given that we use such a wide range of uniformly distributed parameters, all effectively given the same weighting. Filtering with the Bayesian network or partitioning by cluster analysis may be useful techniques for separating the data into more meaningful groups for curve-fitting.

Future studies should consider curve-fitting exercises to formulate new empirical parameterizations for reefs. The data examined here has only been plotted and visually inspected; a formal statistical analysis should be carried out in future investigations (i.e. quantifying correlation, scatter, etc.). In particular, attention should be given to quantifying decay across reef flats and amplification due to low-frequency resonance.

H

Traditional Knowledge & Wave Piloting

The sea is dangerous and its storms terrible, but these obstacles have never been sufficient reason to remain ashore. Unlike the mediocre, intrepid spirits seek victory over these things that seem impossible. It is with an iron will that they embark on the most daring of all endeavors... to meet the shadowy future without fear and conquer the unknown.

Ferdinand Magellan

Traditional knowledge can improve the development of early flood warning systems by supplementing the lack of observations in a data-poor environment and furthering our understanding of wave-island interactions. Applying traditional knowledge can also improve engagement with the communities affected by flooding to make them a part of the solution.

H.1. INTRODUCTION

PEOPLE have lived on the Marshall Islands for over 3000 years, but their ancestral homes are now under threat from climate change. Settling and building a livelihood in the remote archipelago was made possible by their exceptional navigational skills. Of particular relevance to this thesis is their ability to navigate by observing and understanding patterns in swell waves, a practice known as wave piloting[1]. Marshall Islanders have thus long lived in symbiosis with the waves, although now the very same waves that helped them are threatening their survival. Given that they were able to survive for so many centuries by "reading" waves, is it now possible to apply some of their knowledge to help predict the waves that threaten them today?

The Sendai Framework for Disaster Risk Reduction calls for increased use of traditional indigenous knowledge in the implementation of early warning systems, so this could be an ideal opportunity to put it into practice. The framework recognizes that:

> *Indigenous peoples, through their experience and traditional knowledge, provide an important contribution to the development and implementation of plans and mechanisms, including for early warning (UNISDR, 2015, 36(a))*

And it specifically calls to:

> *Ensure the use of traditional, indigenous, and local knowledge and practices, as appropriate, to complement scientific knowledge on disaster risk assessment (UNISDR, 2015, 24(i)).*

Flood risk reduction measures cannot just be imposed from the top down (i.e. at a government level) to work effectively. Engagement with the local communities affected by the flooding is an essential part of the system. For instance, if an early warning system issues an evacuation response, how do you ensure that everyone actually listens and evacuates? That requires buy-in from the locals. Using their traditional knowledge to supplement scientific knowledge could empower people and give them a better sense of ownership/shared responsibility.

Hence, it is important to consider how traditional knowledge of indigenous peoples on low-lying tropical islands can contribute to flood risk reduction.

[1] For a fascinating introduction to wave piloting and an account of recent efforts to link traditional knowledge with modern wave physics, readers are encouraged to read the following article: http://www.nytimes.com/2016/03/20/magazine/the-secrets-of-the-wave-pilots.html?_r=0

H.2. TRADITIONAL KNOWLEDGE

Traditional knowledge is experiential knowledge developed by societies through generations of observing and interacting with their local environments (Becker et al., 2008). Traditional knowledge is often heavily ingrained within the day-to-day lives of indigenous people (Mercer et al., 2007). This deep-rooted understanding includes navigational expertise like wave piloting, but also extends to other concepts relevant to flood risk reduction. Mercer et al. (2007) challenge the assertion that only data collected in a scientific fashion can be useful.

Indigenous people on the tropical islands studied by (Hiwasaki et al., 2014) have developed keen observational skills for their environment which enable them to predict hydrometeorological hazards. For instance, changes in the clouds, wind, sea, and moon may be used as warning signs of impending danger. These abilities, honed over many generations, may form a valuable supplement to other scientific measurement techniques. Mercer et al. (2007) cite numerous examples of cases where indigenous people living in SIDS survived flooding due to cyclones and tsunamis by using traditional knowledge. The inhabitants of these islands are also familiar with the destructive low frequency waves explored in this thesis—in Fiji, they are known to locals as Loka waves (Bosserelle et al., 2015).

In the absence of measured wave or water level records, oral tradition can be a source of anecdotal evidence of past flood events, as used by Smithers and Hoeke (2014) to estimate return periods of extreme swells on Nukutoa, Papua New Guinea.

McAdoo et al. (2009) report that traditional indigenous knowledge of appropriate tsunami responses played a significant role in reducing mortality on the Solomon Islands after a tsunami in April 2007. The local people understood the natural warning signs associated with tsunamis (e.g. earthquake, draining of reef flats and lagoons), and knew to evacuate safely. Fatalities from the tsunami were disproportionately made up of immigrants who lacked the generations of experience that locals had.

Traditional knowledge of appropriate tsunami responses is especially valuable close to the source, where there is insufficient time for an early warning system (McAdoo et al., 2009). However, they suggest that EWS are more useful in regions far away from the source of the tsunami, since exposed populations may not feel the earthquake that caused them. This is analogous to the threat posed by remotely-generated swell, which can arrive at a given island independently of the local conditions. It further underscores the need for EWS on low-lying tropical islands.

Indigenous knowledge does not only extend to disaster response, but also to sustainable land planning practices. Spennemann (1996) notes that original settlement patterns on the Marshall Islands prior to World War II were based around minimizing flood risk (e.g. building only on high ground in more sheltered areas). This is in stark contrast to the situation today, where many residents are clustered in densely-populated urban centres along the windward side of islands. Land reclamation is widespread on urbanized islands like Majuro, RMI (Ford, 2012), and many newer developments are located in low-lying areas at high risk of flooding

H.3. WAVE PILOTING

Marshall Islanders have long held a special relationship with the ocean, dating back to their initial settlement of the archipelago 3000 years ago. Settlement of the Pacific islands began in the second millennium BC and continued gradually spreading outward across thousands of kilometers of open ocean using only simple boats until approximately 1000 AD (Weisler and Woodhead, 1995).

This amazing feat of exploration was possible due to their keen navigational abilities, most specifically their intimate understanding of waves. They were able to "read" the waves in order to pinpoint their position relative to different islands. Wave piloting has a basis in two key physical phenomena: (a) the persistent swell systems originating from consistent source regions and (b) unique diffraction and reflection patterns between islands.

> The Marshall Islanders' unique understanding of the waves has helped them survive for over three thousand years. Is it possible that their knowledge can be used to help them confront the threat that those same waves now pose in the face of climate change?

H.3.1. THE HISTORY OF WAVE PILOTING

As Weisler and Woodhead (1995) remark, "*that Pacific colonists—without the aid of modern instruments—reached nearly every inhabitable island scattered over more than one third of the earth's surface during a relatively brief 3500 year period is truly amazing and stands as one of the great achievements in human history*".

Prevailing winds in the tropical Pacific blow from east to west, and yet many of the islands were settled from west to east. Since early colonists lacked the technology to sail into the wind, Anderson et al. (2006) hypothesize that Pacific islanders may have relied on periodic reversals in prevailing wind direction brought about by the El Niño-Southern Oscillation (ENSO). Their understanding of local climate fluctuations thus would have enabled them to settle remote islands.

The oceanic currents passing through the Marshall Islands are often weak and unsteady, making it a challenge to use them for wayfinding. Finney (1998) posits that this may have contributed to the dependency of Marshallese sailors on interpreting swell patterns to navigate. The low elevation of atolls adds to the challenge of navigation, since they can seldom be seen more than 20 km away Genz et al. (2009).

The swell systems reaching the Marshall Islands were so regular and predictable (on account of persistent trade winds and seasonal fluctuations in remote generation areas) that wave pilots were able identify and rely on them for navigation, even giving them names (Finney, 1998).

Indigenous Pacific Islanders developed an ingenious method for navigating between remote islands by using the relationships between waves and islands, known as wave piloting (van Vledder, 2015). Swell waves generated by distant storms are typically characterized by long crests, steady direction and period. When a swell wave field meets an island, the waves will reflect, refract, or diffract around it, creating characteristic inter-

ference patterns that can be interpreted by someone with knowledge of the local wave climate (Figure H.1). By doing so, they can develop a mental map of their relative position between islands.

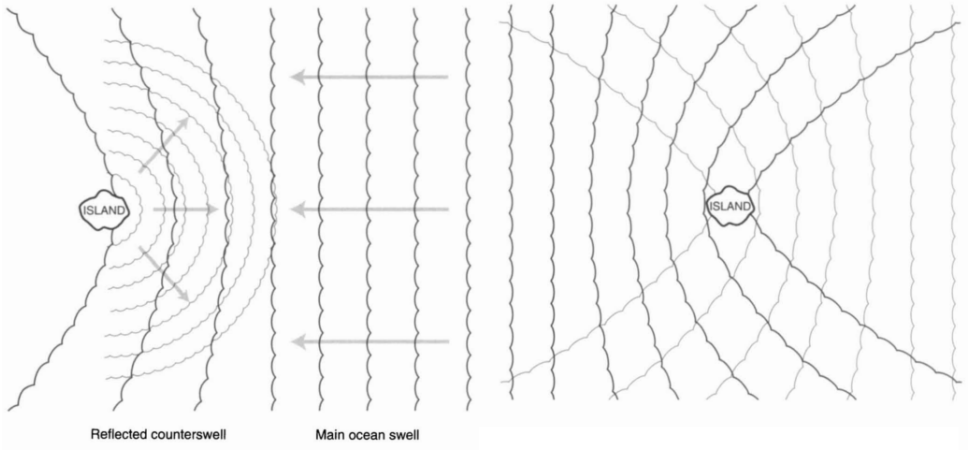

Figure H.1: Simplified schematic of reflection and refraction or diffraction patterns resulting from swell trains interacting with small islands (Source: Finney (1998)).

The wave nodes created by constructive interference from these persistent swells could be used by wave pilots as an indication of nearby islands. These disruptions may form around isolated islands or become yet more complex among small clusters of closely-spaced islands (Finney, 1998). The interference patterns created by islands may extend tens of kilometers offshore, making it possible for observant navigators to determine the relative location and direction of islands even when they are far out of sight (Genz et al., 2009). The Marshallese were able to detect these patterns not just visually, but by feeling the motion of the swell within their canoes (Finney, 1998).

Because the sea is dynamic, so too must be the wave pilots' mental maps of islands and swell patterns. When a large storm-driven swell masks the subtle swell systems normally used for navigation, wave pilots can update their mental maps by interpreting the new patterns it forms (Genz et al., 2009).

To record and transfer this knowledge, the wave pilots made stick charts (Figure H.2) or *rebbelib*, which indicate the relative position of islands and distinctive patterns around them (Hennings, 2015). These tools were used not as navigational charts on voyages, but instead as educational tools and memory aids for making tangible the mental maps developed by wave pilots.

Since World War II, inter-island canoe travel has reduced, making wave piloting a rare skill possessed by few (Finney, 1998). However, there have been recent efforts to revive wave piloting and endow a new generation with these traditions (Tingley, 2016).

H.3.2. SCIENTIFIC ANALYSIS OF WAVE PILOTING

In order to make use of traditional wave piloting knowledge in an operational forecasting system, we must consider how it relates to our scientific understanding of waves. Most

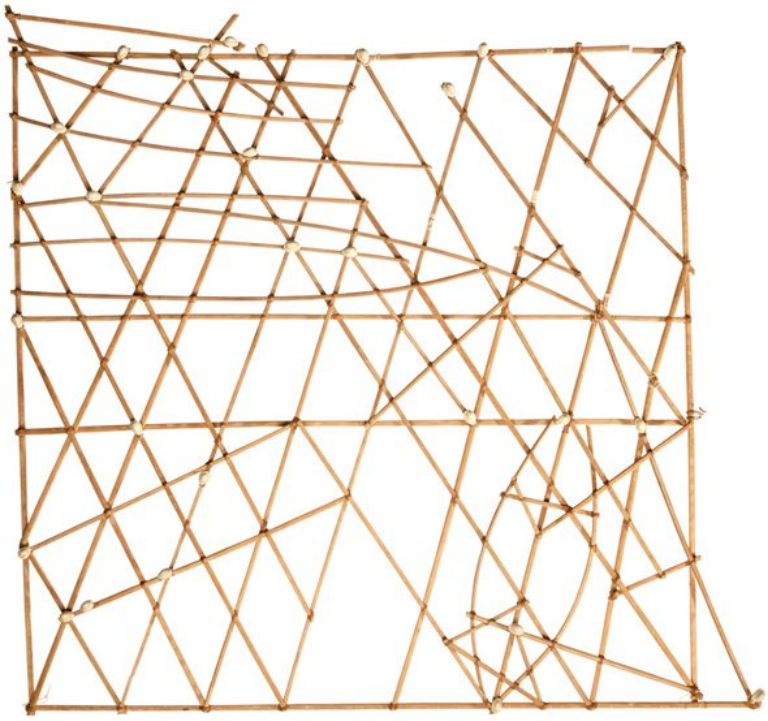

Figure H.2: An example of a stick chart or *rebbelib* used by Marshall Islanders to navigate at sea using swell patterns around islands. The sticks represent characteristic swell systems and interference patterns from diffraction and reflection, while individual islands are represented by shells lashed to the nodes (Source: Smithsonian National Museum of Natural History (2016))

recently, van Vledder (2015) attempted to unite the disparate fields of anthropology and coastal engineering by using numerical wave models to simulate the swell patterns used by Marshall Islanders for navigation.

van Vledder (2015) analyzed the wave climate at Tahiti in French Polynesia, and found that swell waves contributed 80% of all wave energy, with quadruple swells existed 73% of the time. Such persistent, multi-directional swells (independent of local wind conditions) are similar to those that enabled the Marshall Islanders to use waves for navigation. The waves were dependable enough in their frequency, intensity, and direction that islanders often had specific names for different swell systems.

Alves (2006) developed a numerical wave model in WAVEWATCH III (Tolman, 2009) to identify the influence of swell generated in specific regions of the ocean (Figure H.3). Their analysis corroborates the findings of van Vledder (2015), identifying four distinct areas that contribute persistent swell to western Pacific tropical islands. Extratropical regions tend to generate swell via large storms, the same mechanism responsible for many of the wave-induced floods of concern in this thesis. Tropical regions contribute swell via tropical storms and regular trade winds. Steeper waves locally generated by

these trade winds may also be persistent enough to aid in navigation.

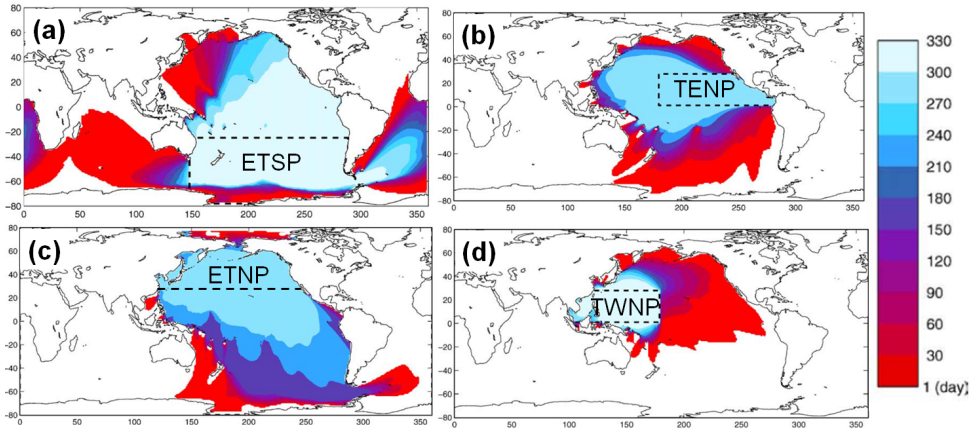

Figure H.3: Persistence of various swell wave sources in the Pacific. The colourmap indicates the number of days per year when a given location is affected by swell originating from the area demarcated by a dashed box. The swell source areas are: (a) Extratropical south Pacific (ETSP); (b) Tropical eastern north Pacific ;(c) Extratropical north Pacific; and (d) Tropical western north Pacific (TWNP). It is these highly persistent swell systems (shown in light blue) that make wave piloting possible in the Marshall Islands. Source: Alves (2006).

Genz et al. (2009) accompanied a Marshallese wave pilot on a 220 km journey between two atolls, deploying wave buoys and developing a numerical wave model in SWAN (Figure H.4). In doing so, they were able to make a clear link between traditional knowledge of swell-island interaction, modern scientific observations, and process-based simulations. More recently, van Vledder (2015) reproduced the wave phenomena observed by indigenous Pacific islanders using the SWASH numerical model to better understand wave blocking by islands at sub-grid scales in regional wave models. Refraction generally does not occur at large scales on atolls because of their steep sides and narrow reef flats, so diffraction around the islands is more common.

In their study, buoys deployed in the Marshall Islands by Genz et al. (2009) were unable to detect waves reflected from the islands. The model results in Section 4 suggest that sea-swell waves are largely attenuated on reefs, although there may be a strong seaward-directed low-frequency wave component generated by the breakpoint mechanism (Pomeroy et al, 2012b).

Baldock et al. (2000) notes that on sandy beaches, breakpoint-generated long waves reflected off the shore are stronger than either reflected bound long waves, outgoing breakpoint-generated long waves, or swell. However, if frictional dissipation is high (i.e. on rough reefs), then infragravity waves reflecting off the shore will decay (Pomeroy et al, 2012b). Hence, outgoing breakpoint-forced long waves are likely to be the dominant reflected signal from atolls. Roeber and Bricker (2015) observed low-frequency energy in deep water offshore of reefs in the Philippines and identified it as free long waves emanating from shore. Thus, it is possible that wave pilots detect breakpoint-generated infragravity waves (which may go unnoticed by less sensitive wave buoys) rather than reflected swell.

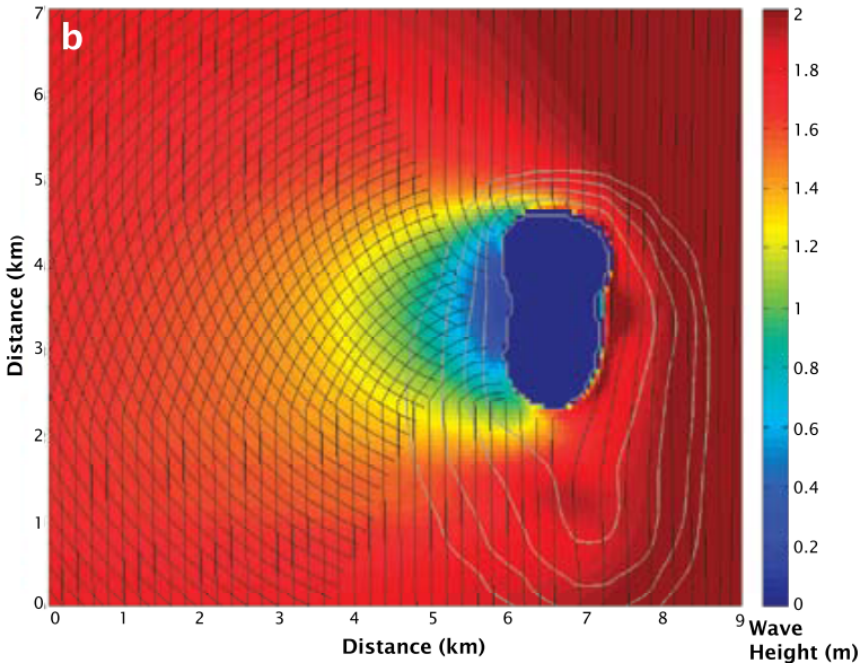

Figure H.4: Simulation of swell wave refraction around Mejit Island, RMI using SWAN (Booij et al., 1999). The contours of the island are indicated in light grey, wave crests in black, and the colour map indicates wave height. Waves travel from right to left in the figure, resulting in a characteristic blocking and interference pattern in the lee of the island (Source: Genz et al. (2009)). By observing these patterns, wave pilots would be able to detect the direction and relative distance of islands even if they were too far over the horizon to be visible to the naked eye.

Rawat et al. (2014) suggest that deep ocean sites in the west Pacific are dominated not by locally-generated infragravity waves, but by those that have travelled from the opposite side of the ocean. They find that the interaction of swell produced by large extratropical depressions with eastern ocean boundaries are better at generating free infragravity waves than hurricanes or other tropical storms. However, they do not specifically investigate low frequency waves generated by reefed coastlines in their analysis.

These atolls would effectively act as small point sources of infragravity waves, and thus their influence may be more difficult to detect at the mid-ocean sites examined by Rawat et al. Although they may transform and increase in size as they move inshore, such low frequency waves are typically O(1 cm) in height on the open sea (Rawat et al., 2014). This challenges the notion that they would be detectable by wave pilots.

The generation of seaward-directed long waves could be further investigated by analyzing the synthetic dataset created in XBeach for this thesis. By conducting a cross-correlation analysis of the incoming and outgoing components, the source and phase relationships of different wave components could be discerned (Gawehn, 2015). If the source and magnitude of reflected waves for each different reef configuration can be determined, it may be possible to develop generalized relationships concerning the waves

that reflect from atolls.

Figure D.8 shows that reflection is most influenced by wave steepness and fore reef slope, which is consistent with the field observations of (Young, 1989). In laboratory experiments, Yao et al. (2012) observed partial standing waves seaward of the reef due to reflection, a trend which increased with increasing fore reef slope. Hence, long-period swell and steep fore reefs are likely to result in greater reflection.

If each island has unique reflective properties based on the characteristics of its reefs, this could be a "signature" that might aid in wave piloting. It would then be interesting to validate these concepts on islands whose reflective characteristics have been documented by wave pilots.

H.4. APPLICATION OF TRADITIONAL KNOWLEDGE

Genz et al. (2009) notes that extreme swell (of primary concern to this thesis) is too strong and irregular to be useful for navigation. Nonetheless, it is possible that the principles on which wave piloting is based may provide some insight that can be useful for predicting its behaviour.

The value of traditional wave piloting knowledge to early flood warning systems is threefold:

1. As interpretations of wave-island interaction which can be used to improve the swell forecasts which drive flood models
2. As a qualitative data source for validating and improving models
3. As a means of increasing community engagement

As the analysis in Section 4 demonstrated, a reliable wave forecast is essential input for the prediction of flooding on low-lying tropical islands. In the absence of measured offshore data, these inputs can be obtained from regional wave models. Island blocking of swell in WAVEWATCH III is currently parameterized, since islands are typically subgrid scale features (Tolman, 2003). By supplementing more detailed models with traditional wave piloting knowledge of reflection, refraction, and diffraction patterns around islands, it may be possible to better quantify these processes and represent them in models (van Vledder, 2015). Improved understanding of wave blocking may thus lead to more accurate early warning systems like the one proposed in this thesis.

Furthermore, as Genz et al. (2009) note, the most astute wave pilots may be able to detect subtleties in swell patterns that are undetected by wave buoys. Hence, they may be able to confirm or refute model findings, or provide leads on where and how to improve scientific monitoring. Since wave pilots can read swell fields from a single wave group, it may be better to represent the sea surface as the sum of wave groups rather the harmonic planar waves assumed by the random phase model (Gerbrant van Vledder, personal communication, June 19, 2016). Thus, wavelet Różyński and Reeve (2005) or Hilbert analysis techniques Huang et al. (1999); Veltcheva (2002) might prove more appropriate than the Fourier analysis typically used for processing wave data.

McAdoo et al. (2009) note that successful evacuations require not only the functional components of an EWS (monitoring, forecasting, and communication), but also an educated population that can properly respond to the warnings. Similarly, Mercer et al. (2007) acknowledge that advancing the science behind early warning systems is essential

but could benefit from incorporating traditional knowledge. Hiwasaki et al. (2014) note that traditional folklore, rituals, and practices may also contribute to disaster resilience by transmitting knowledge to younger generations, raising awareness of hazards, and promoting social cohesion.

Mercer et al. (2007) encourage that the gap between scientific and traditional knowledge be closed in a manner that is both sustainable and culturally compatible. Specifically, McAdoo et al. (2009) call for traditional knowledge to play a more prominent role in disaster risk reduction and response, since it takes into account the human dimensions of effective disaster management.

Top-down policies may be ineffective if they do not engage local communities. Mercer et al. (2007) implore that indigenous people of Small Island Developing States should be the first point of contact in DRR planning. Continued work is thus needed to understand traditional knowledge and find ways to apply effectively it in a scientific framework.

H.5. CONCLUSIONS & RECOMMENDATIONS

Traditional knowledge can improve the development of early flood warning systems by supplementing the lack of observations in a data-poor environment and furthering our understanding of wave-island interactions. Applying traditional knowledge can also improve engagement with the communities affected by flooding to make them a part of the solution.

The research carried out in this thesis also raises several interesting questions for future researchers at this interface of coastal engineering and anthropology:

- What else we learn about reef hydrodynamics from wave piloting practice?
- What can wave piloting teach us about multiple swell systems?
- How might the interaction of waves and islands be important for flood prediction?
- How might shadowing/interference effects observed during normal swell conditions change during extreme swell events? Might these influence flooding (particularly in clusters of nearby islands)?
- Are there critical wave directions for certain islands that may result in greater flooding?
- Could the waves reflecting off one island (or diffracting around it) be modified in frequency and provoke flooding on other islands?
- Can the predictability of swell for wave piloting be transferred to flood forecasting?
- Can knowledge of swell conditions be used to choose representative conditions or bins for a Bayesian network?
- What other traditional knowledge about responses to wave-induced flooding can be used to build resilience against future climate change?
- If climate change modifies the characteristic swell fields within Pacific island chains (also affecting the attenuation of high frequency waves and generation of infragravity waves on reefs), might the patterns relied upon by locals for wave piloting also change?

The recommendations of this thesis (Section 6.2) should be carried out in partnership with the communities on low-lying tropical islands that are affected by flooding,

rather than simply being implemented as a top-down solution. Citizen science, where ordinary citizens are enlisted to record scientific observations, has been an effective strategy for large-scale, long-term data collection in many other science disciplines (Bonney et al., 2009). To make the most of local observations, island residents should be trained to recognize, measure, and report on the phenomena that are of interest here (e.g. undular bores).

Such a bottom-up approach based on traditional knowledge and involvement of local communities may be especially useful on SIDS, since the islands are often remote and disconnected from one another, making centralized disaster risk management more challenging (Mercer et al., 2007). Doing so would also help to compensate for the major scarcity of scientific data that presently limits our understanding of wave-induced flooding on low-lying tropical islands.

Furthermore, traditional knowledge such as wave piloting should be integrated into future studies wherever possible. These remarkable skills have supported the livelihoods of Marshall Islanders for generations, and could continue to play an important role in ensuring a resilient future, in spite of the threats that lie ahead.